INFORMATION TO USERS

This manuscript has been reproduced from the microfilm master. UMI films the text directly from the original or copy submitted. Thus, some thesis and dissertation copies are in typewriter face, while others may be from any type of computer printer.

The quality of this reproduction is dependent upon the quality of the copy submitted. Broken or indistinct print, colored or poor quality illustrations and photographs, print bleedthrough, substandard margins, and improper alignment can adversely affect reproduction.

In the unlikely event that the author did not send UMI a complete manuscript and there are missing pages, these will be noted. Also, if unauthorized copyright material had to be removed, a note will indicate the deletion.

Oversize materials (e.g., maps, drawings, charts) are reproduced by sectioning the original, beginning at the upper left-hand corner and continuing from left to right in equal sections with small overlaps. Each original is also photographed in one exposure and is included in reduced form at the back of the book.

Photographs included in the original manuscript have been reproduced xerographically in this copy. Higher quality 6" x 9" black and white photographic prints are available for any photographs or illustrations appearing in this copy for an additional charge. Contact UMI directly to order.

U·M·I

University Microfilms International
A Bell & Howell Information Company
300 North Zeeb Road, Ann Arbor, MI 48106-1346 USA
313 761-4700 800 521-0600

Order Number 9315465

Monte Carlo studies of three-dimensional chains on a lattice: The equation of state and segment density profile near a repulsive wall

Hertanto, Agung Eko, Ph.D.

City University of New York, 1993

U·M·I
300 N. Zeeb Rd.
Ann Arbor, MI 48106

MONTE CARLO STUDIES OF THREE DIMENSIONAL CHAINS ON A LATTICE: THE EQUATION OF STATE AND SEGMENT DENSITY PROFILE NEAR A REPULSIVE WALL

by

AGUNG EKO HERTANTO

A dissertation submitted to the Graduate Faculty in Physics in partial fulfillment of the requirements for the degree of Doctor of Philosophy, The City University of New York.

1993

This manuscript has been read and accepted for the Graduate Faculty in Physics in satisfaction of the dissertation requirement for the degree of Doctor of Philosophy.

Dec 11, 1992
Date

Chair of Examining Committee

Dec 16, 1992
Date

Executive Officer

Prof. R. Dickman, CUNY

Prof. E. Chudnovsky, CUNY

Prof. R. Mauri, CUNY

Prof. A. Sokal, NYU

Prof. R. Varley, CUNY

Supervisory Committee

THE CITY UNIVERSITY OF NEW YORK.

Abstract

MONTE CARLO STUDIES OF THREE DIMENSIONAL CHAINS ON A LATTICE: THE EQUATION OF STATE AND SEGMENT DENSITY PROFILE NEAR A REPULSIVE WALL

by

AGUNG EKO HERTANTO

Advisor: Professor Ronald Dickman

The equation of state and conformational properties of polymer chains on a regular lattice are investigated using Monte Carlo simulations. Various chain systems are studied: athermal monodisperse and polydisperse linear chains, non-athermal linear chains, and chains with various branch-structures. The chain-length varies from N = 10 to 150. In these simulations, the test-chain insertion method is employed to obtain the insertion factor in the low density regime and to determine the theta-temperature, and the repulsive wall method is used to determine the equation of state in the high density regimes.

This dissertation focuses on comparison between simulation results and predictions of Flory and Flory-Huggins

mean-field theories, and Freed's n-vector model. The results indicate that the Freed's n-vector model provides the best estimate of the osmotic pressure at various densities and solvent qualities. A discrepancy exists for chains with branch structures.

Other conformational properties investigated are the end-to-end distance and the segment density profile near a repulsive wall. Scaling techniques are employed to obtain the scaling exponent ν and the density dependence of the osmotic pressure. Monte Carlo results support de Cloizeaux' scaling law for the pressure. The effect of confinement on the equation of state and the end-to-end distance is also studied for chains at finite concentration. To study the effect of an interface, an analytical calculation is performed to determine the density profile of Gaussian chains adjacent to a repulsive wall. It shows that $\rho \propto z^2$ for $z \to 0$, where z is the distance from the wall. Edwards' model is also used to represent a polymer chain. In this model, the renormalization group equation and the ϵ expansion (up to first order) are presented to determine the scaling exponent of $\rho(z)$ for $z \to 0$. Monte Carlo results also indicate the scaling behavior for athermal chains. For non-athermal chains, a complication arises due to the temperature dependence, which is not represented in Edwards' model.

ACKNOWLEDGMENTS

When this letter was finally written, I had a personal recollection. The questions that came to my mind were why this journey took so long and what the next step would be. This pilgrimage started from supergravity and superstring. All the energy and enthusiasm were spent during those early days to follow the holy grail of theoretical physics, 'to find the theory of everything that represents the phenomenology'. In my journey, it ended nowhere. Even today, the topic that I was assigned of remains unsolved.

Finally I found the reality when Prof. J. Gillespie introduced me to Prof. R. Dickman. Therefore, my first thank goes to Prof. Gillespie.

Prof. R. Dickman deserves a special place. He introduced me Monte Carlo simulations and polymer physics. He suggested the topics for my dissertation. Only through his persistence I moved forward. Without his patience and attention I never finish my graduate program. During the nights I often thought that I wished I could have become his student five years earlier when my youthful energy was still radiant and fresh. Thanks Ron, you give the fine finishing touch in one chapter of my life.

I also thank to Prof. E. Chudnovsky, Prof. R. Mauri, Prof. A. Sokal, and Prof. R. Varley who spent their valuable time to sit in the doctoral committee.

Of many friends who gave encouragement and support, my thank is forwarded to Dr. E. Gozzi, Prof. M. Loebel, Prof. J. Gersten, Prof. T. Boyer, Prof. M. Kaku, Prof. B. Sakita of The City College of New York; Prof. J. Ullman, Prof. C. Engelke, Prof. R. Finnerman, E. Jimenez, L. Stolz, J. Dono, and J. Bernard of H. Lehman College; Prof. M. Barmawi, Dr. M. Hadisoesastro, Dr. H. Hadi, Dr. J. Sudarminto, Rev. G. Oetomo, Rev. I. Warnabinarja, H. Purnomo, R. Atje, H. Suwardi, A. Djaelani, and F. Louis.

Yanti and I also owe our gratitude to Augarten's family, whose support makes our life in New York bearable. Shari and David, how can I express my gratitude for all your support? Samantha and Jessica, you always inspire me of life and hope.

I was fortunate that I could go to the graduate program without a string attached. This was due to Center for Strategic and International Studies - Jakarta, The City University of New York, and The Indonesian Foundation. Their supports were invaluable.

I am also grateful to my parents, brothers, and sisters who always encourage me not to give up. Last but not least, I thank to my wife, Yanti, whose patience, love, and care make this difficult journey easier. Her encouragement, humor, and support are always there in time of need. Therefore, I dedicate this work to her.

As an epilog of my study, I would like to say that my stay at Lehman College was colorful. The people are nice, the campus is small but beautiful. One dark spot that is difficult to erase is my experience with The City University's bureaucracy. It always appalls me.

This dissertation is the final dot in one chapter of my life. A new chapter begins, the pages are still very clean. I already have ideas what to write. It is interesting and better.

TABLE OF CONTENTS

LISTS OF TABLES.

LISTS OF ILLUSTRATIONS.

I. INTRODUCTION: A PEDESTRIAN VIEW OF POLYMER SOLUTIONS.

The properties of polymer systems attracted the interest of physicists early in this century[1-7]. Since then the advancement of technology has made polymer science an essential branch in materials research. The results of polymer research are realized in a wide variety of products in biology and advanced materials. Polymer products exist in several forms: as a liquid or semi-solid it is found in mixtures, solutions, micelles, melts, and gels. Polymers also form glass-like and crystalline solid materials. The rich phenomena of polymers are worthy of theoretical studies, which may yield further understanding of their properties, and better materials.

Early theoretical works[3-6] employed a lattice model to explain the thermodynamic and configurational properties of polymer solutions. In the lattice model a single polymer strand is represented by a chain of which a monomer, irrespective of its size and structure, occupies a single lattice site. A vacant site in the lattice may represent a void or a solvent molecule. An interaction energy between non-bonded nearest neighbor molecules may be included in the model. The calculation of the partition function, which is required to derive the equation of state and other thermodynamic quantities, is formidable since the number of variables involved are tremendous. The question is whether the equation

of state derived using this model can explain the results observed in the experiments and what modification is necessary to improve the predictions.

The advance of computer technology and the computational algorithms provide the opportunity to test the lattice model. Computer simulations have a number of advantages over experiments. For one thing, simulations provide a direct test of the lattice model, which is obviously not acessible experimentally. The parameters that describe the lattice structure, monomer-monomer effective interactions, and branching structure are easily incorporated in simulations. The disadvantages are due to physical limitations of computer memory and time, and the effectiveness to represent the real polymer systems. Taking the disadvantages aside, computer simulations might provide a guide to model-building. The purpose of this work, therefore, is to use computer simulations to explore the accuracy of three dimensional lattice model. More precisely, the equation of state of polymer chains on a three dimensional cubic lattice was studied extensively using Monte Carlo (MC) simulations. The MC results were compared with the predictions of the Flory[8-11] and Huggins[12-14] mean field approximations. The results were also used to test the accuracy of the Freed's recently-devised lattice model[15], in which the bond-correlation is taken into account.

Polymer solutions are generally polydisperse and solvent-quality dependent. The constituent monomers generally have different size and branch structure. The question was what influence the solvent quality and polydispersity implied on the equation of state, and whether it was modified by branch structure. Answering these questions was the main motivation of my work. This thesis, therefore, is the result of my attempt to understand the role of solvent quality, polydispersity, and branch structure in the equation of state. Since polymers are often located near an interface or a wall, the effect of a repulsive wall on the density profile is of considerable interest. This thesis presents my attempt to study the density profile in the proximity of a repulsive wall using scaling theory, renormalization group methods, and Monte Carlo simulations.

In this introduction, early theoretical models and the difficulties encountered in understanding polymer properties are reviewed. One of the early attempts to explain the conformational properties of polymers in dilute solutions was the random walk model[1,2,16,17]. Consider a random walk starting at the origin (O) and ending at F after N steps (see Figure 1.1). For simplicity we may assume that each step has the same length b. If the end-to-end displacement is $\vec{R}$ and the displacement at the i^{th} step is $\vec{r}_i$, the root-mean-square (rms) of the end-to-end distance is given by

$$R = \langle \vec{R}^2 \rangle^{1/2}$$

$$= \left[\sum_{i=1}^{N} \langle \vec{r}_i . \vec{r}_i \rangle + \sum_{i \neq j=1}^{N} \langle \vec{r}_i . \vec{r}_j \rangle \right]^{1/2} = N^{1/2} b \qquad (1.1)$$

where <...> is the average over all configurations. Note that the cross term vanishes because the steps are uncorrelated. In passing to polymer solutions, the path in the random walk model is interpreted as the physical configuration of a long flexible polymer chain. The step length corresponds to the length of the bond, the end-to-end distance is related to the distance between the two ends of the chain, indicating the size of the polymer molecule in the solution, and N corresponds to the number of monomers or chain-segments.

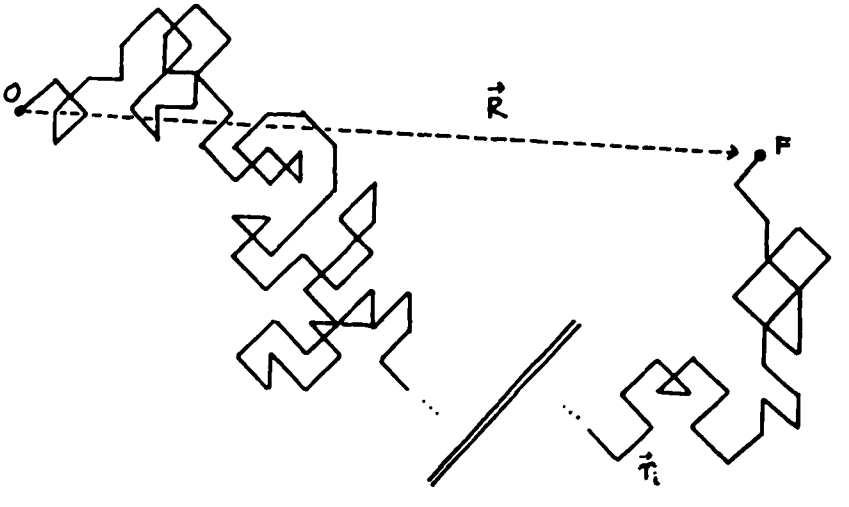

Figure 1.1. An example of a random-walk starting at O and ending at F.

Since in general N is very large, the random walk conformation may be approximated by a Gaussian model[17]. If $P(\vec{R})$ is the probability that a polymer chain has end-to-end displacement $\vec{R}$, then

$$P(\vec{R}) = \left(\frac{2\pi \langle R^2 \rangle}{d} \right)^{-d/2} \exp\left(- \frac{d R^2}{2 \langle R^2 \rangle} \right) \qquad (1.2)$$

The Gaussian model is unphysical since the expression $P(\vec{R})$ does not vanish when $R > R_{max} = Nb$. In addition the Gaussian model allows self-intersection. For real polymers, self-intersection is not permitted since two monomers may not occupy the same space. The Gaussian model is quite popular because of the quadratic nature of the exponent which renders the algebra simple.

The steric restriction that no two segments occupy the same location requires a modification of the random walk. The proper model of a polymer in a dilute solution is the self-avoiding walk (Figure 1.2). In this model, a walk is not allowed to revisit any region of the previous path. This introduces a degree of correlation among the steps. The average of the cross-term in equation (1.1) does not vanish; therefore, the simple relation $R^2 \sim N$ is no longer valid. To achieve self-avoidance, each new step has a tendency to move away from the previous path. This tendency has the effect of making the chain expand. The enlargement to dimensions larger than those expected from the simple random-walk model is known

as the excluded volume effect. Flory was the first to recognize this non-ideality, and to propose that the end-to-end distance is described by[2,18]

$$R = CN^{\nu} \qquad (1.3)$$

where C is a constant with dimensions of length, and ν is an exponent with value $1/2 \leq \nu \leq 1$. Fisher[19] proposed a relation between the value of ν and the space dimensionality d. His derivation was based on a mean field approximation, that a polymer chain might be described by a continuous cloud of monomer segments. The cloud is supposed to be uniformly distributed over a sphere of radius R, hence the segment density, ϕ, is proportional to N/R^d.

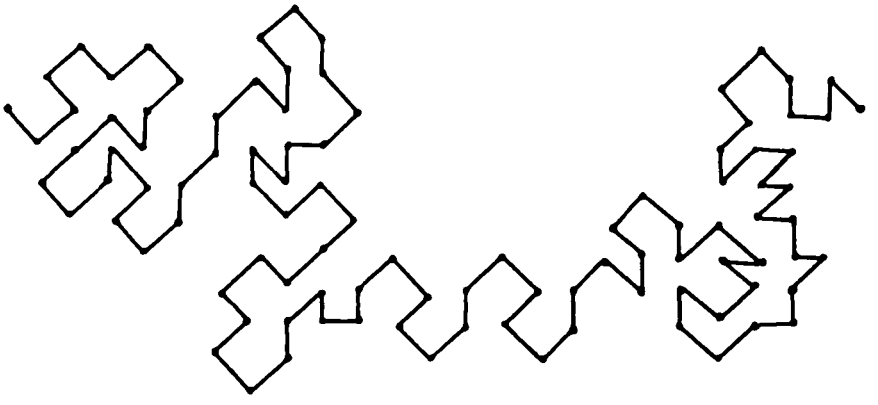

Figure 1.2. An example of a self-avoiding-walk.

The N monomers experience repulsive interactions with total energy given by

$$U = g\int d\vec{R}\,[\phi(\vec{R})]^2 = g\,\frac{N^2}{R^d} \qquad (1.4)$$

g is a measure of the interaction between a pair of monomers. The probability density P(R) is thus generalized to

$$P_F(R) \sim \exp\left[-\frac{dR^2}{2\langle R^2\rangle} - \frac{gN^2}{k_B T R^d}\right] \qquad (1.5)$$

The first and the second terms in the exponent are related to the entropic and energetic contribution to the free energy. If Z is the chain partition function, we can define the partition function of a chain with the end-to-end distance R, Z(R), by

$$Z = \int dR\, Z(R) = \int P_F(R)\, d^d\vec{R} \qquad (1.6)$$

Rewriting $d^d\vec{R}$ in spherical coordinates, we obtain

$$Z(R) = Const.\, R^{d-1} P_F(R) \qquad (1.7)$$

and the corresponding free energy is

$$F(R) = -k_B T \log Z(R) \qquad (1.8)$$

Flory's theory is the mean field estimate of the free energy. It is obtained by minimizing the free energy in equation (1.8) (or equaivalently by maximizing Z(R)). Differentiating Z(R) with respect to R, using the mean field value of $\langle R^2 \rangle = Nb^2$, and equating the result to zero one obtains

$$\frac{R^2}{Nb^2} = \frac{gN^2}{k_B T R^d} + \frac{d-1}{d} \qquad (1.9)$$

Using $R \sim N^{\nu}$ for $d < 4$, the left side and the first term on the right hand side will grow as $N \to \infty$, while the last term remains finite. Equating the exponent of N in this limit yields

$$\nu = \frac{3}{d+2} \qquad d = 1,2,3 \qquad (1.10)$$

For $d \geq 4$, the value $R \sim N^{1/2}$ satisfies equation (1.9) when N is large, and the random walk result is obtained. Although Flory's results provide better agreement with the values of the experimental and simulation results (in d=3: $\nu_{exp}=0.586$[1,20] and $\nu_{sim}=0.579\text{-}0.592$[21-26], in d=2: $\nu_{sim}=0.749$[21,27,28], $\nu_{exact}=3/4$[29], and $\nu_{exp}=0.79(1)$[30]), it is obvious that the mean field

approximation takes into account the monomer-monomer interactions in the crudest fashion, since correlations between chain segments are neglected. The discrepancy between the mean field approximation and the experimental results emerges when one considers the equation of state of a dilute polymer solution. If the number of chains is n_p, and the the solution is so dilute such that the chains never interact one with another, we can generalize the probability density in equation (1.5)

$$P\{R_i\} = \prod_{i=1}^{n_p} C \exp\left[- \frac{dR_i^2}{2\langle R_i^2 \rangle} - \frac{gN^2}{k_B T R_i^d} \right] \qquad (1.11)$$

where we assume that the system is monodisperse. If we also assume that the effective interaction g is very small, the exponential in (1.11) can be Taylor-expanded. To find the partition function, $P\{R_i\}$ is integrated with respect to coordinates of the chain-ends, and assuming there is no integration constraint due to other chains one may obtain

$$Z = V^{n_p}\left(1 - \frac{g}{k_B T} \frac{N^2}{V} \right) \qquad (1.12)$$

where V is the total volume of the system. The pressure can be derived easily using thermodynamic relation

$$P = -\frac{\partial F}{\partial V} = k_B T \frac{\partial \log Z}{\partial V} \qquad (1.13)$$

and the result is given by

$$\frac{P}{k_B T} = \frac{\phi}{M} + \frac{g}{k_B T}\phi^2 \qquad (1.14)$$

ϕ is the mass density in the system and M is the molecular weight which is related to the number of monomers per chain. When the solution is semidilute, the mean field approximation with pair-wise effective interactions between monomers also predicts a quadratic dependence of the pressure on segment density. The experimental results[31,32] showed that $P \sim \phi^{9/4}$. This discrepancy might be caused by correlation between monomers. The need to refine the prediction requires that we devise a better theory. This has led to the application of more sophisticated mathematical tools such as functional integration, scaling concepts, and renormalization group techniques.

Path integration and its functional extensions were pioneered by Feynman in the 1940's[33,34]. It has found application in almost every field of physics[35]. It was introduced in polymer physics by Edwards[36,37] and Saito et.

al.[38]. It was not until Freed[39] that functional integration was widely used to describe the conformational properties of polymer solutions. Basically the work of Freed was a generalization of the random walk model. The probability density is the generalization of equation (1.11) in which he used a generic potential instead of the mean-field potential.

Scaling theory was introduced by Kadanoff[40,41] and the primary application was in critical phenomena[42-45]. It was de Gennes who observed that a polymer solution may be described by the n-vector model in the limit $n \to 0$[46-49]. Scaling theories focus on the long wavelength properties of polymers, as a function of the chain length N and other parameters. The theories then invoke the assumption that when $N \to \infty$ all microscopic parameters are irrelevant and/or enter into equations indirectly through chain dimensions or other macroscopic quantities. Consequently, many models with different microscopic parameters yield the same long wavelength behavior. When applied to concentration-dependent quantities, scaling theories invoke two conditions. In the lower density regime polymer chains are isolated and their behavior can be approximated by that of a single chain. At high concentrations, polymer chains interpenetrate and a monomer cannot distinguish whether its neighbor belongs to the same chain or another. Scaling theories assert that in this regime, static properties should be independent of chain length. As in critical phenomena, a physical quantity (such as

the osmotic pressure) follows a power law in the $N\to\infty$ limit. There are differences, however, between the critical phenomena of the n-vector model and polymer solutions. For example, the reduced temperature in critical phenomena ($\varepsilon=(T-T_c)/T_c$) is associated with the inverse of chain length in polymer solutions (N^{-1}). In reality we cannot devise a polymer chain with infinite length, in contrast to critical phenomena, in which we can approach very closely the critical temperature T_c.

We are interested in more than just the limiting $N\to\infty$ behavior, e.g., in details of how this behavior is approached, since real polymers have finite N. The renormalization group method is one such technique developed to analyze the thermodynamic and conformational properties of polymers. The idea of renormalization group was not new[50-57], and it was primarily applied to critical phenomena[58-64]. Only recently was it applied to polymers[65-87]. The early renormalization group techniques were applied to polymers using the blob model, in which a polymer chain was coarse-grained and replaced by a sequence of blobs, and the polymer - n-vector model analogy[48,49,67]. The calculations were complicated and were not readily adaptable to more general problems. A simpler approach, the so called conformational renormalization group (CRG), was developed by Freed, Oono and coworkers using Edwards' δ-potential model[70-75], and extended to θ-solutions by allowing three-segment interactions[75-78]. The simplicity of

their approach is amenable to a more comprehensive treatment of polymers in semi-dilute solutions[79-82], polymers in confined geometries and near interfaces[83-89], and copolymers[90]. The potential is treated as a perturbation to the ideal chain, therefore, the exponential $e^{-\beta V}$ can be Taylor-expanded. The diagrammatic technique, dimensional regularization[91-93], and ϵ expansion[52,58-64] follow to remedy the pathological behavior of the resulting integrals. In essence, the renormalization group in polymers follows its counterpart in field theory to render singular quantities finite. CRG has found extensive application, and only the most difficult problems remain unsolved (for example: polymers in confined geometries, polymers near interfaces, polymers in two dimensions, etc.)

As useful the CRG is, the fact that it employs the δ-potential means that there is no limit on the density. In this widely used formulation, excluded volume is not properly taken into account, and so the CRG is not suitable for describing dense systems. These difficulties compelled Freed to return to original ideas of the original n-vector model of de Gennes. Note that in de Gennes' model (see Ref. 47 for further explanation), polymer solutions have a wide chain-length distribution. The uncontrollable chain length distribution exposes other deficiencies: its lack of utility for calculating quantities that depend on controlled dispersity, its inability to incorporate segment-segment interactions in non-athermal systems and its inability to take into account

possible differences of monomer/solvent-molecule structure. Recognizing this shortcoming, Freed and coworkers introduced a spin-model defined on a 2n-dimensional complex space and introduced an additional parameter to label the position of a segment along the chain[15,94-105]. The improved version was shown to be equivalent to the packing of polymers on a lattice[102]. The new device enables the calculation of the free energy of mixing, and the equation of state via the Meyer cluster expansion. For instance, Freed and coworkers were able to calculate the free energy of mixing for models with nearest neighbor interactions and various branching-structures[98,99]. In the traditional 'Flory' form[2], it is written as

$$\Delta F_{Mix} = \frac{\Phi}{M}\log\Phi + (1-\Phi)\log(1-\Phi) + \chi\Phi(1-\Phi) \qquad (1.15)$$

The so called χ parameter represents the effective interaction between two segments. In athermal solutions, $\chi = 0$. In Flory theory, the interaction parameter χ is energetic in origin and proportional to $1/T$[2,47]. The experimental results indicate otherwise, that χ has entropic contibutions and also depends on segment concentrations and higher powers of $1/T$[106-108]. The formulation of polymer solutions using the lattice model allows comparison with computer simulations. A major purpose of the research described in this dissertation is to test the accuracy of Freed's lattice model using Monte Carlo simulations.

Computer studies of polymers have been conducted using exact enumeration[109-112] and Monte Carlo simulations. The latter technique employed various algorithms, e.g.: random growth[113-116], reptation[117,118], crank-shaft and internal moves[119-127], the pivot algorithm[21,128-131], and others[132-135]. To obtain the equation of state, the test-chain insertion technique[136-143] was employed. The latter is however inefficient for dense-systems of long chains. A new Monte Carlo method was devised by Dickman to overcome this difficulty[22]. It was then possible for the first time to determine the osmotic pressure of a model polymer system over wide range of densities and chain lengths. The simulation results in two and three dimensions of athermal chains are in good agreement with the Bawendi and Freed's prediction[22,144]. The advent of a new simulation technique opens an opportunity to learn the equation of state of polydisperse systems[145], of polymer solutions with different solvent qualities, and of polymers with branch-structure.

This work is organized as follows. Chapter II reviews the conformational properties and the equation of state of polymers in semidilute solutions. The analysis uses scaling theory. The effect of confinement (e.g., polymers within a narrow channel) is also presented. It is followed in Chapter III with the analysis of the segment density in the presence of a repulsive wall and confining geometries (slabs). The scaling technique and the renormalization group method are

used in the calculations. Chapter IV follows strictly the works of Freed and coworkers that are scattered in several articles over an extended period (1985 - to present). Our contribution is to organize the presentation in a more coherent form, to point out several small corrections, and to calculate the osmotic pressure for chains with a uniform chain-length distribution. We also provide a derivation of Flory-Huggins prediction in this chapter. In Chapter V the predictions, in particular the equations of state derived in Chapter IV, are compared with simulation results for both monodisperse and polydisperse systems. The accuracy of the scaling prediction is also assessed. In this part we also present the results of simulations of chains with different branching structures and different monomer sizes. The conformational properties (end-to-end distance and radius gyration) and segment density as a function of distance from the wall are presented for the previously mentioned polymer models. The results are summarized in Chapter VI. In this final chapter, we also point out the problems that are left behind. Therefore, they indicate the direction for future work.

II. SCALING THEORIES OF POLYMER SOLUTIONS.

Methods for studying polymer solutions have evolved for several decades from the classical approach pioneered by Flory[8-14] to more sophisticated methods such as conformational space renormalization group[69-90] (CRG) and Freed's lattice model[15,94-105]. In the classical approach, the behavior of polymers in solution, and the equation of state were studied in mean field approximation. Flory and Huggins used a lattice model as a representation of polymers in a solution[8-14]. Assuming equal sizes for chain-segments and solvent molecules, (which is generally untrue in real systems), they obtained the probability distribution for chain configurations, and the corresponding equation of state. Using the mean field approximation, as indicated in the introduction, one can obtain the end-to-end distance which shows fractional power law dependence on chain length N : $\langle \vec{R}^2 \rangle \sim N^{2\nu}$ with $\nu = 3/(d+2)$. The fractional power-law signals the presence of correlations between chain-segments which, in turn, reflects the presence of segment-segment interactions. The excluded volume interactions are responsible for the swelling of the chain to dimensions larger than the simple random walk, $\langle \vec{R}^2 \rangle \sim N$. Scaling theories, though, provide the surprising result that excluded volume interactions in multi-chain systems enhance the role of chain segments. Instead of the quadratic dependence on segment density, the osmotic pressure in a semi-dilute solution is

proportional to $\phi^{9/4}$ [69,146]. It seems that the interaction between chains is propagated so that not only the segments in contact contribute to the pressure, but that other segments along the same chain participate as well, although indirectly. Scaling theories were initially introduced in critical phenomena[40-45] and applied to polymer problems by de Gennes and others[46,47]. Originally, de Gennes observed the analogy between polymers and the n-vector model in the $n \to 0$ limit[47]. In this model, he mapped the chain length N to the inverse of the reduced temperature, ϵ^{-1}, in critical phenomena ($\epsilon = (T-T_c)/T_c$). Also the correlation length in critical phenomena is related to the dimensions of a single chain. Recently, Freed, Ohta, Oono and others applied the conformational renormalization group (CRG) method to polymer solutions[69-74]. Here the chains are modeled using Edwards' δ-function repulsive interaction[36,37]. CRG offers the advantage of a controlled chain length distribution.

Before investigating the more intricate renormalization group approach, let us probe in more detail scaling theory as applied to polymer solutions. If N is the chain length and v is the excluded volume parameter, one can obtain the functional dependence of the end-to-end distance R on these parameters.

Let $\{C_i\}$ and $\{D_i\}$ denote the observable macroscopic properties and microscopic parameters respectively. For example, $\{C_i\}$ might be the density, the average size of a polymer strand, and $\{D_i\}$ might be the excluded volume

parameter, the bond length, etc. All microscopic parameters play their role indirectly via the scaled macroscopic quantities[69]. This assumption is the starting point for scaling theories. Another hypothesis invokes the asymptotic power law dependence of a quantity P (for example: the osmotic pressure or the end-to-end distance at fixed concentration) on the asymptotic values $\{C_i\}$. For instance, $P \propto C_1^{q} C_2^{r} f(\{C'_i\})$ where the prime means the first and the second variables are omitted. C_1 and C_2 might represent respectively the chain dimension (proportional to N) and solution concentration. Since the microscopic parameters play an indirect role, models with different interactions may have the same properties. It is as if the effects of the microscopic parameters are washed out, and reemerge in the form of effective interactions hidden in $\{C_i\}$. This is the basis for universality. For instance, it is argued that in three dimensions (d=3), many-body interactions reduce to a simple effective two-body interaction of Edwards' type[69,146]. The δ-potential in turn will affect the osmotic pressure and the end-to-end distance in a multi-chain system indirectly through overlap concentration or $\langle R^2 \rangle$ of a single chain.

Despite their deficiencies, scaling theories are easier to work with and may provide guidance for more detailed calculations. They also provide a qualitative overview of complicated polymer phenomena. The scaling exponents are ready at hand to compare with experimental and simulation results.

If the comparison produces significant discrepancies, it is easier to reconsider the theories or to modify the assumptions implicit in the simulation models. Because of its power and simplicity, we want to explore the scaling theory in this chapter. Most of the results presented in this chapter have been derived by Freed and coworkers[69,146]. However, we also want to clarify the concept of Kuhn length that is often cited in the literature and defined differently by different authors[1,2,69,147,148]. In our simulation results (Chapter V), we use scaling techniques extensively to investigate the equation of state of lattice polymers. We also derived the properties of polymers confined between two walls in the semi-dilute regime.

First of all, in section 2.1 we define the polymer model and the effective bond length. The effective length is different from the so-called Kuhn step length[2,147-149], even though some authors neglect the distinction[69]. In Appendix A we review the original definition of Kuhn length. Its relation to the persistence length[47] is shown in the context of a rigid chain. In section 2.2, we explore the properties of a single chain in solution. The functional dependence of chain dimensions on the excluded volume parameter is derived and the significance of the marginal dimension d=4 is obtained in the $N\to\infty$ limit. This result is used to describe the corresponding behavior at fixed concentration (section 2.3). The scaling theories are also utilized to describe the osmotic pressure at fixed concentration. Analogous to critical phenomena, we

consider the high/low limit of concentration and $N \to \infty$ to obtain the famous result $\pi \sim \phi^{9/4}$.

The presence of confining walls necessitates a modification of the functional form of $\langle R^2 \rangle$ and the osmotic pressure (section 2.4). The models are used as a preliminary to more difficult problems where chain segments interact with the wall. In Chapter III, the density profile near a wall is investigated using scaling techniques and renormalization group methods. The results will be compared to the results of Monte Carlo simulations in Chapter V. This comparison should provide a preliminary indication of scaling relations and critical exponents. The results of wall-segment interactions open new problems such as polymers in a confining tube, polymers in porous media, and polymers at interfaces. This new horizon is of its own interest theoretically and has many applications in technology.

2.1. Polymer Model: The Perturbed Gaussian Chain.

Let us assume that a polymer chain has (N_o+1) monomers or N_o bonds. Denote the set of monomer positions by $\{\vec{r}_i;\ i=0,\ 1,\ 2,\ \ldots,\ N_o\}$. Let $W(\{\vec{r}_i\})$ describe the effective potential energy between monomers in which the effect of the solvent molecules has been taken into account[69]. The distribution function $G(\{\vec{r}_i\})$ can be written as

$$G(\{\vec{r}_i\}) \prod_{i=0}^{N_0} d\vec{r}_i = C \prod_{i=0}^{N_0} d\vec{r}_i \exp\left[-\beta W(\{\vec{r}_i\})\right] \qquad (2.1)$$

where C is a normalization constant and $\beta = 1/(k_B T)$. The potential $W(\{\vec{r}_i\})$ has contributions from the interactions between adjacent monomers along the chain and the interaction between monomers seperated far from each other along the chain but located near each other in the solution. In the literature, the former is called the short-range interaction and the latter is called the long-range interaction. Assume that these types of interactions can be decomposed as

$$W(\{\vec{r}_i\}) = \sum_{i=1}^{N_0} u_i(\vec{r}_i, \vec{r}_{i-1}) + V(\{\vec{r}_i\}) \qquad (2.2)$$

where $u_i(\vec{r}_i, \vec{r}_{i-1})$ corresponds to the short range interaction and $V(\{\vec{r}_i\})$ represents the rest of the interactions. In the pure Gaussian model, where $V(\{\vec{r}_i\})$ vanishes, the short-range potential $u_i(\vec{r}_i, \vec{r}_{i-1})$ has a form which resembles a 'spring-like' potential. The purpose of introducing the Gaussian model is to simplify the mathematics. In the Gaussian model, the short-range interaction is

$$u_i(\vec{r}_i, \vec{r}_{i-1}) = \frac{d}{2} \frac{(\vec{r}_i - \vec{r}_{i-1})^2}{\langle (\vec{r}_i - \vec{r}_{i-1})^2 \rangle} k_B T \qquad (2.3)$$

where $k_B T$ is included for the proper dimensionality of u_i. The potential $V(\{\vec{r}_i\})$ is in general of many-body type. A further simplifying assumption is that the dominant part is given by two-body interactions and that the higher-order interactions can be neglected. If the pair-wise additive potential between monomers i and j, at positions $\vec{r}_i$ and $\vec{r}_j$, is given by $V_{ij}(|\vec{r}_i - \vec{r}_j|)$, then the total potential energy is

$$V(\{\vec{r}_i\}) = \frac{1}{2} \sum_{i,j=0}^{N_0} V_{ij}(|\vec{r}_i - \vec{r}_j|) \qquad (2.4)$$

Hence, the chain distribution function is

$$G(\{\vec{r}_i\}) = C \exp\left[- \sum_{i=1}^{N_0} \frac{d(\vec{r}_i - \vec{r}_{i-1})^2}{2\langle \vec{r}_i - \vec{r}_{i-1} \rangle^2} - \frac{\beta}{2} \sum_{i,j=1}^{N_0} V_{ij}(|\vec{r}_i - \vec{r}_j|) \right] \qquad (2.5)$$

In the long wavelength limit the detailed structure of a polymer strand can be neglected. The monomers may be regarded as if they form a continuous chain. So instead of using the summation over individual chain segments, we construct a hypothetical chain consisting of N spheres, each having an

average size ΔR (figure 2.1).

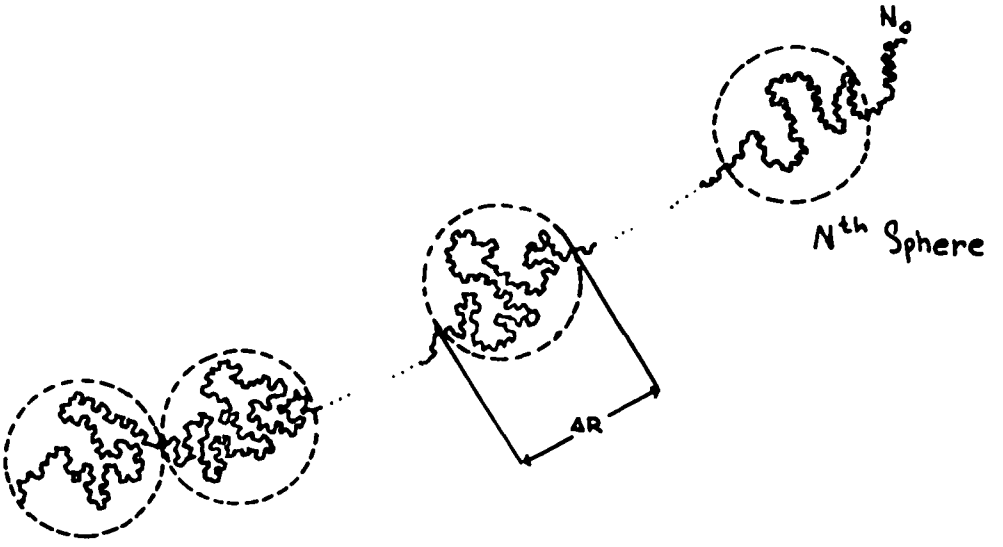

Figure 2.1. A schematic construction of a continuous chain. The discrete chain portion inside a sphere is replaced by a Gaussian segment with the mean-square distance $l\Delta R_{max}$. l is the so-called effective-chain length. ΔR_{max} is the maximum elongation of the original chain portion.

In analogy with the derivation of Kuhn-step-length (see Appendix A), we assume that the chain portion inside the sphere can be replaced by a single Gaussian chain segment of length l such that

$$l = \frac{\langle (\Delta R)^2 \rangle}{\Delta R_{max}} \qquad (2.6)$$

$$\Delta s = \Delta R_{max}$$

ℓ is called the effective length, Δs is the contour length in the equivalent gaussian chain, ΔR_{max} and $<(\Delta R)^2>$ are respectively the maximum extension and the mean square of the end-to-end distance for the chain portion inside the sphere. Using eqs. (2.6), the first term in the exponent in equation (2.5) becomes

$$\frac{d}{2}\sum_{i=1}^{N_0}\frac{(\vec{r}_i-\vec{r}_{i-1})^2}{<(\vec{r}_i-\vec{r}_{i-1})^2>}=\frac{d}{2}\sum_{a=1}^{N}\frac{(\vec{r}_a-\vec{r}_{a-1})^2}{l\,\Delta s}\rightarrow\frac{d}{2l}\int_0^L\left(\frac{dr(s)}{ds}\right)^2 ds \tag{2.7}$$

In the last relation the continuum limit was taken: $N\rightarrow\infty$, $\Delta s\rightarrow 0$ such that $N\Delta s = L$, where L is the contour length of the whole chain. In the continuum limit, eqn. (2.5) can be written as

$$G(\{\vec{r}(s)\})=C\exp\left[-\frac{d}{2l}\int_0^L\left(\frac{d\vec{r}(s)}{ds}\right)^2 ds-\frac{\beta}{2l^2}\int_0^L ds\int_0^L ds'\,V(|\vec{r}(s)-\vec{r}(s')|)\right] \tag{2.8}$$

Note that Freed[69] called l in eqn. (2.8) the Kuhn effective length. Freed's definition is not accurate, since the Kuhn effective length is defined over the whole chain (Appendix A). Following Kuhn's definition, we can also say that the

effective length in eqn. (2.6) is defined by 'averaging' the short range interactions inside the spheres (and replacing them by the gaussian equivalent bond-length), but the long-range interaction is still present and must be taken into account.

2.2. Scaling Theory of A Single Chain.

In this section the scaling theory of a single chain in unconfined space is reviewed; it represents polymers in a dilute solution. The properties of the end-to-end distance are analyzed and will be used to investigate the properties of polymers in a semi-dilute solution (section 2.3).

Consider a polymer chain with distribution given in equation (2.8). The partition function is

$$Z(L) = C^{-1}\int d\{\vec{r}(s)\}\,\exp\{-\int_0^L \frac{d}{2l}\,(\dot{r}(s))^2 ds - \frac{\beta}{2l^2}\int_0^L ds \int_0^L ds_0 V(\vec{r}(s)-\vec{r}(s_0))\} \tag{2.9}$$

The path integral notation $d\{\vec{r}(s)\}$ can be interpreted as shorthand for the product: $\lim_{\substack{N\to\infty \\ \Delta s\to 0}} \prod_{i=1}^{N} d\{\vec{r}_i\}$. If the normalization constant C is chosen such that Z(L) is unity in the absence of interactions (V ≡ 0), then

$$C = \int d\{\vec{r}(s)\} \exp\{-\int_0^L \frac{d}{2l} [\frac{d\vec{r}(s)}{ds}]^2 ds\} \qquad (2.10)$$

The end-to-end distribution in the continuous-chain limit is

$$\begin{aligned} P(\vec{R},L) &= Z^{-1}\int d\{\vec{r}(s)\}\, G\{\vec{r}(s)\}\, \delta(\vec{r}(L)-\vec{r}(0)-\vec{R}) \\ &= Z^{-1} \int_{\vec{r}(0)=0}^{\vec{r}(L)=\vec{R}} d\{\vec{r}(s)\} \exp\{-\int_0^L \frac{d}{2l} (\dot{r}(s))^2 ds \\ &\quad - \frac{\beta}{2l^2}\int_0^L ds \int_0^L ds_0 V(\vec{r}(s)-\vec{r}(s_0))\} \end{aligned} \qquad (2.11)$$

Without lost of generality we assume that $\vec{r}_0 = 0$.

If we restrict ourselves to Edwards' model, the segment-segment interaction $\beta V_{ij}(\vec{r}_i-\vec{r}_j)$ reduces to $v\delta(\vec{r}(s)-\vec{r}(s'))$[36,37]. This means that two segments interact directly only when their positions coincide.

Instead of following the more intuitive de Gennes' approach, here we follow the 'formal' route of Freed[69]. To obtain scaling relations, let use introduce the change of variables

$$\begin{aligned} \vec{r}'(s') &= a_0\vec{r}(s) \\ s' &= b_0 s \qquad \text{with } a_0, b_0 > 0 \end{aligned} \qquad (2.12)$$

the partition function with the Edwards' potential in the new variables will look like

$$Z(L) = C\int d\{\vec{r}'(s')\}\exp\{-\frac{b_0 d}{2a_0^2 l}\int_0^{b_0 L}\left(\frac{d\vec{r}'(s')}{ds'}\right)^2 ds' - \left(\frac{a_0^d \upsilon}{2b_0^2 l^2}\right)\int_0^{b_0 L} ds' \int_0^{b_0 L} ds_0' \,\delta(\vec{r}'(s') - \vec{r}'(s_0'))\} \tag{2.13}$$

Note that in deriving (2.13) the coefficient in the measure $d\{\vec{r}'(s')\}$ is absorbed into the normalization constant C. Also we used the property of the δ-function

$$\delta(\vec{r}(s)) = \delta(a_0^{-1}\vec{r}'(s')) = a_0^d\,\delta(\vec{r}'(s')) \tag{2.14}$$

in the second exponent. Equation (2.13) resembles the partition function of a chain with chain length $L' = b_0 L$, effective length $l' = a_0^2 l/b_0$ and excluded volume parameter $\upsilon' = (a_0^{d+4}/b_0^4)\upsilon$. If we pick $a_0 = (b_0/l)^{1/2}$, which is equivalent to rescaling the chain length such that the effective length is equal to unity, the partition function will become

$$Z(L) = Z(b_0 L, b_0^{\frac{d-4}{2}} \upsilon l^{-\frac{4+d}{2}}) \qquad (2.15)$$

and similarly the end-to-end distribution $G(\vec{R},L)$ becomes

$$G(\vec{R},L,\upsilon) = \left(\frac{b_0}{l}\right)^{\frac{d}{2}} G\left[\left(\frac{b_0}{l}\right)^{\frac{1}{2}}\vec{R}, b_0 L, b_0^{\frac{d-4}{2}} \upsilon l^{-\frac{d+4}{2}}\right] \qquad (2.16)$$

Finally we can always choose $b_0 L = bL/l \equiv bN$ to reduce (2.15) and (2.16) to

$$Z(L) = Z(bN, b^{\frac{d-4}{2}} \upsilon l^{-d}) \qquad (2.17)$$

$$G(\vec{R},L,\upsilon) = (bl^{-2})^{\frac{d}{2}} G(b^{\frac{1}{2}}\vec{R}l^{-1}, bN, b^{\frac{d-4}{2}} \upsilon l^{-d}) \qquad (2.18)$$

Note that if we pick $b=N^{-1}$, the interactions become irrelevant for $d>4$, in the long-chain ($N\to\infty$) limit. A physical quantity such as the mean square end-to-end distance follows straightforwardly from the definition

$$\langle R^2 \rangle = \frac{\int d\vec{R}\, \vec{R}^2 G(\vec{R},L,\upsilon)}{\int d\vec{R}\, G(\vec{R},L,\upsilon)} \qquad (2.19)$$

which becomes, after scaling and changing the integration variables from $\vec{R}$ to $\vec{R}(bl^{-2})^{1/2} = \vec{R}'$,

$$\langle R^2 \rangle = \frac{(b^{-1}l^2)\int d\vec{R}'\,\vec{R}'^2\, G(\vec{R}', bN, b^{\frac{d-4}{2}} v l^{-d})}{\int d\vec{R}'\, G(\vec{R}', bN, b^{\frac{d-4}{2}} v l^{-d})} = b^{-1}l^2 g_R(bN, b^{\frac{d-4}{2}} v l^{-d}) \tag{2.20}$$

where g_R is a so-called scaling function. Scaling theories do not furnish g_R or related scaling functions, but physical considerations imply certain asymptotic behaviors. The renormalization group method provides justification of the scaling limit, and can be used to derive the scaling functions.

Before proceeding, we have to introduce the scaling hypothesis regarding the functional dependence of physical quantities. Suppose the quantity of interest is P. P is a function of various macroscopic parameters (like temperature, end-to-end distance, concentration etc.) and microscopic parameters (like the effective length and monomer-monomer interactions). Let the set of macroscopic parameters be represented by $\{C_i\}$ and the microscopic parameters by $\{D_i\}$. Assume also that the dependence on these parameters can be written as

$$P = P(\{C_i\}, \{D_i\}) \tag{2.21}$$

then the general scaling hypothesis asserts that P can be reexpressed as a product of one or more of the macroscopic variables, raised to various powers, with some function of scaled dimensionless macroscopic variables. The microscopic parameters appear only indirectly, through the macroscopic variables. In this case, P becomes

$$P = \prod_{i=1}^{q} C_i^{m_i} P_1(\{\tilde{C}_i\}) \tag{2.22}$$

where the exponents m_i are dictated by the dimensionality of P and $\{\tilde{C}\}$ is the set of scaled dimensionless macroscopic variables.

The second hypothesis is related to the asymptotic behavior of the scaling function. We usually know the limiting behavior of P when one of the macroscopic variables C_1 (for example: density) approaches zero. Assuming that P may be expressed as a Taylor series in this limit, we have

$$\begin{aligned} P = P(C_1, \{C_i'\}, \{D_i\}) &= P(0, \{C_i'\}, \{D_i\}) \\ &+ C_1 P_1(\{C_i'\}, \{D_i\}) + C_1^2 P_2(\{C_i'\}, \{D_i\}) + \ldots \end{aligned} \tag{2.23}$$

where $\{C_i'\}$ denotes the set $\{C_2, C_3, \ldots C_p\}$. The first term in the right hand side is matched with the known value of P, given the values of $\{C_i'\}$. According to the first hypothesis, all dependence of P on microscopic parameters arises indirectly via $\{C_i\}$.

The second scaling hypothesis further asserts that in the other limit, $(C_1 \to \infty)$, P is governed by a power law. This is analogous to the situation in critical phenomena[44,45].

$$P \to (constant) \times C_i^{y}, \quad \text{where } C_i \to \infty \text{ and } \{C'\} \text{ are given} \tag{2.24}$$

The second scaling hypothesis, therefore, is constructed to recover the known value of the physical quantity in both limits and the obtained exponent is used to study other physical quantities. The drawback of the scaling theories is that first, it is a hypothesis introduced on an ad-hoc basis to produce the known results, not a rigorous first-principle calculation. Second, the functional dependence is not known. And finally, in reality the macroscopic parameters, like the chain length and concentration, are often not in the asymptotic scaling limits. (As is discussed in Freed's book[69], the renormalization group remedies some of the shortcomings of scaling theory.)

Returning to our example, equation (2.20), if we further choose $b=N^{-1}$, the mean square end-to-end distance becomes

$$\begin{aligned} \langle R^2 \rangle &= l^2 N g_R(1, N^{\frac{4-d}{2}} \upsilon l^{-d}) \\ &= l^2 N f_R(N^{\frac{4-d}{2}} \upsilon l^{-d}) \end{aligned} \tag{2.25}$$

Invoking the second scaling hypothesis, we see that for $d > 4$ and $N \to \infty$ the argument of f_R vanishes. From the mean field result derived previously, we have $f_R(x)|_{x\to 0} \to 1$ and

$$\langle R^2 \rangle = l^2 N \qquad \text{for } d>4 \text{ and } N \to \infty \tag{2.26}$$

For $d < 4$, the behavior of $\langle R^2 \rangle$ depends on the parameters υ and N. For a short chain and small enough excluded volume parameter, the product $N^{(4-d)/2}\upsilon l^{-d} << 1$, then

$$\langle R^2 \rangle = l^2 N [\, 1 + O(N^{\frac{4-d}{2}} \upsilon l^{-d}) \,] \tag{2.27}$$

while for large N and/or large excluded volume, the scaling hypothesis requires $f_R(x)$ to take a power law form, $f_R(x) \sim x^y$. In this limit the left hand side will assume the power law given by Flory. Therefore,

$$\langle R^2 \rangle = l^2 N^{2\nu}$$

$$= l^2 N [(N^{\frac{4-d}{2}} \upsilon l^{-d})^{y} + O (N^{\frac{4-d}{2}} \upsilon l^{-d})^{x_1}]$$

$$with\ x_1 < y \qquad (2.28)$$

which gives the following value of y

$$y = \frac{2(2\nu - 1)}{4 - d} \qquad (2.29)$$

In three dimensions, with ν=3/5, this implies y=2/5, and gives $\langle R^2 \rangle \propto l^2 N^{6/5} \upsilon^{2/5} l^{-6/5}$. We can summarize the result; the mean square end-to-end distance of a single chain in d<4 dimensions has the following functional form with its corresponding limits

$$\langle R^2 \rangle = l^2 N f_R (N^{\frac{4-d}{2}} \upsilon l^{-d}) \qquad (2.30a)$$

$$and\ f_R(x) = \begin{cases} \to 1\ as\ x \to 0 \\ \\ \to x^{\frac{2(2\nu-1)}{4-d}}\ as\ x \to \infty \end{cases} \qquad (2.30b)$$

The interesting questions which arise are: What happens to the exponent value and its functional form when we take into consideration a generic potential? Will the many-body

interactions modify these values and the functional dependence? It turns out, as shown by Freed[69], that the Fourier transform of $V_{ij}(\vec{r}_i-\vec{r}_j)$, when expanded in the long wavelength limit, gives coefficients which scale as $N^{(4-d-2m)/2}$, where m corresponds to the degree of the expansion. When m=0, it corresponds to the result of Edwards' δ-potential. In three dimensions, when $N\to\infty$, only the first term need be retained, thereby explaining that the complicated generic potential $V_{ij}(\vec{r}_i-\vec{r}_j)$ is reduced to a simple δ-potential model. The case of d=2 needs careful analysis since all higher-body interactions participate in the approximation. For instance when a many-body interaction involving g segments, $V_{1,2,3,\ldots g}(\vec{r}_1,\vec{r}_2,\ldots\vec{r}_g)$, is taken into account, the long wave-length expansion of its Fourier transform will produce coefficients which scale like $N^{g-(g-1)d/2}$. As $N\to\infty$ (in 3d) this form is small compared to the first term obtained from the two body interaction, justifying the approximation in the Edwards' model. However for d=2, the first coefficients of all many-body interactions scale as N[69]. Retaining these leading parts poses a problem with an infinite number of parameters, which renders the scaling theories of little use. Our aim is to learn the scaling relations and exponents in three dimensions, and we therefore skip the difficult problems in two dimensions. Note that de Gennes' approach to scaling does not rest on the Edwards' δ-function model[47], and many scaling predictions (e.g. $\langle R^2\rangle$, osmotic pressure, etc.) have been verified in 2d[21,22,27-30].

2.3. Scaling Theories of Multi-Chain Solutions.

Scaling theories of many-chain systems are the next step, once single-chain properties have been understood. In this system, a new macroscopic variable ϕ describing segment or mass concentration comes into play, in addition to chain length and excluded volume potential discussed previously. The asymptotic behavior of a physical quantity as a function of concentration, in the low concentration regime, is generally adjusted to reproduce the known results for a single chain (a very dilute solution where chains are almost never in contact may be described by a single isolated chain configuration). On the other hand, in the high density limit, the multi-chain solution is assumed to represent dense/melt behavior where segments in contact with one another cannot distinguish whether their neighbors belong to the same chain or another one.

2.3.1. Scaling of The End-to-End Distance

Let us consider the partition function of n_p chains of length L and Kuhnian length l in volume V. The partition function in equation (2.9) is modified to

$$Z_{n_p} = \frac{V^{n_p}}{n_p!} C^{-1} \prod_{\alpha=1}^{n_p} \int_V d\{\vec{r}_\alpha(s)\}\, e^{+\mathcal{H}[\{\vec{r}_\alpha(s)\};n_p]} \qquad (2.31a)$$

where $\mathcal{H}[\{\vec{r}_\alpha(s)\};n_p]$ and C are, respectively,

$$\mathcal{H}[\{\vec{r}_\alpha(s)\};n_p] = -\frac{d}{2l}\sum_{\alpha=1}^{n_p}\int_0^L [\dot{r}_\alpha(s)]^2\, ds - \frac{v}{2l^2}\sum_{\alpha,\beta=1}^{n_p}\int_0^L ds \int_0^L ds'\, \delta[\vec{r}_\alpha(s) - \vec{r}_\beta(s')] \qquad (2.31b)$$

$$C = \left[\prod_{\alpha=1}^{n_p}\int_V d\{\vec{r}_\alpha(s)\} \exp\left[-\frac{d}{2l}\sum_{\alpha=1}^{n_p}\int_0^L [\dot{r}_\alpha(s)]^2 ds\right]\right]^{-1} \qquad (2.31c)$$

Note that the integration constant C is chosen such that when the interaction is switched-off the partition function will reduce to $V^{n_p}/n_p!$ corresponding to n_p independent chains in volume V. Introducing the change of variables as prescribed in equation (2.9) with the specific values $a_o = (b_o/l)^{1/2}$ and $b_oL = bL/l = bN$, the partition function is

$$Z_{n_p} = (b^{-1}l^2)^{\frac{n_p d}{2}} Z_{n_p}(Nb, b^{\frac{d-4}{2}} v l^{-d}, b^{\frac{d}{2}} l^{-d} V) \qquad (2.32)$$

the extra argument in Z_{n_p} indicates the the volume dependence. To study the effect of concentration on polymer dimensions and the equation of state, consider the end-to-end distance distribution function of chain i in the presence of (n_p-1) other chains. It is given by

$$G_{n_p}^{(i)}(\vec{R}, L; \upsilon, n_p, V) =$$

$$\frac{V^{n_p}}{n_p!} C^{-1} \prod_{\alpha=1}^{n_p} \int_V d\{\vec{r}_\alpha(s)\}\, \delta(\vec{r}_i(L) - \vec{r}_i(0) - \vec{R})\, e^{\mathcal{H}[\{\vec{r}_\alpha(s)\}; n_p]} \tag{2.33}$$

If we rescale the system as prescribed above (see equations (2.11)-(2.14)), the scaling relation between the original and the scaled distribution function is

$$G_{n_p}^{(i)}(R, l; \upsilon, n_p, V) = (b^{\frac{1}{2}} l^{-1})^{(-n_p+1)d} \times G_{n_p}^{(i)}(b^{\frac{1}{2}} l^{-1} R, bN; \upsilon b^{\frac{d-4}{2}} l^{-d}, V(bl^{-2})^{\frac{d}{2}}, n_p) \tag{2.34}$$

The mean square of the end-to-end distance at fixed concentration, $\langle R^2 \rangle_c$, then can be obtained as

$$\langle R^2\rangle_c = \frac{1}{n_p}\sum_{i=1}^{n_p}\frac{\int dR_i\,(R^{(i)})^2\,G_{n_p}^{(i)}(R,L;\upsilon,n_p,V)}{\int dR_i\,G_{n_p}^{(i)}(R,L;\upsilon,n_p,V)} = \frac{l^2}{b}\,\tilde{g}_R(bN,\upsilon b^{\frac{d-4}{2}}l^{-d},V(bl^{-2})^{\frac{d}{2}},n_p) \tag{2.35}$$

where the factor n_p is absorbed into $\tilde{g}_R$. One can pick b = 1/N and equation (3.35) is transformed to

$$\langle R^2\rangle_c = Nl^2\tilde{f}_R(\upsilon l^{-d}N^{\frac{4-d}{2}},V(Nl^2)^{-\frac{d}{2}},n_p) \tag{2.36}$$

In the limit of large volume, $V\to\infty$, the functional dependence of $\langle R^2\rangle_c$ on V and n_p is assumed to appear through their ratio (chain concentration). Therefore, equation (2.36) becomes

$$\langle R^2\rangle_c = Nl^2\tilde{f}_R(\upsilon l^{-d}N^{\frac{4-d}{2}},\phi_c(Nl^2)^{\frac{d}{2}}) \tag{2.37}$$

where $\phi_c = n_p/V$ is the chain density. In the very dilute regime ($\phi \to 0$), the chains do not influence one another, so the end-to-end distance reduces to that for a single chain:

$$\tilde{f}_R(\upsilon l^{-d}N^{\frac{4-d}{2}},\phi_c N^{\frac{d}{2}}l^d)\big|_{\phi_c=0} = f_R(\upsilon l^{-d}N^{\frac{4-d}{2}}) \tag{2.38}$$

We can also learn the properties of $\tilde{f}_R$ as a function of excluded volume parameter. Assuming that the excluded volume interaction is negligible, the chains will assume ideal random walk configurations. To zeroth order in v, $\langle R^2 \rangle_c$ should be proportional to Nl^2, or for $vl^{-d}N^{(4-d)/2} << 1$

$$\langle R^2 \rangle_c = Nl^2 + \tilde{f}_R'(0, \phi_c N^{\frac{d}{2}} l^d)\, v l^{-d} N^{\frac{4-d}{2}} + \ldots \qquad (2.39)$$

equation (2.39) guarantees that at the θ-point, when $v = 0$, $\langle R^2 \rangle_c$ will reduce to the random walk result.

For large excluded volume interactions, corresponding to good solutions, $vl^{-d}N^{(4-d)/2} >> 1$, and zero concentration

$$\tilde{f}_R(v l^{-d} N^{\frac{4-d}{2}}, \phi_c N^{\frac{d}{2}} l^d) = (v l^{-d} N^{\frac{4-d}{2}})^{x_R} \qquad (2.40)$$

$$for \quad \phi_c \to 0, \quad v l^{-d} N^{\frac{4-d}{2}} > 1$$

Equations (2.28) and (2.29) provide the value of the exponent

$$x_R = \frac{2(2\nu - 1)}{4 - d} \qquad (2.41)$$

Using equation (2.30), which is equivalent to $\langle R^2 \rangle^{d/2} = N^{d/2} l^d f_1(vl^{-d}N^{(4-d)/2})$, we can introduce an ansatz

$$\tilde{f}_R(v l^{-d} N^{\frac{4-d}{2}}, \phi_c N^{\frac{d}{2}} l^d) = f_R(v l^{-d} N^{\frac{4-d}{2}})\, g_{c,R}(\phi_c \langle R^2 \rangle^{\frac{d}{2}}) \quad (2.42)$$

so that the mean square end-to-end distance at fixed concentration is related to that of a single chain by

$$\langle R^2 \rangle_c = \langle R^2 \rangle g_{c,R}(\phi_c \langle R^2 \rangle^{\frac{d}{2}}) \quad (2.43)$$

From equation (2.42) we can learn the properties of $g_{c,R}(x)$ as the concentration varies. We expect that in the $\phi_c \to 0$ limit, $\langle R^2 \rangle_c$ should assume the value for an isolated single chain in either good or poor solvent. Therefore,

$$g_{c,R}(x)\,|_{x=0} = 1 \quad (2.44)$$

Also when v is large, with finite chain length N, equations (2.30) and (2.43) yield

$$\langle R^2 \rangle_c = \langle R^2 \rangle g_{c,R}(\phi_c N^{dv} v^{\frac{d(2v-1)}{4-d}} l^{\frac{2d(2-dv)}{4-d}}) \quad (2.45)$$

If the argument of $g_{c,R}$ is small but non-zero, $g_{c,R}$ should have a value less than $g_{c,R}(0)$, reflecting the shrinkage effect due to the presence of other chains. The longer the chain, the

larger is the probability that each chain will interact with other chains even when the density is quite low. This contact and the excluded volume effect will force the chain to assume a smaller size. Freed[146] proposed expanding $g_{c,R}(x) \approx g_{c,R}(0) - x|g_{c,R}'(0)|$; then equation (2.45) becomes

$$\langle R^2 \rangle_c = l^2 N^{2\nu} (\upsilon l^{-d})^{\frac{2(2\nu-1)}{4-d}} \times \left[g_{c,R}(0) - |g_{c,R}'(0)| \phi_c N^{d\nu} \upsilon^{\frac{d(2\nu-1)}{4-d}} l^{\frac{2d(2-\nu d)}{4-d}} \right] \qquad (2.46)$$

As the polymer concentration increases, chains will intertwine and interpenetrate each other. A segment of a given chain will experience the presence of other chains that will compensate the self-excluded volume effect. The net result is the end-to-end distance will exhibit the quasi-ideal behavior of melt/dense system, which is $\langle R^2 \rangle \sim N$. Note that this idea was originated by Flory[2], and has been confirmed in experiments and simulations[150-158]. As $\phi_c \to \infty$, the argument of $g_{c,R}$ is very large and we expect $g_{c,R}$ to follow a power-law form

$$g_{c,R}(\phi_c \langle R^2 \rangle^{\frac{d}{2}}) \sim (\phi_c \langle R^2 \rangle^{\frac{d}{2}})^{y_R} \qquad (2,47)$$

substituting (2.47) into (2.43) and using (2.30), we obtain

$$\langle R^2\rangle_c\big|_{\phi_c>>1} \rightarrow \phi_c^{y_R} l^{y_R d+2} (v l^{-d})^{\frac{(2\nu-1)(y_R d+2)}{4-d}} N^{2\nu+\nu y_R d} \qquad (2.48)$$

Since ϕ_c is the chain concentration, $\phi_c = N^{-1}\phi$, and from the quasi-ideal requirement of the end-to-end distance, y_R is given by

$$y_R = \frac{1-2\nu}{\nu d-1} \qquad (2.49)$$

Therefore,

$$\langle R^2\rangle_c \propto N\phi^{\frac{1-2\nu}{\nu d-1}} l^{\frac{d-2}{\nu d-1}} (v l^{-d})^{\frac{(2\nu-1)(d-2)}{(4-d)(\nu d-1)}} \qquad (2.50)$$

with ϕ corresponds to segment density. In three dimensions with $\nu = 3/5$, we obtain

$$\langle R^2\rangle_c \propto N\phi^{-\frac{1}{4}} l^{\frac{1}{2}} v^{\frac{1}{4}} \qquad (2.51)$$

Note that in the θ-solvent, $\langle R^2\rangle_c \approx N$ (without any v dependence), since $v=0$ and $g(0)=1$. In equation (2.48), even though $\langle R^2\rangle_\phi|_{\phi>>1}$ shows the melt behavior, the v dependence still exists and has positive power. Compared to θ-solutions where $\langle R^2\rangle_{\phi\rightarrow 0} \approx N$, the positive exponent of v reveals the effect of self-excluded volume. We also want to make a remark here, from the renormal-

ization group results at θ-point v is negative in order to compensate for three body interactions. In our discussion we should keep in mind that v is an effective two body interaction where the bare many-body interactions have been renormalized. In experiments, v is usually measured from the second virial coefficient.

2.3.2. Correlation Length at Fixed Concentration.

As has been argued previously, in dense solutions chains start to interpenetrate and screen the interactions between segments on the same chain. The screening effect can be described by introducing the screening length ξ, which is the average distance between contacts (Figure 2.2). De Gennes[47] referred ξ as the average mesh size. In experiments, ξ is measured by observing the structure factor in neutron scattering[11]. Another method, proposed by Benoit[47], is by observing the diffusion of a test-ball of dimension D < R in a polymer solution (R is the average size of a polymer chain). The screening length must scale as $\langle R^2 \rangle^{1/2}$ since it has dimensions of length. However, it does not depend explicitly on N.

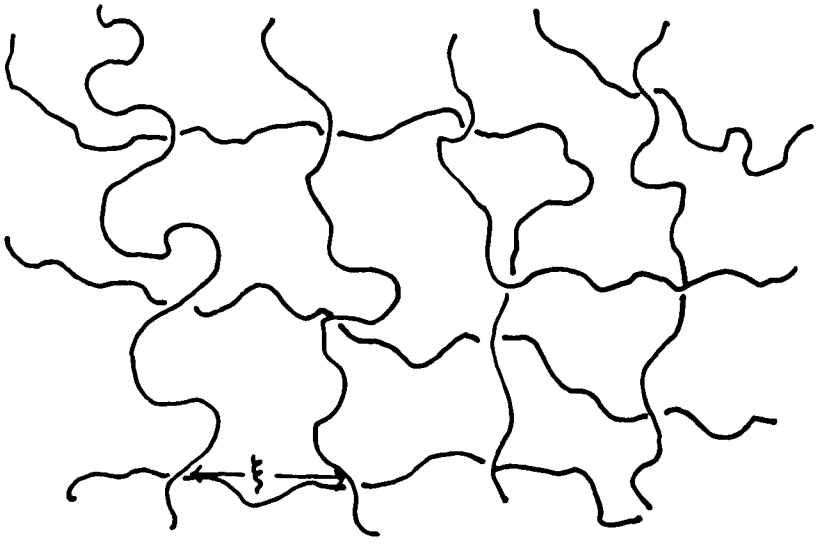

Figure 2.2. Definition of the average mesh-size.

Therefore, we can argue that

$$\xi^2 = l^2 N f_\xi(\phi_c N^{\frac{d}{2}} l^d, v l^{-d} N^{\frac{4-d}{2}}) \qquad (2.52)$$

In a poor solvent, $v \to 0$, and at high concentration, we can neglect the second argument and rewrite (2.52) as

$$\xi^2 = l^2 N f_{1\xi}(\phi_c N^{\frac{d}{2}} l^d) \qquad (2.53)$$

Since, as suggested in section 2.2, $\tilde{f}_{1\xi}$ must have a power law form, we let $\tilde{f}_{1\xi}(z)\,|_{z\to\infty} \propto z^{y_t}$. Then the condition that ξ should be independent of N implies

$$y_{t_p} = \frac{2}{2-d} \tag{2.54}$$

hence

$$\xi^2 \propto \phi^{\frac{2}{2-d}} l^{\frac{4}{2-d}} \qquad \text{when } \upsilon \to 0,\ \phi \text{ or } \phi_c \to \infty \tag{2.55}$$

For three dimensions, equation (2.55) gives $\xi \propto \phi^{-1}$.

In good solutions, where chain dimensions scale as $N^{2\nu}$, equation (2.52) may be analyzed analogous to the derivation of equation (2.45), and it gives

$$\xi^2 = l^2 N^{2\nu} (\upsilon l^{-d})^{\frac{2(2\nu-1)}{4-d}} \times g_{c,\xi}\left[\phi N^{d\nu-1} \upsilon^{\frac{d(2\nu-1)}{4-d}} l^{\frac{2d(2-\nu d)}{4-d}}\right] \tag{2.56}$$

Again assuming that $g_{c,\xi}$ follows a power law for large values of its argument, and writing the exponent as y_{t_ξ} in this case, the independence of N in relation (2.56) implies

$$y_{tg} = -\frac{2\nu}{d\nu - 1} \tag{2.57}$$

which is equal to y_{tp} if we substitute $\nu = 1/2$. Using this result for y_{tg}, equation (2.56) becomes

$$\xi^2 \propto \phi^{-\frac{2\nu}{\nu d-1}} l^{\frac{4(2-d\nu)}{(4-d)(1-d\nu)}} v^{\frac{-2(1-2\nu)}{(4-d)(1-d\nu)}} \tag{2.58}$$

which gives $\xi \propto \phi^{-3/4} l^{-1/2} v^{-1/4}$ for d = 3 and $\nu = 3/5$.

2.3.3. The Scaling of Osmotic Pressure.

Another quantity of interest is the osmotic pressure which is defined by

$$\frac{\Pi V}{k_B T} = V\frac{\partial \log Z_{n_p}}{\partial V} \tag{2.59}$$

If we rescale $\vec{r}'(s') = (b^{1/2}/l)\vec{r}(s)$, where $s' = (b/l)\, s$, and use equation (2.32), we obtain

$$\frac{\Pi V}{k_B T} = \tilde{g}_{\Pi}(Nb, b^{\frac{d-4}{2}} v l^{-d}, V b^{\frac{d}{2}} l^{-d}, n_p) \tag{2.60}$$

Before proceeding, we note that the low density limit of

(2.60) is straightforward, since the partition function may be approximated by the product of single chain partition functions

$$Z_{n_p} = \frac{1}{n_p!} (Z_1)^{n_p} \tag{2.61}$$

where Z_1 is the partition function of a single chain in volume V. Therefore, Π is a function of υ, N and V only:

$$\frac{\Pi V}{k_B T} |_{\phi \to 0} = n_p f_{\Pi}(\upsilon, N, V) \tag{2.62}$$

Relation (2.62) indicates that $\tilde{g}_r$ in equation (2.60) should have an overall proportionality factor n_p, hence, if we factor this extensive quantity the remaining arguments in $\tilde{g}_r$ must have intensive forms. The extensive quantities n_p and $Vb^{d/2}l^{-d}$ will appear as a ratio $n_p/(Vb^{d/2}l^{-d})$ that is proportional to the chain density ϕ_c. With the choice $b = N^{-1}$, the equation of state (2.60) may be reexpressed as

$$\frac{\Pi V}{k_B T} = n_p \tilde{f}_{\Pi}(N^{\frac{4-d}{2}} \upsilon l^{-d}, \phi_c N^{\frac{d}{2}} l^d) \tag{2.63}$$

It is clear from equation (2.62) that the non-ideality of the polymer solution is governed by the excluded volume υ and the

chain concentration ϕ_c, as $N \to \infty$. We must know the behavior of Π in the asymptotic limits of concentration and excluded volume parameter in order to determine the scaling exponents. The demarcation between the low and high concentration regimes is the segment concentration ϕ^*, at which chains start to influence each other. It is given by

$$\phi^* \propto \frac{N}{Vol\ (single\ chain)} \propto N^{1-d\nu} \tag{2.64}$$

If we introduce an ansatz that the arguments of $\tilde{f}_\pi$ appear in the form of the ratio ϕ/ϕ^*, then the two scaling variables of $\tilde{f}_\pi$ have to appear in a combined form

$$N^{d\nu-1} \propto \left(N^{\frac{4-d}{2}} \upsilon l^{-d}\right)^{x_\pi} \phi N^{\frac{d}{2}-1} l^d \tag{2.65}$$

with x_π chosen such that the exponents for N on both sides are equal. This gives

$$x_\Pi = \frac{2\nu d - d}{4-d} \tag{2.66}$$

and the final form of the osmotic pressure, in the long chain limit, is

$$\frac{\Pi}{k_B T} = \frac{\phi}{N}\tilde{f}_{1\Pi}\left(\phi N^{-(1-\nu d)} l^{d} (\upsilon l^{-d})^{\left(\frac{d}{4-d}\right)(2\nu-1)}\right) \qquad (2.67)$$

Using the ratio

$$\frac{\phi}{\phi^*} = \frac{\phi \langle R^2 \rangle^{\frac{d}{2}}}{N} = \phi N^{-(1-\frac{d}{2})} l^{d}\left(f_R (N^{\frac{4-d}{2}} \upsilon l^{-d})\right)^{\frac{d}{2}} \qquad (2.68)$$

the osmotic pressure can be reexpressed in general as

$$\frac{\Pi}{k_B T} = \frac{\phi}{N}\tilde{f}_{1\Pi}(\phi N^{\frac{d}{2}-1} l^{d} [f_R (N^{\frac{4-d}{2}} \upsilon l^{-d})]^{\frac{d}{2}}) \qquad (2.69)$$

As a consistency check, using the $N \to \infty$ asymptotic behavior of f_R for good solutions, equation (2.30), the argument of $\tilde{f}_{1\pi}$ in (2.69) provides the same result as equation (2.67).

To reproduce ideal behavior expected for $\upsilon = 0$ and $\phi \to 0$, we require $\tilde{f}_{1\pi}(0) = 1$. In the limit of high concentration and $\upsilon = 0$, equation (2.69) gives

$$\frac{\Pi}{k_B T} = \frac{\phi}{N}\tilde{f}_{1\Pi}(\phi N^{\frac{d}{2}-1} l^{d}) \qquad (2.70)$$

and the power-law requirement changes the previous equation to

$$\frac{\Pi}{k_B T} = \frac{\phi}{N}[\phi N^{\frac{d}{2}-1} l^d]^{y_{\pi p}} \qquad (2.71)$$

Since chain segments no longer distinguish which segments belong to which chains, it follows that π should be N independent, so $y_{\pi p} = 2/(d-2)$ and

$$\frac{\Pi}{k_B T} = (\phi l^2)^{\frac{d}{d-2}} \qquad (2.72)$$

In good solutions and at low concentrations, equation (2.69) can be rewritten as

$$\frac{\Pi}{k_B T} = \frac{\phi}{N}\tilde{f}_{1\Pi}(\phi N^{\frac{d}{2}-1} l^d (N^{\frac{4-d}{2}} v l^{-d})^{\frac{d(2\nu-1)}{4-d}}) \qquad (2.73)$$

If the combined argument, in very dilute solutions, is small, equation (2.73) may be Taylor-expanded to give

$$\frac{\Pi}{k_B T} = \frac{\phi}{N} + \frac{\phi^2}{N^2}(N^{d\nu} l^{\frac{2d(2-\nu d)}{4-d}} v^{\frac{d(2\nu-1)}{4-d}}) \tilde{f}'_{1\Pi}(0) \qquad (2.74)$$

where $\tilde{f}_{1\pi}'(0)$ is the derivative of $\tilde{f}_{1\pi}$ evaluated at zero. The result in equation (2.74) provides us with the second virial

coefficient A_2 which is

$$A_2 = N^{\nu d-2} l^{\frac{2d(2-\nu d)}{4-d}} \upsilon^{\frac{d(2\nu-1)}{4-d}} \tilde{f}'_{1\mathrm{II}}(0) \qquad (2.75)$$

Another interesting result is obtained when we consider good solutions at high densities. Invoking the power-law form for f_R and $\tilde{f}_{1\pi}$ for $\phi >> \phi^*$, and $\upsilon \to \infty$ we obtain

$$\frac{\Pi}{k_B T} \propto \frac{\phi}{N} [\phi N^{\frac{d}{2}-1} l^d (N^{\frac{4-d}{2}} \upsilon l^{-d})^{\frac{d(2\nu-1)}{4-d}}]^{y_{\Pi g}} \qquad (2.76)$$

In this limit π should be independent of N, which means that the exponent of N vanishes, so $y_{\pi g}$ is given by

$$y_{\Pi g} = \frac{1}{\nu d-1} \qquad (2.77)$$

and the osmotic pressure of a good solution at high concentration becomes

$$\frac{\Pi}{k_B T} \propto \phi^{\frac{d\nu}{d\nu-1}} \upsilon^{\frac{d(2\nu-1)}{(4-d)(d\nu-1)}} l^{\frac{2d(2-d\nu)}{(4-d)(d\nu-1)}} \qquad (2.78)$$

In three dimensions, using the value of ν = 3/5, the previous equation gives the scaling dependence as

$$\frac{\Pi}{k_B T} \propto \phi^{\frac{9}{4}} v^{\frac{3}{4}} l^{\frac{3}{2}} \qquad (2.79)$$

Note that in d=3 the segment density dependence of the osmotic pressure is different from the result of the mean-field approximation, which is proportional to ϕ^2. We may interpret this result as follows: Although the chain is swollen, and so has fewer contacts between segments than in a uniform monomer cloud, the long-range correlation propagates along chain segments of effective size ξ (see Fig 2.2). Since the osmotic pressure is a measure of effective contacts among chain segments, and there is one contact in a volume ξ^3, then $\Pi/(k_B T) \propto \xi^{-3}$. Using the result in eqn. (2.58) we obtain eqn.(2.79).

2.4. Polymers Confined Between Two Walls.

When chains are confined between two walls, it is interesting to learn the effect of the wall distance on the scaling relations of the end-to-end distance $\langle R^2 \rangle$ and of the osmotic pressure $\Pi/(k_B T)$. As noted by Freed[69], by allowing the

distance D between the walls to shrink, one can obtain a recursion relation which relates the critical exponents ν in different dimensions. This interdimensional relation together with the assumed power-law behavior in the $N\to\infty$ limit yields the well-known result for ν originally obtained by Flory. Our interest here is to learn the behavior of $\langle R^2\rangle$ and $\Pi/(k_BT)$ as a function of the excluded volume parameter in a confined region. The analysis is generalized to multichain systems in similar fashion as previous calculations. In the next chapter, we consider the effect of a repulsive wall-segment interaction on the monomer density profile.

2.4.1. The Effect of Confinement on A Single Chain.

Consider a polymer chain confined between two walls separated by a distance D. Let the z axis be directed perpendicular to the walls. The integration involving z (in Eqs. (2.9) and (2.19)) has to be modified accordingly. Under the transformation $\vec{r}'(s') = a_0\vec{r}(s)$ with $a_0 = N^{-1/2}l^{-1}$, the z integration is then transformed to

$$\int_0^D dz = a_0^{-1}\int_0^{a_0D} dz' = (N^{1/2}l)\int_0^{N^{-1/2}l^{-1}D} dz' \qquad (2.80)$$

The partition function and the mean square end-to-end distance

are the same as given by equation (2.9) and (2.19) except that the domain of the z integration is restricted by the walls. Focusing on the end-to-end distance, the scaling relation will be the same, but we also have to incorporate the new parameter D. Denoting the mean square end-to-end distance of a single chain between two walls by $\langle R^2 \rangle_{d,D}$, we have, from eqn. (2.30),

$$\langle R^2 \rangle_{d,D} = l^2 N f_{R,D}(N^{\frac{4-d}{2}} v l^{-d}, DN^{-1/2} l^{-1}) \qquad (2.81)$$

Note that for d>4, when $N \to \infty$ the problem reduces to that of a quasi-ideal chain between two walls, since the excluded volume interaction becomes irrelevant.

For a good solution in d<4, we can write eqn. (2.81) as a product of $\langle R^2 \rangle_d$, the mean-square of the end-to-end distance in free space, and a dimensionless function. Therefore,

$$\langle R^2 \rangle_{d,D} = \langle R^2 \rangle_d f_{1R,D}\left(\frac{D}{\langle R^2 \rangle_d^{1/2}}\right) \qquad (2.82)$$

For a chain in a good solution, the $D \to \infty$ limit has to reproduce the result of a chain in free space. Therefore,

$$f_{1R,D}\left(\frac{D}{\langle R^2 \rangle_d^{1/2}}\right)\Big|_{D\to\infty} = 1 \qquad (2.83)$$

And when D → 0, we invoke the power-law behavior of $f_{1R,D}$:

$$f_{1R,D}(z)\,|_{z=0} = z^{-x_D} \qquad (2.84)$$

so that relation (2.82) becomes

$$\langle R^2\rangle_{d,D} = \langle R^2\rangle_d^{1+x_D/2} D^{-x_D} \qquad (2.85)$$

In this limit, $\langle R^2\rangle_{d,D}$ should exhibit the behavior of a chain in a (d-1)-dimensional hyperplane. Using equation (2.30a) for (d-1) dimensions on the left hand side of eqn. (2.85), we get

$$l^2 N f_{R;d-1}(N^{\frac{(5-d)}{2}} \upsilon l^{-(d-1)}) = D^{-x_D}(l^2N)^{1+x_D/2}\,[f_{R;d}(N^{\frac{(4-d)}{2}} \upsilon l^{-d})]^{(1+x_D/2)} \qquad (2.86)$$

In good solutions, where υ>>1, and in the long chain limit, we may use the asymptotic form in (2.30b). However, the scaling exponent ν on the left side has to be ν_{d-1} , or 3/(d+1) in

Flory's approximation. Equating the exponent of N on both sides yields

$$x_D = \frac{2}{d+1} \tag{2.87}$$

We can summarize the behavior of $f_{1R,D}(x)$ as

$$f_{1R,D}(x) = \begin{cases} 1 & as \quad x \to \infty \\ x^{-\frac{2}{(d+1)}} & as \quad x \to 0 \end{cases} \tag{2.88}$$

The end-to-end distance of a chain in a good solution, when it is located in a slit of width D is

$$\langle R^2 \rangle_{d,D}|_{D<N^{2\nu}} \sim D^{-\frac{2}{1+d}} N^{\frac{2\nu(2+d)}{1+d}} v^{\frac{2(2\nu-1)(2+d)}{(4-d)(1+d)}} l^{\frac{4(2-\nu d)(2+d)}{(4-d)(1+d)}} \tag{2.89}$$

In three dimensions, with ν = 3/5, equation (2.89) yields

$$\langle R^2 \rangle_{3,D}|_{D<N^{2\nu}} \sim D^{-1/2} v^{1/2} l N^{3/2} \tag{2.90}$$

Equation (2.90) indicates that in a narrow slit $\langle R^2 \rangle$ follows the 2d scaling behavior. Since the excluded volume potential is still present, the radius of the disk should be larger than the radius of the (spherical) chain in free space. Also note that the disk size depends on the width of the slit with a negative exponent. For a θ-solvent, where $v=0$ and $f_R(x \to 0)=1$, equation (2.89) is replaced by

$$\langle R^2 \rangle_{d,D}\Big|_{\substack{D\to 0 \\ v=0}} \sim N l^2 \qquad (2.91)$$

The result of (2.91) is not surprising when one considers a random walk. The ideal chain may intersect itself many times without penalty. Confinement will compel the chain to zigzag, without increasing its size.

2.4.2. Semi-Dilute Solution Between Two Walls.

At finite concentration, the semi-dilute regime is given by $\phi > \phi^*$ where $\phi^* \sim N^{1-d\nu}$ for good solvents. When the polymer chains are contained between two walls, the overlap density will be affected by the wall-to-wall distance D through the effective volume of a single chain,

$$\phi^*_{d,D} = \frac{N}{\langle R^2 \rangle_{d,D}^{(d-1)/2} D} \qquad (2.92)$$

Using equations (2.82) and (2.88), and $\nu_d=3/(d+2)$, the overlap density of polymers in a good solvent, confined to a slit of width D is

$$\Phi^*_{d,D}|_{D\sim 0} \sim D^{-\frac{2}{1+d}} N^{\frac{2(2-d)}{1+d}} v^{\frac{1-d}{1+d}} l^{\frac{2(1-d)}{1+d}} \qquad (2.93)$$

In three dimensions it is given by

$$\Phi^*_{3,D}|_{D\sim 0} \sim D^{-1/2} N^{-1/2} v^{-1/2} l^{-1} \qquad (2.94)$$

Other quantities like the end-to-end distance, the mesh-size and osmotic pressure will show D-dependence via the overlap density. For the end-to-end distance at fixed concentration

$$\langle R^2\rangle_{c;d,D} = \langle R^2\rangle_{d,D} \tilde{f}_{R,D}(\Phi/\Phi^*_{d,D}) \qquad (2.95)$$

A particularly interesting problem is the effect of the wall-to-wall distance on the mesh-size and the osmotic pressure. From dimensional analysis one may obtain

$$\xi_D^2 = \langle R^2\rangle_{d,D} \tilde{f}_{\xi}(\Phi/\Phi^*_{d,D}) \qquad (2.96)$$

and

$$\frac{\Pi}{k_B T} = \frac{\phi}{N} \tilde{f}_{\pi}(\phi/\phi^{*}_{d,D}) \qquad (2.97)$$

When $\phi/\phi_{d,D}^{*} >> 0$, the argument in $\tilde{f}_{\xi}$ is large. Assume that

$$\tilde{f}_{\xi}(x)\,|_{x\to\infty} \sim x^{m_{\xi}} \qquad (2.98)$$

then

$$\xi_D^2\,|_{D\to 0} \sim N^{\frac{2\nu(2+d)}{1+d} - m_{\xi}\frac{2(2-d)}{1+d}} \qquad (2.99)$$

Note that we have suppressed all parameters except N in (2.99), for notation convenience. Since, in a dense system, ξ_D^2 should be independent of N, one obtains

$$m_{\xi} = \frac{3}{2-d} \qquad (2.100)$$

Therefore, one can write that the correlation length of chains in the dilute regime, when it is confined between two narrow walls, as

$$\xi_D^2 \sim (\phi^3 D^2 l^2 \upsilon)^{\frac{1}{2-d}} \qquad (2.101)$$

In three dimensions

$$\xi_D|_{D\to 0} \sim \phi^{-3/2} v^{-1/2} D^{-1} l^{-1} \qquad (2.102)$$

We can write equation (2.102) in terms of area density ϕ_a, which is defined by $\phi = \phi_a/D$. Then equation (2.102) becomes

$$\xi_D|_{D\to 0} \sim \phi_a^{-3/2} v^{-1/2} D^{1/2} l^{-1} \qquad (2.103)$$

The proportionality between ξ_D and D (raised to positive power) is interesting. If ξ is a measure of the mesh-size, which is the average of distance between contacts (Fig. 2.2), then as the system is compressed contacts among chain segments occur more frequently over smaller distances. Note also that the area-density dependence in equation (2.103) follows a similar relation as in two dimensions. The analysis for the osmotic pressure follows a similar line. In good solvents, in the semi-dilute regime, the osmotic pressure depends on D via

$$\frac{\Pi}{k_B T} \sim \phi^{\frac{3(1-d)}{2(2-d)}} D^{\frac{1}{d-2}} v^{\frac{1-d}{2(2-d)}} l^{\frac{1-d}{2-d}} \qquad (2.104)$$

The enhancement of the osmotic pressure when the region is compressed can be derived by rewriting equation (2.104) in terms of area density. Assuming that the area density is constant when $D\to 0$, which can be achieved by chains re-configuration, equation (2.104) becomes

$$\frac{\Pi}{k_B T} \sim \phi_a^{\frac{3(1-d)}{2(2-d)}} D^{\frac{5-3d}{2(d-2)}} v^{\frac{1-d}{2(2-d)}} l^{\frac{1-d}{2-d}} \qquad (2.105)$$

In three dimensions, $\Pi/(k_BT) \sim \phi_a^3 D^{-2} v l^2$. This relation shows that the osmotic pressure has the same dependence on the area-density as in two dimensions. The enhancement of the osmotic pressure when the region is compressed is reflected by the negative exponent of D. It is interesting, therefore, to learn the behavior of osmotic pressure when the dimension of the system is varied. Equation (2.105) breaks down for d=2. This difficulty can be explained by expressing the osmotic pressure as a function of contact density.

$$\frac{\Pi}{k_B T} = \frac{1}{\xi_D^{d-1} D} \qquad (2.106)$$

In two dimensions, the system looks similar to a ribbon of a width D. As we squeeze the ribbon ($D \to 0$), polymers are elongated and reduced to one-dimension rods. The average distance between contacts vanishes, and the osmotic pressure described in eqn. (2.106) is undefined.

III. Monomer Density Profile Near a Repulsive Wall.

The study of long flexible chains or polymers near an interface or a wall, is of interest to engineers and scientists, since it has many technological applications. The stabilization of colloids, lubrication, adhesion, plastic-welding, and medical applications are some examples. Several models have been devised. Exact enumeration methods[109-112], Monte Carlo simulations[132-135], scaling theories[47,69], and the renormalization group applied to both the n-vector model[48,49] and Edwards' model[69-74] are examples of methods and simulation techniques devised to attack this problem.

Previous theoretical studies emphasized on the conformational properties of chains in the dilute and semi-dilute regime. Examples were the end-to-end distance of a single chain with one or both ends attached to the wall, the partition function of a chain attached to the wall, etc[79,94,88-90]. The problem of the monomer density profile as a function of distance from the wall was approached using scaling theories or the n-vector model[159,164]. The simulation results for semidilute athermal chains near a hard wall confirmed the prediction of the scaling theories[22]. In this chapter we study the segment density profile of athermal chains as a function of distance from the wall. This problem was first approached using the scaling techniques to obtain the scaling exponent. Since in dense solutions and in θ-solutions, polymers are well

approximated by ideal (random walk) chains, the second section discusses the density profile of ideal chains near an interface, and when the chains are confined between repulsive walls. In the last section we employ the CRG to study the density profile of monomers as a function of distance from a repulsive wall, to the lowest order of perturbation.

3.1. Scaling Relation of Monomer Density Near A repulsive Wall

Consider a single chain near a wall (the plane z=0) with monomer-wall interaction δ_0. The Edwards' model Hamiltonian of the single-chain is

$$H[\{\vec{r}(s)\}] = \frac{d}{2l}\int_0^L [\dot{r}(s)]^2 ds + \frac{v}{2l^2}\int_0^L ds \int_0^L ds' \delta(\vec{r}(s) - \vec{r}(s')) + \delta_0 \int_0^L ds \delta(z(s)) \qquad (3.1)$$

As the last term indicates, we are considering a short range segment-wall interaction. Positive δ_0 corresponds to a repulsive wall, $\delta_0 \to \infty$ represents an impenetrable wall. The chain distribution function, for ends separated by $\vec{R}$, and the s^{th} segment located at $\vec{R}_1$, is given by

$$G(\vec{R}, L; s, \vec{R}_i) = C \int_{\vec{r}(0)}^{\vec{r}(L)=\vec{r}(0)+\vec{R}} d\{\vec{r}(s)\}\, \delta(\vec{r}(s) - \vec{R}_i) \exp[-H\{\vec{r}(s)\}] \tag{3.2}$$

where C is the normalization constant. The integration $d\{\vec{r}(s)\}$ is restricted to $z(s) \geq 0$. In a many-chain system equation (3.2) is generalized to

$$G_{n_p}^{(\alpha)}(\vec{R}, L_\alpha; s, \vec{R}_j; n_p) = C_{n_p} \prod_{\alpha=1}^{n_p} \int_{\vec{r}_\alpha(0)}^{\vec{r}_\alpha(L)=\vec{r}_\alpha(0)+\vec{R}} d\{\vec{r}_\alpha(s)\}\, \delta(\vec{r}_\alpha(s) - \vec{R}_j) \times \exp[-H\{\vec{r}(s), n_p\}] \tag{3.3}$$

where the index α indicates the chain and s corresponds to the segment. For example $\vec{r}_\alpha(s)$ means the position of the s^{th} segment of the α^{th} chain. In equation (3.3), it is located at site $\vec{R}_j$. The Hamiltonian $H\{\vec{r}(s), n_p\}$ is now given by equation (2.31) with the additional monomer-wall interactions. The normalization constant is also modified accordingly, so that the partition function Z = 1.

The segment density at position z, $\rho(z)$, is proportional to the multi-chain distribution function integrated over all possible chain-end positions.

$$\rho(z) \propto \sum_{a=1}^{n_p} \int_0^{L_a} ds \int G_{n_p}^{(a)}(\vec{R}, L_a; s, \vec{R}_j; n_p)\, d\vec{R} d\vec{R}_{j,1} \qquad (3.4)$$

In Eqn. (3.4), we have integrated over all directions parallel to the wall, since we are interested only to the monomer density profile as a function of distance from the wall.

Under scaling relation (2.12) with the choice $a_0=(b_0/l)^{1/2}$ with $b_0L=bL/l=bN$, the monomer-wall interaction term scales as

$$\delta_0 \int_0^L \delta(z(s))\, ds = \delta_0 b^{-1/2} \int_0^{bN} \delta(z'(s'))\, ds' \qquad (3.5)$$

Therefore, the density $\rho(z)$ can be written as

$$\rho(z) = f_\rho(z'; bN, b^{\frac{d-4}{2}} v l^{-d}, b^{-1/2}\delta_0; n_p) \qquad (3.6)$$

Choosing b = 1/N, equation (3.6) can be recast as

$$\rho(z) = f_{1,\rho}\left(\frac{z}{N^{1/2}l}; N^{\frac{4-d}{2}} v l^{-d}, N^{1/2}\delta_0; n_p\right) \qquad (3.7)$$

For general δ_0, the qualitative shape of $\rho(z)$ is as shown in figure (3.1).

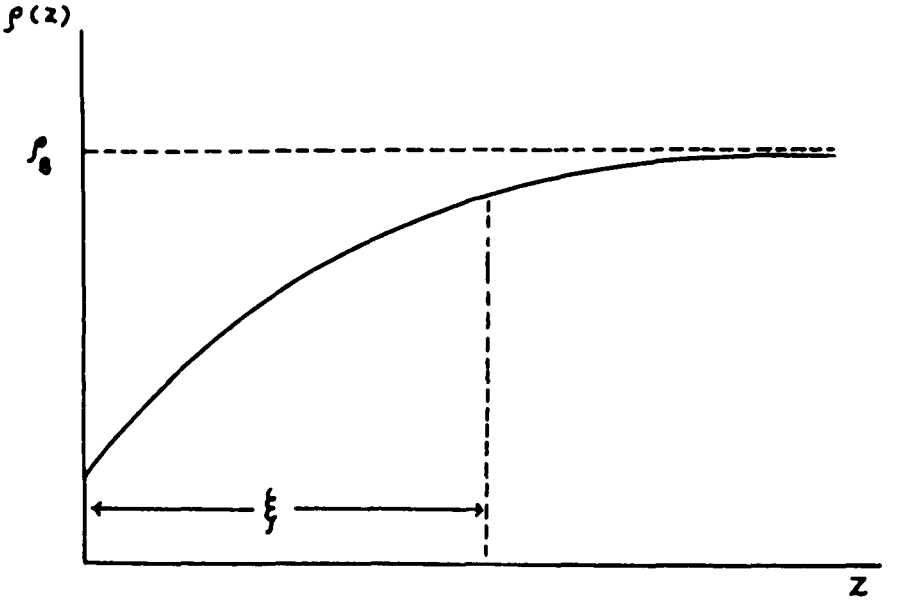

Figure 3.1. A schematic picture of the segment density profile.

In the asymptotic limit $z \to \infty$, $\rho(z)$ will resume the bulk value ρ_B, while for $z \to 0$, ρ will be a function of δ_0. They should depend on the interactions between the polymer and the wall, and on the size of the monomer or Kuhnian length. It also depends on temperature and solvent quality. ξ in figure (3.1) is the correlation length of the polymer solution. It may be interpreted as the distance beyond which the fluid does not 'feel' the presence of the wall due to the screening effect. This correlation length may be approximated by the correlation length of the chains in the bulk (section 2.3.2). In this work

we are only interested on the asymptotic limit $\delta_0 \to \infty$. Assuming that this limit exists, we expect depletion of the monomer density in the region near the wall; for $\delta_0 \to \infty$, $\rho(z) \to 0$ as $z \to 0$. Suppose the $\delta_0 \to \infty$ limit of the right hand side of equation (3.7) exists, i.e.,

$$\lim_{\delta_0 \to \infty} f_{1,\rho}\left(\frac{z}{N^{1/2}l}, N^{\frac{4-d}{2}} v l^{-d}, \delta_0 N^{1/2}, n_p\right) = g_\rho\left(\frac{z}{N^{1/2}l}, N^{\frac{4-d}{2}} v l^{-d}, n_p\right) \tag{3.8}$$

Following the discussion in Chapter II, the dependence on the excluded volume parameter v comes through the macroscopic quantity. In this case, we may pick the correlation length ξ as the macroscopic parameter, then equation (3.7) can be recast to

$$\rho(z) = \rho_B \tilde{g}_\rho\left(\frac{z}{\xi}\right) \tag{3.9}$$

Since ρ_B sets the overall scale and the dimensionality of $\rho(z)$. The argument of $\tilde{g}_\rho$ is a dimensionless ratio of lengths. To satisfy the boundary conditions at $z \to 0$ and $z \to \infty$, $\tilde{g}_\rho$ must have the following asymptotic limits:

$$\tilde{g}_\rho(x) \sim \begin{cases} 0 & as\ x \to 0 \\ 1 & as\ x \to \infty \end{cases} \qquad (3.10)$$

Following the argument of Weibull[160], which was employed by Shih et. al.[161] in their simulations, we may assume that $\tilde{g}_\rho(x)$ takes the following form

$$\tilde{g}_\rho(z/\xi) = 1 - e^{-(\frac{z}{\xi})^m} \qquad (3.11)$$

Note that this form of $\tilde{g}_\rho(x)$ was used also by de Gennes in his early work[159]. To obtain the value of m, we consider the behavior of $\rho(z)$ for $0 < z < \xi$. In this range, equations (3.9) and (3.11) imply that

$$\rho(z) \sim \rho_B[z/\xi]^m \qquad (3.12)$$

Assuming that the osmotic pressure is proportional to the segment density adjacent to the wall[47,159], and using equation (2.78) then

$$\Pi^* \sim \rho_B^{\frac{d\nu}{d\nu-1}} \sim \rho_B \xi^{-m} \qquad (3.13)$$

But the correlation length ξ is related to ρ_B as in equation

(2.58). Therefore, it yields

$$m = \frac{1}{\nu} \tag{3.14}$$

In three dimensions, equation (3.9) gives

$$\rho(z) \sim \rho_B \left(\frac{z}{\xi}\right)^{5/3} \qquad 0 \ll z \ll \xi \tag{3.15}$$

The exponent in equation (3.14) has been confirmed by Shih et. al.[161] in simulations of athermal chains in semidilute solution. Note that the density profile near an attractive wall was obtained by de Gennes[159] and des Cloizeaux[162] as $\rho(z) \sim z^{-d+1/\nu}$.

3.2. Segment Density Profile of Gaussian Chains Near a Repulsive Wall.

In this section we derive the segment-density profile of Gaussian chains near a repulsive wall. First, we will discuss Gaussian chains which interact with a wall via a potential of strength δ_0. The repulsive behavior is obtained by taking the limit $\delta_0 \to \infty$. Segment distribution for chains confined between two repulsive wall follows.

Consider the Edwards' model Hamiltonian for a long flexible chain

$$H[\vec{c}(\tau)] = \frac{1}{2}\int_0^L [\frac{d\vec{c}(\tau)}{d\tau}]^2 d\tau + \frac{u_0}{2}\int_0^L d\tau \int_0^L d\tau' \delta[\vec{c}(\tau) - \vec{c}'(\tau)] \tag{3.16}$$

In equation (3.16) we define $\vec{c}(\tau) = [d/l]^{1/2}\vec{r}(\tau)$ where $\vec{r}(\tau)$ is the position of the τ^{th} segment in d dimensional space. L is the chain length and $u_0 = vd^{d/2}l^{-(4+d)/2}$ is the segment-segment interaction parameter. In the gaussian model of an ideal polymer, $u_0 = 0$. If we have a multichain system, the Hamiltonian is therefore separable and can be studied as an isolated ideal chain.

The end-to-end distribution function $G(\vec{c}, \vec{c}'; L)$ is given by

$$G(\vec{c}, \vec{c}'; L) = \int_{\vec{c}(0)=\vec{c}}^{\vec{c}(L)=\vec{c}'} D[\vec{c}(\tau)] \exp[-H] \tag{3.17}$$

and it satisfies the diffusion equation[69]

$$(\frac{\partial}{\partial L} - \frac{1}{2}\nabla_c^2) G(\vec{c}, \vec{c}'; L) = \delta(\vec{c} - \vec{c}')\delta(L) \tag{3.18}$$

A short-range polymer-wall interaction can be incorporated to the Hamiltonian (3.16) by adding

$$H_{surf} = \delta_0 \int_0^L d\tau\, \delta(c_z(\tau)) \qquad (3.19)$$

δ_0 is a measure of the strength of polymer-wall interaction. If $\delta_0 > 0$ we have a repulsive wall and when $\delta_0 < 0$ it corresponds to an attractive wall. An equivalent description is obtained by imposing appropriate boundary conditions to the diffusion equation instead of adding H_s. In our case, it is equivalent to imposing the following condition[165]

$$\frac{\partial}{\partial c_z} G(\vec{c}, \vec{c}'; L)\,|_{c_z \to 0,\, c'_z \geq 0} = \delta_0 G(\vec{c}, \vec{c}'; L) \qquad (3.20a)$$

such that

$$G(\vec{c}, \vec{c}'; L) \to 0 \qquad \begin{array}{l} as\ c_z\ or/and\ c'_z \to \infty \\ and\ \ |\vec{c} - \vec{c}'| \to \infty \end{array} \qquad (3.20b)$$

Since we are only interested in the z dependence (where z is the direction perpendicular to the wall), we can Fourier-transform all directions parallel to the wall. It is more convenient to work with the ordinary differential equation, therefore the chain-length dependence was Laplace-transformed. The end-to-end distribution function becomes

$$G(\vec{k}; c_z, c_z'; s) = \int_0^\infty dL\, e^{-sL} \int d(\vec{c}_{//} - \vec{c}'_{//})\, e^{-i\vec{k}\cdot(\vec{c}_{//} - \vec{c}'_{//})} \; G(\vec{c}_{//} - \vec{c}'_{//}; c_z, c_z'; L) \tag{3.21}$$

For notational convenience, let us write $G(\vec{k}; c_z, c_z'; s) = G_{FL}(z,z')$. Note that z here is not identical to the third component of $\vec{r}$, but $z \equiv c_z$. The diffusion equation and its boundary conditions now become

$$\left(\frac{p^2}{2} - \frac{1}{2}\frac{\partial^2}{\partial z^2}\right) G_{FL}(z,z') = \delta(z-z') \tag{3.22}$$

where $p^2 = k^2 + 2s$, and

$$\frac{\partial}{\partial z} G_{FL}(z,z')\Big|_{z\to 0} = \delta_0 G_{FL}(z,z')$$

$$\text{and } G_{FL}(z,z') \to 0 \quad \text{as } z \text{ and/or } z' \to \infty \tag{3.23}$$

$$\text{and } |z-z'| \to \infty$$

The solution of (3.22) that satisfies the boundary condition (3.23) is

$$G_{FL}(z,z') = \frac{1}{p}\left\{e^{-p|z-z'|} + \frac{p-\delta_0}{p+\delta_0} e^{-p(z+z')}\right\} \tag{3.24}$$

Using the inverse Laplace transforms

$$\mathcal{L}^{-1}\left\{\frac{e^{-k\sqrt{s}}}{\sqrt{s}(a+\sqrt{s})}\right\} = e^{ak+a^2t}\,erfc(a\sqrt{t}+\frac{k}{2\sqrt{t}}) \qquad (3.25a)$$

$$\mathcal{L}^{-1}\{f(a+s)\} = e^{-at}\mathcal{L}^{-1}\{f(s)\} \qquad (3.25b)$$

$$\mathcal{L}^{-1}\left\{\frac{e^{-k\sqrt{s}}}{a+\sqrt{s}}\right\} = \frac{1}{\sqrt{\pi t}}\,e^{-\frac{k^2}{4t}} - a\,e^{ak+a^2t}\,erfc(a\sqrt{t}+\frac{k}{2\sqrt{t}}) \qquad (3.25c)$$

one may obtain

$$G_p(\vec{k};z,z';L) = (2\pi L)^{-\frac{1}{2}}\,e^{-\frac{k^2}{2}L}\left\{e^{-\frac{(z-z')^2}{2L}} + e^{-\frac{(z+z')^2}{2L}}\right\} - \delta_0\,e^{\delta_0(z+z')+\delta_0^2\frac{L}{2}}\,e^{-\frac{k^2L}{2}}\,erfc(\delta_0\sqrt{\frac{L}{2}}+\frac{z+z'}{\sqrt{2L}}) \qquad (3.26)$$

The end-to-end distribution function in the d dimensional space is the inverse Fourier transform of equation (3.26). Straightforward calculation yields

$$G(\vec{c},\vec{c}';L) = G_{//}(\vec{c}_{//},\vec{c}'_{//};L)\;G_{\perp}(\vec{c}_z,\vec{c}'_z;L) \qquad (3.27a)$$

with

$$G_{//}(\vec{c}_{//},\vec{c}'_{//};L) = (2\pi L)^{-\frac{d-1}{2}}\,e^{-\frac{(\vec{c}_{//}-\vec{c}'_{//})^2}{2L}} \qquad (3.27b)$$

and

$$G_{\perp}(c_z, c_z'; L) = (2\pi L)^{-\frac{1}{2}} \left\{ e^{-\frac{|c_z - c_z'|^2}{2L}} + e^{-\frac{(c_z + c_z')^2}{2L}} \right\}$$

$$- \delta_0 \exp\{\frac{\delta_0^2 L}{2} + \delta_0 (c_z + c_z')\} \, erfc(\delta_0 \sqrt{\frac{L}{2}} + \frac{c_z + c_z'}{\sqrt{2L}}) \qquad (3.27c)$$

Note that the end-to-end distribution function can be factorized into the parallel and perpendicular parts since there is no interaction between chain segments. When $\delta_0 = 0$, we may obtain the distribution function of a gaussian chain confined in the half-space. When $\delta_0 \to \infty$, which corresponds to the infinitely repulsive wall, one can use the property of the error-function

$$erfc\, x|_{x \to \infty} \sim \frac{2}{\sqrt{\pi}} e^{-x^2} [\frac{1}{2x} - \frac{1}{2^2 x^3} + \ldots .] \qquad (3.28)$$

to obtain

$$G_{\perp}(c_z, c_z'; L) = (2\pi L)^{-\frac{1}{2}} \{ e^{-\frac{|c_z - c_z'|^2}{2L}} - e^{-\frac{(c_z + c_z')^2}{2L}} \} \qquad (3.29)$$

Equation (3.29) indicates that when c_z and/or c_z' $\to$ 0, $G(\vec{c},\vec{c}';L)$ vanishes. We expect this behavior since the segment occupancy at the infinitely repulsive wall has to be zero.

Let us consider the segment density as a function of the distance from the wall

$$\rho(c_z; L) = A\int d(\vec{c}_{//}-\vec{c}'_{//}) \int d(\vec{c}_{//}-\vec{c}''_{//}) \int_0^{\infty} dc'_z \int_0^{\infty} dc''_z \int_0^{L} d\tau\, G(\vec{c}-\vec{c}';\tau)\, G(\vec{c}-\vec{c}'';L-\tau) \tag{3.30}$$

A is the normalization constant defined such that $\rho/\rho_B|_{z\to\infty} = 1$, where ρ_B is the bulk density. If we Laplace-transform $\rho(c_z; L)$, equation (3.30) becomes

$$\mathcal{L}[\rho(c_z;L)] = A\int_0^{\infty} dc'_z \int_0^{\infty} dc''_z\, \mathcal{L}[\int_0^{L} d\tau\, G(\vec{k}=0, c'_z, c_z;\tau)\, G(\vec{k}=0, c_z, c''_z; L-\tau)] \tag{3.31}$$

Using a convenient notation $c_z \equiv z$ and the Laplace-transform of the convolution integral, one may obtain

$$\mathcal{L}[\rho(z;L)] = A\int_0^{\infty} dz' \int_0^{\infty} dz''\, G_{FL}(\vec{k}=0, z', z; s)\, G_{FL}(\vec{k}=0, z, z''; s) \tag{3.32}$$

We now integrate Eqn. (3.32) with respect to z' and z" coordinates. Substituting relation (3.24) for k = 0 in equation (3.32), it yields

$$\mathcal{L}[\rho(z;L)] = A\left[\frac{1}{s} - \frac{\delta_0 e^{-\sqrt{2s}z}}{s(\sqrt{2s}+\delta_0)}\right]^2 \qquad (3.33)$$

Using the following inverse Laplace-transforms

$$\mathcal{L}^{-1}\left\{\frac{a e^{-k\sqrt{s}}}{s^2(a+\sqrt{s})}\right\} = erfc\left(\frac{k}{2\sqrt{t}}\right)\left[\frac{1}{2a^2}(2ak+2+a^2k^2+2a^2t)\right] + e^{-\frac{k^2}{4t}}\left[-\frac{2}{a}\sqrt{\frac{t}{\pi}} - k\sqrt{\frac{t}{\pi}}\right] - \frac{e^{ak+a^2t}}{a^2} erfc\left(a\sqrt{t}+\frac{k}{2\sqrt{t}}\right) \qquad (3.34a)$$

and

$$\mathcal{L}^{-1}\left\{\frac{a e^{-k\sqrt{s}}}{s^2(a+\sqrt{s})^2}\right\} = \left[\frac{1}{2a^3}(4ak+6+a^2k^2+2a^2t)\right] erfc\left(\frac{k}{2\sqrt{t}}\right) + \left[\frac{k}{a^2}+\frac{2at}{a^2}-\frac{3}{a^3}\right] e^{ak+a^2t} erfc\left(a\sqrt{t}+\frac{k}{2\sqrt{t}}\right) + \left[-\frac{6}{a^2}\sqrt{\frac{t}{\pi}} - \frac{k}{a}\sqrt{\frac{t}{\pi}}\right] e^{-\frac{k^2}{4t}} \qquad (3.34b)$$

After tedious calculation and by setting $\rho(c_z, L)|_{c_z=-\infty}=\rho_B$ one obtains

$$\frac{\rho(c_z,L)}{\rho_B} = 1 - \frac{2}{L}\left\{\left(\frac{2c_z}{\delta_0} + \frac{2}{\delta_0^2} + c_z^2 + L\right) erfc\left(\frac{c_z}{\sqrt{2L}}\right)\right.$$

$$\left. - \left(\frac{2}{\delta_0}\sqrt{\frac{2L}{\pi}} + c_z\sqrt{\frac{2L}{\pi}}\right) e^{-\frac{c_z^2}{2L}} - \frac{2}{\delta_0^2}\, e^{\delta_0 c_z + \delta_0^2 \frac{L}{2}}\, erfc\left(\delta_0\sqrt{\frac{L}{2}} + \frac{c_z}{\sqrt{2L}}\right)\right\}$$

$$+ \left(\frac{8c_z}{\delta_0 L} + \frac{6}{\delta_0^2 L} + \frac{4c_z^2}{L} + 1\right) erfc\left(c_z\sqrt{\frac{2}{L}}\right) - \left(\frac{6\sqrt{2}}{\delta_0\sqrt{L\pi}} + \frac{2c_z\sqrt{2}}{\sqrt{L\pi}}\right) e^{-2\frac{c_z^2}{L}}$$

$$+ \frac{\delta_0}{L\sqrt{2}}\left(\frac{4c_z\sqrt{2}}{\delta_0^2} + \frac{2\sqrt{2}L}{\delta_0} - \frac{6\sqrt{2}}{\delta_0^3}\right) e^{2\delta_0 c_z + \delta_0^2 \frac{L}{2}}\, erfc\left(\delta_0\sqrt{\frac{L}{2}} + c_z\sqrt{\frac{2}{L}}\right)$$

(3.35)

From equation (3.35) the segment density at the wall is given by

$$\frac{\rho_N}{\rho_B} = \frac{\rho(c_z=0;L)}{\rho_B}$$

$$= \frac{2}{\delta_0^2 L} - \frac{2\sqrt{2}}{\delta_0\sqrt{L\pi}} + \left(2 - \frac{2}{\delta_0^2 L}\right) e^{\delta_0^2 \frac{L}{2}}\, erfc\left(\delta_0\sqrt{\frac{L}{2}}\right) \qquad (3.36)$$

Let us discuss the limiting case in which $\delta_0 \to \infty$, corresponding to the infinitely repulsive wall. Equation (3.35) becomes

$$\frac{\rho(c_z, L)}{\rho_B} = 1 - 2\left[\{1 + \frac{c_z^2}{L}\} erfc(\frac{c_z}{\sqrt{2L}}) - \frac{c_z\sqrt{2}}{L\pi} e^{-\frac{c_z^2}{2L}}\right]$$

$$+ (1 + \frac{4c_z^2}{L}) erfc(\frac{c_z\sqrt{2}}{\sqrt{L}}) - \frac{2c_z\sqrt{2}}{\sqrt{L\pi}} e^{-2\frac{c_z^2}{L}} \qquad (3.37)$$

When $c_z^2 \ll L$ and $c_z \sim 0$, the segment density near the repulsive wall will decrease to zero as

$$\frac{\rho(c_z, L)}{\rho_B} \sim \frac{2c_z^2}{L} \qquad (3.38)$$

The exponent of c_z in (3.38) is in agrrement with the previous result in equation (3.12) provided ν=1/2 for the ideal chain.

The case of strongly attractive wall $\delta_0 < 0$ and $|\delta_0| \gg 1$ can be analyzed in similar fashion. The segment density and its value at the wall are respectively given by

$$\frac{\rho(c_z, L)}{\rho_B} = 1 - 2(1 + \frac{c_z^2}{L}) erfc(\frac{c_z}{\sqrt{2L}}) + \frac{2c_z\sqrt{2}}{\sqrt{L\pi}} e^{-\frac{c_z^2}{2L}}$$

$$+ (1 + \frac{4c_z^2}{L}) erfc(c_z\sqrt{\frac{2}{L}}) - \frac{2c_z\sqrt{2}}{\sqrt{L\pi}} e^{-2\frac{c_z^2}{L}}$$

$$+ 4\exp[-2c_z|\delta_0| + \delta_0^2\frac{L}{2}] \qquad (3.39)$$

and

$$\frac{\rho_N}{\rho_B} = 4\, e^{\delta_0^2 \frac{L}{2}} \tag{3.40}$$

The results in our discussion agree with the results obtained by Eisenriegler[164] using the polymer-magnet analogy.

For an ideal chain confined between two walls, the boundary condition for the end-to-end distribution function in equation (3.23) is replaced by

$$\frac{\partial}{\partial z} G_{FL}(z, z') \Big|_{z=0(H)} = \pm \delta_0 G_{FL}(z, z') \Big|_{z=0(H)} \tag{3.41}$$

The solution of the diffusion equation which satisfies these boundary conditions is

$$\begin{aligned} G_{FL}(z, z'; H) = {} & \frac{2}{p}\left[\frac{p+\delta_0}{p-\delta_0} e^{pH} - \frac{p-\delta_0}{p+\delta_0} e^{-pH}\right]^{-1} \\ & \{\cosh[pH - p(z+z')] + \cosh[pH - p|z-z'|] \\ & + \frac{\delta_0}{p-\delta_0} e^{p(H-|z-z'|)} - \frac{\delta_0}{p+\delta_0} e^{-p(H-|z-z'|)}\Big\} \end{aligned} \tag{3.42}$$

Note that when $H \to \infty$, $G_{FL}(z,z';H) \to G_{FL}(z,z')$ of equation (3.24).

When the wall is infinitely repulsive, the distribution function becomes

$$G_{FL,R}(z,z';H)=\frac{1}{p\sinh pH}\left[\cosh\{pH-p|z-z'|\}-\cosh\{pH-p(z+z')\}\right] \tag{3.43}$$

and the segment density is

$$\rho(z;L)=\int_0^H dz'\int_0^H dz''\int_0^L d\tau\, G_{F,R}(\vec{k}=0,z',z;\tau,H)\,G_{F,R}(\vec{k}=0,z,z'';L-\tau,H) \tag{3.44}$$

with $G_{F,R}$ is given by

$$G_{F,R}(\vec{k}=0;z',z;\tau,H)=\mathcal{L}^{-1}\{G_{FL,R}(z,z';H)\}$$

$$=\frac{1}{H}\sum_{n=1}^{\infty}e^{-\frac{n^2\pi^2}{2H^2}\tau}\left(\cos\frac{n\pi|z-z'|}{H}-\cos\frac{n\pi(z+z')}{H}\right) \tag{3.45}$$

Integrating with respect to z' and z" we obtain

$$\rho(c_z;L)=\frac{16L}{\pi^2}\left\{\sum_{n=1}^{\infty}\frac{\sin^2(\frac{2n-1}{H}\pi c_z)}{(2n-1)^2}e^{-\frac{(2n-1)^2\pi^2}{2H^2}L}+2\sum_{n=1}^{\infty}\sum_{m>n}\frac{\sin(\frac{2n-1}{H}\pi c_z)\sin(\frac{2m-1}{H}\pi c_z)}{(2n-1)(2m-1)}I_{m,n}(\frac{\pi^2L}{2H^2})\right\} \tag{3.46a}$$

where

$$I_{m,n}(x) = \frac{1}{x}\frac{e^{-(2n-1)^2x} - e^{-(2m-1)^2x}}{(2m-1)^2 - (2n-1)^2} \qquad m \neq n \qquad (3.46b)$$

Note that when c_z is equal to 0 or H, $\rho(c_z, L)$ vanishes as we expect it for the strongly repulsive wall. In figure (3.2) we plot segment density as a function of distance for various values of H and chain-length L. To make this plot we have truncated the infinite sums, and retained the first 25 terms.

3.3. A Renormalization Group Analysis for Segment Density Near A Strongly Repulsive Wall.

The problem of the segment density profile near a repulsive wall has been analyzed using various methods. In addition to the scaling technique, the renormalization group method has been applied to polymer systems via the n-vector model[164,165]. In this section, the conformational renormalization group method and perturbation techniques are employed to derive the scaling property of the segment density profile of a single chain near a repulsive wall at $z \to 0$. The calculation was done to $O(\epsilon)$, where $\epsilon = 4-d$. By a repulsive wall, we mean that no chain segment may occupy any site at the wall. If δ_0 is the parameter describing the strength of the wall-segment interaction, the repulsive-wall condition is obtained by taking $\delta_0 \to \infty$. This condition also simplifies the calculation.

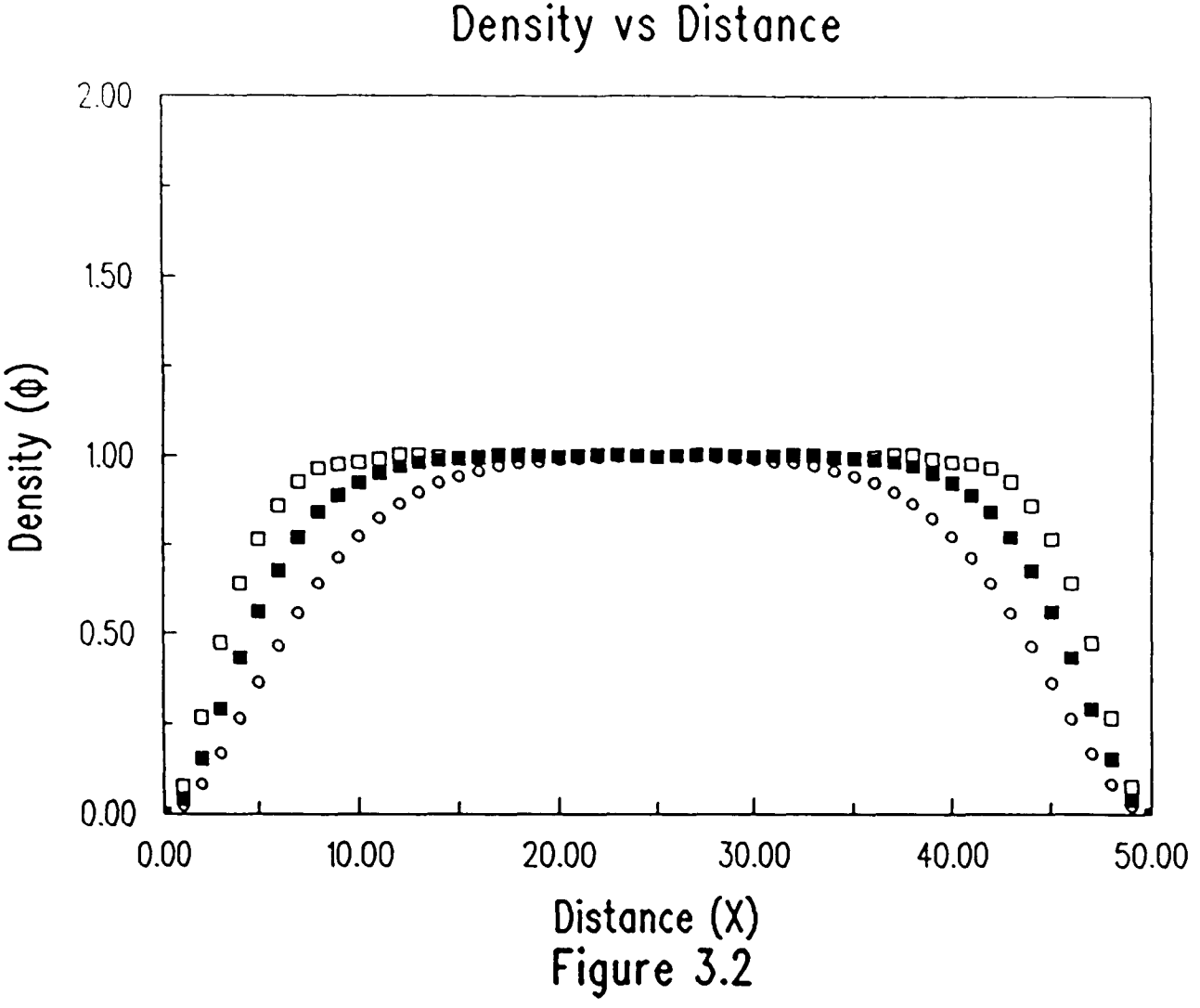
Density vs Distance
2.00
1.50
1.00
0.50
0.00
Density (ϕ)
0.00
10.00
20.00
30.00
40.00
50.00
Distance (X)

Figure 3.2

Let $\rho(z)$ be the segment linear-density at a distance z from the wall. For a system with fixed concentration, one expects that as $z\to\infty$, $\rho(z)$ will assume its bulk value ρ_B. The situation is not obvious for a single chain, since $\rho(z)\to 0$ as $z\to\infty$. Also $\rho(z)=0$ if we consider the whole half space. In our calculation, therefore, we are only interested in the segment density profile of a single chain occupying a box adjacent to the wall (see figure 3.3). This box has a volume V=LA, where A is the area of the plane parallel to the wall and L is the linear-size of the box along the perpendicular direction. The area A will be cancelled after integrating the coordinates parallel to the wall ($\tilde{\rho}$), and we expect that $L\rho(z) \propto z^m$ as $z\to 0$. The calculation of $\rho(z)$ is performed up to the lowest order (a one-loop calculation), and for simplicity of calculation some approximation are made (e.g., $L \to \infty$ etc.).

Consider a single chain of length N_0 and with excluded volume parameter u_0. The subindices indicate that those parameters are unrenormalized. They are called 'bare' parameters in field theories. Let the chain-ends be at $\vec{c}_0$ and $\vec{c}_N$ and $\vec{c}$ be the coordinate of a point on this chain. The corresponding distribution function is

$$G_0(\vec{c}_0, \vec{c}, \vec{c}_N; N_0, \tau; u_0) = \int_{\vec{c}_0;\, z(s)\geq 0}^{\vec{c}_N} D[\vec{c}(\tau')]\, \delta[\vec{c}(\tau)-\vec{c}]\, e^{-H} \qquad (3.47)$$

where $z(s) \equiv c_1(s)$ is the vector component perpendicular to the wall. H is the Hamiltonian given in eqn. (3.16). The constraint $z(s) \geq 0$ is imposed by requiring that the chain never crosses the wall.

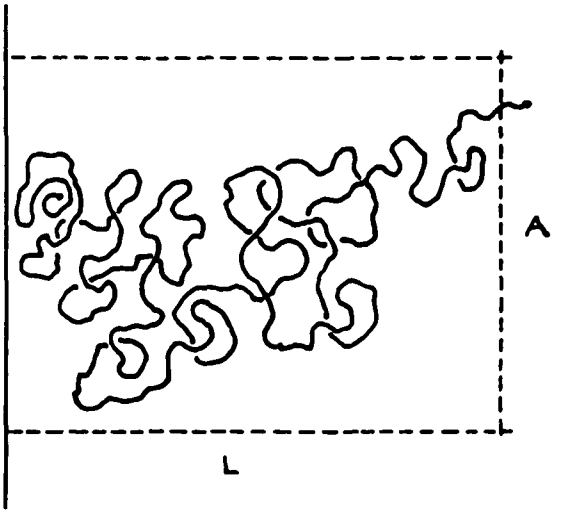

Figure 3.3. A polymer chain near a repulsive wall

The segment density at a distance z from the wall, irrespective of end-segment positions, is

$$L\rho_0(z) = \frac{L}{V}\int d\vec{c}_0 \int d\vec{c}_N \int d\vec{c}_{//} \int_0^{N_0} d\tau\, G_0(\vec{c}_0, \vec{c}, \vec{c}_N; N_0, \tau; u_0) \quad (3.48)$$

We then assume that the excluded volume potential is as a perturbation to the ideal Gaussian chain. Expanding the exponent in eqn. (3.47), we obtain

$$L\rho_0(z) = \frac{L}{V}\int d\vec{c}_0 \int d\vec{c}_N \int d\vec{c}_{//} \int_0^{N_0} d\tau \{G_0^{(0)}(\vec{c}_0, \vec{c}; \tau)\, G_0^{(0)}(\vec{c}, \vec{c}_N; N_0 - \tau) -$$

$$- \frac{u_0}{2} \int_{\vec{c}_0;\, z(s)\geq 0}^{\vec{c}_N} D[\vec{c}(\tau')]\, \delta[\vec{c}(\tau) - \vec{c}] \int_0^{N_0} ds \int_0^{N_0} ds'\, \delta[\vec{c}(s) - \vec{c}(s')]\, e^{-H_g} \tag{3.49}$$

where $G_0^{(0)}$ is the ideal chain distribution defined over the half-space. H_g is the Hamiltonian of the gaussian chain. We can represent the location of the segment τ by (×) and the point of contact between two segments by (o). If the SAW chain is represented by a double line (====) and the gausian chain by a single line (----), eqn. (3.49) may be expressed diagrammatically as

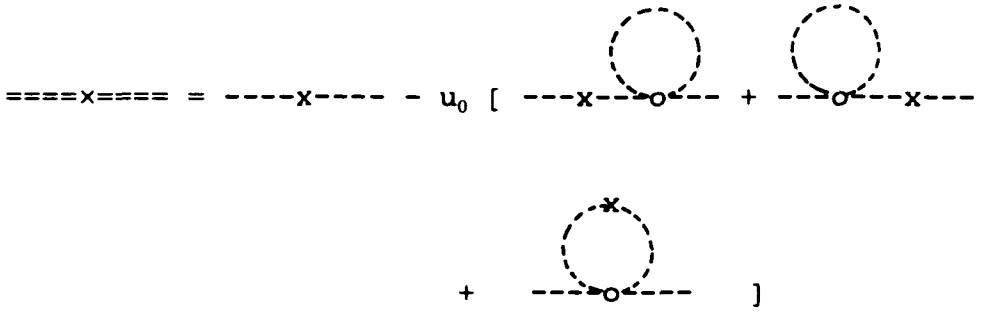

Figure 3.4. A diagrammatic representation of the segment density calculations.

The factor 1/2 in u_0 is cancelled out because of the symmetry related to the choice of contour direction. The segment τ may reside on the chain portion between contact segments or outside the loop. Note that by symmetry the first two diagrams give identical contributions.

Let us consider the first diagram. The distribution function for a gaussian chain in half space is obtained from eqn (3.27) by allowing $\delta_0 \to \infty$.

$$G_0^{(0)}(\vec{\rho}-\vec{\rho}';z,z';N_0) = (2\pi N_0)^{-d/2} e^{-\frac{(\vec{\rho}-\vec{\rho}')^2}{2N_0}} \{e^{-\frac{|z-z'|^2}{2N_0}} - e^{-\frac{(z+z')^2}{2N_0}}\} \tag{3.50}$$

Inserting eqn.(3.50) into (3.49) and integrating the end-segment coordinates, $\vec{\rho}_0$ and $\vec{\rho}_N$, we obtain

$$L\rho^{(0)}(z,N_0) = \int dz_0 \int dz_N \int_0^{N_0} d\tau\, [2\pi\tau]^{-1/2} [2\pi(N_0-\tau)]^{-1/2} \times \tag{3.51}$$
$$\times \{e^{-\frac{|z-z_0|^2}{2\tau}} - e^{-\frac{(z+z_0)^2}{2\tau}}\} \{e^{-\frac{|z-z_N|^2}{2(N_0-\tau)}} - e^{-\frac{(z+z_N)^2}{2(N_0-\tau)}}\}$$

We can Laplace-transform the N_0 parameter in $\rho^{(0)}$ and obtain

$$L\rho^{(0)}(z,s_0) = L\mathcal{L}\rho^{(0)}(z,N_0)$$

$$= \int dz_0 \int dz_N f(z,z_0;s_0)\, f(z,z_N;s_0) \qquad (3.52)$$

where

$$f(z,z';s_0) = \frac{1}{\sqrt{(2s_0)}}\{e^{-\sqrt{(2s_0)}|z-z'|} - e^{\sqrt{(2s_0)}(z+z')}\} \qquad (3.53)$$

Integrating with respect to z_0 and z_N, eqn. (3.52) yields

$$L\rho^{(0)}(z,s_0) = \frac{1}{s_0^2}\{1 - e^{-z\sqrt{2s_0}}\}^2 \qquad (3.54)$$

In the limit $z \to 0$, the previous equation gives

$$L\rho^{(0)}(z,s_0) \sim \frac{2z^2}{s_0} \qquad (3.55)$$

The calculation of the first diagram is tedious. Let us call the position of (x) along the chain τ_1, and let the positions along the contour of the self-intersection, (o), as τ_2 and τ_3. These points are located at $(\vec{\rho},z)$ and $(\vec{\rho}',z')$, respectively (see figure 3.5)

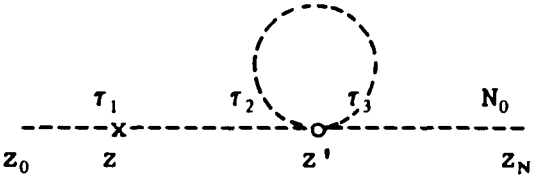

Figure 3.5. A one-loop diagram for the calculation of the segment density to $O(\epsilon)$.

This diagram is represented by the following integral

$$I = \frac{L}{V}\int d\vec{\rho}\int d\vec{c}_0\int d\vec{c}_N\int d\vec{c}'\int_0^{N_0} d\tau_3\int_0^{\tau_3} d\tau_2\int_0^{\tau_2} d\tau_1\, G_0^{(0)}(\vec{\rho}_0-\vec{\rho};z_0,z;\tau_1)\times$$

$$\times\, G_0^{(0)}(\vec{\rho}-\vec{\rho}';z,z';\tau_2-\tau_1)\, G_0^{(0)}(\vec{\rho}'-\vec{\rho}';z',z';\tau_3-\tau_2)\times$$

$$\times\, G_0^{(0)}(\vec{\rho}'-\vec{\rho}_N;z',z_N;N_0-\tau_3) \qquad (3.56)$$

Fourier transforming with respect to the coordinates parallel to the wall, and Laplace transforming with respect to N_0 yields

$$L\rho^{(1)}(z,s_0) = \int dz_0\int dz_N\int dz'\int \frac{d\vec{k}}{(2\pi)^{d-1}}\, G_{FS}^{(0)}(k=0;z_0,z;s_0)\times$$

$$\times\, G_{FS}^{(0)}(k=0;z,z';s_0)\, G_{FS}^{(0)}(k;z';z';s_0)\, G_{FS}^{(0)}(k=0;z',z_N;s_0) \qquad (3.57)$$

with

$$G_{FS}^{(0)}(k;z,z';s_0) = \frac{1}{p}\{e^{-p|z-z'|} - e^{p(z+z')}\} \qquad (3.58)$$

and $p = (2s_0+k^2)^{1/2}$. Integration of z_0 and z_N will reduce equation (3.57) to

$$L\rho^{(1)}(z,s_0) = \frac{1}{s_0^{5/2}\sqrt{2}}\{1 - e^{-z\sqrt{2s_0}}\}\{\rho_A^{(1)} - \rho_B^{(1)}\} \qquad (3.59)$$

where

$$\rho_B^{(1)} = \int_0^\infty dz'\{e^{-|z-z'|\sqrt{2s_0}} - e^{-(z+z')\sqrt{2s_0}}\}\{1 - e^{-z'\sqrt{2s_0}}\} \times$$

$$\times \int \frac{d\vec{k}}{(2\pi)^{d-1}} \frac{e^{-(z'+z'')\sqrt{2s_0+k^2}}}{\sqrt{2s_0+k^2}}\Big|_{z''\to z'} \qquad (3.60)$$

and $\rho_A^{(1)}$ has the same form as equation (3.60) except that the 'momentum' integration is replaced by

$$\int \frac{d\vec{k}}{(2\pi)^{d-1}} \frac{e^{-|z'-z''|\sqrt{2s_0+k^2}}}{\sqrt{2s_0+k^2}}\Big|_{z''\to z} \qquad (3.61)$$

Equation (3.60) involves an integration of the following form

$$I_0 = \int \frac{d\vec{k}}{(2\pi)^{d-1}} e^{i\vec{k}\cdot\vec{\rho}} \frac{e^{-2z'p}}{p}\Big|_{\vec{\rho}=0}$$

$$= \frac{1}{(2\pi)^{d-1}\rho^{\frac{d-3}{2}}} \int_0^\infty dk\, k^{\frac{d-1}{2}} J_{\frac{d-3}{2}}(k\rho) \frac{e^{-2z'p}}{p}\Big|_{\vec{\rho}=0} \qquad (3.62)$$

where $J_\nu(x)$ is the Bessel function of the first kind. Using the following definition of the modified Bessel function [see Ref. 166, Eqn. 8.432.3]

$$K_\nu(z) = \frac{\frac{z^\nu}{2}\Gamma(\frac{1}{2})}{\Gamma(\nu+\frac{1}{2})}\int_1^\infty e^{-zt}(t^2-1)^{\nu-\frac{1}{2}}\,dt \qquad (3.63)$$

$$[Re(\nu+\tfrac{1}{2})>0, |\arg z|<\tfrac{\pi}{2}; \text{or } Re\, z = 0 \text{ and } \nu = 0]$$

and the following relation [Ref. 166, Eqn. 6.596.7]

$$\int_0^\infty \frac{J_\nu(\beta x)\,K_\mu(\alpha\sqrt{x^2+z^2})\,x^{\nu+1}}{\sqrt{(x^2+z^2)^\mu}}\,dx = \frac{\beta^\nu}{\alpha^\mu}\left(\frac{\sqrt{\alpha^2+\beta^2}}{z}\right)^{\mu-\nu-1} K_{\mu-\nu-1}(z\sqrt{\alpha^2+\beta^2})$$

$$[\alpha>0, \beta>0, Re\,\nu>-1, |\arg z|<\tfrac{\pi}{2}] \qquad (3.64)$$

I_0 in equation (3.59) becomes

$$I_0 = \frac{1}{(2\pi)^{d-1}}\sqrt{\frac{2}{\pi}}\left(\frac{4z^2}{2s_0}\right)^{-\frac{d-2}{4}} K_{\frac{d-2}{2}}(2z\sqrt{2s_0}) \qquad (3.65)$$

In deriving (3.64) we also use the symmetric property of the modified Bessel function $K_{-\nu}(x) = K_{\nu}(x)$. In the renormalization group calculation of polymer in full space and half space[69,84], u_0 is of $O(\epsilon)$, so we can set d = 4 for the loop-diagram calculations. The integral in Eqn. (3.60) now becomes

$$\rho_B^{(1)} = \frac{\sqrt{2s_0}}{(2\pi)^2} [I_1 - I_2 - I_3 + I_4] \qquad (3.66a)$$

The four terms inside the bracket are

$$I_1 = \int_0^\infty dz' \{ e^{-|z-z'|\sqrt{2s_0}} \frac{K_1(az')}{z'} \} \qquad (3.66b)$$

$$I_2 = \int_0^\infty dz' \{ e^{-(z+z')\sqrt{2s_0}} \frac{K_1(az')}{z'} \} \qquad (3.66c)$$

$$I_3 = \int_0^\infty dz' \{ e^{-|z-z'|\sqrt{2s_0} - z'\sqrt{2s_0}} \frac{K_1(az')}{z'} \} \qquad (3.66d)$$

$$I_4 = \int_0^\infty dz' \{ e^{-(z+2z')\sqrt{2s_0}} \frac{K_1(az')}{z'} \} \qquad (3.66e)$$

where $a=2\sqrt{2s_0}$. Here we give the calculation of I_2, since it involves the simplest integration and others follow a similar line. In this calculation it is necessary to introduce a cut-off Λ when $z' \to 0$, otherwise the integral is singular.

Physically the cut-off may be explained by recognizing that the chain segment never touches the wall. So Λ has the dimension of a monomer size. At the end of the calculation this singularity will be cancelled by a renormalization constant.

To calculate I_2, we use the series expansion of $K_n(z)$ [Ref. 166, Eqn. 8.446]

$$K_n(z) = \frac{1}{2}\sum_{k=0}^{n-1}(-)^k \frac{(n-k-1)!}{k!\,(z/2)^{n-2k}} + \\ + (-)^{n+1}\sum_{k=0}^{\infty}\frac{(z/2)^{n+2k}}{k!\,(n+k)!}\left[\log\frac{z}{2} - \frac{1}{2}\psi(k+1) - \frac{1}{2}\psi(n+k+1)\right] \tag{3.67}$$

where $\psi(k)$ is the digamma function. This integration involving $(1/z^2)\exp[-z\sqrt{2s_0}]$, which comes from the first term of Eqn. (3.67), is singular because of the vanishing lower-bound. Therefore, we introduce a cut-off:

$$\int_0^{\infty} dz' \frac{e^{-z'\sqrt{2s_0}}}{z'^2} \to \int_{\Lambda}^{\infty} dz' \frac{e^{-z'\sqrt{2s_0}}}{z'^2} = \frac{1}{\Lambda}E_2(\Lambda\sqrt{2s_0})\big|_{\Lambda\to 0} \sim \frac{1}{\Lambda} \tag{3.68}$$

where $E_n(x)$ is the exponential integral. Using the following Laplace transforms[167]

$$\int_0^\infty dz' e^{-z'p} (z')^n = \frac{n!}{p^{n+1}} \tag{3.69}$$

$$\int_0^\infty dz' e^{-z'p} (z')^{\nu-1} \log z' = \Gamma(\nu) p^{-\nu} [\psi(\nu) - \log p] \tag{3.70}$$

we obtain

$$I_2 = e^{-z\sqrt{2s_0}} \left[\frac{1}{\Lambda 2\sqrt{2s_0}} - \sum_{k=0}^{\infty} \frac{(2k)!}{k!\,(k+1)!} \left\{ \frac{1}{2} \psi(k+1) + \right. \right. \tag{3.71}$$

$$\left. \left. + \frac{1}{2} \psi(k+2) - \psi(2k+1) \right\} \right]$$

Calculations of I_1, I_3, and I_4 follow a similar line. After taking the limit $z \to 0$, the dominant term of $\rho_B^{(1)}$ is given by

$$\rho_B^{(1)} \sim -\left[\frac{2s_0}{(2\pi)^2}\right](z \log z/\Lambda) \tag{3.72}$$

Returning to the first part of $\rho^{(1)}$, the integration is also plagued by singularities. For example, equation (3.61) is divergent when z=z' and d = 4. To avoid this, we also introduce the cut-off Λ, so Eqn. (3.61) is proportional to $K_1(\Lambda 2\sqrt{2s_0})/\Lambda$. The calculation is then simplified. We obtained the dominant terms, one is proportional to Λ^{-2}, and the other

is proportional to $z[\log(z/\Lambda)]$. The coeficient of $z\log(\Lambda)$ is the same as the one in Eqn. (3.72). Summing up $\rho_A^{(1)}$ and $\rho_B^{(1)}$, in the limit $z \to 0$, the dominant terms of Eqn. (3.59) are

$$L\rho^{(1)} \sim \left[\frac{z^2}{(2\pi)^2 s_0^2}\frac{1}{2\Lambda^2} + \frac{2z^2}{(2\pi)^2 s_0}\log z\right] \qquad (3.73)$$

The calculation of the third loop diagram is also performed using Fourier-Laplace transform. Consider the following diagram

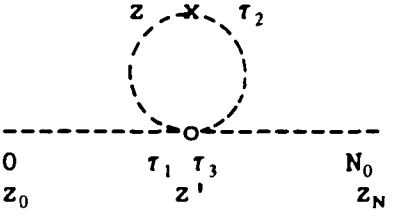

Figure 3.6. Another one-loop diagram.

The corresponding integration is given by

$$L\rho^{(2)} = \frac{L}{V}\int d\vec{\rho}\int d\vec{c}_0\int d\vec{c}_N\int d\vec{\rho}'\int dz'\int_0^{N_0} d\tau_3\int_0^{\tau_3} d\tau_2\int_0^{d}\tau_2 d\tau_1\, G_0^{(0)}(\vec{\rho}_0-\vec{\rho}';z_0,z';\tau_1)\times$$

$$\times\, G_0^{(0)}(\vec{\rho}'-\vec{\rho};z',z;\tau_2-\tau_1)\, G_0^{(0)}(\vec{\rho}'-\vec{\rho};z',z;\tau_3-\tau_2)\times$$

$$\times\, G_0^{(0)}(\vec{\rho}'-\vec{\rho}_N;z',z_N;N-\tau_3) \qquad (3.74)$$

Integrating the end segment coordinates and Fourier-Laplace transforming the previous equation, we obtain

$$L\rho^{(2)} = \int dz' \int \frac{d\vec{k}}{(2\pi)^{d-1}} \left[\frac{1}{s_0} (1 - e^{-z'\sqrt{2s_0}}) G_{FS}^{(0)}(\vec{k}; z'; z; s) \right]^2 \tag{3.75}$$

When z << 1, we can use the following approximation of the distribution function

$$G_{FS}^{(0)} = \frac{1}{\sqrt{2s_0+k^2}} \left[e^{-(z-z')\sqrt{k^2+2s_0}} - e^{-(z'+z)\sqrt{k^2+2s_0}} \right] \theta(z-z') + z' \leftrightarrow z \tag{3.76}$$

We can neglect the first term involving $\int_0^z dz'$, for $z \to 0$, since it is insignificant compared to terms with $\int_z^\infty dz'$. Letting x = z'-z and using the definition of K, in Eqn. (3.63), and the integration in (3.64), equation (3.75) becomes

$$L\rho^{(2)}(z, s_0) = II_1 + II_2 + II_3 \tag{3.77}$$

where

$$II_1 = \frac{8z^2}{(2\pi)^2 s_0} \int_0^\infty dx \frac{K_2(2x\sqrt{2s_0})}{x} \tag{3.77a}$$

$$II_2 = \frac{8z^2}{(2\pi)^2 s_0} \int_0^\infty dx \, \frac{K_2(2x\sqrt{2s_0})}{x} \, e^{-2x\sqrt{2s_0}} \qquad (3.77b)$$

$$II_3 = \frac{16z^2}{(2\pi)^2 s_0} \int_0^\infty dx \, \frac{K_2(2x\sqrt{2s_0})}{x} \, e^{-x\sqrt{2s_0}} \qquad (3.77c)$$

Evaluation of II_1 can be easily worked out by inverse-Laplace transforming the s_0 parameter. Using the following relation [Ref. 167, Eqn. 5.16.39]

$$\mathcal{L}^{-1}[p^{-\frac{1}{2}\nu} K_\nu(2\alpha^{\frac{1}{2}} p^{\frac{1}{2}})] = \frac{1}{2} t^{\nu-1} e^{-\frac{\alpha}{t}} \alpha^{-\frac{1}{2}\nu} \qquad (3.78)$$

equation (3.77a) becomes

$$\mathcal{L}^{-1}[II_1] = \frac{z^2 N_0}{2\pi^2} \int_\Lambda^\infty dx \, \frac{e^{-\frac{2x^2}{N_0}}}{x^3} \qquad (3.79)$$

As $\Lambda \to 0$, the integral diverges as $1/(2\Lambda^2)$, and

$$\mathcal{L}^{-1}[II_1] \sim \frac{z^2 N_0}{2\pi^2} \left(\frac{1}{2\Lambda^2}\right) \qquad (3.80)$$

Calculation of II_2 can be easily performed if we expand $K_2(x)$ as in (3.67). The dominant terms are

$$II_2 \sim \frac{2z^2}{s_0\pi^2}\left[\int_0^\infty dx\, e^{-2x\sqrt{2s_0}}\left\{\frac{1}{4s_0x^3} - \frac{1}{2x}\right\}\right] \qquad (3.81)$$

The first part in (3.81) gives

$$II_2(1^{st}\ part) \sim \frac{2z^2}{s_0\pi^2}\left[\frac{1}{8\Lambda^2 s_0}\right] \qquad (3.82)$$

The second part is easily performed using the inverse-Laplace transform of the s_0 parameter and using the following relation

$$\mathcal{L}^{-1}[p^{-1}e^{-\alpha p^{\frac{1}{2}}}] = Erfc\left(\frac{1}{2}\alpha t^{-\frac{1}{2}}\right) \qquad (3.83)$$

By straightforward calculation and using

$$\int_0^\infty e^{-pt}\frac{\log t}{t^{\frac{1}{2}}}\,dt = -\pi^{\frac{1}{2}}p^{-\frac{1}{2}}\log(4\gamma p), \quad Re\ p>0 \qquad (3.84)$$

we obtain

$$\mathcal{L}^{-1}[II_2(2^{nd}\ part)] = \frac{2z^2}{\pi^2}\left[-\frac{1}{2}\log\left(\frac{N_0^{\frac{1}{2}}}{\Lambda\sqrt{2}}\right) + \frac{1}{4}\log 4\gamma\right] \qquad (3.85)$$

Summing (3.85) and (3.82) gives

$$\mathcal{L}^{-1}[II_2] \sim \frac{2z^2}{\pi^2}\left[\frac{N_0}{8\Lambda^2} + \frac{1}{2}\log\Lambda\right] \qquad (3.86)$$

Calculation of II_3 follows a similar line as the one of II_2, and it gives

$$\mathcal{L}^{-1}[II_3] \sim -\frac{4z^2}{\pi^2}\left[\frac{N_0}{8\Lambda^2} + \frac{1}{2}\log\Lambda\right] \qquad (3.87)$$

After Laplace transforming N_0 parameter, Eqs. (3.80), (3.86), and (3.87) give

$$L\rho^{(2)}(z, s_0) \sim -\frac{z^2}{\pi^2 s_0}\log\Lambda \qquad (3.88)$$

The idea of renormalization group is to absorb the divergences using a renormalization constant. In our case, it is employed to absorb the Λ-dependence in previous results. Since we are only interested in the z-dependence of the density profile, here we only collect terms which are finite and depend on z^2 and $z^2\log(z)$. Collecting our results in Eqs. (3.55), (3.73), and (3.88), we get

$$L\rho(z,s_0) \sim \frac{2z^2}{s_0}\left[1 - \frac{2u_0 \log z}{4\pi^2}\right] \qquad (3.89)$$

Here we use the result of Ref. 84 that at fixed point $u_0 \sim \epsilon\pi^2/2$. Inserting this value into (3.89), and Laplace-transform s_0 parameter, we obtain

$$\begin{aligned} \rho(z) &\sim \frac{2}{L} z^2 \left[1 - \frac{\epsilon}{4} \log z\right] \\ &\sim \frac{2}{L} z^{2\left(1-\frac{\epsilon}{8}\right)} \end{aligned} \qquad (3.90)$$

Thus $m = 2(1-\epsilon/8)$. If $m = 1/\nu$ as given by scaling theories [see Eqn.(3.14)], then $\nu = 1/2+\epsilon/16$ which is in agreement with the result in Ref. 69. Note that the nearest neighbor interaction between non-bonding segments is not explicitly expressed in Edwards' δ-potential, therefore, simulation results of non-athermal chains cannot be easily compared with (3.90). Monte Carlo results for the density profile of athermal and non-athermal self-avoiding chains are presented in Chapter V.

CHAPTER IV. THE LATTICE MODEL OF POLYMER SOLUTIONS.

In our simulations (Chapter V), we employed polymer chains on a regular lattice. The polymer model described in previous chapters are defined on continuum space, and therefore, are not suitable for comparison. In this chapter, we introduce lattice models of polymer solutions; Flory and Flory-Huggins mean field theories[8-14], and Freed's n-vector model[15]. The equation of state obtained in these models will be compared with Monte Carlo results in the next chapter. In the following discussion, we review the deficiencies of Edwards' model.

The conformational space renormalization group (CRG) was built on Edwards' δ-potential model[36,69]. The potential was treated as a perturbation to the random walk model, and the standard techniques of ϵ-expansion and renormalization were performed to remove the singularities (see Chapter III). The δ-potential was the result of approximating a generic potential V_{ij}; this approximation was validated in three dimensions by means of scaling theory[69,146]. The original purpose of Edwards' model was to take into account the excluded volume effect. However, the characteristics of δ-potential allows two monomers to approach arbitrarily close to one another. The potential does not impose an upper-bound on the segment density, which is of course contrary to experimental results. Because of this deficiency, the

application of the model is restricted to dilute and semi-dilute solutions. The problems of polymers in dense solutions or melts, in which the excluded volume effect is significant, must be addressed through different model.

An early attempt to resolve this difficulty was by incorporating higher order interactions into Edwards' model[163]. The idea is that the many-body interactions would place a constraint on the monomer occupancy. The extended model seems artificial, and calculation of physical quantities was cumbersome. Another approach, which lends itself to computer simulations, is to use the n-vector model on a lattice[46,47]. The monomer size is presumably equivalent to the lattice cell. As shown in the Introduction, the original n-vector model of de Gennes suffers several difficulties. For example, dispersity is not controlled, so this model cannot be used to calculate quantities that are sensitive to chain length distribution. The Flory-Huggins equation of state cannot be derived, therefore, any attempt to improve on this prediction fails or relies on improved probabilistic recounting. Also, the polymer-polymer interactions and solvent quality are not easily incorporated in de Gennes' n-vector model.

Realizing that de Gennes' model could be improved, Freed and coworkers introduced an internal degree of freedom for each spin, which represents the segment position along the chain[15]. In addition, the n-vector model is also extended to

complex spin-space. The spin $\vec{S}_i$ in de Gennes' model is replaced by a pair $\{ \vec{S}_{i,\alpha} , \vec{S}_{i,\alpha}^{\dagger} \}$, where i indicates the lattice site and α corresponds to the position along the chain. $\vec{S}_{i,\alpha}$ is an n-component complex vector, and $\vec{S}_{i,\alpha}^{\dagger}$ is its complex conjugate. As it stands, the model describes flexible athermal chains, the monomer-monomer interaction may be incorporated through further modifications. By controlling the position index α (imposing constraints on the new internal degree of freedom), one may control chain length distribution. Freed and Bawendi also showed that their model was equivalent to a model of polymer packing, in which polymers are represented by a set of sequentially occupied sites on a lattice[102]. In polymer packing, the chain correlation and monomer-monomer interactions can be conveniently described. The packing model is quite natural and can easily be extended to polydisperse solutions, and to include different steric architectures and solvent qualities[97-105].

The purpose of this chapter is to present the derivation of the Flory-Huggins equation of state and its generalization using the insertion probability[143,168]. To improve the Flory-Huggins predictions, one has to rely on Freed's n-vector model. Since the calculation of Freed and coworkers will be utilized extensively in analyzing our computer simulation results, we present their derivation in this chapter. Our presentation is more systematic (Freed and coworkers' works are scattered over many articles over several years). We also

note some minor corrections and derive the osmotic pressure for systems with a uniform length distribution.

4.1. The Equation of State of Polymer Solutions: Flory-Huggins Mean Field Approximation.

In the lattice model, a monomer is associated with an occupied site and a solvent molecule or void is represented by an unoccupied site[2,8-11]. The calculation of the equation of state proceeds via the insertion probability method (section 4.1.1)[143,168], with segment-segment correlations neglected. This approximation was improved by Huggins[12-14], taking into account nearest neighbor segments along the chain. The improved Flory-Huggins predictions are in better agreement with Monte Carlo results[22,144] (presented in the next chapter). Since segment-segment correlations are not taken into account, both methods are mean field approximations.

4.1.1. Calculation of Chain-Segment Insertion Probability.

Consider a lattice of N_l sites. Let n_p chains, each of length N (the number of segments is N+1), occupy this lattice. In this model, a lattice site may be occupied by a void or a chain segment. Figure (4.1) describes a one-chain configuration.

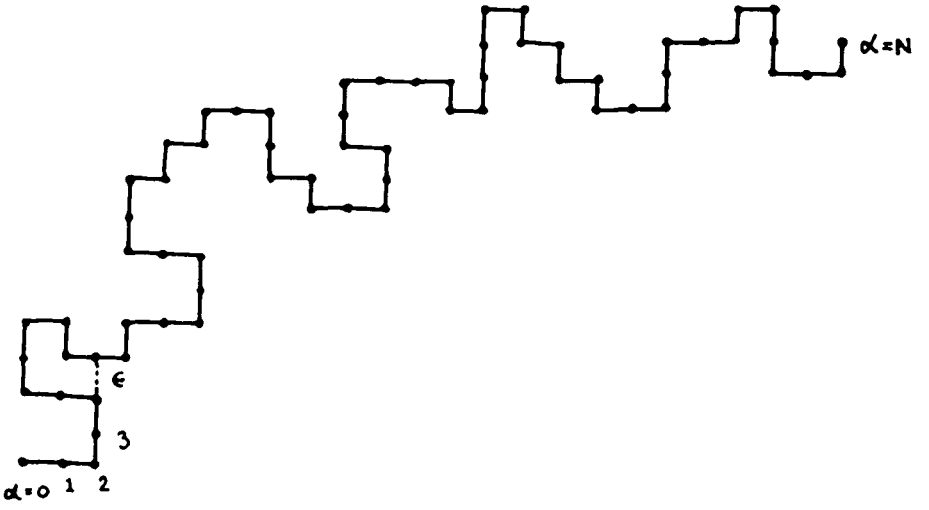

Figure 4.1. A polymer chain on a lattice.

If $P(\nu_k|\nu_{k-1},\nu_{k-2},\ldots,\nu_1)$ is the probability of placing the k^{th} segment when (k-1) segments have been successfully placed without overlap, then the single-chain insertion probability is given by

$$P(n_p-1) = (1-\phi)\prod_{k=2}^{N+1} P(\nu_k|\nu_{k-1},\nu_{k-2},\ldots,\nu_1) \qquad (4.1)$$

where ϕ is the segment density. The first factor corresponds to the placement of the first segment.

Flory employed a mean field approximation in which the insertion of each segment is an independent event; the presence of other connected segments does not affect the placement of the subsequent segments. The insertion is then

given by

$$P(\nu_k \mid \nu_{k-1}, \nu_{k-2}, \ldots, \nu_1) = (1-\phi) \qquad (4.2)$$

and equation (4.1) becomes

$$P_F = (1-\phi)^{N+1} \qquad (4.3)$$

If we have more than one species, we suppose that there are $n_p(i)$ chains of length N_i; then the insertion probability of a single chain belonging to the i^{th} species is given by

$$P_{i,F} = (1-\phi)^{N_i+1} \qquad (4.4)$$

with ϕ now the total density. In nature, polymers do not always consist of identical chemical units. Monomers may have different sizes and structures, which may be described by multi-site occupancy. However, the Flory approximation disregards the monomer architecture as well as the chain connectivity. Consequently, the insertion probability is still given by equation (4.4), where the exponent (N_i+1) is now replaced by $M_i = (N_i+1)s_i$, where s_i indicates the number of sites occupied by a monomer.

The next simplest approximation, which we call the Flory-Huggins approximation, was due to Huggins. He took into

account the presence of nearest-neighbor bonded segments. In this approximation the insertion of segment k is not affected by the presence of previous chain segments except for the segment k-1, so that

$$P(\nu_k \mid \nu_{k-1}, \nu_{k-2}, \ldots, \nu_1) = P(\nu_k \mid \nu_{k-1}) = (1-\tilde{\phi}) \tag{4.5}$$

where $\tilde{\phi}$ is the effective segment density, slightly modified from the average value due to the presence of nearest neighbor segments. The insertion of a single chain in equation (4.1) becomes

$$P_{FH}(n_p=1) = (1-\phi)[1-\tilde{\phi}]^N \tag{4.6}$$

The problem, therefore, is reduced to that of obtaining the value of $\tilde{\phi}$ in terms of ϕ and the lattice coordination number z. Let us consider polymers with a simple branching structure, as in figure (4.2). Except for the end points, the monomers possess b branches as indicated in the right side of figure (4.2). For simplicity, one can assume that each branch end has a single monomer; the case of longer branch follows trivially. If M is the total number of segments per molecule, n_b is the number of back-bone segments, and b corresponds to the number of branches attached to internal back-bone segments, it is

evident that

$$M = (1+b)\,n_b - 2b \tag{4.7}$$

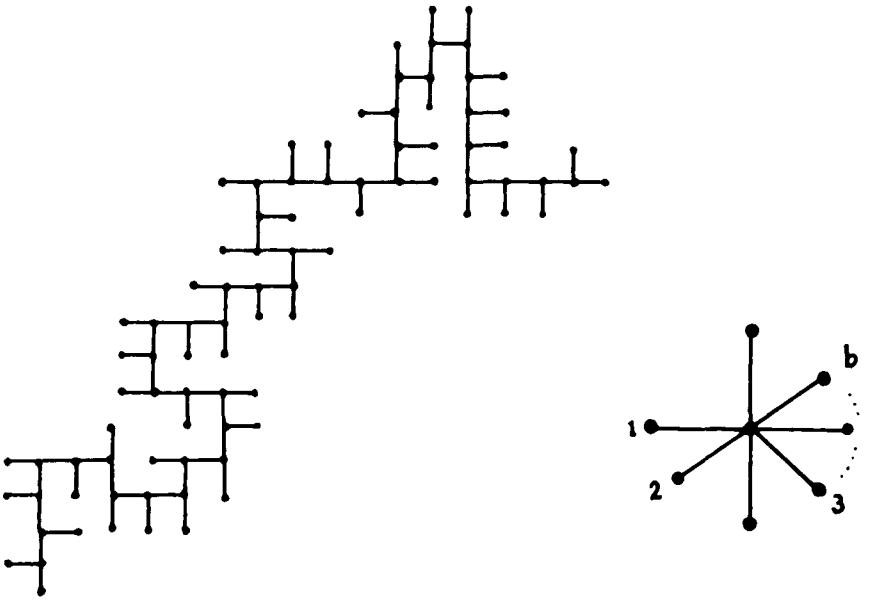

Figure 4.2. An example of a polymer chain with branch-structure.

For linear-unbranched-chains; b=0 and $M=n_b$. The fraction of end segments, internal back-bone segments, and dangling sites are given respectively by

$$\phi_e = \frac{2}{M}\phi \tag{4.8a}$$

$$\phi_i = \frac{n_b - 2}{M}\,\phi \qquad (4.8b)$$

$$\phi_{ds} = \frac{b(n_b - 2)}{M}\,\phi \qquad (4.8c)$$

where ϕ is the fraction of occupied sites in the lattice. To find the insertion probability one has to consider the fraction of occupied sites in the neighborhood of the chain segments; in the neighborhood of the end-segments it is given by

$$\phi_{ne} = \frac{1}{z} + \frac{z-1}{z}\,\phi \qquad (4.9a)$$

in the neighborhood of internal backbone segments and dangling sites is, respectively,

$$\phi_{ni} = \frac{2+b}{z} + \frac{z-b-2}{z}\,\phi \qquad (4.9b)$$

$$\phi_{nds} = \frac{1}{z} + \frac{z-1}{z}\,\phi \qquad (4.9c)$$

The total fraction of the occupied sites, therefore, must be

$$\phi = [\,\phi\,\frac{2}{M}\,]\,\phi_{ne} + [\,\phi\,\frac{n_b - 2}{M}\,]\,\phi_{ni} + [\,\phi\,\frac{b(n_b - 2)}{M}\,]\,\phi_{nds} \qquad (4.10)$$

Substituting equation (4.9) into equation (4.10), one obtains

$$\tilde{\phi} = \frac{\phi\,[1 - \frac{2}{z}(1 - \frac{1}{M})]}{1 - \frac{2}{z}\phi(1 - \frac{1}{M})} \qquad (4.11)$$

This result indicates that since in Flory-Huggins approximation one considers the nearest-neigbor segments, irrespective of the chain architecture, the effective density should be a function of lattice coordination number and segment density. Details of the chain architecture do not enter. (In fact, this shortcoming motivated Freed and coworkers to devise a model which is able to distinguish between different segment architectures). The insertion probability in equation (4.6) is then given by

$$P_{FH} = \frac{(1-\phi)^M}{(1 - \frac{2}{z}\phi\,[1 - \frac{1}{M}])^{M-1}} \qquad (4.12)$$

In the presence of nearest neighbor interactions, with interaction parameter given by $-\epsilon$, the insertion probability in (4.12) is multiplied by η^A where $\eta = \exp(\epsilon/k_BT)$ and A is equal to the number of bonds linking non-bonded nearest-neighbor occupied sites. In the mean field approximation equation (4.12) is then modified to

$$P_{FH}(\eta) = P_{FH}(\eta=1)\,\eta^{[(z-1)(2+bn_b-2b)+(n_b-2)(z-2-b)]\phi} \qquad (4.13)$$

The factor $P_{FH}(\eta=1)$ is the athermal result, equation (4.12). The first term and the second terms in the exponent correspond, respectively, to the average number of bonds at the end and at internal segments. In simple case of linear chains, (b = 0, M = n_b = N+1),

$$P_{FH,lin}(\eta) = \frac{(1-\phi)^M}{(1-\frac{2}{z}\phi[1-\frac{1}{M}])^{M-1}}\,\eta^{\frac{(zM-2[M-1])^2\phi}{(zM-2\phi[M-1])}} \qquad (4.14)$$

4.1.2. The Equation of State: Flory-Huggins predictions[168].

Consider chains of M segments on a lattice, which interact via a pairwise segment-segment interaction (figure 4.1). Suppose the system consists of n_p chains and the pairwise segment-segment potential is given by $U(|\vec{X}_i^{(\mu)}-\vec{X}_j^{(\nu)}|)$, and suppose further that there is an external potential $W_g(\{\vec{X}_i^{(\mu)}\})$, where the $\vec{X}_i^{(\mu)}$ denotes the position of the μ th segment of the i^{th} chain. The total potential energy of the multichain system is then

$$U_{n_p} = \frac{1}{2} \sum_{i \neq j=1}^{n_p} \sum_{\mu,\nu=1}^{M} U(|\vec{X}_i^{(\mu)} - \vec{X}_j^{(\nu)}|) + \sum_{i=1}^{n_p} \sum_{\mu=1}^{M} W_g(\{\vec{X}_i^{(\mu)}\}) \quad (4.15)$$

The configurational partition function for a multi-chain system consisting of n_p M - mers on lattice of N_l sites is given by

$$Z(n_p, M, N_l, \beta) = \frac{1}{n_p!} \sum_{\vec{X}_1^{(1)} \in \Lambda_{N_l}}' \cdots \sum_{\vec{X}_{n_p}^{(M)} \in \Lambda_{N_l}} e^{-\beta U_{n_p}} \quad (4.16)$$

where Λ_{N_l} is a region in the lattice, and $\beta = 1/k_B T$.

A quantity of interest is the insertion probability of a single chain into the n_p-chain configuration, which is related to the osmotic pressure via a simple relation. If Y denotes a configuration of an M-mer chain, and X denotes a configuration of n_p M-mers on a lattice of N_l sites, the insertion factor is given by the following relation

$$P(n_p, M, N_l, \beta) = \langle \langle e^{-\beta U_T} \rangle_Y \rangle_X \quad (4,17)$$

U_T is the potential energy between the test-chain Y when it is inserted into the multi-chain configuration X, and <...> indicates an ensemble average over all possible chain configurations X and test-chain configurations Y. Using

equation (4.16), one can obtain

$$P(n_p, M, N_1, \beta) = \frac{\sum_{\vec{x}_1^{(1)} \in \Lambda_{N_1}} \cdots \sum_{\vec{x}_{n_p+1}^{(M)} \in \Lambda_{N_1}} e^{-\beta U_{n_p+1}}}{\sum_{\vec{x}_1^{(1)} \in \Lambda_{N_1}} \cdots \sum_{\vec{x}_{n_p}^{(M)} \in \Lambda_{N_1}} e^{-\beta U_{n_p}} \cdot \sum_{\vec{x}_1^{(1)} \in \Lambda_{N_1}} \cdots \sum_{\vec{x}_1^{(M)} \in \Lambda_{N_1}} e^{-\beta U_1}} \tag{4.18}$$

$$= (n_p+1) \frac{Z(n_p+1, M, N_1, \beta)}{Z(n_p, M, N_1, \beta)\, Z(1, M, N_1, \beta)}$$

The partition function, therefore, can be written iteratively as

$$Z(n_p, M, N_1, \beta) = \frac{[\, Z(1, M, N_1, \beta)\,]^{n_p}}{n_p!} \prod_{j=1}^{n_p-1} p(j, M, N_1, \beta) \tag{4.19}$$

Here $p(j,M,N_1,\beta)$ is the insertion factor for placing a single chain on a lattice of size N_1 at temperature $1/\beta$ when j chains are already present. If we use the statistical thermodynamic relations for the free energy and the chemical potential

$$\mu n_p = E - TS + \pi N_1 \tag{4.20}$$

$$A(n_p, M, N_1, \beta) = E - TS$$
$$= k_B T \log Z(n_p, M, N_1, \beta) \qquad (4.21)$$

and

$$\mu(n_p, M, N_1, \beta) = -k_B T [\log Z(n_p+1, M, N_1, \beta) - \log Z(n_p, M, N_1, \beta)] \qquad (4.22)$$

then one can obtain

$$\pi^*(n_p, M, N_1, \beta) = N_1^{-1} \{ \sum_{j=1}^{n_p-1} \log p(j, M, N_1, \beta) - n_p \log p(n_p, M, N_1, \beta) + n_p \log(n_p+1) - \log n_p! \} \qquad (4.23)$$

where $\pi^* \equiv \beta\pi$.

Taking the thermodynamic limit N_1, $n_p \to \infty$ such that the fraction of occupied sites $\phi = Mn_p/N_1$ is finite, the osmotic pressure can be reexpressed as

$$\pi^*(\phi, M, \beta) = \frac{\phi}{M} [1 - \log p(\phi, M, \beta)] + \frac{1}{M} \int_0^{\phi} \log p(\phi', M, \beta)\, d\phi' \qquad (4.24)$$

The derivation of equations (4.15) to (4.24) can be found in Dickman and Hall[168]. We can generalize the results to polydisperse systems. If we have f classes of dispersity each with n_p^i chains of length M_i, the steps from Eqn. (4.18) to (4.24) can be repeated. In this case the chain insertion probability of type i is given by

$$p_i = \frac{(n_p^i+1)\, Z(n_p^1, n_p^2, \cdots, n_p^{i-1}, n_p^i+1, n_p^{i+1}, \cdots, n_p^f)}{Z_i(1)\, Z(n_p^1, n_p^2, \cdots, n_p^i, \cdots, n_p^f)} \qquad (4.25)$$

and equation (4.19) is changed to

$$Z(n_p^1, n_p^2, \cdots, n_p^f) = \prod_{i=1}^{f} \frac{[Z_i(1)]^{n_p^i}}{n_p^i!} \prod_{j_i=0}^{n_p^i-1} p(j_i, n_p^1, n_p^2, \cdots, n_p^{i-1}; N_1, \beta) \qquad (4.26)$$

where $p(j_i, n_p^1, n_p^2, \ldots, n_p^{i-1}; N_1, \beta)$ is the insertion probability when $\sum_{I=1}^{i-1} n_p^I + j_i$ chains are already present. Using the thermodynamic relation $\pi N_1 = -A + \sum_{i=1}^{f} \mu_i n_p^i$ one can obtain immediately the osmotic pressure of a polydisperse system

$$\pi^* = \sum_{i=1}^{f} \left[\left(\frac{\phi_i}{M_i} \right) \left[1 - \log p_i(\phi_1, \phi_2, \cdots, \phi_f, \beta) \right] + \frac{1}{M_i} \int_0^{\phi_i} \log p(\phi', \phi_1, \phi_2, \cdots, \phi_{i-1}, \beta)\, d\phi' \right] \tag{4.27}$$

Using equation (4.24) and the insertion probability of Flory and Flory-Huggins (P_F and P_{FH}) derived in the previous section, one may obtain the compressibility factor, $W = \pi^* M/\phi$, in the athermal case

$$W_F = 1 - M[\log(1-\phi) + \phi]/\phi \tag{4.28}$$

and

$$W_{FH} = W_F + \frac{Mz}{2\phi}\left[\log\left(1 - \frac{2\phi}{z}\left(1-\frac{1}{M}\right)\right) + \frac{2\phi}{z}\left(1-\frac{1}{M}\right)\right] \tag{4.29}$$

where M is the number of segments per molecule or equal to polymerization index for a linear chain. The non-athermal case is

$$W_{FH}(\eta) = W_{FH}(\eta=1) + \frac{Mz[M(z-2)+2]^2 A \log\eta}{2(1-M)[zM-2\phi(M-1)]} - \frac{Mz[M(z-2)+2]^2}{4\phi(1-M)^2}(A\log\eta)\log\left[1 - \frac{2\phi(M-1)}{zM}\right] \tag{4.30a}$$

where

$$A = \frac{[(z-1)(2+bn_b-2b) + (n_b-2)(z-b-2)]}{[M(z-2)+2]} \qquad (4.30b)$$

The first term in eqn. (4.30a) is the compressibility factor in the athermal case, and for linear chains A=1, and M = N+1.

4.2. The Equation of State in Freed's N-Vector Model: Athermal Case.

As indicated in the Introduction and at the beginning of this chapter, the conformational renormalization group of Edwards' model is suitable for polymer solutions with volume fraction much less than unity. The problem of polymers at higher densities was approximated using the n-vector model on a lattice by de Gennes[46,47] and was generalized by Freed and coworkers[15,94-105]. The motivation to employ these models on a lattice is to include the excluded volume effect appropriately in the high-density regime, in which the excluded volume is considered comparable to that of a lattice cell. Freed and coworkers generalized the n-vector model in order to control the chain length distribution. They also employ the generalized n-vector model to derive systematic corrections to mean field results of the entropy and energy of mixing[95]. Their description is also suitable for polymers with a branched structure[97].

4.2.1. Generalized N-Vector Model: A Mean Field Approximation.

Consider the complex n-vector $\{\bar{S}_{i\alpha}, \bar{S}_{i\alpha}^{\dagger}\}$ where the internal symmetry index α runs from 0 to N_0. The index α corresponds to the position along the chain. The index i denotes the lattice site. Let us impose the following condition

$$Tr_S[\exp(i\vec{k}.\vec{S}^{*}_{j\alpha} + i\vec{k}^{*}.\vec{S}_{m,\beta}] = 1 - \vec{k}.\vec{k}^{*}\delta_{\alpha\beta}\delta_{jm}$$
$$Tr_S[\vec{S}_{j,\alpha}.\vec{S}_{m,\beta}] = Tr_S[\vec{S}^{*}_{j,\alpha}.\vec{S}^{*}_{m,\beta}] = 0 \qquad (4.31)$$

All traces of higher than quadratic order are defined to be zero. Unlike the original definition of traces in the n-vector model[47], which describes a magnet, the traces in eqn (4.31) are imposed so that we may recover the correct set of chain configurations. We may regard the spin variable as a book-keeping device. Using the 2n-component complex spin model, the grand partition function of polymers with chain length distribution P_{N_o} is

$$Z = Tr_S\left[\exp\{K\sum_{\langle ij\rangle}\sum_{\alpha=0}^{\infty}\vec{S}^{*}_{i,\alpha+1}.\vec{S}_{j,\alpha} + \sum_{i}(\vec{H}.\vec{S}^{*}_{i,0} + \vec{H}^{*}.\vec{S}_{i,N_0}\frac{P_{N_0}}{2})\}\right] \qquad (4.32)$$

where <ij> denotes the nearest neighbor sites i and j. K is a constant which may be set to unity. H and $H^{\dagger}$ represent external fields, and their coefficients have a role of initiating and terminating chains, respectively. Note that when the direction of chain-segment sequence is chosen by ordering the index α, the backward and forward directions of chain contour are assumed to be different, while physically they are of course indistinguishable. The factor 1/2, therefore, is included to correct the overcount. The chain length distribution P_{N_o} controls the polymer dispersity; for a monodisperse solution $P_{N_o} = \delta_{N,N_0}$. Expanding the exponent in the grand partition function and using equation (4.31), we find

$$Z = Tr_S \Big(\prod_{\langle ij \rangle} \prod_{\alpha=0}^{\bar{\ }} \left(1 + K \vec{S}^{\dagger}_{i,\alpha+1} . \vec{S}_{j,\alpha} + \cdots \right) \times \prod_{m} \left(1 + \vec{H} . \vec{S}^{\dagger}_{m,0} + \vec{H}^{\dagger} . \vec{S}_{m,N} \frac{P_{N_o}}{2} + \cdots \right) \Big) \tag{4.33}$$

and the partition function of n_p chains is given by

$$Z_{n_p} = \frac{1}{n_p!} \frac{\partial^{n_p}}{\partial (\vec{H}\vec{H}^{\dagger})^{n_p}} Z \Big|_{\vec{H}=\vec{H}^{\dagger}=0} \tag{4.34}$$

Let us limit the calculation to a monodisperse solution with the chain length N. Introducing the complex random fields $\vec{\Phi}_{i,\alpha}$, and its complex conjugate, $\vec{\Phi}_{i,\alpha}^{\dagger}$, one may obtain the following identity (the derivation can be found in Appendix B)

$$\exp\left[K\sum_{\langle ij\rangle}\vec{S}^{*}_{i,\alpha+1}\cdot\vec{S}_{j,\alpha}\right]$$

$$= \int\prod_{i} d\vec{\Phi}^{*}_{i,\alpha}\, d\vec{\Phi}_{i,\alpha}\exp\Big[\sum_{i}\vec{S}^{*}_{i,\alpha+1}\cdot\vec{\Phi}_{i,\alpha}$$

$$+ \vec{S}_{i,\alpha}\cdot\vec{\Phi}^{*}_{i,\alpha} - \sum_{i,j}\tilde{V}_{ij}\vec{\Phi}_{i,\alpha}\cdot\vec{\Phi}_{j,\alpha}\Big]$$

$$\times\left[\int\prod_{i} d\vec{\Phi}^{*}_{i,\alpha}\, d\vec{\Phi}_{i,\alpha}\exp\Big(-\sum_{ij}\tilde{V}_{ij}\vec{\Phi}^{*}_{i,\alpha}\cdot\vec{\Phi}_{j,\alpha}\Big)\right]^{-1} \tag{4.35}$$

where

$$\tilde{V}_{ij} = \sum_{k}\exp\left[\,i\vec{k}\cdot(\vec{r}_{i}-\vec{r}_{j})\,\right]\left[N_{1}Kf(\vec{k})\right]^{-1} \tag{4.36}$$

and

$$f(\vec{k}) = \sum_{\{\vec{a}_{i}\}}\exp\left(i\vec{k}\cdot\vec{a}_{i}\right) \tag{4.37}$$

In equation (4.37), $\{\,\vec{a}_{i}\,\}$ is the set of lattice vectors to the nearest neighbor sites. Substituting Eqs. (4.35 - 4.37) into the partition function yields

$$Z = Tr_S\left[C\int\prod_i\prod_{\alpha=0}^{N-1} d\Phi^*_{i,\alpha}d\Phi_{i,\alpha}\exp\{\sum_i\sum_{\alpha=0}^{N-1}\ (\vec{S}^*_{i,\alpha+1}\cdot\Phi_{i,\alpha} + \vec{S}_{i,\alpha}\cdot\Phi^*_{i,\alpha}\right.$$

$$\left. + \sum_i \vec{H}.\vec{S}^*_{i,0} + \frac{\vec{H}^*}{2}.\vec{S}_{i,N} - \sum_{i,j}\sum_{\alpha=0}^{N-1}\tilde{V}_{ij}\Phi^*_{i,\alpha}.\Phi_{j,\alpha}\}\right] \qquad (4.38a)$$

where the constant C is given by

$$C = \left[\int\prod_{i=1}^{N_l}\prod_{\alpha=0}^{N-1} d\Phi^*_{i,\alpha}d\Phi_{i,\alpha}\exp\{-\sum_{ij}\sum_{\alpha=0}^{N-1}\tilde{V}_{ij}\Phi^*_{i,\alpha}.\Phi_{j,\alpha}\}\right]^{-1} \qquad (4.38b)$$

The condition on traces in equation (4.31) will simplify a lot of the calculation since the surviving terms after taking the trace with respect to spin S are the coefficients of the products $\vec{S}_{i,\alpha}{}^{\dagger}.\vec{S}_{i,\alpha}$ and unity, which are

$$1 + X_i = 1 + \frac{\vec{H}}{2}.\Phi^*_{i,0} + \sum_{\alpha=1}^{N-1}\Phi^*_{i,\alpha}.\Phi_{i,\alpha-1} + \vec{H}^*.\Phi_{i,N-1} \qquad (4.39)$$

and the partition function is transformed to

$$Z = C\int D[\Phi^*\Phi]\prod_i(1+X_i)\exp(-\sum_{ij}\sum_{\alpha=0}^{N-1}\tilde{V}_{ij}\Phi^*_{i,\alpha}.\Phi_{j,\alpha}) \qquad (4.40)$$

where $D[\vec{\Phi}^{*}\vec{\Phi}] = \prod_{i=1}^{N_l}\prod_{\alpha=0}^{N-1} d\vec{\Phi}^{*}_{i,\alpha} d\vec{\Phi}_{i,\alpha}$. In the mean field approximation we retain only the k=0 component of $\tilde{V}_{ij}$, and neglect the variation of X_i from site to site. In other words, we are treating the system as if there were random mixing of all segments. By dropping the position index in Eqn. (4.39) and setting X_i=X, the product in equation (4.40) becomes

$$Z_{MF} = C' \int D'[\vec{\Phi}^{*}\vec{\Phi}] \ (1+X)^{N_l} \exp\left(-\frac{N_l}{Kz}\sum_{\alpha} \vec{\Phi}^{*}_{\alpha}\cdot\vec{\Phi}_{\alpha}\right) \qquad (4.41)$$

where C' is a new normalization constant and $D'[\vec{\phi}^{*}\vec{\phi}]$ is a measure in which the site index i is omitted. For simplicity we pick $\vec{H}$ along the x_1 direction so that the vector sign can be dropped. Also note that the index α is decoupled (there is no cross-term in the exponent). Using the multinomial expansion

$$\left(1+\sum_{i=1}^{p} a_i\right)^{N_l} = \sum_{\substack{m_1, m_2, \ldots, m_p \\ \sum_{\alpha=1}^{p} m_\alpha \le N}} \frac{N_l!}{\left(N_l - \sum_{i=1}^{p} m_i\right)! \prod_{i=1}^{p} m_i!} \prod_{i=1}^{p} a_i^{m_i} \qquad (4.42)$$

equation (4.41) becomes

$$Z_{MF} = \sum_{\{\ldots\}} \frac{N_1!}{(N_1 - \sum_{\alpha=0}^{N} m_\alpha)! \prod_{\alpha=0}^{N} m_\alpha!} \times \left\langle \left(\frac{H}{2}\Phi_0\right)^{m_0} \prod_{\alpha=1}^{N-1} (\Phi_\alpha^* \Phi_{\alpha-1})^{m_\alpha} (H^* \Phi_{N-1})^{m_N} \right\rangle \tag{4.43}$$

where the summation constraint {...} is identical to the one in Eqn. (4.42). <...> indicates an average weighted with the Gaussian distribution of equation (4.41). Since the index α is decoupled and using the following identity

$$\langle (\Phi_\alpha^*)^m (\Phi_\alpha)^l \rangle = C \int \prod_{\alpha=1}^{N-1} d\Phi_\alpha^* d\Phi_\alpha \, (\Phi_\alpha^*)^m (\Phi_\alpha)^l \, e^{-\frac{N_1}{KZ} \sum_{\alpha=0}^{N-1} \Phi_\alpha^* \Phi_\alpha} = m! \, \delta_{l,m} \left(\frac{KZ}{N_1}\right)^m \tag{4.44}$$

we see that all the exponents of Φ_α are the same, $m_0 = m_1 = \ldots = m_N$, which is equal to the number of chains n_p.

In the mean-field approximation, the partition function of n_p chains should give Z_{MF}, then using Eqn. (4.34) we get:

$$Z_{n_p, MF} = \frac{N_1!}{[N_1 - (N+1)\, n_p]!\, n_p!} \left(\frac{KZ}{N_1}\right)^{n_p N} \tag{4.45}$$

The corresponding entropy is defined by

$$S_{n_p}^{MF} = k_B \log Z_{n_p,MF} \tag{4.46}$$

Using Stirling's approximation for the factorial

$$x! \sim x^x e^{-x} \sqrt{(2\pi x)} \qquad x \gg 1 \tag{4.47}$$

one may obtain the entropy per site:

$$\frac{S_{n_p}}{k_B N_l} = \phi \log N_l - (1-\phi) \log (1-\phi) - \phi - \frac{\phi}{M} \log \frac{2\phi N_l}{M} + \frac{\phi}{M} + (\phi - \frac{\phi}{M}) \log \frac{Kz}{N_l} \tag{4.48}$$

with M = (N + 1) the number of segments per unit chain.

The entropy of mixing is defined as the difference between the entropy obtained in equation (4.48) and the entropy of polymeric melt,

$$\Delta S^{MIX} = S(\phi) - \phi S(\phi=1) \tag{4.49}$$

For monodisperse systems of linear chains, the mean-field expression for the entropy of mixing is

$$\frac{\Delta S^{MIX}}{k_B N_1} = -(1-\phi)\log(1-\phi) - \frac{\phi}{M}\log\phi \qquad (4.50)$$

This result is the standard Flory expression for the mixing entropy. In the mean field approximation, we assume X_i, hence $\vec{\phi}_{i,\alpha}$ and $\vec{\phi}_{i,\alpha}^{\dagger}$, to be independent of lattice site i and the position index α. Therefore, one may expect that by retaining the site dependence, we may derive corrections to the mean-field results.

4.2.2. Systematic Corrections to Mean Field Theory.

To see the effect of chain connectivity we retain the position (i) dependence of the random fields $\{\vec{\phi}_{i,\alpha}, \vec{\phi}_{i,\alpha}^{\dagger}\}$. Instead of working directly with spatial indices, it is easier to use the Fourier coefficients (in q-space) of the random fields. The mean field approximation in q-space is represented by the $\vec{q}=0$ component of the Fourier coefficients. Non-zero wave vectors correspond to corrections wherein the locality of the random field is not discarded. The Fourier transform of the random fields ϕ is defined so:

$$\Phi_{i,\alpha} = \sum_{\vec{q}} e^{i\vec{q}\cdot\vec{r}_i}\Phi_{\vec{q},\alpha}$$

$$\Phi_{\vec{q},\alpha} = \frac{1}{N_l}\sum_{i} e^{-i\vec{q}\cdot\vec{r}_i}\Phi_{i,\alpha} \qquad (4.51)$$

and the complex conjugate transforms accordingly (with $e^{i\vec{q}\cdot\vec{r}} \rightarrow e^{-i\vec{q}\cdot\vec{r}}$). In the Fourier representation, the argument of the Gaussian exponential becomes

$$\sum_{ij}\sum_{\alpha=0}^{N-1} \tilde{V}_{ij}\Phi^{*}_{i,\alpha}\cdot\Phi_{j,\alpha} = \sum_{\alpha=0}^{N-1}\sum_{\vec{q}} \Phi^{*}_{\vec{q},\alpha}\cdot\Phi_{\vec{q},\alpha}\left[\frac{N_l}{f(\vec{q})}\right] \qquad (4.52)$$

and X_i is given by

$$X_i = \vec{H}\cdot\sum_{\vec{q}} e^{i\vec{q}\cdot\vec{r}_i}\Phi^{*}_{\vec{q},0} + \sum_{\alpha=1}^{N-1}\sum_{\vec{q},\vec{q}'} e^{i(\vec{q}-\vec{q}')\cdot\vec{r}_i}\Phi^{*}_{\vec{q}',\alpha}\cdot\Phi_{\vec{q},\alpha-1}$$
$$+ \frac{1}{2}\vec{H}^{*}\cdot\sum_{\vec{q}} e^{i\vec{q}\cdot\vec{r}_i}\Phi_{\vec{q},N-1} \qquad (4.53)$$

The grand partition function, after setting K equal to unity, is

$$Z = \int D''[\Phi\Phi^{*}]\prod_i (1+X_i)\exp\left[-\sum_{\alpha=0}^{N-1}\sum_{\vec{q}}\frac{N_l}{f(\vec{q})}\Phi^{*}_{\vec{q},\alpha}\cdot\Phi_{\vec{q},\alpha}\right] \qquad (4.54)$$

The measure in Eqn. (4.54) is defined over Fourier components $\{\vec{\phi}_{\vec{q},\alpha}, \vec{\phi}_{\vec{q},\alpha}^{+}\}$. To see the effect of site dependence, the $\vec{q}$=0 components in X_i are seperated from the non-zero coefficients

$$X_i = X(\vec{q}=0) + \delta X_i^{(1)} + \delta X_i^{(2)} \qquad (4.55a)$$

with

$$\delta X_i^{(1)} = \vec{H}.\sum_{\vec{q}}{}'\exp(-i\vec{q}.\vec{r}_i)\,\vec{\Phi}^{*}_{\vec{q},0} + \sum_{\alpha=1}^{N-1}\sum_{\vec{q}}{}'\,[e^{i\vec{q}.\vec{r}_i}\vec{\Phi}^{*}_{\vec{q}=0,\alpha}\vec{\Phi}_{\vec{q},\alpha-1}$$

$$+ e^{-i\vec{q}.\vec{r}_i}\vec{\Phi}^{*}_{\vec{q},\alpha}.\vec{\Phi}_{\vec{q}=0,\alpha-1}] + \frac{1}{2}\vec{H}^{\dagger}.\sum_{\vec{q}}{}'\exp(i\vec{q}.\vec{r}_i)\,\vec{\Phi}_{\vec{q},N-1}$$

$$\delta X_i^{(2)} = \sum_{\alpha=1}^{N-1}\sum_{\vec{q},\vec{q}'}{}'e^{i(\vec{q}-\vec{q}').\vec{r}_i}\vec{\Phi}_{\vec{q}',\alpha}\vec{\Phi}^{*}_{\vec{q},\alpha-1} \qquad (4.55b)$$

Σ' means the summation with respect to non-zero momenta. Note that $X_i^{(1)}$ and $X_i^{(2)}$ have terms linear and quadratic in $\vec{\Phi}_{\vec{q}\neq 0}$. The coefficient of H initiates the chain configuration since the index α = 0 and the coefficient $H^{\dagger}$ terminates the chain contour with α = N. Since the Gaussian average with a single $\vec{\Phi}_{\vec{q},\alpha}$ or $\vec{\Phi}_{\vec{q},\alpha}^{\dagger}$ vanishes, a pair of $X_i(1)$'s are required to provide a non-zero correction. One may suggest that $X_i^{(1)}$ is required to initiate, to propagate and to terminate a chain configuration, while $X_i^{(2)}$ functions as the propagator of the

chain construction. Using equation (4.55),

$$\langle \prod_i (1+X_i) \rangle = \langle \prod_i (1+X(\vec{q}=0)+\delta X_i^{(1)}+\delta X_i^{(2)}) \rangle$$

$$\sum_{\substack{2m+l=n \\ m\geq 0}} \sum_{\substack{i_1 \neq i_2 \neq \ldots \neq i_{2m} \\ \neq j_1 \neq j_2 \neq \ldots \neq j_l}} \frac{1}{(2m)!\,l!} \langle (1+X)^{N_l-n} \delta X_{i_1}^{(1)} \ldots \delta X_{i_{2m}}^{(1)} \delta X_{j_1}^{(2)} \ldots \delta X_{j_l}^{(2)} \rangle \qquad (4.56)$$

where $X = X(\vec{q}=0)$.

Consider the lowest order correction, m=1 and l =0. The equation (4.56) now becomes

$$Z^{(2)} = \frac{1}{2!} \sum_{i_1 \neq i_2} \langle (1+X)^{N_l-2} \delta X_{i_1}^{(1)} \delta X_{i_2}^{(1)} \rangle \qquad (4.57)$$

Taking the ensemble average over $\Phi_{\vec{q}\neq 0}$ and using a modified form of equation (4.44)

$$\langle (\Phi_{\vec{q},\alpha}^{*})^m (\Phi_{\vec{q},\beta})^l \rangle = m! \left[\frac{f(\vec{q})}{N_l}\right]^m \delta_{l,m} \delta_{\alpha,\beta} \qquad (4.58)$$

one may obtain

$$Z^{(2)} = \sum_{1\neq 2}\sum_{\vec{q}}{}' \exp\left[-i\vec{q}.(\vec{r}_1-\vec{r}_2)\right]\frac{f(\vec{q})}{N_1}$$

$$\times\left[\langle H(1+X)^{N_1-2}\Phi^{+}_{\vec{q}=0,1}\rangle_{\Phi_{\vec{q}=0}} + \sum_{\alpha=1}^{N-2}\langle(1+X)^{N_1-2}\Phi_{\vec{q}=0,\alpha-1}\Phi^{+}_{\vec{q}=0,\alpha+1}\rangle_{\Phi_{\vec{q}=0}}\right.$$

$$\left. + \langle\frac{1}{2}H^{+}(1+X)^{N_1-2}\Phi_{\vec{q}=0,N-2}\rangle_{\Phi_{\vec{q}=0}}\right] \qquad (4.59)$$

Let us call the three terms in the ensemble average over $\Phi_{\vec{q}=0}$ on the right side I_1, I_2, and I_3 respectively. One finds these terms to be equal;

$$I_1 = I_2 = I_3 = \sum_{\substack{m_0 \\ m_0(N+1)+m_\alpha=N_1}} \frac{(N_1-2)!\,m_0}{2^{m_0}m_\alpha!\,m_0!}\left[\frac{z}{N_1}\right]^{Nm_0-1} \qquad (4.60)$$

Since there are N such terms and using the result of $Z_{m_0,MF}$, the correction may be rewritten as

$$Z^{(2)} = \sum_{(N+1)m_0+m_\alpha=N_1} \frac{Nm_0}{N_1(N_1-1)} Z_{m_0,MF}(HH^{+})^{m_0}P_2 \qquad (4.61a)$$

with

$$P_2 = \sum_{1\neq 2}\sum_{\vec{q}}{}' e^{-i\vec{q}.(\vec{r}_1-\vec{r}_2)}\left[\frac{f(\vec{q})}{z}\right] \qquad (4.61b)$$

The partition function of n_p chains, therefore, is

$$Z_{n_p}^{(2)} = \frac{Nn_p}{N_1(N_1-1)} P_2 Z_{n_p,MF} \qquad (4.62)$$

Equation (4.62) is the lowest order correction to the mean field approximation of n_p-chain partition function. It takes partial account of chain correlations. The factor Nn_p indicates the number of ways to put a pair of bonded nearest neighbor segments in the n_p-chain configuration. Equivalently, it is equal to the number of ways to place a single bond on Nn_p bonds available in the system. $N_1(N_1-1)$ in the denominator is the number of choices to pick two $\delta^{(1)}$ s or to place two segments on N_1 sites in an ordered fashion. P_2 depends only on the lattice architecture. The calculation of P_2 follows immediately by recognizing that

$$\sum_{1\neq 2} = \sum_{1,2} (1-\delta_{1,2}) \qquad (4.63)$$

and

$$\sum_{\vec{q}}{}' f(\vec{q}) = \sum_{\vec{q}} f(\vec{q}) - f(0) = -z \qquad (4.64)$$

Therefore,

$$P_2 = N_1 \qquad (4.65)$$

and

$$Z_{n_p}^{(2)} = \frac{N n_p}{(N_1 - 1)} Z_{n_p, MF} \qquad (4.66)$$

The next order of corrections come with m=1 and l=1, and

$$Z^{(3)} = \sum_{1 \neq 2 \neq 3} \frac{1}{2!} \langle (1+X)^{N_1 - 3} [\delta X_1^{(1)} \delta X_2^{(1)} \delta X_3^{(2)}] \rangle \qquad (4.67)$$

Expanding $\delta X^{(i)}$ and taking the ensemble average of $\Phi_{q \neq 0}$, equation (4.67) becomes

$$Z^{(3)} = \sum_{1 \neq 2 \neq 3} \sum_{\vec{q}_1, \vec{q}_2}{}' [\frac{z}{N_1}]^2 [\frac{f(\vec{q}_1) f(\vec{q}_2)}{z^2}] e^{-i(\vec{q}_1 \cdot \vec{r}_1 - (\vec{q}_1 - \vec{q}_2) \cdot \vec{r}_2 - \vec{q}_2 \cdot \vec{r}_3)}$$

$$\times \{\langle H(1+X)^{N_1 - 3} \Phi^{+}_{\vec{q}=0,2} \rangle_0 + \sum_{\alpha=1}^{N-3} \langle (1+X)^{N_1 - 3} \Phi_{\vec{q}=0,\alpha-1} \Phi^{+}_{\vec{q}=0,\alpha+2} \rangle_0$$

$$+ \langle \frac{H^*}{2} (1+X)^{N_1 - 3} \Phi_{\vec{q}=0,N-3} \rangle_0 \} \qquad (4.68)$$

The calculation of the ensemble average on the righthand side is similar to the one in equation (4.59). All yield the same value and the correction to the partition function $Z_{n_p}^{(3)}$ can

be expressed as

$$Z_{n_p}^{(3)} = \frac{(N-1)\,n_p}{N_1(N_1-1)\,(N_1-2)}\, Z_{n_p,\,MF} P_3 \qquad (4.69)$$

with

$$P_3 = \sum_{1\neq 2\neq 3} \sum_{q_1,\,q_2}{}' e^{-i\,[\vec{q}_1\cdot\vec{r}_1-(\vec{q}_1-\vec{q}_2)\cdot\vec{r}_2-\vec{q}_2\cdot\vec{r}_3]}\, \frac{f(\vec{q}_1)\, f(\vec{q}_2)}{z^2} \qquad (4.70)$$

Note that

$$\begin{aligned} \sum_{1\neq 2\neq 3} &= \sum_{1,2,3} (1-\delta_{1,2})\,(1-\delta_{1,3})\,(1-\delta_{2,3}) \\ &= \sum_{1,2,3} (1-\delta_{1,2}-\delta_{1,3}-\delta_{2,3}+2\delta_{1,2,3}) \end{aligned} \qquad (4.71)$$

Equation (4.71) and its generalization are easily pictured using a Venn - diagram. Some notation requires explanation. $\delta_{1,2,3}$ means that the sites $\vec{r}_1$, $\vec{r}_2$, and $\vec{r}_3$ coincide, and it is equivalent to $\delta_{1,2}\delta_{1,3}$, $\delta_{1,2}\delta_{2,3}$, $\delta_{1,3}\delta_{2,3}$, and $\delta_{1,2}\delta_{1,3}\delta_{2,3}$. The calculation of P_3, described in Appendix C, yields

$$P_3 = -\frac{N_1^3}{z} + N_1^2 + 2N_1 \qquad (4.72)$$

Since the calculations of $Z^{(2)}$ and $Z^{(3)}$ involve two- and three-

segment correlations, we call them the second and third order corrections respectively. The third order correction to the n_p-chain partition function is

$$Z^{(3)}_{n_p} = \frac{(N-1)\,n_p}{N_1(N_1-1)(N_1-2)} Z_{n_p,MF}\left[-\frac{N_1^3}{z} + N_1^2 + 2N_1\right] \qquad (4.73)$$

Up to this order, observing the polymerization indices on the non-zero momentum random fields evidently shows that working with random fields is equivalent to describing the polymer system in terms of the bond configurations. In transforming to random fields from the spin variables, we translate the description of chain segments into polymeric bonds. If $S_{i,\alpha}^{\dagger}$ and $S_{i,\alpha}$ correspond to to the 'creation' and 'annihilation' of a chain segment with polymerization index α, then $\Phi_{i,\alpha}^{\dagger}$ and $\Phi_{i,\alpha}$ denote the 'creation' and 'annihilation' of bond α. For example, the two pairs of non-zero momentum random fields in $Z^{(3)}$ occur with consecutive polymerization indices ($\Phi_{\vec{q},\alpha}^{\dagger}\Phi_{\vec{q},\alpha}$ $\Phi_{\vec{q},\alpha+1}^{\dagger}\Phi_{\vec{q},\alpha+1}$). It indicates the role of two consecutive bonds in the partition function.

The previous remark can be easily visualized by using diagrammatic expansion of Freed and coworkers[94]. If (o) indicates a chain segment and (-----) describes a bond, then the second and third order contribution can be depicted as in figure (4.3)

(second order) (third order)

Figure 4.3. Diagrams representing second and third order corrections to the MF partition function.

With this diagram, it is easier to explain equation (4.69). The numerator $(N-1)n_p$ corresponds to the number of possible placements of two consecutive bonds in n_p N-bond chains. The denominator corresponds to the number of choices to place three segments in an ordered fashion and P_3 is a correction due to lattice-architecture. The next correction comes from the correlation of four segments fashioned either by two non-consecutive bonds or by three consecutive bonds. Since the former can be placed on a single chain or on different chains, we require different diagrams to distinguish them. If two bonds are placed non-consecutively in a single chain, we separate them with a wiggly line. The fourth order correction is depicted in the following picture

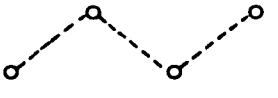

(a)

(b)

Figure 4.4. Diagrams contributing to forth order corrections.

The calculation in Appendix C shows that

$$Z_{n_p}^{(4a)} = Z_{n_p,MF}\frac{(N-2)\,n_p}{N_1(N_1-1)\ldots(N_1-3)}\left[\frac{N_1^4}{z^2}-\frac{8N_1^3}{z}+N_1^3+7N_1^2+6N_1\right] \tag{4.74a}$$

and

$$Z_{n_p}^{(4b)} = Z_{n_p,MF}\left\{\frac{Nn_pN(n_p-1)}{2N_1\ldots(N_1-3)} + \frac{n_p(N-1)(N-2)}{2N_1\ldots(N_1-3)}\right\} \times\left[\frac{2N_1^3}{z}-N_1^2-6N_1\right] \tag{4.74b}$$

In equation (4.74a), $(N-2)n_p$ corresponds to the placement of three consecutive bonds on n_p chains, while $Nn_pN(n_p-1)$ and $n_p(N-1)(N-2)$ in equation (4.74b) are the number of ways of placing two non-consecutive bonds on different chains and on a single chain respectively. In the thermodynamic limit ($N_l\to\infty$, $n_p\to\infty$) such that $\phi = [(N+1)n_p]/N_l$ is fixed, the partition function of n_p chains, including corrections up to fourth order is

$$Z_{n_p} = Z_{n_p,MF} + Z_{n_p}^{(2)} + Z_{n_p}^{(3)} + Z_{n_p}^{(4a)} + Z_{n_p}^{(4b)}$$

$$= Z_{n_p,MF}\left[1+\phi\left(1-\frac{1}{N}\right)+\phi\left(1-\frac{2}{N}\right)\left(-\frac{N_1}{z}-\frac{3}{z}+1\right)\right.$$

$$+\phi\left(1-\frac{3}{N}\right)\left(\frac{N_1}{z^2}-\frac{8}{z}+1+\frac{6}{z^2}\right)+\frac{\phi^2}{2}\left(1-\frac{2}{N}\right)\left(2\frac{N_1}{z}-1+\frac{12}{z}\right)$$

$$\left.-\frac{\phi}{z}\left(N-1+\frac{1}{N}\right)+\frac{\phi}{z}\left(N-4+\frac{6}{N}\right)\right] \tag{4.75}$$

which can be rearranged to give

$$Z_{n_p} = Z_{n_p,MF}\left[1+\phi\left(\frac{5}{2}-\frac{8}{z}+\frac{6}{z^2}\right)+\phi\frac{N_1}{z}\left(1-\frac{3}{N}\right)\right.$$

$$\left.+\phi(1-\phi)\left\{\frac{N_1}{z}\left(-1+\frac{2}{N}\right)+\frac{1}{2}-\frac{6}{z}\right\}+\ldots+O\left(\frac{1}{N_1},\frac{1}{N},\frac{1}{z^3}\right)\right] \tag{4.76}$$

Note that the result in equation (4.76) may be regarded as an expansion in 1/z. For two different lattice structures, this expansion gives different results, although these lattices have the same coordination number[94] (see comment in Appendix D). The entropic correction per lattice site is given by

$$\frac{(S_{n_p}-S_{n_p,MF})}{N_1 k_B} = \frac{1}{z}\left[-\left(1-\frac{1}{z}\right)\phi(1-\phi)\right.$$

$$\left.+\phi^2\left(3-\frac{16}{z}+\frac{20}{z^2}-\frac{6}{z^3}\right)+O\left(\frac{1}{N_1},\frac{1}{N},\phi^3\right)\right] \tag{4.77}$$

From equation (4.77) we notice the entropic contribution to the parameter χ in equation (1.20) as the coefficient of $\phi(1-\phi)$. In general the entropic contribution is a function of $(1/z)$ and segment density ϕ. This result is in contrast to Flory's prediction in which χ is energetic in origin and independent of monomer density. Experimental results also indicate an entropic contribution to χ. However, the lattice model cannot be compared with experimental (off-lattice) results. A more direct and useful test of the theory is a comparison with the results of lattice-polymer simulations, which is the subject of the next chapter.

4.2.3. The Equation of State of Athermal Monodisperse Chains.

In the previous section the entropy of polymer solutions was studied using field theories. By introducing random fields in momentum space, the partition function was expressed in terms of Gaussian functional. As given in the previous section, the formulation is rather cumbersome and inefficient to work with for higher order corrections. The interaction energy between monomers cannot be interpreted easily. In fact, Bawendi and Freed introduced the interaction energy in an ad-hoc fashion and utilized Grassmann variables (non-commutative variables) to derive the extended mean field approximation[96]. This approximation generalized Flory's theory to a non-athermal system by disregarding chain correlations, and by

taking into account the locality of the Grassman variables. This difficulty led Bawendi and Freed to introduce the approach of polymer packing[102].

The polymer packing approach, in fact, is equivalent to the field theory. Consider the n_p-chain partition function given in equation (4.34) derived from the grand canonical ensemble of equation (4.54-55). Without loss of generality, we can consider the problem of a single polymer-chain with N bonds in a lattice of N_l sites. Expand the product of $(1+X_i)$ and take a single derivative with respect to $(\vec{H}^{\dagger}\vec{H})$. Since we have only one chain, the result is

$$Z_1 = \frac{N_l!}{N!} \sum_{\substack{\vec{q}_1,\vec{q}_2,\ldots,\vec{q}_N \\ \vec{p}_1,\ldots,\vec{p}_N}} \exp\left[-i\left(\vec{q}_1\cdot\vec{r}_1+\vec{q}_2\cdot\vec{r}_2+\cdots+\vec{q}_N\cdot\vec{r}_N-\vec{p}_1\cdot\vec{r}_2-\cdots-\vec{p}_N\cdot\vec{r}_{N+1}\right)\right]$$

$$\times \langle \Phi^{\dagger}_{\vec{q}_1,0}\cdot\Phi_{\vec{p}_1,0}\Phi^{\dagger}_{\vec{q}_2,1}\cdot\Phi_{\vec{p}_2,1}\cdots\Phi^{\dagger}_{\vec{q}_N,N-1}\cdot\Phi_{\vec{p}_N,N-1}\rangle \qquad (4.78)$$

where <...> is an ensemble average with respect to the Gaussian functional in equation (4.54). Using the second moment

$$\langle \Phi^{\dagger}_{\vec{q},\alpha}\cdot\Phi_{\vec{p},\beta}\rangle = \delta_{\vec{q},\vec{p}}\delta_{\alpha,\beta}\left[\frac{f(\vec{q})}{N_l}\right] \qquad (4.79)$$

the partition function of a single chain is

$$Z_1 = \frac{N_1!}{2N!} \prod_{\alpha=1}^{N} \sum_{\vec{q}_\alpha} e^{-i\vec{q}_\alpha \cdot (\vec{r}_\alpha - \vec{r}_{\alpha-1})} \frac{f(\vec{q}_\alpha)}{N_1} \Big|_{\vec{r}_1 \neq \vec{r}_2 \neq \ldots \neq \vec{r}_{N-1}} \qquad (4.80)$$

Using definition of $f(\vec{q}_\alpha)$ in equation (4.37), together with the following representation of the Kronecker-δ

$$\delta(\vec{r}_i, \vec{r}_j + \vec{a}_\alpha) = \frac{1}{N_1} \sum_{\vec{q}} e^{i\vec{q} \cdot (\vec{r}_i - \vec{r}_j - \vec{a}_\alpha)} \qquad (4.81)$$

Z_1 may be transformed so;

$$Z_1 = \frac{N_1!}{2N!} \prod_{\alpha=1}^{N} \sum_{\beta_\alpha=1}^{z} \delta(\vec{r}_\alpha, \vec{r}_{\alpha+1} + \vec{\beta}_\alpha) \Big|_{\vec{r}_1 \neq \vec{r}_2 \neq \ldots \neq \vec{r}_{N-1}} \qquad (4.82)$$

The constraint in the previous equation that no two segments sit on the same lattice site, and the factorial $(N_1!)/N!$ are equivalent to the restricted summation, hence

$$Z_1 = \frac{1}{2} \sum_{\vec{r}_1 \neq \vec{r}_2 \neq \ldots \neq \vec{r}_{N+1}=1}^{N_1} \prod_{\alpha=1}^{N} \sum_{\beta_\alpha=1}^{z} \delta(\vec{r}_\alpha, \vec{r}_{\alpha+1} + \vec{\beta}_\alpha) \qquad (4.83)$$

Equation (4.83) can be interpreted as the number of configurations for a set of (N+1) segments on an N_1-site lattice without overlap. Note that $\delta(\vec{r}_\alpha, \vec{r}_{\alpha+1} + \vec{\beta}_\alpha)$ means that

the position of two segments has to be separated by a lattice vector. Summation over β explains the allowed orientation of the lattice vector in a lattice with coordination number z. The product over α, together with the argument of the Kronecker-δ indicates that all segments are linked in sequence. And the condition that the segments are not allowed to overlap is given by the restricted sum. If we have n_p chains, the partition function is

$$Z_{n_p} = \frac{1}{2^{n_p} \Pi_p!} \sum_{\substack{\vec{r}_1^1 \neq \vec{r}_2^1 \neq \ldots \neq \vec{r}_{N+1}^1 \\ \vec{r}_1^2 \neq \vec{r}_2^2 \neq \ldots \neq \vec{r}_{N+1}^2 \\ \neq \ldots\ldots\ldots\ldots\ldots \neq \\ \vec{r}_1^{n_p} \neq \vec{r}_2^{n_p} \neq \ldots \neq \vec{r}_{N+1}^{n_p} = 1}}^{N_1} \prod_{m=1}^{n_p} \prod_{\alpha=1}^{N} \sum_{\vec{\beta}_\alpha^m = 1}^{z} \delta(\vec{r}_\alpha^m, \vec{r}_{\alpha+1}^m + \vec{\beta}_\alpha^m) \tag{4.84}$$

Equation (4.84) is the partition function for the so called polymer packing problem of n_p chains, each having (N+1) segments, on a lattice of size N_l[102]. The calculation of the mean field entropy and its correction is equivalent to the cluster expansion of equation (4.84). This expansion may be derived by writing

$$\sum_{\vec{\beta}_\alpha}^{z} \delta(\vec{r}_\alpha^m, \vec{r}_{\alpha+1}^m + \vec{\beta}_\alpha^m) = \frac{z}{N_l} \{ 1 + \frac{1}{z} \sum_{\vec{\beta}_\alpha} \sum_{\vec{q} \neq 0} e^{i\vec{q} \cdot (\vec{r}_\alpha^m - \vec{r}_{\alpha+1}^m - \vec{\beta}_\alpha^m)} \}$$

(4.85)

If we define Y_α^m by

$$Y_\alpha^m = \sum_{\vec{q}_\alpha \neq 0} \frac{f(\vec{q}_\alpha)}{Z} e^{i\vec{q}_\alpha \cdot (\vec{r}_\alpha^m - \vec{r}_{\alpha-1}^m)} \tag{4.86}$$

which is the factor associated with a bond (Appendix C), then (4.84) may be reexpressed

$$Z_{n_p} = \frac{1}{2^{n_p} n_p!} \sum_{\cdots\cdots} \prod_{m=1}^{n_p} \prod_{\alpha=1}^{N} (1 + Y_\alpha^m) \frac{Z}{N_l} \tag{4.87}$$

Notice that Y_α^m depends explicitly on the position of the two segments forming the α-bond on the m^{th} chain, hence Y_α^m represents the correction arising from the correlation of the monomer positions. The leading contribution to the partition function comes from the unity. Since it does not depend on the connectivity index α and the site location, it will yield the mean field result

$$Z_{n_p,MF} = \frac{1}{2^{n_p} n_p!} \sum_{\cdots} \prod_{n=1}^{n_p} \prod_{\alpha=1}^{N} \frac{z}{N_l}$$

$$= \frac{1}{2^{n_p} n_p!} \sum_{\cdots} \left(\frac{z}{N_l}\right)^{n_p N} \qquad (4.88)$$

The restricted sum will give $N_l! / [N_l-(N+1)n_p]!$, hence the mean field result in equation (4.45) is recovered. Expanding the product in Y_α^m corresponds to a bond-cluster expansion; a term linear in Y_α^m is a correction due to one bond, a term with two Y_α^m's is required for two-bond correlation, etc. The diagrammatic rules follow immediately as shown in Appendix C.

The cluster expansion becomes more complicated as the number of bonds increases. In general, for example see equations (4.67,73-75), the partition function may be expanded as

$$Z_{n_p} = Z_{n_p,MF} [\, 1 + \sum_B \gamma_D D_B \,] \qquad (4.89)$$

where the summation is over the number of bonds B involved in the diagram, γ_D is the number of ways of selecting a particular bond diagram from n_p chains of (N+1) segments. Since a chain may have branches, γ_D depends on the chain architecture. D_B is a product of a combinatorial factor α which accounts for the number of distinct arrangements, and a diagrammatic factor d_B (see Appendix C). α is given by

$$\alpha = s[N_1(N_1-1)\ldots.(N_1-n_v+1)]^{-1} \qquad (4.90)$$

where s indicates the symmetry factor arising from identical diagrams, and

$$d_B = \sum_c f_{B,c} R_{B,c} \qquad (4.91)$$

In equation (4.91) c is the counting index. $f_{B,c}$ is a factor coming from the contraction of the original diagram into diagram $R_{B,c}$ because of $\delta[m_1]\delta[m_2]\ldots\delta[m_p]$,

$$f_{B,c} = \prod_{\alpha=1}^{p} (-1)^{m_\alpha - 1} (m_\alpha - 1)! \qquad (4.92)$$

For example, consider two-non-consecutive-bond diagram in Fig. 4.4b. Since there are two bonds, B=2. There are two possible diagrams for the placement of two bonds; on a single chain which yields $\gamma_1 = n_p(N-1)(N-2)$, and on different chains with $\gamma_2 = n_p(n_p-1)N^2$. The factor α in both cases is given by $1/2[N_1\ldots(N_1-3)]^{-1}$. $f_{B,c}$ corresponds to the coefficients of Kronecker-δ in equation (C.14). In the thermodynamic limit only $R_{2,1}$ survives, which corresponds to the second diagram of Appendix E. This diagram comes from the $\delta[2]\delta[2]$ terms, hence $f_{2,1} = (-1)^{1+1}((2-1)!)^2$. There are two possible ways to obtain $R_{2,1}$ from Fig. 4.4b. With this value of $R_{2,1}$ one obtains

$$[\gamma_1 + \gamma_2]\, D_2 = \frac{[n_p(N-1)\,(N-2) + n_p(n_p-1)\,N^2]}{2N_1 \ldots (N_1-3)} \left[\frac{2N_1^3}{z} - 2N_1^2\right] \tag{4.93}$$

The calculation of the entropy follows from eqn. (4.89),

$$S_{n_p} = k \log Z_{n_p,MF} + \sum_B \gamma_B D_B - \frac{1}{2}\left(\sum_B \gamma_B D_B\right)^2 + \frac{1}{3}\left(\sum_B \gamma_B D_B\right)^3 + \ldots \tag{4.94}$$

The expansion of the logarithmic terms in the previous equation is equivalent to a cumulant expansion. Examples of the effect of the expansion on the bond diagram can be seen in Fig. 4.5.

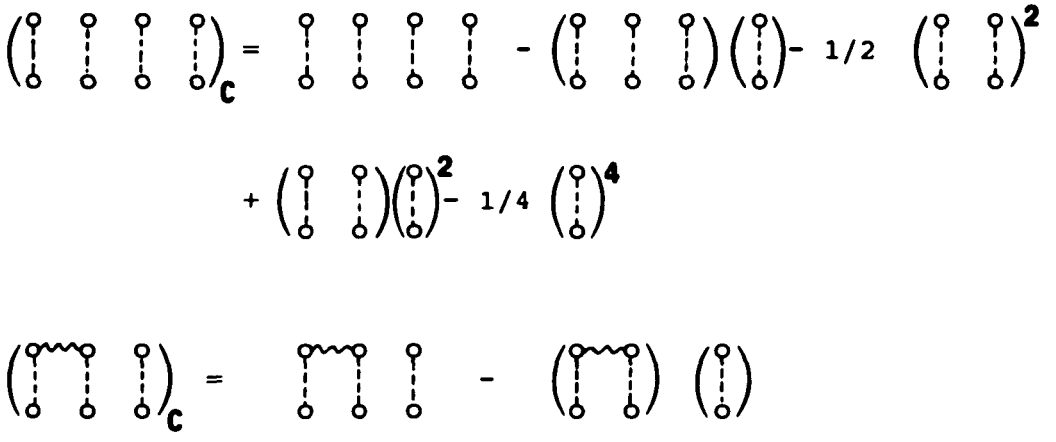

Figure 4.5. Examples of a cumulant expansion.

In figure 4.5 diagrams on the right side inside the parenthesis correspond to higher order terms in the expansion (4.94), and the indices c on the left side stand for the cumulant. Working with the cumulant simplifies the calculation and also eliminates higher powers of N_l. The entropy is proportional to N_l as expected for an extensive quantity. To obtain the entropy of mixing we subtract from Eqn. (4.94) the entropy of the pure system.

$$\Delta S^{mix} = S_{n_p} - \sum_i \phi_i S_i$$

$$\Delta S^{mix} = S_{n_p} - \sum_i \phi_i S_i \qquad (4.95)$$

where the entropy of the pure species i, S_i, is $S_{n_p}(\phi_i=1)$.

Diagram set I in Appendix H is required to calculate the equation of state up to $O(z^{-2})$. After some calculations, one may obtain the cumulant values for a monodisperse solution, as shown in Appendix G. All the calculations of the cumulant were performed in the thermodynamic limit ($N_l \to \infty$) such that the segment density $\phi=[n_p(N+1)]/N_l$ is fixed. In the monodisperse case, the pressure can be obtained from ΔS^{mix}. Writing $\Delta S^{mix} = N_l \Delta s^{mix}$, and using $\phi=N_t/N_l$ (N_t is the number of segments), then

$$\frac{\Pi}{T} = \frac{\partial}{\partial N_l}[N_l \Delta s^{mix}]$$

$$= \left(1 - \phi \frac{\partial}{\partial \phi}\right) \Delta s^{mix} \qquad (4.96)$$

where we assume that the volume of the lattice cell is unity. The compressibility factor of linear chains with M = N+1, defined as $W = \pi M/(\phi k_B T)$, is

$$W_{lin} = -\frac{M}{\phi}\log(1-\phi) - (M-1)$$
$$-\phi\left\{\frac{N^2}{z(N+1)} + \frac{3N^2-6N+1}{z^2(N+1)}\right\}$$
$$-\phi^2\left\{\frac{-20N^3+24N^2}{3z^2(N+1)^2}\right\}$$
$$-\phi^3\left\{\frac{6N^4}{z^2(N+1)^3}\right\} + O(z^{-3}) \qquad (4.97)$$

which was obtained by Bawendi and Freed[96]. The compressibility factor for monodisperse solutions is in good agreement with simulation results in two and three dimensions[22,144].

For chains with branched structure, such as shown in figure 4.6.,

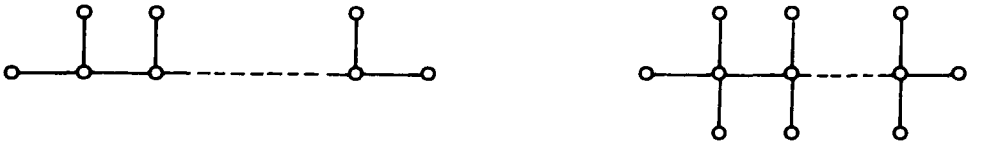

Structure 1 Structure 2

Figure 4.6. Chains with branch-structure.

the partition function is

$$Z_{n_p} = \frac{1}{2^{n_p} n_p!} \sum_{\cdots} \prod_{m=1}^{n_p} \left[\prod_{\alpha=1}^{N} \sum_{\beta_\alpha^m=1}^{z} \delta(\vec{r}_\alpha^m, \vec{r}_{\alpha+1}^m + \vec{\beta}_\alpha^m) \prod_{\omega=1}^{b} \prod_{\mu=2}^{N} \sum_{\beta_{\mu,\omega}^m=1}^{z} \delta(\vec{r}_\mu^m, \vec{r}_{\nu,\omega}^m + \vec{\beta}_{\mu,\omega}^m) \right] \tag{4.98}$$

where b denotes the number of branches and $\vec{r}_{\nu,\omega}^{\,m}$ indicates the position of the dangling site of branch ω eminating from the back-bone site $\vec{r}_\mu^{\,m}$. Using the definition of Y_α^m, Eqn. (4.86) and

$$Y_{\mu,\omega}^m = \frac{1}{z} \sum_{\vec{q} \neq 0} f(\vec{q})\, e^{i\vec{q}\cdot(\vec{r}_\mu^m - \vec{r}_{\nu,\omega}^m)} \tag{4.99}$$

the partition function can be recast into similar form as for linear chains.

$$Z_{n_p} = \frac{1}{n_p!\, 2^{n_p}} \sum_{\cdots} \prod_{m=1}^{n_p} \prod_{\xi=1}^{N} [1 + Y_\xi^m] \frac{z}{N_1} \tag{4.100}$$

where $Y_\xi^m = \{Y_\alpha^m,\ Y_{\nu,\omega}^m\}$. The analysis and diagrammatic rules follow similarly as in linear chains[97]. However, we have to include diagrams F, O, P, and Q of Appendix H to account for the monomer structures. The compressibility factor for the first branched structure is

$$W_{branch\text{-}1} = -\frac{M}{\phi}\log(1-\phi) - (M-1)$$
$$-\phi\left\{\frac{(M-1)^2}{zM} + \frac{\frac{25}{4}M^2-29M+25}{z^2M}\right\}$$
$$-\phi^2\left\{(M-1)^2\frac{-32M+68}{3z^2M^2}\right\}$$
$$-\phi^3\left\{\frac{6(M-1)^4}{z^2M^3}\right\} + O(z^{-3}) \qquad (4.101)$$

For the second branched structure, it is given by

$$W_{branch\text{-}2} = -\frac{M}{\phi}\log(1-\phi) - (M-1)$$
$$-\phi\left\{\frac{(M-1)^2}{zM} + \frac{10M^2-52M+46}{z^2M}\right\}$$
$$-\phi^2\left\{(M-1)^2\frac{-44M+92}{3z^2M^2}\right\}$$
$$-\phi^3\left\{\frac{6(M-1)^4}{z^2M^3}\right\} + O(z^{-3}) \qquad (4.102)$$

The first two terms are equivalent to the result for linear chains. It corresponds to Flory's mean field approximation where segment correlations and chain structure are neglected and, therefore, do not affect the equation of state. Our simulation results for branch polymers are presented in the next chapter.

4.2.4. The Equation of State of Polydisperse Chains with Uniform Distribution.

Real polymer fluids are almost never realized in strictly monodisperse form. Monte Carlo simulations and theoretical model should therefore be used to learn the effect of polydispersity. In this section, we apply Freed's polymer packing model to obtain the equation of state in a regular lattice. The effect of polydispersity on conformational properties was studied by Ohta and Oono[72] in the framework of conformational renormalization group; the simulation results are presented in the next chapter.

In the polymer-packing model, the partition function is almost the same as for monodisperse chains. The only modification is the requirement to include species indices; the diagrammatic rules remain the same. Little complication arises when we consider diagrams with non-consecutive bonds, since they may reside on different species. The partition function has the following form

$$Z_{n_p,k} = Z_{n_p,k;MF}\left[1 + \frac{(N_1 - \sum_{\tau=1}^{k} n_\tau M_\tau)!}{N_1!} \times \sum_{\{\ldots\}} \{ \sum_{\tau,a_\tau,m_\tau} Y_{a_\tau;\tau}^{m_\tau} + \sum_{\{\tau,a_\tau,m_\tau\}>\{\tau',a'_{\tau'},m'_{\tau'}\}} Y_{a_\tau;\tau}^{m_\tau} Y_{a'_{\tau'};\tau'}^{m'_{\tau'}} + \ldots \right] \tag{4.103}$$

where the index τ indicates the species, and M_τ is the number of segments in species τ. Our calculation is in agreement with the result of J. Dudowicz and K. F. Freed[103,105]. Here we also present the result for uniformly distributed linear chains. The correction to the mixing entropy per site is

$$\frac{\Delta S_{pd}^{mix,corr}}{N_l} = \sum_{\mu,\nu=1}^{k} \phi_\mu \phi_\nu A_{\mu,\nu} + \sum_{\mu,\nu,\tau=1}^{k} \phi_\mu \phi_\nu \phi_\tau B_{\mu,\nu,\tau} + \sum_{\mu,\nu,\tau,\lambda=1}^{k} \phi_\mu \phi_\nu \phi_\tau \phi_\lambda C_{\mu,\nu,\tau,\lambda}$$
$$- \sum_{\mu=1}^{k} (A_{\mu,\mu} + B_{\mu,\mu,\mu} + C_{\mu,\mu,\mu}) \phi_\mu \qquad (4.104)$$

where k is the number of species,

$$A_{\mu,\nu} = \frac{N(1,\mu)N(1,\nu)}{z} - \frac{4N(1,\mu)N(2,\nu)}{z^2} - \frac{6N(1,\mu)N(\perp,\nu)}{z^2}$$
$$- \frac{2N(1,\mu)N(3,\nu)}{z^2} + \frac{N(2,\mu)N(2,\nu)}{z^2} - \frac{2N(1,\mu)N(1,2;\nu)}{z^2}$$
$$+ \frac{2N(1,\mu)N(1,\nu)N(2,\nu)M_\nu}{z^2} \qquad (4.105)$$

$$B_{\mu,\nu,\tau} = \frac{8}{3z^2} N(1,\mu)N(1,\nu)N(1,\tau) + \frac{4}{z^2} N(1,\mu)N(1,\nu)N(1,1;\tau)$$
$$- \frac{2}{z^2} N(1,\mu)N(1,\nu)N(1,\tau)^2 M_\tau \qquad (4.106)$$

and

$$C_{\mu,\nu,\tau,\lambda} = \frac{2}{z^2} N(1,\mu) N(1,\nu) N(1,\tau) N(1,\lambda) \qquad (4.107)$$

In the previous equations we use the following notation: $N_{i,\mu}$ is the number of ways to place an i consecutive bonds on a chain of species μ, $N_{i,j,\mu}$ is the number of ways to place two bond-sequences, one with i consecutive bonds and the other with j consecutive bonds, on a chain of species μ (see Appendix F for monodisperse chains). Let us define $N(i;\mu) = N_{i,\mu}/M_\mu$, $N(i,j;\mu) = sN_{i,j,\mu}/M_\mu$, with $s=(2 - \delta_{i,j})/2$. In this section we are interested in a distribution in which the chain densities for k species ranging from N to N+k-1 are equal, $\phi_c = \phi_\mu/M_\mu$. We call this a uniform distribution, then the correction to the osmotic pressure is

$$\frac{\Delta\Pi_{pd}^{corr}}{k_B T} = -\phi_c^2 \sum_{\mu,\nu=1}^{k} M_\mu M_\nu A_{\mu,\nu} - 2\phi_c^3 \sum_{\mu,\nu,\tau=1}^{k} M_\mu M_\nu M_\tau B_{\mu,\nu,\tau} - 3\phi_c^4 \sum_{\mu,\nu,\tau,\lambda=1}^{k} M_\mu M_\nu M_\tau M_\lambda C_{\mu,\nu,\tau,\lambda} \qquad (4.108)$$

For linear chain, after a straightforward but long calculation, equation (4.108) becomes

$$\frac{\Delta\Pi_{pd}^{corr}}{k_BT} = -\phi_c^2\left[\frac{k^2}{4z}(2N+k-1)^2+\frac{k^2}{z^2}\{1+\frac{3}{4}(2N+k-1)(2N+k-5)\}\right]$$

$$+\phi_c^3\left[\frac{k^3}{12z^2}(2N+k-1)^2(20N+10k-34)\right]$$

$$-\phi_c^4\left[\frac{3k^4}{8z^2}(2N+k-1)^4\right] \qquad (4.109)$$

where N is the number of bonds in the shortest chain. Note that the chain-length average $\bar{N} = (2N+k-1)/2$. The osmotic pressure, then is given by $\pi = \pi^{MF} + \Delta\pi_{pd}^{corr}$

$$\frac{\Pi_{MF}}{k_BT} = \phi_c\sum_{\mu=1}^{k}[1-M_\mu] - \log(1-\sum_{\mu=1}^{k}\phi_\mu) \qquad (4.110)$$

and the compressibility factor follows accordingly, $W_{pd} = \pi/\phi_c$.

4.3. The Equation of State of Non-Athermal Monodisperse Linear Chains.

Consider the chain configuration in figure (4.1), with a nearest-neighbor effective interaction between monomers ϵ (in units of k_BT). The total energy is given by

$$\exp\Big(\sum_{i,j\in S\subset\Lambda} \epsilon^{\langle ij\rangle}\Big) = \prod_{i,j\in S} \Big[1 + \sum_{\beta=1}^{z} \delta(i, j+\beta) f\Big] \qquad (4.111)$$

where f = e'-1 and S is the set of lattice sites occupied by monomers. <ij> denotes a pair of nearest neighbor sites and $\delta(i,j+\beta) = \delta(\vec{r}_i, \vec{r}_j+\vec{a}_\beta)$. The partition function in the presence of interaction is

$$Z_{n_p} = \frac{1}{n_p!\, 2^{n_p}} \sum_{(\ldots)} \prod_{m=1}^{n_p} \prod_{\alpha=1}^{N} \sum_{\beta_\alpha^m=1}^{z} \delta(i_\alpha^m, i_{\alpha+1}^m+\beta_\alpha^m) \exp\Big(\sum_{i,j\in S} \epsilon^{\langle ij\rangle}\Big) \qquad (4.112)$$

The product in equation (4.111) can be expanded as (Mayer expansion)

$$\prod_{i,j\in S} \Big[1 + \sum_{\beta=1}^{z} \delta(i, j+\beta) f\Big] = 1 + \sum_{\beta=1}^{z} \sum_{i>j} \delta(i, j+\beta) f + \sum_{\beta,\beta'=1}^{z} \sum_{(i>j)\neq(i'>j')} \delta(i, j+\beta)\delta(i', j'+\beta') f^2 + \ldots \qquad (4.113)$$

Terms with $\delta(i,j+\beta)f$ are represented by solid lines (see Appendix H) to distinguish them from the correlating-bond diagrams. The diagrammatic expansion of the partition function, therefore, includes both correlating bonds and interaction lines. For each interaction line one has

$$f\sum_{\beta=1}^{z}\delta(i,j+\beta) = \frac{zf}{N_1}\sum_{\vec{q}} e^{-i\vec{q}\cdot(\vec{r}_i-\vec{r}_j)}\,\frac{f(\vec{q})}{z} \qquad (4.114)$$

In equation (4.114) the summation is with respect to all momentum values, in contrast to the correlating-bond diagrams where the summation is restricted to non-zero momenta. Also we have an additional factor N_1^{-1} from the definition of the Kronecker-δ function. Following Dudowics[105], one can always separate the $\vec{q}=0$ and $\vec{q}\neq 0$ components of (4.114) so that the product in equation (4.111) can be reexpressed as

$$e^{\sum_{i,j\in s} e^{\langle ij\rangle}} = \prod_{\substack{i,j\in S\\ i>j}} \left[1 + \frac{fz}{N_1} + \frac{fz}{N_1}\sum_{\vec{q}\neq 0} e^{-i\vec{q}\cdot(\vec{r}_i-\vec{r}_j)}\,\frac{f(\vec{q})}{z}\right] \qquad (4.115)$$

$$= \prod_{\substack{i,j\in S\\ i>j}} \left[1 + \frac{fz}{N_1}\right]\left[1 + \frac{fz}{N_1\left[1+\frac{fz}{N_1}\right]}\sum_{\vec{q}\neq 0} e^{-i\vec{q}\cdot(\vec{r}_i-\vec{r}_j)}\,\frac{f(\vec{q})}{z}\right]$$

Since the first factor does not depend on the coordinates, the product over i,j yields

$$e^{\sum_{i,j\in s} e^{\langle ij\rangle}} = \left[1 + \frac{fz}{N_1}\right]^{\frac{n_p N(n_p N-1)}{2}} \times \prod_{\substack{i,j\in S\\ i>j}} \left[1 + \frac{fz}{N_1\left[1+\frac{fz}{N_1}\right]}\sum_{\vec{q}\neq 0} e^{-i\vec{q}\cdot(\vec{r}_i-\vec{r}_j)}\,\frac{f(\vec{q})}{z}\right] \qquad (4.116)$$

The free energy is

$$\frac{F}{k_BT} = -\frac{fz}{2}\phi^2 N_1$$

$$- \log\left[\frac{1}{n_p!\,2^{n_p}}\sum_{(\ldots)}\prod_{m=1}^{n_p}\prod_{a=1}^{N}\frac{z}{N_1}\{1+\sum_{\vec{q}\neq 0}\frac{f(\vec{q})}{z}e^{-i\vec{q}\cdot(\vec{r}_{i_a}-\vec{r}_{i_{a-1}})}\}\right.$$

$$\left.\times\prod_{\substack{i,j\in s\\ i>j}}\{1+\frac{fz}{N_1[1+\frac{fz}{N_1}]}\sum_{\vec{p}\neq 0}\frac{f(\vec{p})}{z}e^{-i\vec{p}\cdot(\vec{r}_i-\vec{r}_j)}\}\right] \qquad (4.117)$$

Equation (4.117) indicates that the calculation of the interaction lines follows a similar pattern as that for the correlating bond except that for each interaction line we have to include a factor $fz/(N_1)$. When we take $\vec{q}=0=\vec{p}$, the second term together with the lowest order in ϵ of first term correspond to the mean-field result in non-athermal systems. If we retain $\vec{q} \neq 0$ and $\vec{p} = 0$, the right side corresponds to the correction due to correlating-bonds as obtained in the athermal case. Terms with $\vec{q} = 0$ and $\vec{p} \neq 0$ are related to the extended mean field approximation of Bawendi and Freed[95], where all energy diagrams are taken onto account disregarding segment correlations. Terms with $\vec{q}\neq 0\neq\vec{p}$ correspond to energetic corrections to the mean-field value, with correlation bonds also included. The free energy can be written as

$$\frac{F}{k_BT} = -N_1\frac{fz}{2}\phi^2 - \log Z_{n_p,MF} - \log\{1+\sum_{B,1}\gamma_{d,1}D_{B,1}\} \qquad (4.118)$$

where $\gamma_{D,l}$ is a factor depends on the chain architecture and $D_{B,l}$ is a factor which comes from the contracted diagrams of B bonds and l interaction lines. By considering equation (4.117) and the comments that follow it, the calculation of diagrams with B bonds and l interaction lines is similar to the diagrams with (B+l) correlating bonds with the end result multiplied by $(fz/N_t)^l$. We may also encounter diagrams involving loops, since the interaction lines might connect sites linked by a sequence of bonds. These loop diagrams are never present in the ordinary correlating bond diagrams, however, the rule of contraction remains valid and all the procedures follow similarly. $\gamma_{D,l}$ requires explanation. It comes from the choice of placing B bonds on n_p chains, the number of ways extracting sites involved in the interaction exclusive of the ones in the bonds, and the number of ways to construct the interaction lines. In the first diagram of figure (4.7), with $N_t = Mn_p$ is the number of segments,

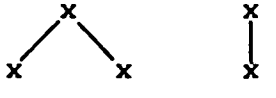

$$\binom{N_t}{3}\binom{N_t-3}{2} \quad (3)$$

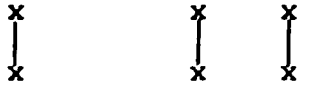

$$\binom{N_t}{2}\binom{N_t-2}{2}\binom{N_t-4}{2}\,1/3!$$

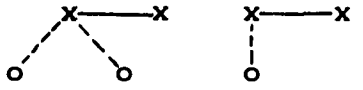

$$N_2 n_p N_1 (n_p - 1) \binom{N_t - 5}{2} \quad (4)$$

Figure 4.7. Examples of diagrams with interaction lines.

There are $\binom{N_t}{3}$ ways to pick the first three sites, $\binom{N_t - 3}{2}$ ways of the last two sites and three ways to link sites on each grouping. The factor $N_2 n_p N_1 (n_p - 1)$ associated with the last diagram corresponds to the number of ways of selecting the correlating bonds out of n_p chains, $\binom{N_t - 5}{2}$ is the number of ways of selecting two cross vertices from the rest of the segments, multiplied by four to construct interaction lines. The calculation of the free energy up to $O(\epsilon^4, z)$ for energy diagrams involving no correlating bonds, $O(\epsilon, z^{-1})$ for diagrams with correlating bonds and a single interaction line, and to $O(\epsilon^2, z^0)$ for diagrams with correlating bonds and two interaction lines, can be found in Dudowicz et. al[105]. For convenience we include the diagram sets in Appendix H and the result of calculation in Appendix G. Our calculation for a monodisperse system for the free energy of mixing yields

$$\frac{\Delta F^{mix}}{N_1 k_B T} = \frac{1}{N_1 k_B T}(\Delta F^{I} + \Delta F^{II} + \Delta F^{III} + T\Delta S^{mix}) \qquad (4.119)$$

where ΔS^{mix} is the athermal result,

$$\begin{aligned}\frac{\Delta S^{mix}}{k_B N_1} &= -\frac{\phi}{M} - (1-\phi)\log(1-\phi) \\ &+ (\phi^2-\phi)\left[\frac{\{N(1)\}^2}{z} - \frac{4N(1)N(2)}{z^2} - \frac{6N(1)N(\perp)}{z^2} - \frac{2N(1)N(3)}{z^2}\right. \\ &\left. + \frac{N(2)N(2)}{z^2} - \frac{2N(1)N(1,2)}{z^2} + \frac{2N(1)N(1)N(2)}{z^2}\right] \\ &+ (\phi^3-\phi^2)\left[\frac{8}{3z^2}\{N(1)\}^3 + \frac{4}{z^2}\{N(1)\}^2 N(1,1) - \frac{2}{z^2}\{N(1)\}^4 M\right] \\ &+ (\phi^4-\phi^3)\left[\frac{2}{z^2}\{N(1)\}^4\right] \qquad (4.120)\end{aligned}$$

ΔF^{I} comes from diagram set II,

$$\begin{aligned}\frac{\Delta F^{I}}{N_1 k_B T} &= \frac{ez}{2}\phi(1-\phi) - \frac{e^2 z}{4}\phi^2(1-\phi)^2 - \frac{e^3 z}{12}\phi^2(1-\phi)^2(1-2\phi)^2 \\ &- \frac{e^4 z}{48}\phi^2(1-\phi)^2[1-6\phi(1-\phi)(3\phi^2-3\phi+2)] \qquad (4.121)\end{aligned}$$

ΔF^{II} and ΔF^{III} come from diagram sets III and IV respectively,

$$\frac{\Delta F^{II}}{N_1 k_B T} = -eN(1)\phi(1-\phi)^2 + \frac{e}{z}[\phi(1-\phi)^2\{2N(2)+N(3)+3N(\perp)$$

$$+N(1,2)-N(1)N(2)M\} - 2\phi^2(1-\phi)^2\{2N(1)N(1)$$

$$+2N(1)N(1,1) - N(1)N(1)N(1)M\} - \phi^3(1-\phi)^2\{4N(1)^3\}] \qquad (4.122)$$

and

$$\frac{\Delta F^{III}}{N_1 k_B T} = -\frac{e^2}{2}N(1)\phi(1-\phi)^2(1-2\phi)^2 - e^2N(2)\phi(1-\phi)^3$$

$$- e^2N(1)^2\phi^2(1-\phi)^3(1-3\phi) + \frac{e^2}{2}N(1)^2M\phi(1-\phi)^4$$

$$- e^2N(1,1)\phi(1-\phi)^4 \qquad (4.123)$$

For linear chains with M = (N+1), equations (4.119 - 123) yield the compressibility factor

$$W_{lin}(e) = W_{lin}(athermal) + \sum_{i=1}^{7} a_i\phi^i \qquad (4.124)$$

with the coefficients of ϕ^i :

$$a_1 = \frac{e}{z}\frac{4M^2-14M+6}{M} + 2e(M-1) - \frac{Mez}{2} + e^2\left[1 - \frac{(M-1)^2}{M}\right]$$

$$- \frac{Me^2z}{4} - \frac{Me^3z}{12} - \frac{Me^4z}{48} \qquad (4.125a)$$

$$a_2 = \frac{e}{z}\frac{-18M^3+62M^2-48M+8}{M^2} - 2e(M-1) + e^2\frac{11M^2-29M+12}{M}$$

$$+ Me^2z + Me^3z + \frac{7}{12}Me^4z \qquad (4.125b)$$

$$a_3 = \frac{e}{z}\frac{30M^3-96M^2+90M-24}{M^2} + e^2\frac{-33M^2+78M-36}{M}$$

$$- \frac{3}{4}Me^2z - \frac{13}{4}Me^3z - \frac{55}{16}Me^4z \qquad (4.125c)$$

$$a_4 = -\frac{16e(M-1)^3}{zM^2} - e^2\frac{-38M^2+82M-40}{M} + 4Me^3z + 9Me^4z \qquad (4.125d)$$

$$a_5 = -\frac{15e^2(M-1)^2}{M} - \frac{5}{3}Me^3z - \frac{25}{2}Me^4z \qquad (4.125e)$$

$$a_6 = 9Me^4z \qquad (4.125f)$$

$$a_7 = -\frac{21}{8}Me^4z \qquad (4.125g)$$

In the next chapter we present simulation results for non-athermal chains over wide range of densities to test the accuracy of equation (4.124).

V. MONTE CARLO SIMULATIONS AND RESULTS.

With the advance of mathematical tools, the properties of polymer solutions and melts have become the focus of renewed attention. Application of functional integration[39,69], scaling theories[69,146], the conformation space renormalization group[69-90], and various lattice models[94-105] have revived interest in scaling behavior and the equation of state of polymer chains. Some of these analytical techniques have been discussed in previous chapters. However, understanding of the equation of state for polymer solutions and melts is not complete unless it is confirmed by experiments.

The earliest polymer equations of state are of the well-known Flory and Flory-Huggins lattice mean field theories[8-14]. The latter theory is a correction to the Flory mean field approximation. Both approximations and their extension to the nonathermal system had been discussed in Chapter IV. Although the Flory-Huggins theory is quite accurate at high densities, it overestimates the pressure in the dilute regime. The Flory and Flory-Huggins theories ignore important correlation effects associated with chain structure. The discrepancy between the predictions and experimental and simulation results grows with increasing chain length. Bawendi, Freed and others[94-105] improved the predictions for the equation of state of polymer chains by using the complex n-vector model defined on a regular lattice. Their lattice model was an extension of

the original n-vector model of de Gennes[46,47] supplemented with an extra parameter required to control the chain length[15]. It was shown that Freed's n-vector model was equivalent to a model of packing polymers on a regular lattice[102]. Systematic corrections to Flory-Huggins theory can then be derived, and segment-segment interactions can be introduced, which is not feasible in the original n-vector model. The detailed discussion of the Freed's lattice model was presented in Chapter IV. The Bawendi Freed correction for simple linear chains provides better agreement with Monte Carlo simulations in two and three dimensions[22,144].

In recent years, the progress of computer hardware and Monte Carlo simulations has had a significant impact on polymer physics[132-135]. Computer simulation yields much useful information since the parameters in the model systems are known explicitly and can be fine-tuned easily. In contrast, theoretical models are generally not exactly solvable and physical parameters are arbitrarily defined. Any discrepancy with experimental results might be caused by the model itself, by the choice of parameters or perhaps by the mathematical approximation. All theoretical predictions and simulation results have to be confirmed by experiments. However, the experiments are often hampered by impurities, and some quantities cannot be measured directly. These problems render model building more difficult. Computer simulations represent a bridge between model building (theory) and experiments. The

information provided by computer simulations is often designed to determine the accuracy of approximation and the physical parameters involved in theoretical calculations.

Monte Carlo simulation is an efficient way to test mean-field and scaling theories of chain molecules. The initial Monte Carlo studies of the equation of state were by Bellemans, Okamoto and co-workers[136-142], who determined the pressure via the test-chain insertion method. Ottinger and Khalatur et al.[115,116] tested scaling theory predictions for the partition function and osmotic pressure in simulations employing the scanning method of Meirovitch[114]. These methods, however, are restricted to low densities and short chain lengths. To circumvent these difficulties, Dickman devised a new method, in which the pressure is related to the segment density in a repulsive layer adjacent to a hard wall[22]. The repulsive-wall method permits determination of the osmotic pressure over wide range of densities (up to $\phi \approx 0.9$), even for long chains. In this chapter, I report my main original contributions in the study of polymer conformational properties. The emphasis of the study is on the chain-segment-density profile near a wall and the equation of state of polymer chains in three dimensional lattice models.

In the next section, we describe the basics of Monte Carlo simulation. It is followed, in section 5.2, by a description of the polymer models and Monte Carlo algorithms employed in our study. Section 5.3 discusses the simulation

procedures; this is followed by results of various studies in section 5.4. All data and graphics are presented in sections 5.5 and 5.6, respectively.

5.1. Monte Carlo Simulations: A Simplistic View.

Consider a chain configuration described in Fig. 5.1 (see section 5.6). Let this configuration be called $\vec{X}$, and assume that at time t it has the probability $P(\vec{X},t)$. The probability $P(\vec{X},t)$ satisfies the Markovian master equation[135,169]

$$\frac{dP(\vec{X},t)}{dt} = -\sum_{\vec{X}'} W(\vec{X}\rightarrow\vec{X}')\,P(\vec{X},t) + \sum_{\vec{X}'} W(\vec{X}'\rightarrow\vec{X})\,P(\vec{X}',t) \quad (5.1)$$

where $W(\vec{X}\rightarrow\vec{X}')$ is the transition probability from configuration $\vec{X}$ to $\vec{X}'$. In the limit $t \rightarrow \infty$, and assuming there is no problem with ergodicity, $P(\vec{X},t)$ will relax toward equilibrium. $P(\vec{X},t)$ is then replaced by its steady-state solution $P_{eq}(\vec{X})$, which satisfies

$$P_{eq}(\vec{X})\,W(\vec{X}\rightarrow\vec{X}') = W(\vec{X}'\rightarrow\vec{X})\,P_{eq}(\vec{X}') \quad (5.2)$$

If the configuration $\vec{X}$ has a total energy $E(\vec{X})$ at temperature T, the probability is

$$P_{eq}(\vec{X}) = \frac{1}{Z} e^{-\frac{E(\vec{X})}{k_B T}} \qquad (5.3)$$

where Z is the partition function, and k_B is Boltzmann's constant.

Monte Carlo simulation in equilibrium statistical mechanics was devised to approximate the sampling of the probability distribution P_{eq}. In practice, the set of configurations $\{\vec{X}_1, \vec{X}_2, \vec{X}_3, \ldots, \vec{X}_Q; Q \gg 1\}$ is generated consecutively. Using Eqs. (5.2) and (5.3), the new configuration $\vec{X}_j$ is obtained from the old configuration $\vec{X}_{j-1}$ according to

$$W_{\vec{X}_{j-1}\to\vec{X}_j} \equiv W_{j-1,j} = \begin{cases} \exp[-\delta E/(k_B T)] & \text{if } \delta E > 0 \\ 1 & \text{otherwise} \end{cases} \qquad (5.4)$$

where $\delta E = E(\vec{X}_j) - E(\vec{X}_{j-1})$. Equation (5.4) requires an explanation. If $W_{j-1,j}$ is zero, the old configuration is retained and counted once more in the configurational set, and the procedure is repeated. If $W_{j-1,j}$ is unity, the new configuration is accepted and counted, and the procedure is iterated. If $0 < W_{j-1,j} < 1$, a random number $0 \le r \le 1$ is generated and $W_{j-1,j}$ is compared with r. If it is greater than r, the new configuration is accepted and counted, otherwise it is

rejected and the old configuration is retained and counted, and the iteration is resumed. This simulation process is known as the Metropolis algorithm[170].

Suppose we are interested to measure a quantity $A(\vec{X})$ (for example: the radius of gyration). Statistical mechanics provides the procedure to obtain the average value

$$\langle A \rangle = \frac{1}{Z} \int d\vec{X} A(\vec{X}) \, e^{-E(\vec{X})/(k_B T)} \qquad (5.5)$$

The evaluation of (5.5) is performed over the whole configurational space, which is of course not available in the simulation process. Instead of using the complete configurational space, one obtains a sample of M_s configurations. If all configurations are equally likely to appear in the sample, and the average in Eqn. (5.5) is replaced by

$$\overline{A} = \frac{\sum_{I=1}^{M_s} A(\vec{X}_I) \exp[-E(\vec{X}_I)/(k_B T)]}{\sum_{I=1}^{M_s} \exp[-E(\vec{X}_I)/(k_B T)]} \qquad (5.6)$$

This method of averaging is random sampling[113]. For each configuration $\vec{X}_I$, we compute $A(\vec{X}_I)$ and the corresponding weight factor $P(\vec{X}_I) = \exp[-E(\vec{X}_I)/(k_B T)]$. The average of $A(\vec{X})$ is calculated using eqn. (5.6). However, the random sampling is

not efficient if the density of states g(E) favors high values of E. The randomly sampled contribution from the low E portion will be underrepresented resulting in poor statistics. Another method is called importance sampling method, i.e., the Metropolis[170] algorithm mentioned above. This method replaces equation (5.2) with

$$\overline{A} = \frac{1}{M_s} \sum_{I=1}^{M_s} A(\vec{X}_I) \qquad (5.7)$$

The average of $A(\vec{X})$ is now given by the mean over the samples, since each configuration occurs with its canonical probability.

In the simulation process, the averaging of $A(\vec{X})$ is performed after the system has already relaxed and at interval $\Delta t \geq \tilde{N}$, where $\tilde{N}$ is the total number of monomers in the system. Therefore, if Q is the number of Monte Carlo iterations, $M_s = Q/\Delta t$. For relaxation criteria, one may investigate the polymer properties in the system. For example: the value of $A(\vec{X})$ should be steady; segment density and bond-orientation, in the absence of external potential or stiffness, should be uniformly distributed (see section 5.3).

5.2. Polymer Models and Monte Carlo Algorithms.

5.2.1. The Lattice Model.

In our simulation we employed a cubic lattice, in which each site may be occupied by a chain segment or by a solvent molecule (a void). To emulate the excluded volume effect, double occupancy is prohibitted. Figure 5.1 shows linear chains in a square lattice. ϵ is the effective interaction, and ℓ is the bond-length, which is equal to a unit lattice distance. In the non-athermal system, the interaction energy is of the nearest-neighbor type. Note that the bond-length in the lattice model might correspond to the real bond-length of a short polymer, it might also represent the effective bond-length of a long polymer.

5.2.2. The Iteration Techniques.

In our simulations, we mainly employed two different techniques to realize the Monte Carlo iterations of equation (5.4). One is the reptation or slithering snake-like motion[117,118], the other is an internal move (a variant of the kink-jump motion[119-122]), as shown in Fig. 5.2.

Starting from an arbitrary configuration, a chain is selected at random and one of the chain-ends, randomly selected, is allowed to move one step subject to condition

(5.4). In the athermal case δE is equal 0 or ∞ corresponding to a movement to a vacant or an occupied site, so W = 1 or 0. This condition reflects the excluded volume constraint: a move is successful if the target site is unoccupied. In the non-athermal case, in addition to the excluded volume contraints, δE is governed by the change in the total energy of the chain configuration, so that the move is accepted with the probabilty $p=\min(1,\exp[-\delta E/(k_B T)])$. If the move is successful, the rest of the segments slither along the chain contour. The reptation algorithm proves very efficient when applied to polymers with branched-structures. This algoritm, however, is not strictly ergodic[21]. In branched polymers, in which there are b dangling sites emanating from a backbone segment, a chain is allowed to reptate if in the neighborhood of the chain end there are at least (b+1) vacant sites. The locked-in configurations, where all nearest-neighbor sites of the chain ends are occupied, are inaccessible from other configurations via reptation. We adopt the usual assumption that the number of such configurations in three dimensions is very small, and does not give significant contribution.

In addition to reptation, we also employed internal moves algorithm in our simulations. One third to one half of the attempted moves in our simulations were of this kind. The exception was the simulations of polymers with branched-structure, for which internal moves were inefficient, so only reptation was employed. The internal move is a simplified

kink-jump motion. In such moves, a segment i ($i \neq 1$ or N), at position $\vec{x}_i$, and such that $\vec{x}_{i-1}$, $\vec{x}_i$, and $\vec{x}_{i+1}$ are not colinear, is reflected about the line joining $\vec{x}_{i-1}$ and $\vec{x}_{i+1}$. In the non-athermal system, non-overlapping trial configurations were accepted with probability $P=\min(1,\exp(-\Delta n\epsilon/k_BT))$ where $\Delta n=n_f-n_i$ is the difference between the final and initial numbers of nearest neighbor occupied sites. ϵ/k_BT is the monomer-monomer interaction parameter. As in the reptation technique, this algorithm also suffers from non-ergodicity by neglecting the locked-in configurations. A method had been devised to overcome this problem by allowing the bond-length to vary. This method was used primarily in simulations of the so-called fluctuating-bond model[135,173,174].

5.2.3. Determination of Insertion Probability and The Osmotic Pressure.

Our studies focused on the equation of state at various densities, segment density profiles as a function of distance from the wall, and other conformational properties like the end-to-end distance. To obtain the equation of state at low densities, we employed the test-chain insertion technique, while at high densities we used the more efficient repulsive-wall method[22].

A. The Test-Chain Insertion Method[143].

In our simulations, the test-chain and the main configuration evolve independently, via the Metropolis algorithm rule described above. Assuming X is the test chain configuration, the insertion probability is estimated from the success rate of placing X in the main configuration. In the nonathermal case, we have to take the monomer-monomer interaction into consideration (see Section 4.1). After getting the insertion probability at various densities, the osmotic pressure may be obtained from equation (4.24).

The test-chain insertion method, when applied to a non-athermal system, can be used to obtain the θ-temperature. Consider a dilute solution ($\phi < \phi^*$, where ϕ^* is the overlap density). The pressure takes the form

$$\Pi^* = \frac{\Phi}{M} + A_2\phi^2 + \ldots \tag{5.8}$$

where A_2 is the second virial coefficient, and M is the number of segments in a chain. The osmotic pressure is also given by Eqn. (4.24). For ϕ near zero, one can assume a linear relation between log $p(\phi)$ and log $(1-\phi)$. Expanding $\log(1-\phi)$ to $O(\phi)$ and equating Eqn. (4.24) with (5.8), one can find

$$A_2 = \frac{1}{2M} \frac{\log P}{\log (1-\phi)} \qquad (5.9)$$

The θ-temperature, by definition, is the temperature at which the second virial coefficient vanishes[7]. Equation (5.9) vanishes provided $p(\phi)$ is identically equal to unity. In simulations of non-athermal systems, the insertion factors $p(\phi)$ may be taken at different temperature, and θ-temperature is obtained by interpolating $p(\phi) = 1$ on the resulting graph.

Monte Carlo simulations employing test-chain insertion are limited to low density and short chains. The insertion probability for a chain of length M at density ϕ is roughly proportional to $(1 - \phi)^M$, so succesful insertions become rare events for long chains and/or high densities. Dickman, extending his work on off-lattice simulations, invented an efficient technique (repulsive-wall method) in which one may obtain the osmotic pressure directly[22].

B. The Repulsive-Wall Method[22].

Consider a d-dimensional cubic lattice, of length L in d-1 dimensions, and of length H in the remaing direction, with which we associate the coordinate x. There is an infinite repulsive potential at x = 0 and x = H + 1; in the other directions, periodic boundary conditions are assumed. If $Z(n_p,M,L,H)$ denotes the partition function for a system of n_p

M-mer chains on the lattice, then

$$Z(n_p, M, L, H) = \frac{1}{n_p!} \sum_{\vec{x}_1, \vec{x}_2, \ldots, \vec{x}_{Mn_p}} e^{-\beta U(\vec{x}_1, \ldots, \vec{x}_{Mn_p})} \qquad (5.10)$$

where the segment coordinates $\vec{x}_1$, $\vec{x}_2, \ldots \vec{x}_{Mn_p}$, are restricted to the lattice, and the potential U incorporates restrictions which define the chain structure and include the excluded volume constraint and other segment-segment interactions. In the continuous space model, one may obtain the pressure from

$$\Pi^* = \frac{\partial}{\partial V} \log Z(n_p, M, L, H) = L^{-(d-1)} \frac{\partial}{\partial H} \log Z(n_p, M, L, H) \qquad (5.11)$$

The analogous expression for the lattice model is

$$\Pi^* = L^{-(d-1)} [\log Z(n_p, M, L, H) - \log Z(n_p, M, L, H-1)] \qquad (5.12)$$

Now modify the model by associating with each occupied site in the plane x = H the Bolzmann factor $\lambda = e^{-\beta V}$ $(0<\lambda<1)$, which may be viewed as a repulsive potential in the vicinity of the wall. The partition function becomes

$$Z(n_p, M, L, H, \lambda) = \frac{1}{n_p!} \sum_{\vec{R}_1, \vec{R}_2, \ldots, \vec{R}_{Mn_p}} e^{-\beta U(\vec{R}_1, \ldots, \vec{R}_{Mn_p})} \lambda^{N(H)} \quad (5.13)$$

where N(H) is the number of occupied sites in the plane at x=H. Clearly, $Z(n_p,M,L,H,\lambda=1)=Z(n_p,M,L,H)$, and $Z(n_p,M,L,H,\lambda=0) = Z(n_p,M,L,H-1)$. Using equations (5.10) and (5.11) we may write

$$\Pi^* = L^{-(d-1)} \int_0^1 \frac{\partial \log Z}{\partial \lambda} d\lambda = \int_0^1 \frac{d\lambda}{\lambda} \rho_H(\lambda) \quad (5.14)$$

where $\rho_H(\lambda)$ is the site occupation fraction at x = H. The pressure is determined by performing simulations at several values of λ, and evaluating the right hand side of equation (5.11) numerically. This method was applied in the studies of two- and three-dimensional athermal chains and was found in excellent agreement with the test-chain insertion results[22].

When applied to longer chains, this procedure has several inconvenient aspects. Associated with the incremental variation of λ is the need for interpolation of $\rho_H(\lambda)$, and for the relaxation following each change in λ. There is, moreover, a slight increase in bulk density (the site occupation fraction far from the wall) as λ is reduced. To circumvent this problem, the parameter λ may be varied spatially rather than temporally[144]. The parameter λ is now varied along either

wall (i.e., at x=1 and x=H). We partitioned each wall into five slabs and assigned different value of λ for each slab. For x = 1, λ varied incrementally from 0.1 to 0.5, and at x = H, λ = 0.6 - 1.0. The osmotic pressure in (5.12) is now approximated by

$$\Pi^{*} = \sum_{m=1}^{5} \left(\frac{\rho_{x=1}(m)}{m} + \frac{\rho_{x=H}(m)}{m+5} \right) \qquad (5.15)$$

where $\rho_{x=1}(m)$ and $\rho_{x=H}(m)$ is the segment density at x=1 and x=H, respectively, over the portion of the wall with λ=m/10.

5.3. Simulation Procedures.

The model studied in the simulations consists of lattice chains, i.e., collections of self and mutually avoiding random walks on a simple cubic lattice (see Fig. 5.1 in section 5.6). The system is characterized by the number of monomers per chain M, the number of chains n_p, and the number of lattice sites N_l. For a strictly linear chain, M is equal to the number of backbone segments n_b. In the model of polymers with branched-structure, one or two branches emanate from the backbone segment except the end segments (figure 4.6). The internal unit, therefore, occupies two or three sites. In the athermal case, there is no additional interaction except the

self-avoiding constraint. In the nonathermal model, only nearest neighbor interactions were considered.

To test for relaxation, we imposed several criteria. First, the simulation cell was partitioned into several slabs (6 - 10 slabs depending on the size of simulation cell), oriented parallel to the walls. The center-of-mass distribution over the slabs, chain orientations, the mean-square end-to-end distance, and the distribution of segments over the simulation cell were monitored in the simulations. To ensure relaxation, we tested: 1) isotropy of bond orientations, 2) steady values of the mean square end-to-end distance, 3) steady values of the segment density near the wall, and 4) uniformity of the center-of-mass distribution over the inner slabs. Secondly, we also investigated whether the measured quantity (for example: the insertion probability and the osmotic pressure) had already settled to a steady value.

In each series of simulations, an ordered initial configuration was generated at the highest density, and allowed to relax, prior to any data-taking. To obtain statistically independent data, we followed the criteria of Ref. 135; data were collected every p Monte Carlo steps, where $p \geq 1$ and one Monte Carlo step is equal to the number of segments in the lattice. Statistically independent data could also be gauged from the average center-of-mass displacement. One expects successive runs and samplings to be essentially

uncorrelated if the mean-square center-of-mass displacement ΔR equals the effective chain diameter $D_c = 2S$ (S is the root-mean-square radius-of-gyration). To save computer time, after previous samplings were completed, chains were removed to achieve progressively lower densities and were allowed to relax. The sampling process was then repeated.

5.3.1. Athermal Lattice Chains in Three Dimensions.

In the test-chain insertion technique, the configuration space was sampled via the reptation method. The evolution of the test-chain is also governed by reptation, independent of the multichain configuration. In the M = 5, 10, and 20 chain-insertion simulations, a cubic cell of size L=20 was employed, while for M=40 we used L=50. A simulation for M=20 and ϕ=0.5, but with L=30, yielded an insertion probability identical with the L=20 result, to within an uncertainty of less than 1%, thereby ruling out finite size effects. Relaxation required 1-3X10^6 trial moves for M=5 in the low density regime ($\phi \approx 0.1$), and 7.5-10X10^7 trial moves for M=20 at moderate density ($\phi \approx 0.5$). To estimate $p(n_p,M,N_l)$, 10-25 insertion attempts were performed per configuration. Estimates for the insertion probability were derived from averages over seven runs, with the number of configurations per run ranging from 0.5X10^6 at the lowest density to 3X10^6 at the highest density. The

simulation results for the insertion probability are displayed in Table I.

The repulsive wall method was employed to obtain the segment densities adjacent to the wall, $\rho_H(\lambda)$, for λ=0.1, 0.3, 0.5, 0.7, and 0.9. A cell of length L=40 and H=50 was used. The site occupancy fraction at x=1, where there is no repulsive potential, furnishes $\rho_H(\lambda=1)$. The osmotic pressure is obtained via equation (5.14). The configuration space was sampled via reptation and internal moves. Nonoverlapping trial configurations were accepted with the probability P=min $(1,\lambda^{\Delta N(H)})$, where $\Delta N(H)$ is the change in the number of occupied sites at x=H.

After a relaxation period of 3-10 X 10^7 trial moves, estimates for $\rho_H(\lambda)$ and the associated uncertainty were determined from the average and variance over 5-8 runs, each consisting of 1.5-3 X 10^7 configurations. The bulk density ϕ_B was estimated by averaging over the columns at distance 10 or greater from the walls. The test-chain insertion and the repulsive-wall method yield pressures which agree to within 0.5 % for M = 20 and ϕ = 0.5. Excellent agreement between the two methods was also found in low-density simulations of 40-mers. Table II summarizes the simulation results for the compressibility factor $Z = \pi^*/\phi_c$ (where ϕ_c is the chain density) as a function of bulk density.

5.3.2. Athermal Lattice Chains: A Polydisperse System.

In real experiments, it is difficult to prepare monodisperse solutions, so it is useful to examine the effects of polydispersity in simulations. In the present study, we are particularly interested in the effects of polydispersity on the equation of state, and therefore wish to avoid any change in length distribution as the density is varied. Note that there are alternative methods where the length distribution is not controlled (see Mansfield[171] and Madden[172]).

The simulations employed the repulsive-wall method only. The hard wall was placed perpendicular to the x direction, and periodic boundaries were used in the y and z directions. The simulation cell was a cube with 50 sites to a side. In one series of simulations, the chain length distribution was uniform on the range M=30 to M=50; the other series was of a bimodal distribution - equal numbers of 10 and 70-mers. The degree of polydispersity can be gauged by the ratio $\mu = \langle M \rangle^2 / \langle M^2 \rangle$; here μ = 0.98 and 0.84 for the uniform and bimodal distributions, respectively. In addition, we simulated bimodal systems with extreme disparities of chain lengths: equal numbers of dimers and 78-mers (μ = 0.526), and single-monomers and 79-mers (μ = 0.513), at a density of about 0.3. Even for the largest chain lengths employed, the cell length is four times the root mean-square end-to-end distance, so that finite-size effects should not be significant.

Typical relaxation periods consisted of 1-3x10^8 trial moves. Estimates for the segment density at the wall $\rho_H(\lambda)$, and the associated uncertainty were determined from the mean and standard deviation over 8-14 runs, each consisting 2-8x10^7 configurations. This choice was based on the statistical independence of the quantities computed over successive runs. At a density $\phi \approx 0.85$ in the bimodal distribution, we found the mean-square CM displacement $\Delta R = 6.46$, while the effective chain diameter $2S = 6.63$; in the simulation of the uniform chain-length distribution, at density 0.8, we found $\Delta R = 5.8$ and $2S = 6.5$, while at density 0.75 $\Delta R = 7.60$ and $2S = 6.53$. (The ΔR values are for runs of 7x10^7 steps.) Thus, even at the highest densities, the mean-square CM displacement is comparable to the chain diameter, so that we can trust the uncertainty estimates, which are the standard deviations of the mean, calculated over a sample of 8 - 14 runs. At worst, the uncertainty in the pressure is about 3%, with most of the results obtained to a precision of 2% or better.

5.3.3. Nonathermal Lattice Chains.

In simulations of non-athermal lattice chains, the test-chain insertion and the repulsive-wall method were employed. At low densities and at large value of $\eta = \exp(-\epsilon/k_BT)$ (low temperature), the test-chain insertion method is very efficient. We used this method to obtain the osmotic pressure

of 40-mer solutions at low densities ($\phi \leq 0.06$) for $\eta = 1.20$, 1.291 and 1.40. The test-chain insertion method was also used to determine the θ-temperature, $\eta_\theta = \exp[1/(k_B\theta)]$, for various chain-lengths (M = 20 - 150).

In the test-chain insertion method, the configuration space and the test-chain evolved independently via reptation and internal moves. Insertions were performed every 1-16 Monte Carlo iterations, where the higher figure corresponds to insertion attempts in a system of short chains at low density. For M=30, 50, 60, 70, and 80, a lattice of size 55x55x84 was employed. For M=20 and 40, we used lattice cells of size 30x30x56 and 40x40x100, respectively. Long chains required larger cell size: the insertion studies of 100-mer chains required a cubic lattice of L = 65, while simulations for M=150 were performed in a lattice of L=85. For every chain length, the cell size was larger than four times the size of a polymer-coil at the lowest density and the highest temperature, so the finite size effect should not be significant. Relaxation required $3\text{-}4.5\text{x}10^7$ trial moves for $M \leq 80$, and $6\text{x}10^7$ for M=100 and 150. Estimates for the insertion factors were obtained from averages over 10-15 runs, with the number of configurations $1\text{-}3\text{x}10^6$ per run. For each chain-length M, the test-insertion factor $P(M,\phi,\eta)$ was obtained from at least five different densities, and at each density this factor was sampled at more than seven different values of

temperature (η). The values of θ-temperature obtained via insertion method are presented in Table V.

To study the conformational properties and the equation of state, we employed the repulsive-wall method in simulations of non-athermal chains with length M=20, 40, and 80. In these simulations, we spatially varied the parameter λ to gain efficiency. The chain configurations evolved via reptation and internal moves. If the non-overlapping condition was not violated, new configurations were accepted with probability p = $\min(1, \eta^{-\Delta B})$, where ΔB is the change in the number of bonds linking nearest-neighbor sites. Chains were allowed to move to the sites adjacent to the wall with probability P_w = $\min(1, \lambda_1^{\Delta N(1)}/\lambda_2^{\Delta N(2)})$, where λ_1 and $\Delta N(1)$ are the value of parameter λ and the change in the number of occupied site at the wall due to the chain-end moves, while λ_2 and $\Delta N(2)$ are the corresponding values due to the movement of the other chain-end. The osmotic pressure was determined via Eqn. (5.15). Chain configurations were generated at the highest density and were allowed to relax. The criteria listed in section (5.2) were used to gauge whether the system had relaxed. For M=80, it required 5×10^8 steps, while for M=20 the relaxation period was 3×10^8 trial moves.

Simulations of 20-mer chains were performed using the repulsive-wall method at η = 1.20, η_θ = 1.281, and η = 1.35. A lattice of size 30x30x56 was employed. For M=40, cells of different sizes were used. At η=1.20, a lattice of size

50x50x50 was used for densities, ϕ, higher than 0.100. In these simulations, the repulsive-wall method was employed. At lower densities, the test-chain insertion method was used in a lattice of 40x40x100. At the θ-temperature, η_θ = 1.291, the lattice cell was 40x40x75, and the repulsive-wall method was used to obtain the osmotic pressure at ϕ>0.01. At densities 0.0150 and lower, the test-chain insertion technique was used and the lattice size was 40x40x100. Below the θ-temperature (η=1.400), we applied test-chain insertion method for $\phi \leq$ 0.006 on a lattice of 40x40x100, and the repulsive-wall method for $\phi \geq$ 0.2723 on a lattice of 50x50x70. To test the finite size effect, we also employed the repulsive-wall method on a lattice of 40x40x100 at densities ϕ = 0.4875, 0.2810, and 0.012-0.2186. The result was negative. The simulations of 80-mer chains at the θ-temperature, η_θ = 1.296, employed the repulsive-wall method on a lattice of size 55x55x84.

In the repulsive-wall method, the osmotic pressure, segment distribution, and the RMS end-to-end distance, and their uncertainties were determined from the average and variance over 8-15 runs, each run consisting of 3-8x10^7 configurations. At lower densities, the test-chain insertion methods were employed and run at least 12 times. Each run consists of 1-3x10^6 configurations. The bulk densities, ϕ_B, were estimated by averaging over the columns at distance x from the wall, where x $\geq$ 5, 8, and 10 for M = 20, 40, and 80,

respectively. Table VI summarizes the simulation results for compressibility factor and the RMS end-to-end distance as a function of bulk density.

5.3.4. Athermal Lattice Chains: Branched-Polymers.

In this section, we describe the simulation procedures of branched-polymers. Two types of branched structure were studied; the first type involved one dangling monomer emanating from every backbone segment, the other was a chain with two branches attached to every backbone monomer (see Fig. 4.6).

The repulsive wall and the test-chain insertion methods were employed to obtain the osmotic pressure via Eqs. (4.24) and (5.15). For the first structure, N_B=11 and 21 were studied, where N_B is the number of backbone segments. Therefore, the number of monomers M is equal to 20 and 40 respectively. The second structure involved N_B = 8 and 15 giving M = 20 and 41. The relaxation criteria of section 5.2 were employed during simulations. To obtain statistically independent data, samples were taken at an interval ΔN_t such that the average chain displacement is larger than the chain size. For N_B = 8, we used a lattice of size 30x30x56. Relaxation required 2-3x10^8 iterations, the osmotic pressure and its uncertainties were determined from the average and variance of 9-15 runs, each consisting of 2-5x10^7

configurations. Chains with N_B=15 were simulated on a lattice of 40x40x70. It required $3x10^8$ Monte Carlo trial moves before the system was relaxed. The osmotic pressure and other conformational properties were sampled from 10-14 runs. Each run has $2\text{-}5x10^7$ configurations. For the first structure, chains with N_B = 11 and 21 were simulated on a lattice of size 30x30x56 and 40x40x70 respectively. Simulations were performed in 10-14 runs, each run generating $2\text{-}5x10^7$ configurations. Statistics were performed after relaxation of $3x10^8$ Monte Carlo trial moves. In all cases we found that the lattice cell is on the average five times larger than the average size of a single chain, so the finite size effect is expected to be insignificant. The results of simulations are presented in Tables VII and VIII.

5.4. Results of Various Studies.

In this section, we present the results of our simulations. Scaling properties and the equation of state are analyzed and compared with theoretical predictions discussed in the previous chapters. The effects of dispersity and chain structure are studied. We also study other conformational properties, such as the mean-square end-to-end distance and density profile near a wall.

5.4.1. Athermal Lattice Chains in Three Dimensions: A Monodisperse System[72].

A. Equation of State and Scaling Exponents.

In figure (5.3) we plot the result of Monte Carlo simulations obtained with the chain insertion method. The graph shows $-M^{-1}$ log p as a function of -log $(1-\phi)$. Also plotted are the predictions of the Flory approximation (Eqn. 4.3) and the Flory-Huggins approximation (Eqn. 4.12). The Bawendi-Freed approximation for the chain insertion can be obtained from Eqn. (4.18) and the method discussed in section 4.2.3. Up to order z^{-2}, the insertion probability is[95]

$$
\begin{aligned}
M^{-1}\log P_{BF} = \log(1-\phi) &+ \frac{2\phi}{z}\left(\frac{M-1}{M}\right)^2 \\
&+ \frac{2\phi}{z^2M^4}\left[3(M-1)^4 - 8(M-1)^2 - 4(M-1) + 1\right] \\
&- \frac{2\phi^2}{z^2M^4}\left[5(M-1)^4 - (M-1)^3 - 6(M-1)^2\right] \\
&+ \frac{8\phi^3}{z^2}\left(\frac{M-1}{M}\right)^4 + O(z^{-3})
\end{aligned}
\qquad (5.18)
$$

where z is the cordination number of the lattice (z = 6 for simple cubic lattice). Of the three predictions, we find that

the Bawendi-Freed theory is the most accurate. For M = 20 all of the predictions underestimate $p(\phi,M)$, but the BF prediction remains the most accurate one.

We turn now to the compressibilty factor Z. The Flory, Flory-Huggins, and Bawendi-Freed predictions are respectively given by equations (4.28), (4.29), and (4.97). These predictions, and our simulation results, are compared in Table II and, for M = 20 and 40, in Figs. 5.4. For M = 5 and 10 the FH and BF predictions lie quite close to the simulation data, and their accuracy is best judged from Table II. For M = 20, the BF (solid line) and FH (dashed line) theories show an excellent agreement with simulations, except in the dilute and semi-dilute regimes. For M = 40, the overestimate of the compress ibility factor in the low-density regime is more prominent. In both cases, however, the discrepancy is significantly smaller for the BF theory. The BF and FH predictions are virtually identical at high densities, where they match the simulation data very closely. Figure 5.4 also illustrates the excellent agreement between chain-insertion and repulsive-wall simulations, as may be judged (for M=20) by comparison of the circles and squares, and (for M=40) by comparison of the diamonds and the open circles.

In Fig. 5.5 the scaling behavior of the compressibility factor is analyzed. The scaling theory of des Cloizeaux predicts that the pressure of the semidilute polymer solution in the long-chain limit has the scaling form (see Chapter II',

$$\Pi^* = \phi f(\phi/\phi^*) \qquad (5.19)$$

where ϕ^* is the overlap concentration and $f(x) \propto x^{1/(3\nu-1)}$ (see equations (2.73) and (2.74) for more accurate formulation). Note that in the semidilute regime, the segment density ϕ is restricted by $\phi^* << \phi << 1$, where $\phi^* \approx M^{1-d\nu}$. In three dimensions, using the Flory exponent $\nu = 3/5$, one then has $\phi^* \approx M^{-4/5}$, and $f(x) \propto x^{5/4}$ in the semidilute regime. Figure 5.5 may be interpreted as showing a preliminary indication of scaling. On the other hand, the range of power-law behavior seems rather limited, extending from $\phi = 0.17$ to $\phi = 0.42$ for $M = 40$.

The results of the present study should be compared with those of Khalatur et al[115]. for off-lattice chains composed of $M = 40$ hard spheres. The continuous space model in their simulations appears to exhibit a more rapid (with chain length) approach to asymptotic power-law behavior. Their work employed the scanning method[114], and is therefore limited to low density regime ($\phi/\phi^* = 2 - 20$). The high density regime is not accessible.

Another work that yielded definitive evidence for scaling was that of Ottinger[116], who introduced the quantity

$$G(y) = \int_0^y \frac{Z(y') - 1}{y'} dy' \qquad (5.20)$$

Z is the compressibility factor and the scaling variable y, defined (in our notation) as

$$y = (M-1)^{3\nu}\left[\frac{n_p - 1}{M}\right] \qquad (5.21)$$

is essentially a measure of ϕ/ϕ^*. One expects $G \propto y^{1/(3\nu-1)}$ in the semidilute regime. Ottinger's[116] simulations of simple cubic lattice chains with M = 60 and 80 show convincing power-law behavior, yielding $\nu = 0.579 \pm 0.001$, as compared with the RG estimate $\nu = 0.588 \pm 0.001$, and the data of Khalatur et al.[115] $\nu = 0.565 \pm 0.002$. In Fig. 5.6 we plot log G vs. log y, as computed from our pressure data for M = 20 and 40. In contrast to Fig. 5.5, here we see definitive evidence of scaling. The straight line drawn through the M = 40 points corresponds to $\nu = 0.576$. Thus, a plot of compressibility factor, such as Fig. 5.5, provides a more sensitive test of the des Cloiseaux law than does the plot of the quantity G where the ideal gas contribution ($\sim 1/n_p$) is removed, eliminating a finite-size effect. The latter analysis does, however, yield useful estimates of the exponent.

In dilute solutions ($\phi < \phi^*$) the pressure takes the form of equation (2.11). Scaling[47] and renormalization group analyses[69] predict that the second virial coefficient A_2 scales with chain length M such that $M^{2-3\nu}A_2$ is constant. The second virial coefficient is readily extracted from the chain-

insertion data (see eqn. (5.10)). Our estimates for the second virial coefficient are presented in Table III, where they are compared with the previous Monte Carlo results of Bellemans and Janssens[175]. There is excellent agreement except for M = 40, where our value exceeds the earlier estimate by about 6%. It is also evident that $M^{2-3\nu}A_2$ is approximately constant.

B. Mean-Square End-to-End Distance.

Another scaling theory prediction is that the mean-square end-to-end distance decreses with density (for $\phi>\phi^*$) according to equation (2.47). Evidence of such scaling behavior has been analyzed by Bishop et. al.[176], for a variety of chain lengths. In figure 5.7 we plot $\log[\langle R^2\rangle/M]$ vs $\log \phi$. Using the Flory exponent $\nu = 3/5$, one expects the data to approach a straight line of slope -1/4, while $\nu = 0.588$ implies a slope of -0.23. The data suggest an approach to power-law behavior, but clearly do not provide a strong confirmation of equation (2.47) at this chain length. We also examined the dependence of $\langle R^2\rangle$ on the location of chains relative to the wall. In the simulations of chains with M = 40 we gathered statistics on $\langle R^2\rangle$ with center of mass in each of the ten bins (with bin j extending from x = 5j-4 to 5j) parallel to the walls. Chains with the center of mass in the bin adjacent to the wall have a mean-square length about 10% less than the bulk value. Their dimensions in the directions parallel to the walls have to

swell to compensate the decrease in the other direction. Other wise, $\langle R^2 \rangle$ does not vary significantly from bin to bin.

C. The Ratio of The Osmotic Pressure and Wall-Contact Density.

Another interesting quantity is the relation between the wall wall-contact density $\rho_H(1)$ and the pressure. The ratio B = $\rho_H(1)/\pi^*$ was found to decrease monotonically, in conflict with a conjecture[47] that the ratio would be constant (similar behavior is also observed in two dimensions). Fig. 5.8 indicates that B approaches a constant value in the zero-density limit, and is otherwise a decreasing function of pressure. The (rather limited) data for M = 20 suggest that B is essentially independent of M. The semilogarithmic plot (inset) shows two forms of limiting behavior: constant B at low pressure, and B = a - b ln π (with b $\simeq$ 0.875) at higher pressures.

5.4.2. Athermal Lattice Chains: A Polydisperse System.

A. The Equation of State of Polydisperse Chains.

Table IV summarizes our results for the polydisperse case. Figure 5.9 shows the compressibility factor W = $\langle M \rangle \pi^*/\phi$ as a function of density. For uniform chain distribution, the compressibility factor in Eqn. (4.28) is replaced by

$$Z_F = 1 - \frac{1}{\phi_c}\left[\log(1-\bar{\phi}) + \bar{\phi}\right] \qquad (5.20)$$

where ϕ_c is the total chain density and $\bar{\phi}$ is the total segment density. The Flory-Huggins approximation in Eqn. (4.29) becomes

$$Z_{FH} = Z_F + \frac{z}{2\phi_c}\left[\log\left\{1 - \frac{2}{z}(\bar{\phi} - \phi_c)\right\} + \frac{2}{z}(\bar{\phi} - \phi_c)\right] \qquad (5.21)$$

Note that Flory and Flory-Huggins theories predict that polydispersity has no influence on the equation of state, i.e., the pressure depends only on the average chain length. The compressibility factor for a polydisperse system with a uniform chain distribution as predicted by Bawendi and Freed is given by equation (4.110). Comparison with our simulation results indicates that the FH and BF are in excellent agreement with simulation, except in the dilute and semidilute regimes, where both approximations overestimate the pressure. The discrepancy is significantly smaller for the BF theory. Figure 5.9 also illustrates dramatically the insignificance of dispersity regarding the compressibility factor. Even in the extreme cases of dimers and 78-mers, or monomers and 79-mers, there is no significant change in the compressibility factor due to polydispersity.

B. Mean-Square End-to-End Distance versus Polydispersity.

We also study the distribution-sensitive quantity proposed by Ohta and Oono[72] - the dependence of $\langle R^2\rangle/\langle R^2\rangle_{\phi\to 0}$ upon $h(\phi)=(Z-1)/A_2\phi$, where $\langle R^2\rangle$ is the mean square end-to-end distance and A_2 is the second virial coefficient. A renormalization group calculation predicts that systems with a greater degree of dispersity (i.e., smaller μ), exhibit a larger ratio of $\langle R^2\rangle/\langle R^2\rangle_{\phi\to 0}$ for a given $h(\phi)$. Though Ohta and Oono's calculation is for Edwards' continuum model, we try to investigate this subtle behavior with our lattice simulations for the density range ϕ=0.08-0.8. This density range includes the semidilute regime, defined by the condition $\phi^* \ll \phi \ll 1$ where ϕ^* is the overlap treshold. Since $\phi^* \propto M^{-4/5}$ in three dimensions, for $\langle M\rangle$=40 we obtain $\phi^* \propto 0.05$. Our system realizes semidilute conditions for $0.1<\phi<0.4$; in this range, the behavior of the pressure is consistent with the des Cloizeaux scaling law. Our results for the relation between $Y=\langle R^2\rangle/\langle R^2\rangle_{\phi\to 0}$ and $h(\phi)$ are presented in Fig. 5.10. Although we obtain encouraging results for the uniform distribution (μ=0.98), the results for the bimodal distribution (μ=0.84) appear to contradict Ohta and Oono's prediction (i.e., Y is smaller than for the monodisperse system). It is not possible to draw a definite conclusion from the present results, however. In particular, we note that $\langle R^2\rangle$ has only a weak dependence on density, in chains of only 10 segments. Studies on longer chains and over

wide range of dispersity will be needed to explore the scaling.

As in the monodisperse case, it is of interest to examine the behavior of the wall-contact density, $\rho_H(1)$ as a function of pressure. In monodisperse systems the ratio $\rho_H(1)/\pi^*$ decreases monotonically. As is seen from Fig. 5.11, the polydisperse systems exhibit precisely the same behavior.

5.4.3. NONATHERMAL LATTICE CHAINS.

A. Determination of θ-temperature.

The chain insertion method was employed to estimate the second virial coefficient A_2 in equation (5.9). The results for the insertion factors at various densities ($\phi \leq 0.02$) and temperatures ($\eta = 1/k_BT$) are shown in Figs. 5.12a-e. In these graphs, η ranges from 1.200 to 1.400, and $P(\phi,\eta)$ is the corresponding insertion factor. Note that all curves intersect almost at the same point. The temperature at which $P(\phi,\eta)=1$ is defined as the θ-temperature, since the second virial coefficient vanishes. The average over results at various densities ϕ of η at the θ-point, $\langle\eta_\theta(M)\rangle$, depends on the chain length and are presented in Table V. Our simulation results are in good agreement with the previous studies[127,137,141,177]. In Fig. 5.13, we plot $\langle\eta_\theta(M)\rangle$ vs 1/M to obtain the θ-temparature in the limit $M\to\infty$. This yields $\eta_\theta(\infty)=1.301(2)$, which is within

the range of the previous estimates[127,177] (see Table V). Note that in the M→∞ limit, the θ-temperature should converge with the collapse temperature T_c[127,177,178]. In our simulations, we use $<\eta_\theta(M)>$ to study the equation of state and other conformational properties at the θ-temperature for M=20, 40, and 80.

B. The Equation of State of Nonathermal Chains.

The bulk density, the compressibility factor, and the mean-square end-to-end distance are presented in Table VI. In this table, we also provide the predictions of Flory (F), Flory-Huggins(FH), Bawendi-Freed(BF), and Dudowicz et. al. (DFM). In the BF approximation (also called the extended mean-field approximation), the bond correlation was used to determine the entropic correction only and did not play any role in the enthalpic calculation[95]. The DFM approximation is employed in Ref. 103 to obtain the mixing energy. In their approach, the correlating bonds were considered to calculate the entropic and enthalpic parts. Our simulations indicate that the DFM approximation gives the best prediction. In Figs. 5.14a-g, we plot the compressibility factor vs. density (for clarity, each figure corresponds to a certain value of chain length M and θ).

To see the effect of temperature, we present the compressibility factor for M=20 at various η in the same picture (Fig. 5.15a). The simulation results are compared with

the most accurate prediction of DFM. η = 1.00 corresponds to an athermal system. At the lowest temperature (η=1.350) and small densities, the slope of compressibility factor is negative, and it is almost flat at the θ-temperature. The same results are observed for M=40 (Fig. 5.15b). Note that the finite size effect has no significant role in our system as can be seen from Table VI or Figs. 5.15b and 5.14f. For example, at density ϕ = 0.2723 a system with lattice size of 50x50x70 yields almost the same value of the compressibility factor as a system of 40x40x100 at ϕ = 0.2810. (See section 5.3 for further details).

Figure 5.16 describes the equation of state at the θ-temperature for polymer solutions with different chain-lengths. The results are compared with the predictions of the Flory-Huggins approximation and Dudowicz et.al.[103]. The simulation results sit rather nicely on curves depicting the DFM predictions.

Following Ottinger[116] and Dickman[179], we plot the excess pressure over an ideal gas, π^*-ϕ/N, vs ϕ on a logarithmic scale. N here is the chain length, which is equal to M for a linear chain. Figure 5.17a describes the excess pressure for N=40 at various temperature, and Fig. 5.17b is the corresponding graph for N = 20, 40, and 80 at the θ-temperature. At the θ-temperature and low densities, the MC results lie on a straight line which has a slope of 3 corresponding to the exponent of density in the third term of the virial expansion.

C. Mean-Square End-to-End Distance.

$\langle R^2 \rangle / M$ is plotted vs density on a logarithmic scale in Figures 5.18a and 5.18b, corresponding to chains of length M = 20 and 40, respectively. In Fig. 5.18c, we compare $\langle R^2 \rangle / M$ for various chain lengths at the θ-temperature. Note that above the θ-temperature, the chain dimension contracts as the density increases. At the θ-temperature, we observe that the chain dimension increases as the density increases, and reaches a maximum value at $\phi_m \sim 0.35$ before contracting. These phenomena were observed for all chain lengths, and also noticed in two dimensions[179]. The swelling of the chain is prominent below the θ-point. It may indicate that at or below the θ-temperature and at densities about ϕ_m, the attractive interchain interactions outweigh the intrachain interactions as well as the excluded volume. Above ϕ_m, however, the excluded volume effects play more significant role, thus the chains contract again.

D. Wall-Contact Density vs Pressure.

As in our analysis of the athermal systems, we also plot the ratio of the wall contact density to the osmotic pressure, $B=\rho_H(1)/\pi^*$, vs the osmotic pressure. Figure 5.19a shows this ratio for M=20 at η = 1.200, 1.281, and 1.350. Figure 5.19b corresponds to M=20,40, and 80 at the θ-temperature. de Gennes

assumes proportionality between the osmotic pressure and segment density at the layer adjacent to the wall[47], which is indicated in our results for $\pi^* \leq 0.10$.

5.4.4. ATHERMAL CHAINS WITH MULTISITE MONOMERS

A. The Equation of State of Polymers with Branched Structures.

The bulk density and compressibility factor are presented in Table VII. Predictions of Flory, Flory-Huggins, and Freed's lattice models are also given. In Freed's model, correction due to bond correlation was given to the lowest order of branch-structure (see Appendix H). In Fig. 5.20a, we plot the compressibility factor (Z) vs the density (ϕ) for chains of structure 1 and 2 with M=20. The graph indicates that Freed's correction is almost insignificant compared to FH mean-field approximation. It also shows considerable discrepancy between MC results and theoretical predictions. This discrepancy is also noticed for polymers with longer chain length (M=40), see Fig. 5.20b. To see the effect of the excessive pressure, we plot $\log(\pi^*-\phi/M)$ vs $\log(\phi)$ in Fig. 5.21. The lower osmotic pressure might indicate stiffness present in corresponding branch-polymer models. To check the accuracy of these models, it is necessary to perform simulations with longer chains and with different algorithms, or by incorporating higher order corrections in Freed's lattice model.

B. Mean-Square End-to-End Distance and Radius of Gyration.

Figure 5.22 summarizes our MC results indicating the chain dimension as a function of density. The top symbols correspond to the mean-square end-to-end distance. Similar figures in the lower part of the picture are the radius of gyration. From this picture, it is obvious that the chain dimension remains constant as the density varies. It may indicate that chains with structure are stiff, so that, in contrast to strictly linear chains, the presence of other chains does not significantly affect their configurations. Since our simulations are limited to short chains, further studies involving longer chains are required.

5.4.5. SEGMENT AND CHAIN DENSITY DISTRIBUTION.

We turn now to some aspects of the polymer-wall interaction. One interesting question is the behavior of the segment density $\rho(x)$, as a function of distance from the wall. Scaling arguments suggest that the density is reduced from its bulk value ϕ_B in a region of width ξ, where the mesh-size $\xi \propto \phi_B^{-3/4}$. de Gennes[47] has also predicted the power law behavior of $\rho(x) \propto x^{1/r}$ in the vicinity of the wall. In Fig. 5.23 we plot the normalized density $n(x) = \rho(x)/\phi_B$ vs $\phi_B^{3/4}x$, for M = 40 athermal chains at 12 values of bulk density. The scaling of

n(x) is confirmed rather nicely, although the present data do not provide clear evidence of the predicted power law.

As in the monodisperse case, it is also interesting to examine the behavior of the segment-density $\rho(x)$ as a function of distance from the wall. In Fig. 5.24 the normalized density profile $n(x) = \rho(x)/\phi_B$ is plotted versus $x\phi_B^{3/4}$, which shows that both monodisperse and polydisperse solutions follow the predicted scaling behavior that $n(x) \rightarrow 1$ for $x\phi_B^{3/4} \gg 1$. Note however that Fig. 5.24 shows only the aggregate behavior of n(x) in the polydisperse samples.

For nonathermal chains, there is no evidence of scaling behavior when the normalized density profile was plotted vs $\phi_B^{3/4}x$. Following Dickman[179], we plot n(x) vs $y=x/x_{1/2}$, where $x_{1/2}$ is the point at which the density attains one half of its bulk value (see Table IX). The results for M=20 and 40 at various temperature are presented in Figs. 5.25a and 5.25b, respectively. Fig 5.25c is the picture for M=20, 40, and 80 at the θ-temperature. In all those pictures, density profiles fall nicely into the same curve. The dependence of n(x) on temperature and densities in the nonathermal case is still not obvious .

Now we turn to a system of branched polymers with the structures depicted in Fig. (4.6). In Fig. 5.26, we plot the normalized density profile vs $x(\phi_B/b)^{3/4}$. b is the number of occupied sites per repeat unit. For structure 1, b = 2, since the repeat unit consists of the backbone monomer and one

dangling site. And b = 3 for structure 2. The purpose of dividing ϕ_B by b is the assumption that the mesh-size ξ is proportional to $\phi^{-3/4}$, where ϕ is the density of the repeat units. In Fig. 5.26, the normalized densities of structure 1 and 2 collapse into a single curve. Our simulation results are for $\phi_B > 0.3$. It would be very interesting to study whether the same behavior is observed at lower densities.

Following Shih et.al[116] (see also chapter III), the density profile may be described by an expression of the form $n(x) = 1-\exp\{-(x/\xi)^m\}$, where $m = 1/\nu$. In Figure 5.27a, we plot -log (1-n(x)) vs x using the log-log plot for the athermal chains of M=20, 40, and 80. Note that all simulation results lie on straight lines (indicated by the dashed lines) with a common slope $m=1/\nu$, with $\nu=3/5$. The most interesting case is when we plot -log(1-n(x)) vs y for the nonathermal chains. Figure 5.27b indicates that all data collapse into a single line, even when we plot the athermal chains. As in the previous analysis, the relation between the mesh-size ξ and $x_{1/2}$ (or ξ and ϕ_B) in the nonathermal systems is not obvious. This observation is of interest to further studies.

We also gathered statistics on the number of chains with center of mass in each of ten bins. The behavior of $f_{cm}(i)$, the fraction of chains with center of mass in bin i, is shown in Fig. 5.28 At low density (ϕ = 0.0552), there is the expected depletion of the bin adjacent to the wall, as well as a surprising enhancement of the c.m. fraction in the bin but one

removed from the wall. At higher densities there is a slight enhancement of the c.m. fraction in the bin adjacent to the wall. This curious tendency for chain centers of mass to accumulate near a wall has also been noticed by Madden in simulations of polydisperse systems (N_{av}=100) of athermal chains.[172]

In polydisperse case, we observed that the density of segments belonging to shorter chains is enhanced near the wall, as indicated in Fig. 5.29. This reflects the lower penalty in entropy associated with placing short chains near the wall. This behavior is also confirmed when we plot of $n_{cm}(j)=n_{cm}N_{bin}/N_{class}$ versus j (Fig. 5.30), where $n_{cm}(j)$ is the number of chains with center of mass in bin j, N_{bin} is the number of bins (equal to 10), and N_{class} is the number of chains with the same length. For the shorter chains the distribution is peaked in the bin adjacent to the wall, while the CM density for the longer chains is maximum in the bin but one from the wall, and is strongly reduced in the bin closest to the wall.

The distribution of CM fraction over bins parallel to the wall at the θ-temperature is presented in Figures 5.31a-c. At high densities, chains almost evenly distributed. At lower densities, the number of chains located in bins next to the walls is slightly reduced. These phenomena are noticed also in the athermal systems. The effect of temperature on CM distribution is described in Fig. 5.32a-c. At lower temperature,

chains tend to aggregate in the middle of the vessel, especially at low densities (Fig. 5.32c). It may indicate that interchain interactions play significant influence on the distribution. In higher-density systems, the excluded volume effect may compensate interchain interactions, and polymers are distributed more evenly. Note that at higher temperature, we observed the same phenomena as in athermal case.

5.5. Results of Monte Carlo Simulations.

Table I. Test-chain insertion probability $p(\phi)$. M = number of segments per chain, ϕ = fraction of occupied sites. Figures in the second to the forth columns corespond to $-(1/M) \log p(\phi)$ of Freed, Freed-Huggins, and Bawendi-Freed theories, while the last column indicates the results of Monte Carlo simulations. In the simulations, a cubic lattice of size L = 20 is used. Also included is the result for M = 20, ϕ = .5, and L = 30 .

ϕ	F	FH	BF	Monte Carlo
M = 5				
0.005	0.0053	0.0042	0.0039	0.00374 ± 0.00002
0.010	0.0104	0.0082	0.0076	0.00749 ± 0.00003
0.015	0.0154	0.0121	0.0113	0.01125 ± 0.00003
0.020	0.0205	0.0162	0.0151	0.01500 ± 0.00002
0.025	0.0256	0.0202	0.0189	0.01884 ± 0.00002
0.030	0.0308	0.0243	0.0227	0.02261 ± 0.00006
0.035	0.0359	0.0284	0.0266	0.02669 ± 0.00004
0.040	0.0411	0.0325	0.0305	0.03043 ± 0.00005
0.045	0.0464	0.0366	0.0344	0.03445 ± 0.00005
0.050	0.0516	0.0408	0.0383	0.03844 ± 0.00002
0.10	0.1057	0.0840	0.0796	0.07972 ± 0.00003
0.15	0.1629	0.1302	0.1244	0.12461 ± 0.00024
0.20	0.2235	0.1796	0.1729	0.1728 ± 0.0003

(table I continued)

0.30	0.3571	0.2903	0.2829	0.2823 ± 0.0003
0.40	0.5113	0.4210	0.4138	0.4135 ± 0.0005
0.50	0.6937	0.5792	0.5727	0.5729 ± 0.0006
0.60	0.9170	0.7775	0.7718	0.7694 ± 0.0018
0.70	1.2050	1.0396	1.0342	1.0348 ± 0.0024
0.875	2.0818	1.8692	1.8617	1.8702 ± 0.0031
M = 10				
0.005	0.0056	0.0041	0.0035	0.00306 ± 0.00002
0.010	0.0107	0.0078	0.0067	0.00614 ± 0.00001
0.015	0.0157	0.0115	0.0099	0.00925 ± 0.00002
0.020	0.0208	0.0152	0.0132	0.01249 ± 0.00004
0.025	0.0259	0.0190	0.0164	0.01559 ± 0.00002
0.030	0.0311	0.0228	0.0197	0.01887 ± 0.00007
0.035	0.0362	0.0266	0.0231	0.02228 ± 0.00004
0.040	0.0414	0.0304	0.0265	0.02536 ± 0.00008
0.045	0.0467	0.0343	0.0299	0.02888 ± 0.00012
0.050	0.0519	0.0382	0.0334	0.03217 ± 0.00008
0.10	0.1060	0.0784	0.0699	0.06761 ± 0.00043
0.15	0.1632	0.1216	0.1101	0.1065 ± 0.0004
0.20	0.2239	0.1680	0.1544	0.1496 ± 0.0004
0.30	0.3575	0.2725	0.2565	0.2502 ± 0.0004
0.40	0.5118	0.3966	0.3802	0.3714 ± 0.0014
0.50	0.6943	0.5479	0.5320	0.5221 ± 0.0012
0.60	0.9178	0.7390	0.7240	0.7136 ± 0.0058
0.70	1.2060	0.9936	0.9789	0.9660 ± 0.0038

(table I continued)

M = 20				
0.005	0.0063	0.0044	0.0036	0.00255 ± 0.00001
0.010	0.0113	0.0079	0.0064	0.00515 ± 0.00002
0.015	0.0164	0.0115	0.0094	0.00775 ± 0.00005
0.020	0.0215	0.0151	0.0123	0.01050 ± 0.00004
0.025	0.0266	0.0187	0.0153	0.01396 ± 0.00011
0.030	0.0317	0.0223	0.0183	0.0160 ± 0.0001
0.035	0.0369	0.0260	0.0214	0.0187 ± 0.0001
0.040	0.0421	0.0296	0.0245	0.0215 ± 0.0001
0.045	0.0474	0.0333	0.0277	0.0244 ± 0.0002
0.050	0.0526	0.0371	0.0308	0.0276 ± 0.0002
0.10	0.1068	0.0758	0.0647	0.0568 ± 0.0006
0.15	0.1640	0.1174	0.1026	0.0942 ± 0.0005
0.20	0.2247	0.1621	0.1446	0.1342 ± 0.0014
0.30	0.3585	0.2632	0.2426	0.2307 ± 0.0012
0.40	0.5129	0.3838	0.3624	0.3452 ± 0.0007
0.50	0.6957	0.5315	0.5106	0.4950 ± 0.0040
M = 20, ϕ = 0.50, L = 30				
0.50	0.6957	0.5315	0.5106	0.4915 ± 0.0038
M = 40				
0.0192	0.01939	0.01328	0.01051	0.00863 ± 0.00003
0.0384	0.03916	0.02691	0.02157	0.01795 ± 0.00008
0.0576	0.0593	0.0409	0.0332	0.0281 ± 0.0001
0.0763	0.07937	0.05489	0.04508	0.00368 ± 0.0001
0.0832	0.08687	0.06014	0.04960	0.0423 ± 0.0001

Table II. Compressibility factor as a function of density. Z_F, Z_{FH}, and Z_{BF} are Flory, Flory-Huggins, and Bawendi-Freed predictions for the compressibility factor. Z_{MC} for M = 5, 10, 20, $\phi < 0.5$, and M = 40, $\phi < 0.074$ were calculated from the test-chain insertion data, using equation (4.29). The remaining data were obtained using the repulsive wall method.

ϕ	Z_F	Z_{FH}	Z_{BF}	Z_{MC}
M = 5				
0.025	1.064	1.051	1.048	1.048 ± 0.003
0.050	1.130	1.103	1.097	1.098 ± 0.002
0.075	1.198	1.158	1.149	1.150 ± 0.004
0.10	1.269	1.214	1.204	1.205 ± 0.003
0.15	1.418	1.336	1.324	1.324 ± 0.005
0.20	1.580	1.469	1.456	1.454 ± 0.005
0.25	1.755	1.615	1.602	1.593 ± 0.008
0.30	1.946	1.777	1.765	1.762 ± 0.006
0.40	2.387	2.157	2.149	2.149 ± 0.006
0.50	2.933	2.640	2.637	2.639 ± 0.006
0.60	3.638	3.279	3.280	3.270 ± 0.016
0.70	4.603	4.176	4.178	4.184 ± 0.018
0.875	7.893	7.337	7.330	7.350 ± 0.021
M = 10				
0.025	1.130	1.096	1.083	1.080 ± 0.011

(Table II continued)

0.050	1.262	1.193	1.169	1.166 ± 0.009
0.075	1.398	1.295	1.263	1.256 ± 0.011
0.10	1.540	1.401	1.361	1.351 ± 0.022
0.15	1.838	1.629	1.578	1.559 ± 0.019
0.20	2.161	1.879	1.823	1.798 ± 0.018
0.25	2.512	2.156	2.098	2.065 ± 0.022
0.30	2.894	2.462	2.406	2.376 ± 0.015
0.40	3.777	3.188	3.142	3.100 ± 0.027
0.50	4.871	4.118	4.087	4.042 ± 0.024
0.60	6.282	5.358	5.339	5.298 ± 0.083
0.70	8.214	7.110	7.097	7.039 ± 0.063
M = 20				
0.025	1.267	1.188	1.155	1.135 ± 0.054
0.050	1.531	1.375	1.315	1.292 ± 0.046
0.075	1.804	1.570	1.488	1.446 ± 0.042
0.10	2.086	1.775	1.673	1.585 ± 0.064
0.15	2.685	2.215	2.085	2.016 ± 0.050
0.20	3.331	2.699	2.553	2.471 ± 0.083
0.25	4.033	3.234	3.083	3.024 ± 0.088
0.30	4.798	3.830	3.682	3.605 ± 0.076
0.40	6.566	5.245	5.122	4.961 ± 0.053
0.50	8.757	7.067	6.980	6.891 ± 0.135
0.51	9.005	7.278	7.193	6.917 ± 0.268
0.61	11.896	9.781	9.727	9.494 ± 0.122
0.71	15.860	13.339	13.296	13.085 ± 0.224

(table II continued)

0.81	21.848	18.902	18.839	18.600 ± 0.285
0.91	33.090	29.699	29.570	29.600 ± 0.319
M = 40				
0.056	2.16	1.80	1.66	1.51 ± 0.07
0.075	2.57	2.09	1.91	1.72 ± 0.07
0.093	2.99	2.38	2.17	1.89 ± 0.08
0.109	3.35	2.64	2.40	2.13 ± 0.06
0.140	4.09	3.18	2.90	2.63 ± 0.08
0.176	5.00	3.84	3.53	3.11 ± 0.09
0.212	5.94	4.54	4.21	3.84 ± 0.09
0.262	7.38	5.62	5.28	4.79 ± 0.12
0.314	8.95	6.83	6.50	6.19 ± 0.26
0.412	12.56	9.69	9.42	9.02 ± 0.16
0.512	17.04	13.39	13.20	12.56 ± 0.23
0.611	22.83	18.35	18.22	17.92 ± 0.25
0.710	30.77	25.43	25.33	25.04 ± 0.32
0.808	42.76	36.51	36.37	36.67 ± 0.46

Table III. Second virial coefficient A_2 as a function of chain length M. $A_{2,MC}$ are the results of chain insertion, $A_{2,BJ}$ are the earlier results of Bellemans and Janssens[162].

M	$A_{2,MC}$	$A_{2,BJ}$	$M^{2-3\nu}A_{2,MC}$	
			$\nu=3/5$	$\nu=0.588$
5	0.373 ± 0.002	0.372	0.515 ± 0.003	0.545 ± 0.003
10	0.305 ± 0.002	0.306	0.483 ± 0.003	0.525 ± 0.003
20	0.255 ± 0.001	0.253	0.464 ± 0.002	0.517 ± 0.002
40	0.217 ± 0.001	0.205	0.454 ± 0.002	0.518 ± 0.002

Table IV. Compressibility factor Z, and mean-square end-to end distance $\langle R^2 \rangle$ as a functions of bulk density ϕ_B from Monte Carlo simulations of polydisperse systems with uniform (M = 30-50) and bivariate chain-length distributions. n_p is the number of chains.

n_p	ϕ_B	Z_{MC}	$\langle R^2 \rangle$
M = 30-50			
2835	0.9126 ± 0.0028	61.24 ± 0.64	62.32 ± 0.05
2667	0.8608 ± 0.0029	45.67 ± 0.33	62.53 ± 0.21
2520	0.8149 ± 0.0029	37.21 ± 0.33	63.55 ± 0.20
2310	0.7488 ± 0.0026	28.57 ± 0.27	64.27 ± 0.12
2100	0.6826 ± 0.0024	22.59 ± 0.20	65.51 ± 0.13
1890	0.6161 ± 0.0020	17.87 ± 0.24	66.70 ± 0.03
1680	0.5493 ± 0.0017	14.44 ± 0.17	68.02 ± 0.09
1470	0.4825 ± 0.0015	11.52 ± 0.19	69.48 ± 0.15
1260	0.4156 ± 0.0012	9.04 ± 0.21	71.13 ± 0.16
1050	0.3483 ± 0.0010	7.18 ± 0.15	72.84 ± 0.07
840	0.2808 ± 0.0007	5.28 ± 0.13	74.99 ± 0.08
630	0.2132 ± 0.0006	3.92 ± 0.08	77.36 ± 0.08
525	0.1791 ± 0.0004	3.15 ± 0.08	78.66 ± 0.07
420	0.1445 ± 0.0004	2.63 ± 0.07	79.92 ± 0.06

(table IV continued)

M = 10 & 70			
2650	0.8553 ± 0.0065	44.43 ± 0.88	62.93 ± 1.35
2550	0.8240 ± 0.0065	38.70 ± 0.94	63.70 ± 1.05
2450	0.7929 ± 0.0061	33.92 ± 1.12	65.25 ± 0.55
2350	0.7613 ± 0.0059	30.61 ± 0.96	65.59 ± 0.52
2200	0.7142 ± 0.0056	24.70 ± 0.64	66.57 ± 0.33
2050	0.6668 ± 0.0050	21.64 ± 0.78	67.59 ± 0.62
1900	0.6194 ± 0.0048	18.24 ± 0.76	68.86 ± 0.65
1700	0.5559 ± 0.0039	14.64 ± 0.58	70.24 ± 1.02
1500	0.4923 ± 0.0033	11.77 ± 0.55	71.86 ± 0.36
1300	0.4284 ± 0.0028	9.47 ± 0.67	73.25 ± 0.59
1100	0.3646 ± 0.0023	7.49 ± 0.36	75.52 ± 0.18
900	0.3007 ± 0.0021	5.69 ± 0.49	77.73 ± 0.28
700	0.2365 ± 0.0014	4.32 ± 0.25	80.80 ± 0.27
500	0.1716 ± 0.0010	3.17 ± 0.21	84.38 ± 0.25
250	0.0886 ± 0.0004	1.87 ± 0.12	89.87 ± 0.39
M = 2 & 78			
900	0.3011 ± 0.0017	5.72 ± 0.31	79.99 ± 0.31
M = 1 & 79			
900	0.3010 ± 0.0009	5.58 ± 0.12	-

Table V. Values of $\langle \eta_\theta(M) \rangle$ as a function of the chain length. The value at $M \to \infty$ is the extrapolation result (see figure 5.13). In this table, we include the results of Monte Carlo simulations from several authors.

M	$\eta_\theta(M)$	Other MC Results
20	1.2812(4)	1.28[179], 1.287[141]
30	1.2880(6)	1.5[137]
40	1.2912(5)	1.293[179], 1.292[141]
50	1.2928(8)	
60	1.2942(6)	
70	1.2952(7)	
80	1.2958(12)	1.295[179], 1.297[141]
100	1.2970(3)	
150	1.2983(3)	
∞	1.306(2)	1.305[141], 1.309[179], 1.30(6)[127]

Table VI. Compressibility factor of nonathermal linear chains in a cubic lattice. $\eta = \exp(1/k_BT)$. ϕ is the fraction of occupied sites. F: the predictions of Flory theory; FH: the predictions of Flory-Huggins theory, BF: the results of extended-mean-field approximation calculated from Bawendi-Freed paper [Ref. 95]; DFM: the results of approximation calculated from Dudowicz-Freed-Madden paper [Ref. 103]

ϕ	F	FH	BF	DFM	MC	R^2
M = 20, η = 1.200						
0.8262(1)	17.334	14.040	12.428	12.695	12.71(4)	29.12(3)
0.7986(2)	15.308	12.239	10.770	11.032	10.98(4)	29.34(5)
0.7708(2)	13.603	10.749	9.414	9.666	9.62(2)	29.53(5)
0.7425(2)	12.130	9.484	8.276	8.514	8.52(4)	29.66(3)
0.7144(2)	10.873	8.424	7.331	7.554	7.48(3)	29.80(4)
0.6855(2)	9.750	7.494	6.509	6.716	6.71(4)	29.92(3)
0.6570(2)	8.782	6.705	5.818	6.010	5.98(2)	30.06(3)
0.5982(3)	7.122	5.387	4.675	4.841	4.82(5)	30.28(4)
0.5393(3)	5.808	4.377	3.807	3.959	3.95(3)	30.63(3)
0.4798(3)	4.743	3.585	3.127	3.278	3.26(3)	30.73(2)
0.4186(3)	3.858	2.946	2.579	2.736	2.67(2)	30.97(2)
0.3568(2)	3.134	2.438	2.141	2.310	2.25(1)	31.18(2)
0.2935(2)	2.535	2.027	1.786	1.963	1.90(2)	31.39(2)
0.2399(2)	2.119	1.747	1.545	1.723	1.64(2)	31.49(1)

(table VI continued)

0.1839(1)	1.760	1.508	1.345	1.510	1.49(2)	31.67(2)
0.1277(1)	1.466	1.313	1.190	1.326	1.34(1)	31.77(2)
0.0707(4)	1.227	1.154	1.078	1.164	1.12(2)	31.93(3)
0.0355(1)	1.105	1.072	1.031	1.077	1.07(1)	31.91(2)

M = 20, η = 1.281

0.8311(2)	15.565	12.128	10.032	10.398	10.42(4)	29.24(6)
0.8042(1)	13.588	10.407	8.505	8.862	8.96(5)	29.25(4)
0.7772(3)	11.940	9.004	7.281	7.622	7.65(5)	29.40(5)
0.7494(2)	10.510	7.813	6.261	6.581	6.68(3)	29.51(5)
0.7217(1)	9.297	6.824	5.428	5.726	5.71(3)	29.59(5)
0.6658(3)	7.328	5.271	4.150	4.404	4.43(3)	29.90(4)
0.6081(2)	5.785	4.107	3.219	3.441	3.48(2)	30.07(3)
0.5506(3)	4.599	3.253	2.548	2.756	2.81(2)	30.20(2)
0.4910(4)	3.644	2.596	2.038	2.250	2.30(2)	30.32(3)
0.4299(3)	2.885	2.098	1.654	1.883	1.88(1)	30.44(2)
0.3668(4)	2.283	1.722	1.364	1.614	1.59(1)	30.51(2)
0.3022(3)	1.820	1.446	1.152	1.417	1.37(2)	30.51(2)
0.2462(3)	1.520	1.275	1.026	1.288	1.24(1)	30.48(1)
0.1888(2)	1.295	1.152	0.945	1.182	1.16(1)	30.53(1)
0.1305(2)	1.138	1.069	0.909	1.095	1.06(1)	30.44(2)
0.0712(1)	1.042	1.021	0.920	1.030	1.05(2)	30.29(2)
0.03581(4)	1.012	1.006	0.951	1.006	1.00(2)	30.28(3)

(table VI continued)

M = 20, η = 1.350

0.8359(2)	14.207	10.636	8.165	8.614	8.69(7)	29.06(5)
0.8101(1)	12.289	8.995	6.756	7.192	7.18(3)	29.11(5)
0.7829(2)	10.621	7.603	5.590	6.003	6.17(5)	29.33(5)
0.7570(3)	9.289	6.519	4.705	5.091	5.14(4)	29.40(3)
0.7295(2)	8.089	5.569	3.946	4.303	4.41(3)	29.49(4)
0.6758(4)	6.223	4.148	2.850	3.153	3.27(3)	29.65(3)
0.6206(4)	4.783	3.112	2.086	2.350	2.47(2)	29.79(4)
0.5641(4)	3.668	2.356	1.549	1.798	1.93(2)	29.88(3)
0.5063(4)	2.804	1.809	1.171	1.430	1.52(2)	29.94(2)
0.4454(4)	2.124	1.409	0.903	1.189	1.22(1)	29.95(3)
0.3793(6)	1.594	1.126	0.717	1.040	1.07(1)	29.94(1)
0.3125(5)	1.229	0.956	0.614	0.960	0.98(2)	29.82(3)
0.2536(3)	1.023	0.878	0.580	0.922	0.88(1)	29.68(2)
0.1943(3)	0.906	0.851	0.595	0.899	0.86(2)	29.56(3)
0.1326(2)	0.865	0.865	0.662	0.889	0.89(1)	29.30(2)
0.0722(1)	0.892	0.912	0.781	0.906	0.93(1)	29.11(3)
0.0359(4)	0.937	0.953	0.880	0.940	0.995(14)	28.88(4)

M = 40, η = 1.200

0.8929(2)	48.054	40.046	35.896	36.406	41.30(9)	61.36(10)
0.8478(4)	37.455	30.284	26.694	27.254	31.93(4)	62.53(09)
0.8019(3)	30.061	23.678	20.597	21.152	25.60(6)	62.96(17)
0.7578(1)	24.795	19.110	16.463	16.983	17.10(4)	63.60(11)
0.7113(2)	20.490	15.485	13.239	13.707	13.62(5)	64.18(11)

(table VI continued)

0.6645(1)	17.049	12.673	10.777	11.192	11.17(4)	64.87(7)
0.6018(2)	13.425	9.808	8.303	8.661	8.58(3)	65.60(5)
0.5384(2)	10.581	7.641	6.451	6.778	6.72(2)	66.26(6)
0.4747(4)	8.324	5.982	5.038	5.363	5.15(3)	67.11(7)
0.4107(3)	6.514	4.694	3.940	4.284	4.10(2)	67.84(5)
0.3456(2)	5.037	3.674	3.067	3.439	3.18(1)	68.58(3)
0.2798(3)	3.842	2.869	2.377	2.767	2.53(2)	69.26(6)
0.2122(2)	2.865	2.224	1.832	2.212	1.98(1)	69.98(6)
0.1606(1)	2.261	1.830	1.514	1.854	1.66(1)	70.41(5)
0.1081(1)	1.755	1.500	1.268	1.534	1.37(1)	70.91(3)
0.0620	1.389	1.260	1.115	1.285	1.169(1)	71.11(33)
0.0370	1.219	1.148	1.056	1.163	1.096(1)	71.60(31)
0.0200	1.114	1.077	1.026	1.085	1.055(1)	71.45(28)
0.0150	1.084	1.057	1.018	1.063	1.041(1)	72.02(21)
0.0110	1.061	1.042	1.013	1.046	1.029(1)	71.83(23)
0.0070	1.039	1.026	1.008	1.029	1.017(1)	72.12(55)
0.0050	1.027	1.019	1.005	1.021	1.010(1)	72.55(28)

M = 40, η = 1.291

0.8304(1)	29.500	22.470	18.023	18.820	18.35(9)	62.38(14)
0.7994(1)	25.048	18.632	14.658	15.430	15.29(7)	62.84(11)
0.7683(1)	21.433	15.597	12.056	12.784	12.75(7)	63.12(11)
0.7374(1)	18.464	13.168	10.019	10.694	10.58(6)	63.36(10)
0.7059(2)	15.925	11.145	8.358	8.977	9.02(9)	63.68(12)
0.6583(2)	12.797	8.734	6.425	6.969	7.08(5)	64.18(16)

(table VI continued)

0.6107(2)	10.313	6.895	4.988	5.478	5.49(5)	64.23(8)
0.5622(3)	8.281	5.450	3.881	4.346	4.45(4)	64.73(7)
0.5135(2)	6.634	4.327	3.033	3.499	3.50(6)	65.09(8)
0.4636(5)	5.270	3.434	2.366	2.857	2.94(4)	65.30(6)
0.4125(4)	4.147	2.731	1.841	2.373	2.42(4)	65.52(6)
0.3599(5)	3.230	2.180	1.432	2.006	2.02(4)	65.74(9)
0.3077(5)	2.517	1.772	1.132	1.734	1.60(1)	65.68(6)
0.2528(3)	1.946	1.459	0.913	1.512	1.38(3)	65.81(8)
0.1962(3)	1.518	1.237	0.779	1.327	1.29(3)	65.72(5)
0.1384(1)	1.225	1.094	0.732	1.172	1.14(2)	65.54(4)
0.0991(1)	1.099	1.036	0.753	1.087	1.05(1)	65.27(8)
0.0597(1)	1.024	1.005	0.817	1.025	1.02(2)	65.15(7)
0.0279(4)	0.999	0.996	0.901	0.999	1.004(22)	64.97(9)
0.0119(2)	0.997	0.997	0.955	0.996	1.00(3)	64.74(10)
0.0150	0.997	0.997	0.944	0.996	1.00(1)	-
0.0070	0.998	0.998	0.973	0.997	1.00(1)	-
0.0050	0.998	0.999	0.980	0.998	0.999(1)	-
0.0040	0.998	0.999	0.984	0.998	0.999(2)	-

M = 40, η = 1.400

0.8325(8)	24.442	17.180	11.672	12.737	11.05(15)	62.61(20)
0.7813(2)	17.791	11.690	7.208	8.174	6.91(15)	62.88(12)
0.7313(4)	13.196	8.109	4.473	5.307	4.38(6)	63.79(9)
0.6729(3)	9.315	5.273	2.448	3.143	2.80(3)	63.82(9)
0.6046(4)	6.112	3.115	1.022	1.627	2.10(2)	63.82(6)

(table VI continued)

0.5410(2)	4.013	1.830	0.238	0.845	1.38(3)	63.86(7)
0.4875(3)	2.725	1.118	-0.166	0.495	0.96(2)	63.26(5)
0.4001(4)	1.317	0.454	-0.502	0.294	0.66(2)	63.17(7)
0.3385(2)	0.721	0.247	-0.569	0.303	0.50(1)	62.74(4)
0.2810(2)	0.396	0.192	-0.533	0.356	0.46(1)	62.13(4)
0.2723(3)	0.364	0.193	-0.520	0.366	0.44(1)	61.57(5)
0.2186(3)	0.252	0.246	-0.394	0.426	0.43(1)	60.89(5)
0.1551(1)	0.290	0.392	-0.146	0.500	0.53(1)	59.97(6)
0.0920(1)	0.485	0.604	0.220	0.607	0.64(1)	58.82(6)
0.0300(1)	0.805	0.862	0.710	0.821	0.86(1)	57.23(5)
0.0120(2)	0.919	0.944	0.880	0.921	0.95(1)	56.78(9)
0.0060	0.959	0.972	0.939	0.959	0.97(1)	-
0.0050	0.966	0.976	0.949	0.966	0.984(2)	-
0.0030	0.979	0.986	0.969	0.979	0.994(2)	-

M = 80, η = 1.296

0.7364(1)	35.298	24.644	18.183	19.586	19.99(23)	133.28(49)
0.7067(1)	30.532	20.869	15.112	16.405	16.55(23)	133.99(55)
0.6766(2)	26.406	17.687	12.573	13.764	13.78(14)	134.62(27)
0.6463(2)	22.835	15.003	10.472	11.575	11.76(16)	134.81(58)
0.6159(2)	19.736	12.735	8.726	9.761	10.23(14)	136.02(42)
0.5858(2)	17.068	10.834	7.283	8.274	8.58(16)	135.64(23)
0.5559(2)	14.752	9.226	6.077	7.049	7.22(7)	136.66(44)
0.5252(2)	12.671	7.820	5.033	6.008	6.31(9)	136.93(31)
0.4945(2)	10.853	6.623	4.150	5.149	5.32(9)	137.37(17)

(table VI continued)

0.4634(2)	9.243	5.593	3.394	4.433	4.63(4)	138.03(38)
0.4313(2)	7.796	4.692	2.735	3.827	4.04(8)	138.59(38)
0.3837(3)	5.999	3.612	1.948	3.126	3.26(4)	138.44(31)
0.3344(3)	4.512	2.757	1.329	2.582	2.53(7)	138.77(28)
0.2841(3)	3.326	2.107	0.872	2.156	1.91(5)	138.66(23)
0.2323(4)	2.403	1.625	0.561	1.806	1.69(7)	138.47(45)
0.1803(2)	1.736	1.298	0.399	1.512	1.41(6)	138.91(34)
0.1271(2)	1.288	1.093	0.386	1.260	1.30(5)	138.29(31)
0.0909(1)	1.102	1.016	0.465	1.122	1.11(4)	138.40(35)
0.0547(1)	1.002	0.982	0.619	1.025	1.06(5)	137.03(41)
0.0292(2)	0.980	0.981	0.774	0.991	1.01(1)	136.31(26)

Table VII. Compressibility factor of athermal chains with branch-structures. F: the predictions of Flory theory; FH: the predictions of Flory-Huggins theory; NBF: the predictions calculated from Nemirovsky-Bawendi-Freed paper [Ref. 97]; MC: Monte Carlo simulation results. M is the number of monomer units in a chain.

ϕ	F	FH	BF	MC
STRUCTURE 2, CHAIN LENGTH = 8, M = 20				
0.0346(1)	1.354	1.249	1.113	1.25(3)
0.0650(1)	1.680	1.481	1.240	1.56(5)
0.1288(2)	2.411	2.012	1.589	1.71(5)
0.1926(3)	3.216	2.611	2.057	1.92(3)
0.2558(2)	4.100	3.286	2.648	2.35(3)
0.3177(2)	5.066	4.041	3.361	2.73(4)
0.3786(2)	6.134	4.895	4.211	3.14(4)
0.4390(1)	7.334	5.877	5.220	3.89(4)
0.4795(1)	8.235	6.628	6.006	4.24(4)
0.5192(2)	9.209	7.451	6.874	4.87(7)
0.5582(3)	10.269	8.361	7.839	5.65(5)
0.5981(1)	11.482	9.417	8.960	6.31(4)
0.6373(2)	12.827	10.606	10.221	7.34(6)
0.6764(1)	14.360	11.979	11.674	8.52(5)
0.7570(4)	18.376	15.654	15.534	12.03(13)

(table VII continued)

STRUCTURE 1, CHAIN LENGTH = 11, M = 20

0.0264(1)	1.269	1.189	1.121	1.39(9)
0.0787(2)	1.831	1.590	1.410	1.63(4)
0.1318(3)	2.447	2.039	1.771	1.70(4)
0.1832(4)	3.092	2.518	2.190	1.90(4)
0.2354(4)	3.804	3.059	2.689	1.93(4)
0.2856(5)	4.551	3.637	3.247	2.34(3)
0.3366(4)	5.384	4.293	3.900	2.57(4)
0.3877(4)	6.305	5.033	4.651	2.91(5)
0.4372(3)	7.296	5.845	5.486	3.24(5)
0.4872(3)	8.417	6.780	6.455	3.73(4)
0.5367(2)	9.671	7.846	7.563	4.24(3)
0.5851(2)	11.071	9.058	8.822	5.07(4)
0.6339(1)	12.704	10.496	10.313	5.97(4)
0.6819(2)	14.594	12.189	12.062	7.09(3)
0.7295(2)	16.846	14.241	14.170	8.69(4)
0.8052(1)	21.630	18.697	18.715	13.74(2)
0.8334(4)	24.008	20.949	20.998	15.77(4)

STRUCTURE 2, CHAIN LENGTH = 15, M = 41

0.8248(1)	46.585	40.014	39.783	32.41(13)
0.7890(7)	40.851	34.629	34.201	28.67(16)
0.7763(2)	39.087	32.986	32.491	23.17(15)
0.6944(2)	29.995	24.658	23.754	15.66(22)
0.6226(2)	24.170	19.475	18.265	11.41(10)

(table VII continued)

0.5506(1)	19.560	15.484	14.027	8.56(7)
0.4778(2)	15.751	12.279	10.646	6.42(6)
0.4039(2)	12.516	9.634	7.913	4.98(9)
0.3296(1)	9.742	7.432	5.728	3.95(6)
0.2916(3)	8.473	6.447	4.797	3.19(8)
0.2543(1)	7.309	5.558	3.992	2.83(4)
0.2155(2)	6.177	4.706	3.264	2.65(5)
0.1774(1)	5.134	3.933	2.650	2.22(4)
0.1291(1)	3.899	3.035	2.010	1.98(7)
0.0799(1)	2.731	2.202	1.507	1.72(3)
0.0321(1)	1.672	1.462	1.159	1.58(6)

STRUCTURE 1, CHAIN LENGTH = 21, M = 40

0.8286(2)	46.144	39.706	39.689	27.72(19)
0.7954(1)	40.794	34.671	34.574	23.66(10)
0.7620(1)	36.354	30.542	30.362	20.31(10)
0.7165(2)	31.372	25.975	25.681	13.96(10)
0.6474(3)	25.407	20.619	20.155	10.01(11)
0.5779(1)	20.700	16.503	15.880	7.20(12)
0.5067(2)	16.784	13.170	12.408	6.00(9)
0.4530(2)	14.272	11.084	10.242	4.66(9)
0.3981(2)	12.009	9.245	8.346	4.00(8)
0.3432(3)	9.995	7.643	6.720	3.32(5)
0.2878(2)	8.171	6.225	5.315	2.79(6)
0.2308(2)	6.477	4.937	4.088	2.50(6)

(table VII continued)

0.1827(2)	5.171	3.965	3.207	2.38(7)
0.1351(2)	3.973	3.091	2.465	2.19(7)
0.0840(2)	2.780	2.238	1.803	1.86(9)
0.0585(1)	2.218	1.842	1.522	1.72(4)
0.0310(1)	1.633	1.435	1.256	1.63(9)

Table VIII. The mean-square of the end-to-end distance and the radius of gyration of athermal chains with branch-structures. N, N_B, and M are the number of backbone segments, the number of branches emanating from a backbone segment, and the number of monomer units in a chain, respectively. ϕ is the segment density.

N = 8, N_B= 2, M = 20			N = 11, N_B = 1, M =20		
ϕ	R^2	R_g^2	ϕ	R^2	R_g^2
0.0346(1)	12.49(3)	2.503(1)	0.0264(1)	17.55(3)	3.214(4)
0.0650(1)	12.51(2)	2.506(1)	0.0787(2)	17.57(3)	3.213(2)
0.1288(2)	12.54(4)	2.507(1)	0.1318(3)	17.60(2)	3.215(2)
0.1926(3)	12.51(2)	2.506(1)	0.1832(4)	17.57(2)	3.212(1)
0.2558(2)	12.53(1)	2.507(1)	0.2354(4)	17.53(1)	3.207(1)
0.3177(2)	12.50(2)	2.507(1)	0.2856(5)	17.53(1)	3.207(1)
0.3786(2)	12.46(2)	2.504(1)	0.3366(4)	17.53(1)	3.206(1)
0.4390(1)	12.47(2)	2.505(1)	0.3877(4)	17.52(1)	3.205(1)
0.4795(1)	12.43(1)	2.503(1)	0.4372(3)	17.46(1)	3.202(1)

(table VIII continued)

0.5192(2)	12.40(1)	2.500(1)	0.4872(3)	17.45(1)	3.200(1)
0.5582(3)	12.38(1)	2.500(1)	0.5367(2)	17.40(1)	3.196(1)
0.5981(1)	12.35(1)	2.498(1)	0.5851(2)	17.37(1)	3.192(1)
0.6373(2)	12.31(1)	2.496(1)	0.6339(1)	17.26(2)	3.184(1)
0.6764(1)	12.27(1)	2.492(1)	0.6819(2)	17.24(1)	3.182(1)
0.7570(4)	12.15(2)	2.486(1)	0.7295(2)	17.13(1)	3.172(1)
			0.8052(1)	17.03(1)	3.161(1)
			0.8334(4)	16.97(1)	3.155(1)

N = 21, N_s = 1, M = 40			N = 15, N_s = 2, M = 41		
ϕ	R^2	R_g^2	ϕ	R^2	R_g^2
0.8286(2)	33.37(8)	6.980(11)	0.7763(2)	27.21(15)	6.138(2)
0.7954(1)	33.54(7)	6.954(5)	0.6944(2)	27.68(6)	6.172(6)
0.7620(1)	33.76(9)	7.012(10)	0.6226(2)	27.74(4)	6.177(3)
0.7165(2)	34.45(16)	7.076(5)	0.5506(1)	27.73(5)	6.181(3)

0.6474(3)	34.60(6)	7.108(5)	0.4778(2)	27.96(3)	6.201(3)
0.5779(1)	34.82(5)	7.129(5)	0.4039(2)	28.10(4)	6.205(4)
0.5067(2)	34.92(6)	7.134(5)	0.3296(1)	28.08(3)	6.195(3)
0.4530(2)	35.07(5)	7.147(5)	0.2916(3)	28.07(4)	6.190(3)
0.3981(2)	35.14(7)	7.147(6)	0.2543(1)	28.15(2)	6.192(4)
0.3432(3)	35.25(7)	7.153(6)	0.2155(2)	28.14(3)	6.189(3)
0.2878(2)	35.08(5)	7.133(6)	0.1774(1)	28.06(5)	6.175(5)
0.2308(2)	35.29(3)	7.138(5)	0.1646(2)	28.14(3)	6.180(3)
0.1827(2)	35.15(5)	7.129(5)	0.1241(2)	28.09(4)	6.176(2)
0.1428(2)	35.28(6)	7.143(4)	0.0837(1)	28.15(3)	6.177(3)
0.0616(2)	35.23(12)	7.128(9)	0.0421(1)	28.12(4)	6.171(3)

Table IX. Values of $X_{1/2}$ vs density. $X_{1/2}$ is the distance (in unit lattice cell) at which the density attains one half of the the bulk value.

M = 20		M = 40		M = 80	
ϕ	$X_{1/2}$	ϕ	$X_{1/2}$	ϕ	$X_{1/2}$
Athermal					
0.0661	1.81	0.0742	2.31	0.0524	3.25
-	-	-	-	0.1021	2.31
Above the θ-temperature					
η = 1.200		η = 1.200			
0.068	2.10	0.094	2.51		-
0.517	0.96	0.485	1.09		-
0.744	0.65	0.741	0.60		-
At the θ-temperature					
η = 1.281		η = 1.291		η = 1.296	
0.068	2.17	0.096	3.00	0.089	4.00
0.526	1.20	0.496	1.40	0.483	1.70
0.748	0.69	0.746	0.70	0.720	0.75
Below the θ-temperature					
η = 1.350		η = 1.400			
0.069	2.24	0.099	4.10		-
0.540	1.49	0.527	2.60		-
0.754	0.71	0.755	0.90		-

5.6. Graphs of Simulation Results.

Figure 5.1. A snapshot of two-dimensional lattice chains. ε indicates the nearest neighbor interaction. ℓ is the bond length, which is equal to the lattice spacing.

Figure 5.2. Monte Carlo moves. Top figure is the slithering snake-like move (reptation). The lower figure illustrates the effect of two internal moves.

Figure 5.3. $-M^{-1}\log(p)$ vs $-\log(1-\phi)$ for athermal chains in the simple cubic lattice for chains of M = 5, 10, and 20 monomer units. (▪▪▪▪▪) is the prediction of Flory theory, (---) is the prediction of Flory-Huggins theory, and (———)is the results of Bawendi-Freed approximation through order z^{-2}. • is the Monte Carlo simulation results. The inset shows an enlargment of the low density region.

Figure 5.4. The compressibility factor $Z = \phi_c^{-1}\pi^*$ vs segment density, ϕ, where ϕ_c is the chain density. •-•-•: Flory theory; ---: Flory-Huggins theory; ———: Bawendi-Freed approximation through order z^{-2}; •: Monte Carlo (MC) simulation results using the chain-insertion method for M=20; ■; MC results using the repulsive-wall method for M=20. For M=40, ○: MC results using the repulsive-wall method; ◇: MC results using the chain-insertion method.

Figure 5.5. Scaling of the compressibility factor: log(Z) vs $\log(\phi/\phi^*)$. ○, •, and □ correspond to M = 10, 20, and 40, respectively. The dashed line with a slope of 5/4 indicates the scaling behavior expected from the des Cloizeaux law.

Figure 5.6. Scaling behavior of G(y), defined in Eq. (5.20). •: M = 40; ○: M = 20.

Figure 5.7. Dependence of chain dimensions on the segment density for M=40. ——and --- have slopes of -1/4 and -0.23, respectively (see Eq. (2.47) and the discussion in Sec. 5.4.1)

Figure 5.8. The ratio of the wall-contact density to pressure vs pressure. ○: M = 20; and •: M = 40.

Figure 5.9. Compressibility factor Z vs volume fraction for polydisperse athermal chains in the cubic lattice. •-•-•: Flory theory; ---: Flory-Huggins theory; ———:Bawendi-Freed approximation through order z^{-2}. Symbols denote the results of MC simulations: +, monodisperse system , M=40; x, uniform distribution, M=30-50; □, bimodal distribution, M=10 and 70. The arrow indicates the position of two data points for extreme bimodal distributions with M=2 and 78, and M=1 and 79.

Figure 5.10.The normalized mean-square end-to-end distance Y = $\langle R^2\rangle/\langle R^2\rangle_{\phi\to 0}$ vs $h(\phi)=(Z-1)/(A_2\phi)$. □: uniform distribution (μ=0.98); +: bimodal distribution (μ=0.84, M=10 and 70); ○: monodisperse system (μ=1.).

Figure 5.11. The ratio of the wall-contact density to pressure ($B=\rho_H(1)/\pi^*$) vs pressure π^*. +: μ=0.84; x: μ=0.98; and ○: μ=1.

Figure 5.12. The insertion factor vs η ($\eta=\exp(1/k_BT)$ at low-density region. Fig. a: M=20; b: M=40; c: M=60; d: M=80; and e: M=100. Note that $P(\phi,\eta)=1$ determines η at θ-temperature.

Figure 5.13. θ-temperature vs. 1/M. Note that $\langle\eta_\theta\rangle$ is used instead of temperature. $\langle\eta_\theta\rangle$ is obtained by averaging the values of η_θ at various densities.

Figure 5.14. Compressibility factor vs volume fraction at various temperatures. ••••: Flory theory; -•-•-; Flory-Huggins theory; ---: the extended-mean-filed approximation of Bawendi and Freed (calculated from Ref. 95); ——:the results obtained from Dudowic-Freed-Madden (see Eqn. 4.125); □: Monte Carlo simulation results. Fig. a: M=20, η=1.200; b: M=20, η=1.281; c: M=20, η=1.350; d: M=40, η=1.200; e: M=40, η=1.291; f: M=40, η=1.400; g: M=80, η=1.296.

Figure 5.15. Compressibility factor vs density for linear chains at various temperatures. Fig. a: M = 20; and b: M = 40.

Figure 5.16. Compressibility factor vs density for linear chains at the θ-temperature. The MC simulation results were compared with the predictions of Flory-Huggins theory and Freed's n-vector model (see Eqn. 4.125, which is calculated from Dudowicz-Freed-Madden[103]).

Figure 5.17. The log. of excess pressure vs log(ϕ). The dashed line has a slope of 3. In Fig. a the monomer units per chain is 40, and the simulation results are denoted by the following symbols: □, η=1.00 (athermal system); ◇, η=1.200 (above θ-temperature); ■, η=1.291 (θ-temperature); ○, θ=1.300 (slightly below θ-temperature). Fig. b is the results at θ-temperature. □: M = 20; ◇: M = 40; and ■: M = 80.

Figure 5.18. Log(R^2/M) vs -log(ϕ). Fig. a: M=20 and □, ■, and ◇ correspond to η=1.200, 1.281, and 1.350, respectively. Fig. b: M=40 and □, ■, and ◇ correspond to η=1.200, 1.291, and 1.400, respectively. ○ denotes the athermal results. Fig. c: □, ■, and ◇ correspond to simulation results at θ-temperature for M = 20, M = 40, and M = 80, respectively.

Figure 5.19. The ratio of the wall-contact density to pressure ($B=\rho_H(1)/\pi^*$) vs pressure π^*. Fig. a: M = 20 and □, ■, and ◇ correspond to η=1.200, 1.281, and 1.350, respectively. Fig. b: □, ■, and ◇ respectively correspond to M=20, M=40, and M=80 at the θ-temperature.

Figure 5.20. Compressibility factor vs segment density for athermal chains with various structures. ○: MC results for linear chains; ■: MC results for chains with struture 1; □: MC results for chains with structure 2; ———:Flory theory; ---: Flory-Huggins theory; -•-•-: Nemirovski-Bawendi-Freed (NBF) predictions for chains with structure 1; and ••••: NBF predictions for chains with structure 2. Fig. a and b

correspond to M = 20 and M = 40, respectively.

Figure 5.21. The Log. of excessive pressure vs log(ϕ). ◆: M=40, linear chains; ○: M=40, structure 1; ◇: M=20, stucture 2; •: M=20, linear chains; ■: M=20, structure 1; and □: M=20, structure 2. Dashed line is a visual aid corresponding to linear chains.

Figure 5.22. The mean-square of the end-to-end distance and the radius of gyration vs density. ■: M=40, structure 1; ◇: M=41, structure 2; □: M=20, structure 1; and ○: M=20, structure 2.

Figure 5.23. The normalized density vs $\phi_B^{3/4}x$ (distance from the wall scaled to mesh-size $\xi \sim \phi_B^{-3/4}$). The symbols correspond to MC simulation results of M=40 chains for various density values.

Figure 5.24. The normalized density vs $\phi_B^{3/4}x$ for various density and chain-length distributions. μ = 1.00 (monodisperse system): □, ϕ=0.802; ◇, ϕ=0.408; ○, ϕ=0.209; *, ϕ=0.108; μ = 0.98 (uniform distribution): △, ϕ=0.610; •, ϕ=0.143; μ = 0.84 (bimodal distribution): ■, ϕ=0.755; ▲, ϕ=0.550; +, ϕ=0.361.

Figure 5.25. The normalized density vs distance (normalized to the distance at which the density attains one half its bulk value, $x_{1/2}$). Fig. a corresponds to M = 20 and the following symbols: η=1.200: +, ϕ=0.744; x, ϕ=0.517; □, ϕ=0.068; η=1.281: ■, ϕ=0.748; ◇, ϕ=0.526; ○, ϕ=0.068; η=1.350: •, ϕ=0.754; △, ϕ=

0.540; ▲, ϕ=0.069. Fig. b is the MC results for M = 40, and the symbols mean as follows: η=1.200: +, ϕ=0.741; x, ϕ=0.485; □, ϕ=0.094; η=1.291: ■, ϕ=0.746; ◇, ϕ=0.496; ○, ϕ=0.096; η=1.400: •, ϕ=0.755; △, ϕ=0.527; ▲, ϕ=0.099. Fig. c is the MC results at θ-temperature with the symbols meaning as follows: M=20: +, ϕ=0.748; x, ϕ=0.526; □, ϕ=0.068; M=40: ■, ϕ=0.746; ◇, ϕ=0.496; ○, ϕ=0.096; M=80: △, ϕ=0.720; ◆, ϕ=0.483; •, ϕ=0.089.

Figure 5.26. The normalized density vs $(\phi_s/b)^{3/4}x$ (b is the number of occupied sites per monomer unit). Structure 1, b=2: +, M=40, ϕ=0.717; ○, M=40, ϕ=0.398; □, M=20, ϕ=0.730; x, M=20, ϕ=0.437. Structure 2, b=3: •, M=41, ϕ=0.776; ◆, M=41, ϕ=0.478; ◇, M=20, ϕ=0.757; and ■, M=20, ϕ=0.480.

Figure 5.27. Scaling analysis of the density profile. Fig. a shows the scaling property of athermal chains. n is the normalized density, and x is the distance from the wall. The symbols mean as follows: M=80: ■, ϕ=0.1021; ◇, ϕ=0.0524; M=40: □, ϕ=0.1433; x, ϕ=0.0742; M=20, +, ϕ=0.0661. The dashed line has a slope of 5/3. Fig. b shows the scaling of density of athermal and nonathermal chains. $Y = X/X_{1/2}$ (X is the distance from the wall, and $X_{1/2}$ is the distance from the wall at which the density is half of the balk value). Athermal: M=80: △, ϕ= 0.1021; ◆, ϕ=0.0524; M=40: ◻, ϕ=0.0742; and M=20: ▲, ϕ=0.0661. Nonathermal: M=20: +, η=1.200, ϕ=0.068; x, η=1.281, ϕ=0.068; □, η=1.350, ϕ=0.069; M=40: ■, η=1.200, ϕ=0.094; ◇, η=1.291, ϕ=0.096; ○, η=1.400, ϕ=0.100; M=80: •, η=1.296, ϕ=0.089.

Figure 5.28. Fraction of chains vs Bin Number for the athermal chains at various densities. M=40.

Figure 5.29. Short-chain and aggregate normalized density profiles for bimodal systems. The x-axis corresponds to the distance from the wall. +, ϕ=0.237, M=10 only; □, ϕ=0.237, aggregate (M=10 and 70); x, ϕ=0.301, M=10 only; ◇, ϕ=0.301, aggregate; •, ϕ=0.301, M=2 only; ○, ϕ=0.301, aggregate (M=2 and 78).

Figure 5.30. Fraction of chains vs Bin Number for a bimodal system with M = 10 and 70. x, ϕ=0.237, M=10; ○, ϕ=0.237, M=70; +, ϕ=0.0301, M=10; □, ϕ=0.0301, M=70.

Figure 5.31. Fraction of chains with center-of-mass (CM) located at Bin j. Figure a, b, and c correspond to 20-, 40-, and 80-mer chains at θ-temperature.

Figure 5.32. Fraction of chains vs Bin Number for 40-mer chains. Fig. a: η=1.200 (above θ-temperature); Fig. b: η=1.300 (slightly below θ-temperature); and Fig. c: η=1.400 (well below θ-temperature).

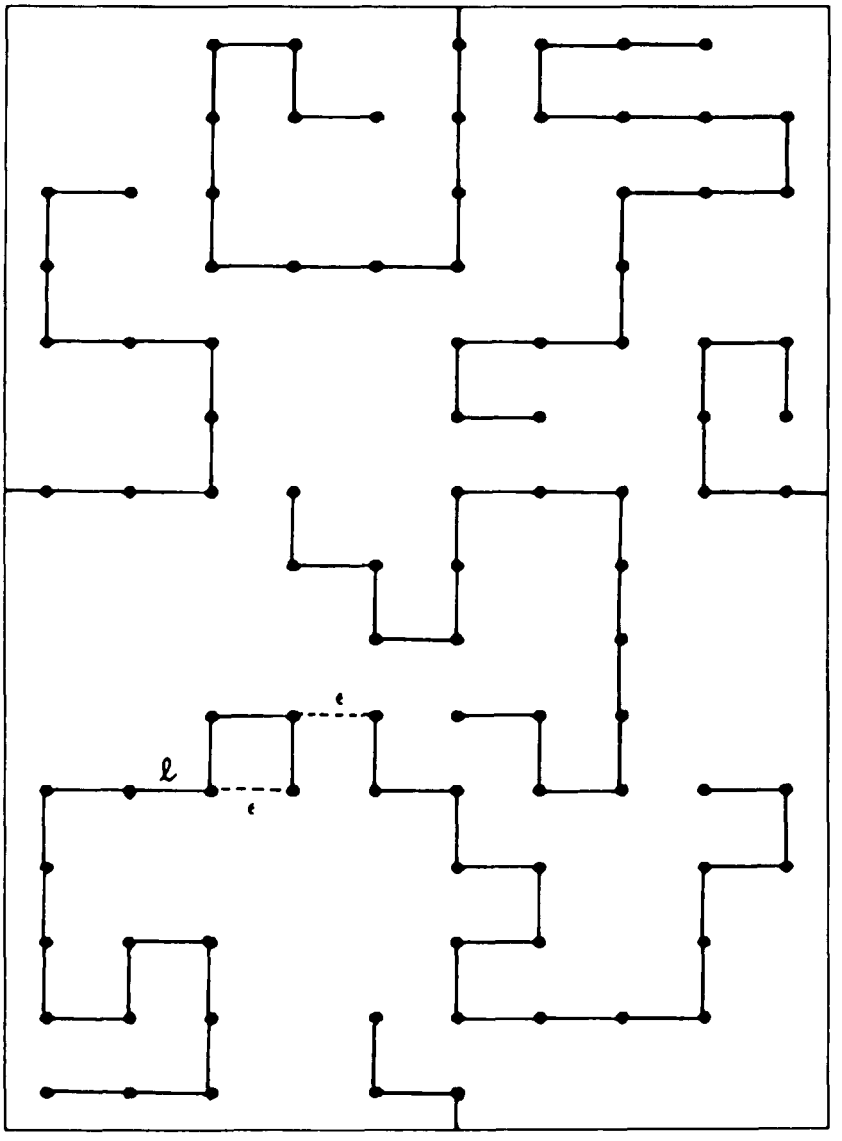

Figure 5.1

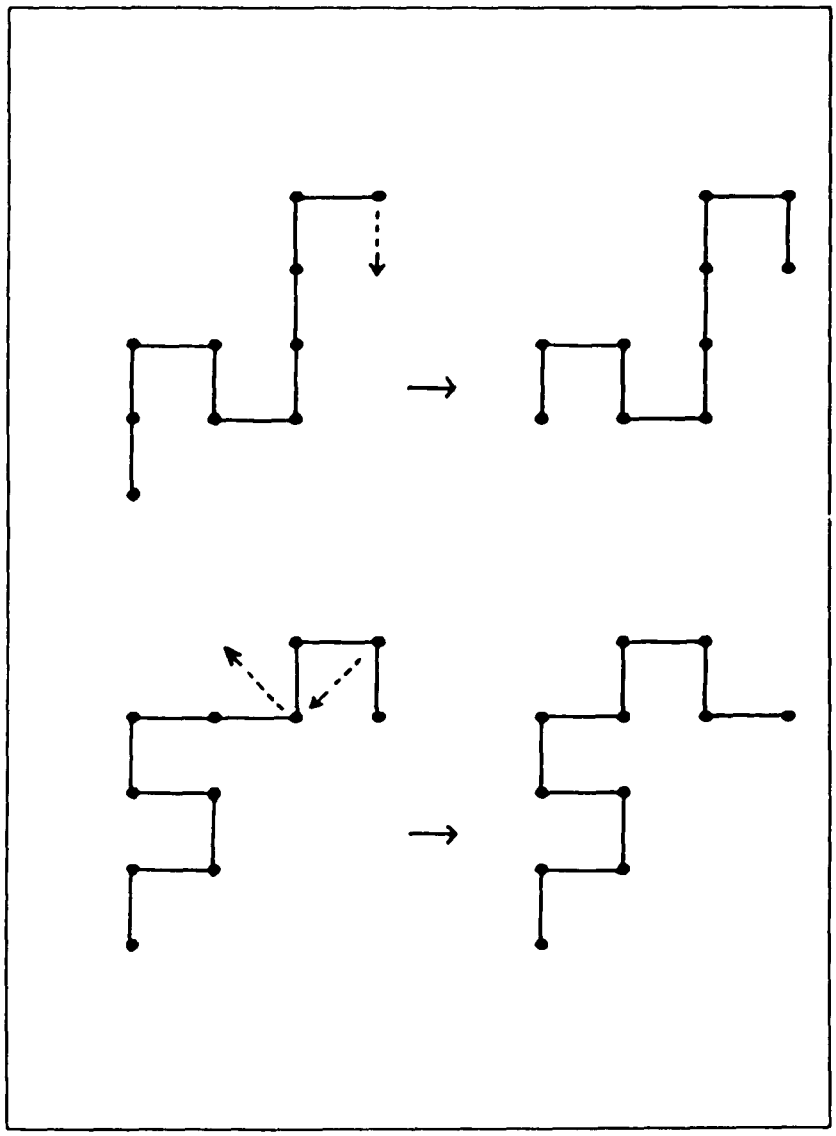

Figure 5.2

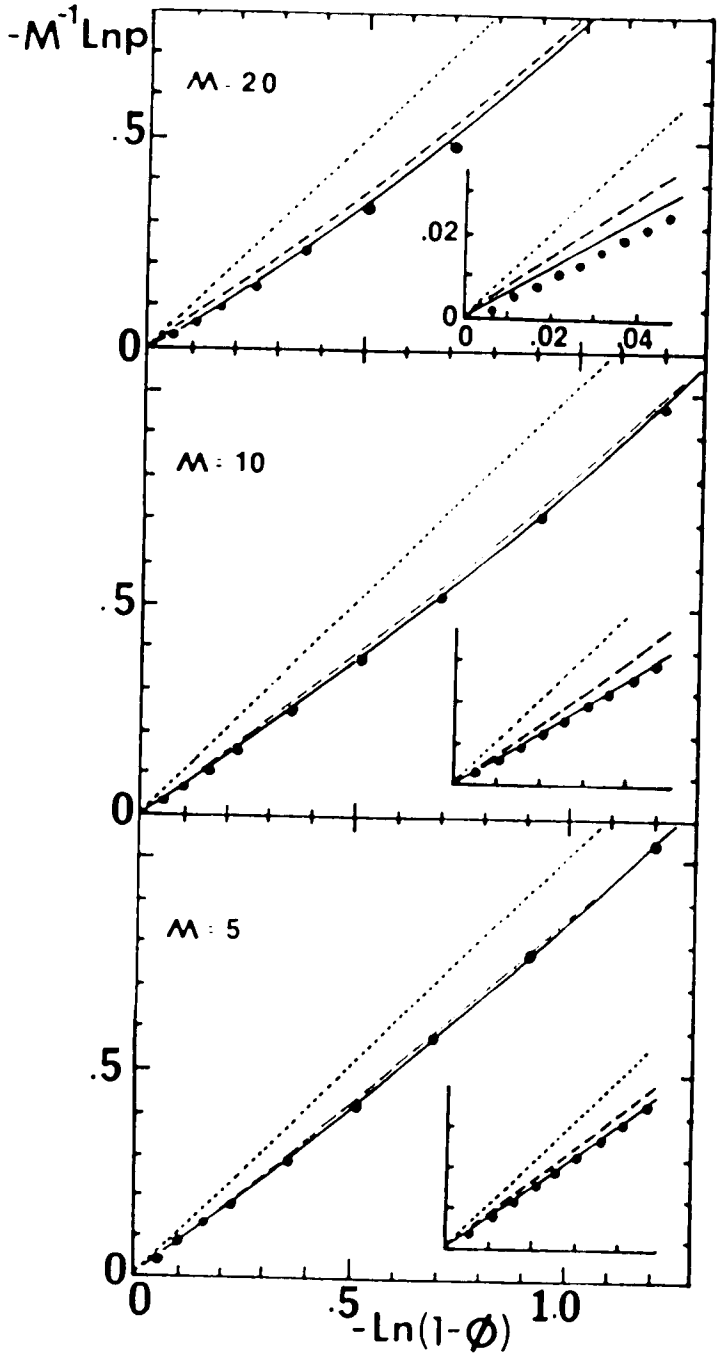

Figure 5.3

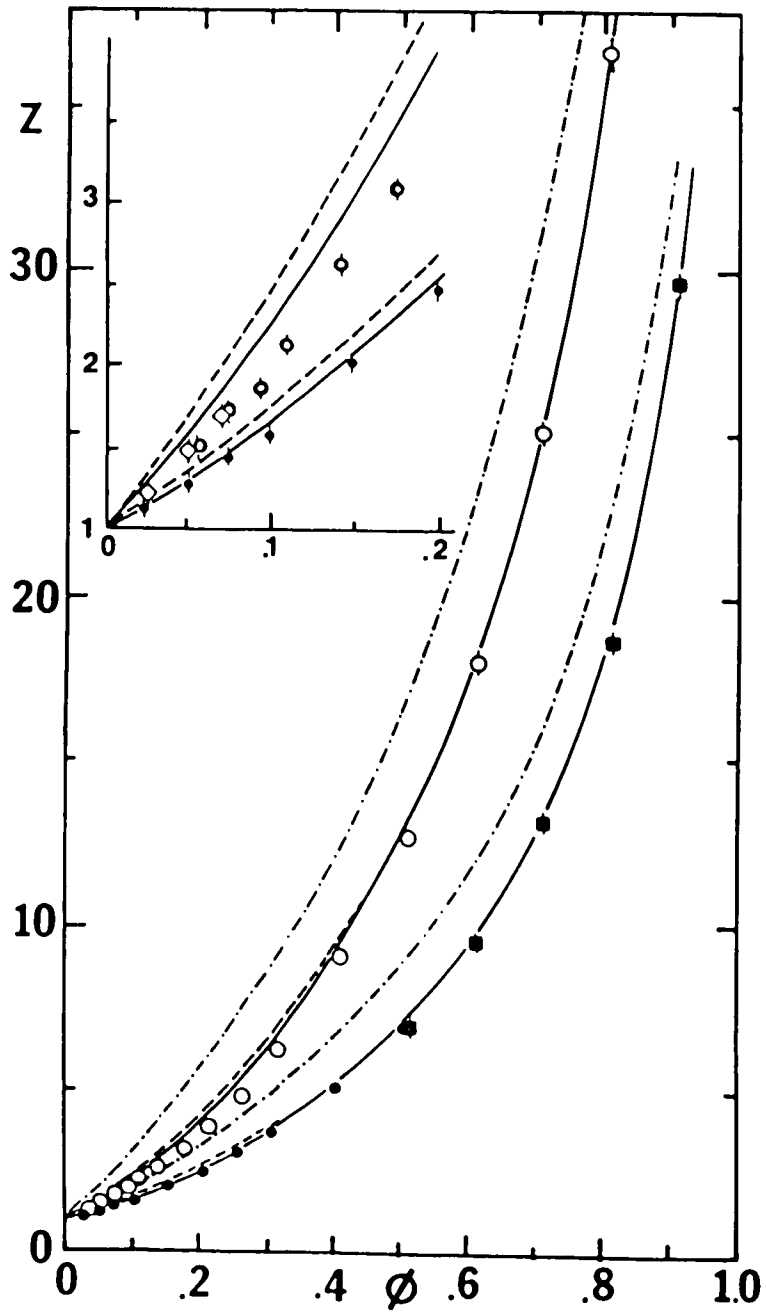

Figure 5.4

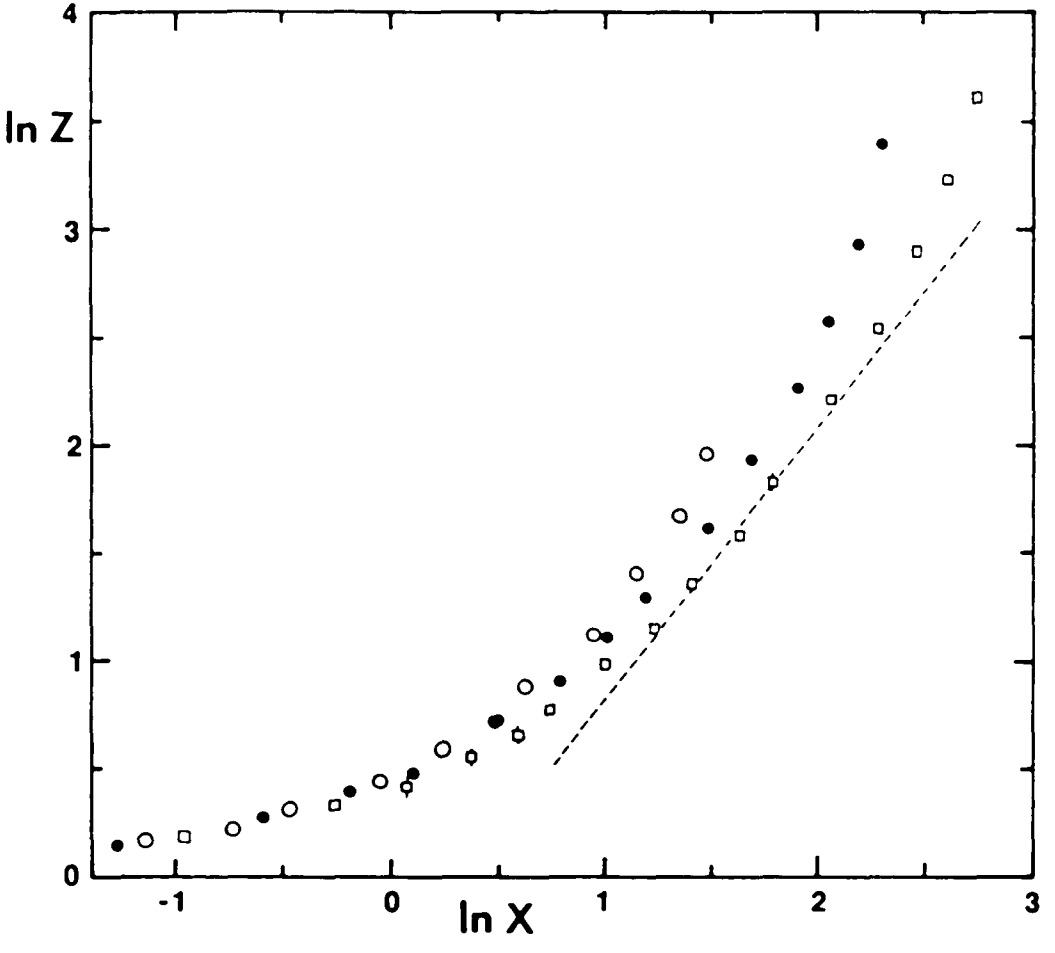

Figure 5.5

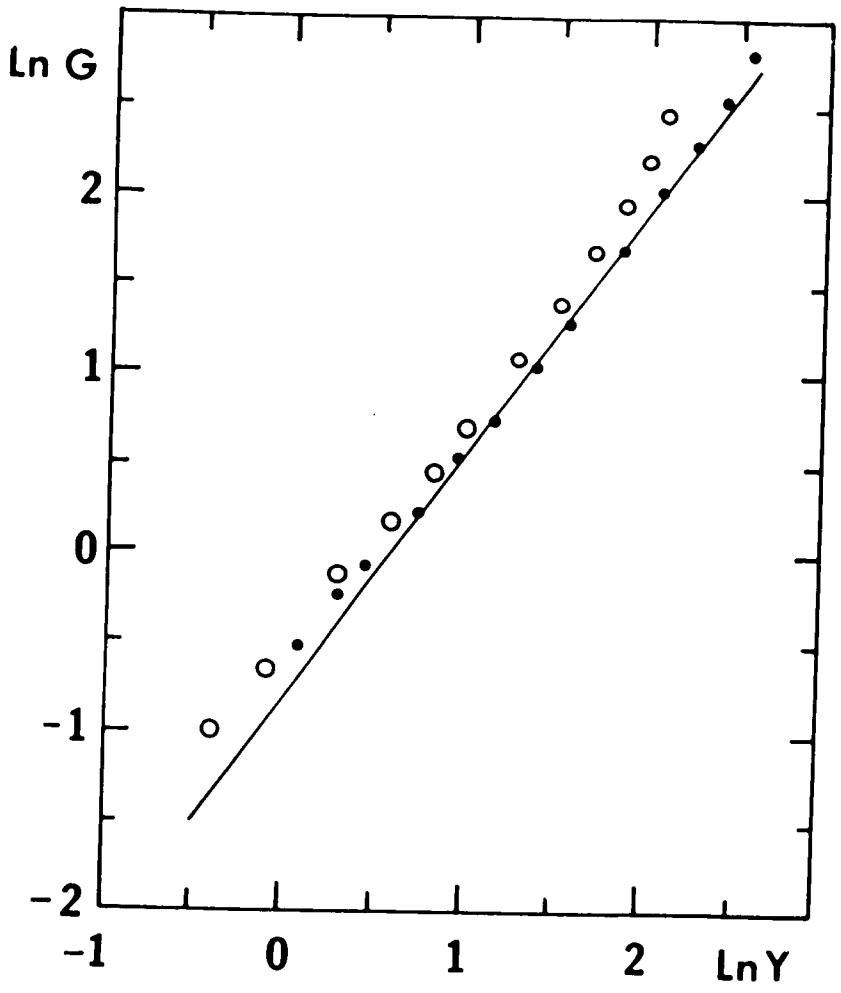

Figure 5.6

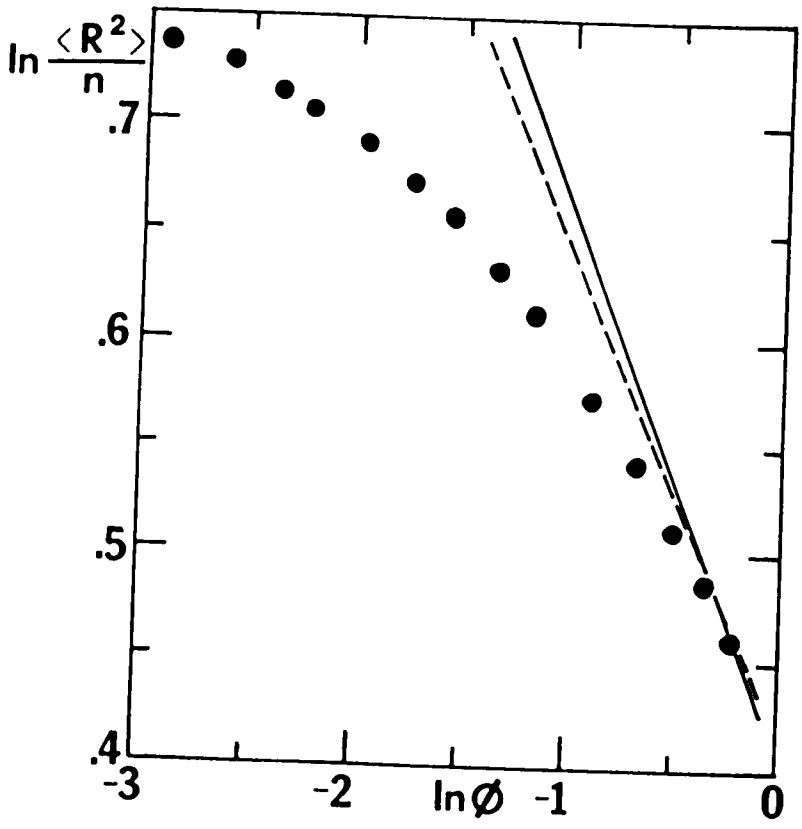

Figure 5.7

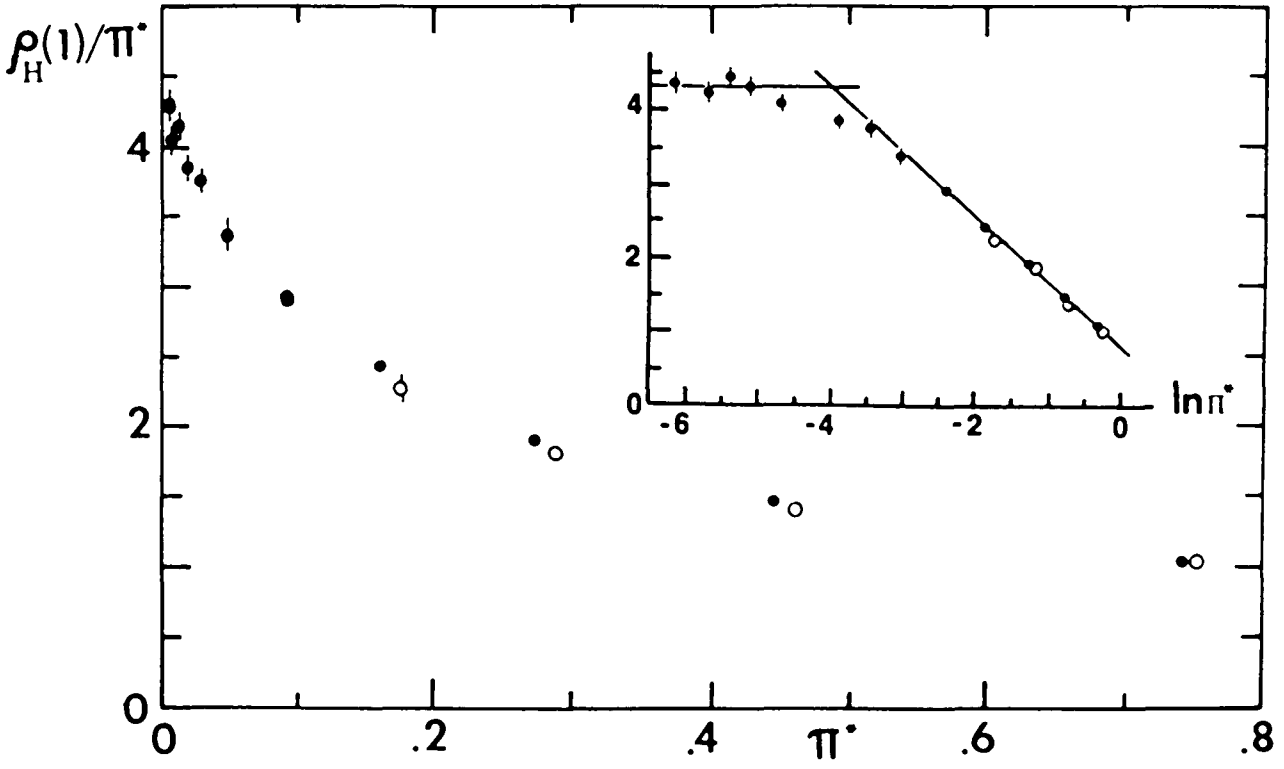

Figure 5.8

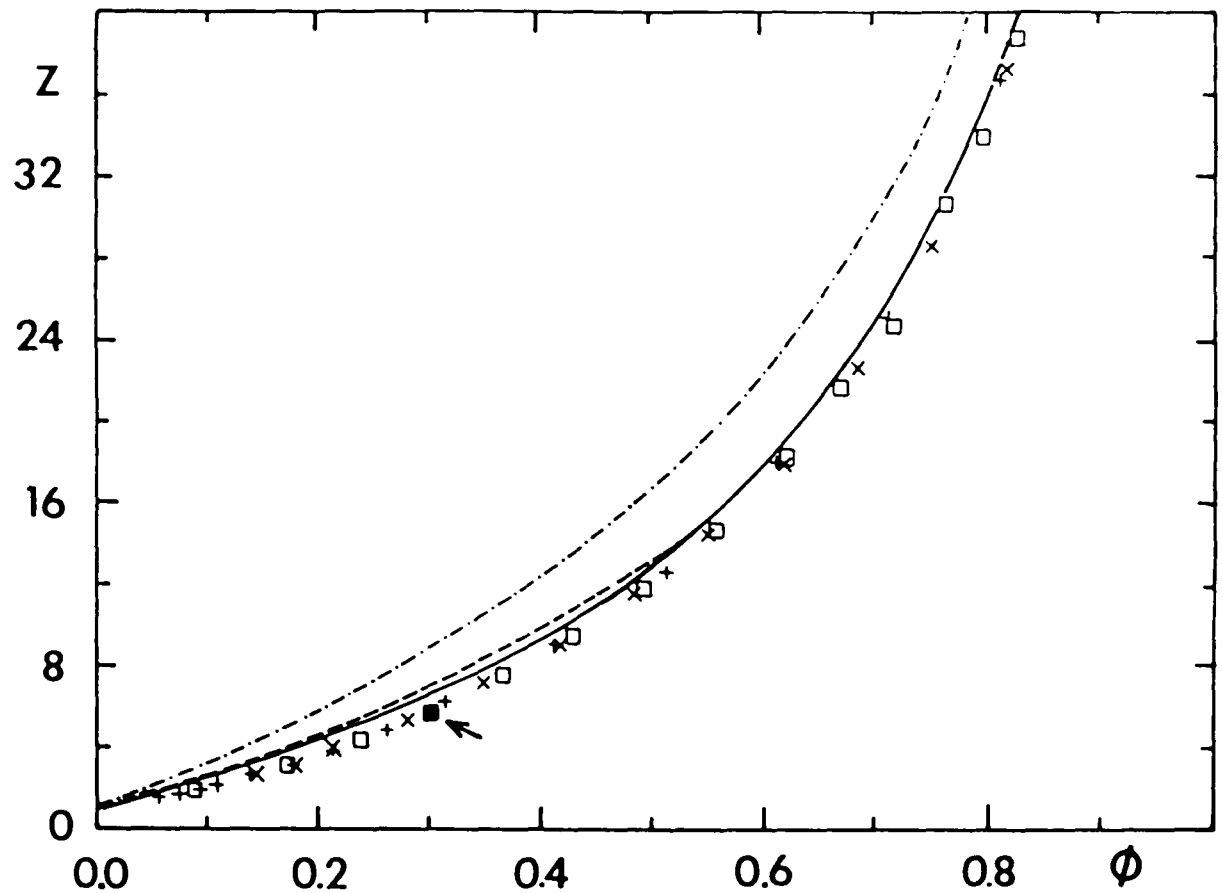

Figure 5.9

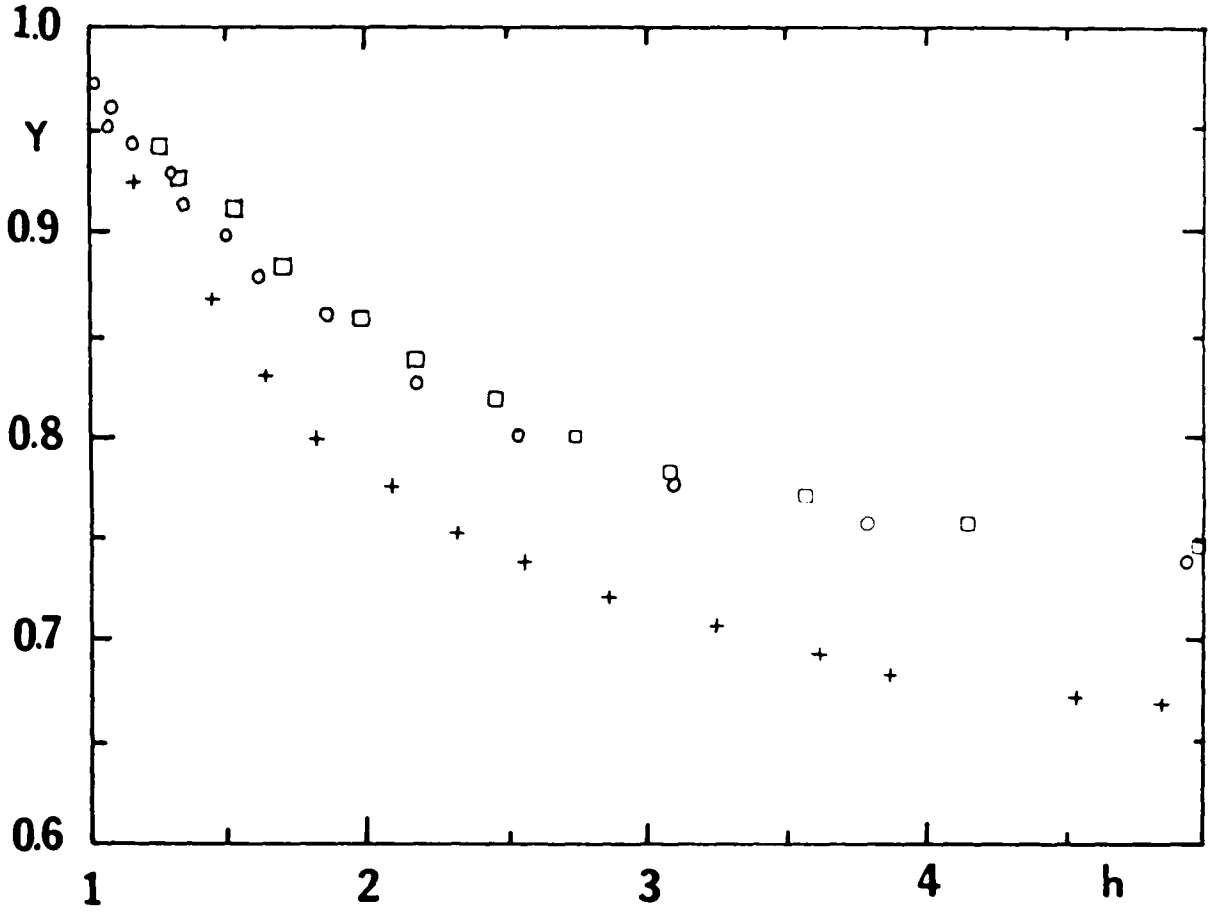

Figure 5.10

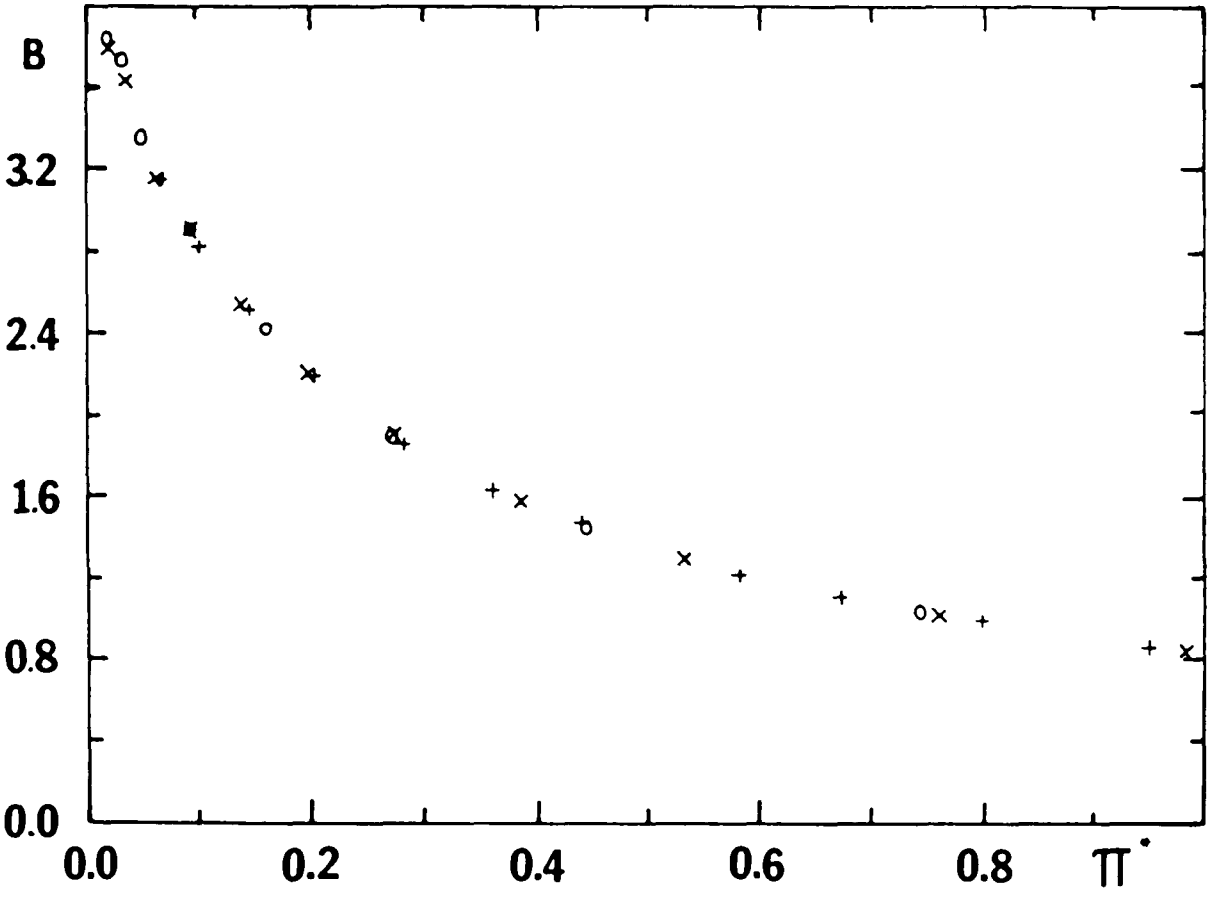

Figure 5.11

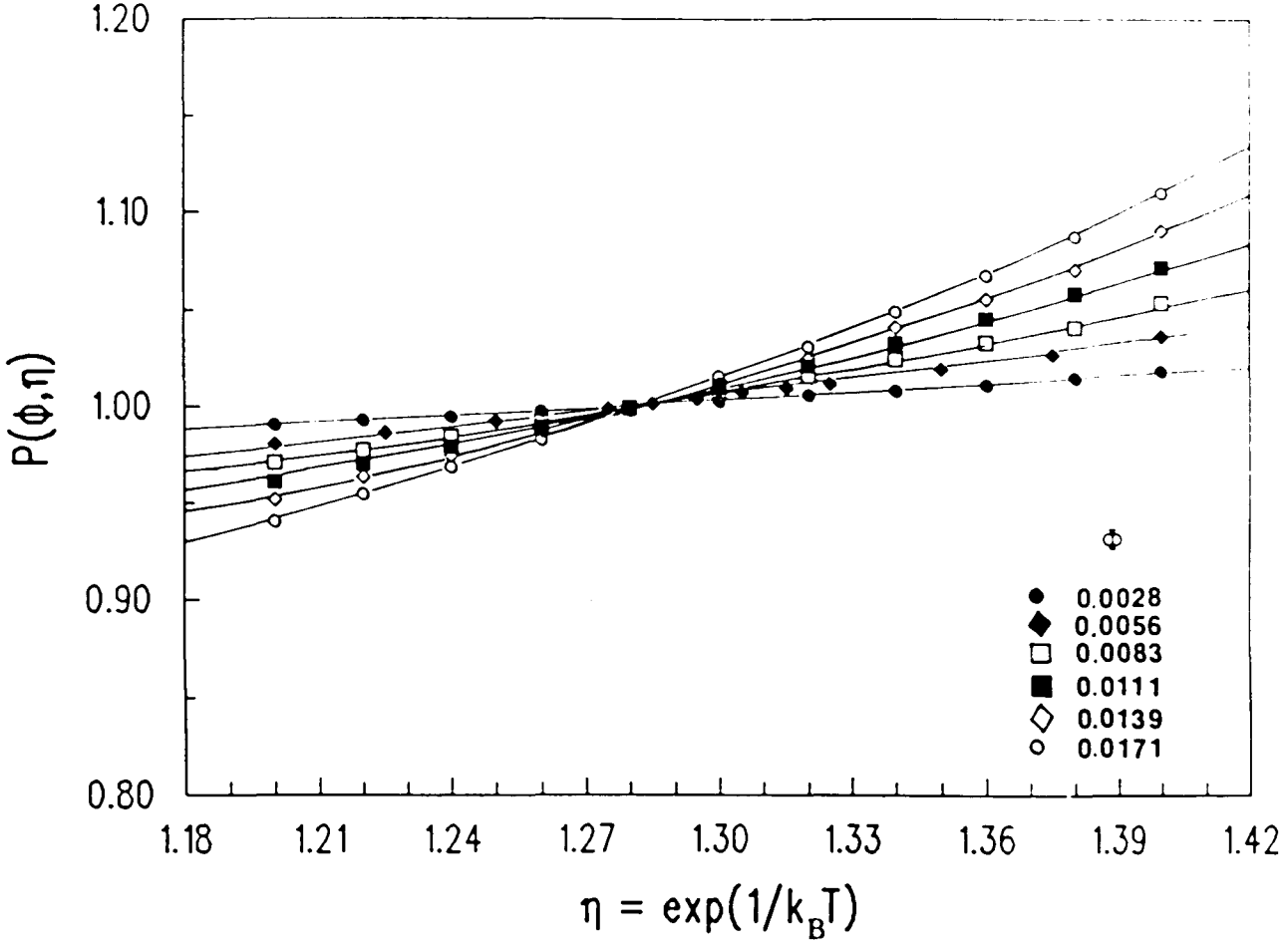
1.20
1.10
1.00
0.90
0.80
P(ϕ,η)
1.18
1.21
1.24
1.27
1.30
1.33
1.36
1.39
1.42
η = exp(1/k_BT)
Φ
0.0028
0.0056
0.0083
0.0111
0.0139
0.0171

FIGURE 5.12a

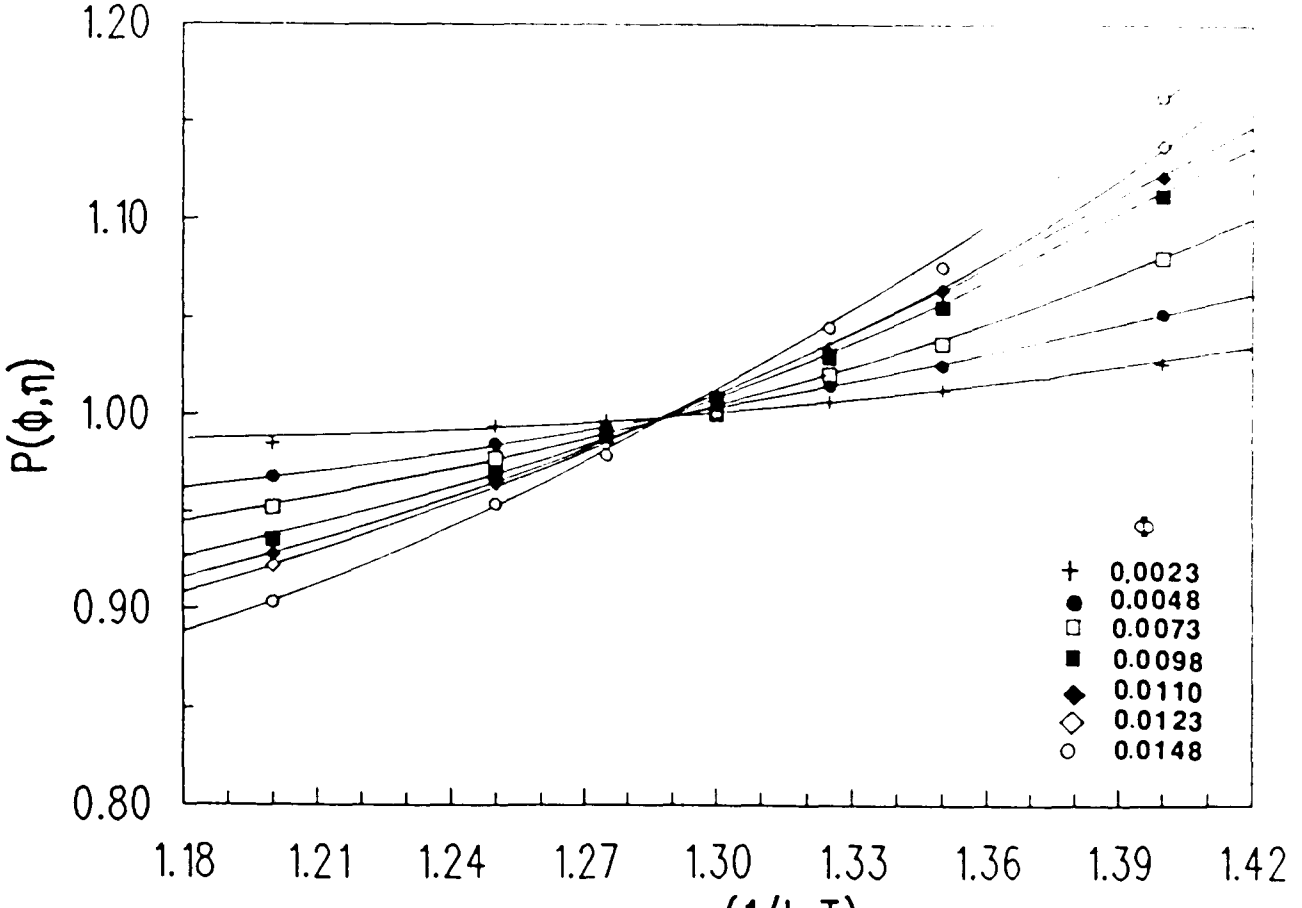
1.20
1.10
1.00
0.90
0.80
P(φ,η)
1.18
1.21
1.24
1.27
1.30
1.33
1.36
1.39
1.42
η = exp(1/k_BT)
φ
0.0023
0.0048
0.0073
0.0098
0.0110
0.0123
0.0148

Figure 5.12b

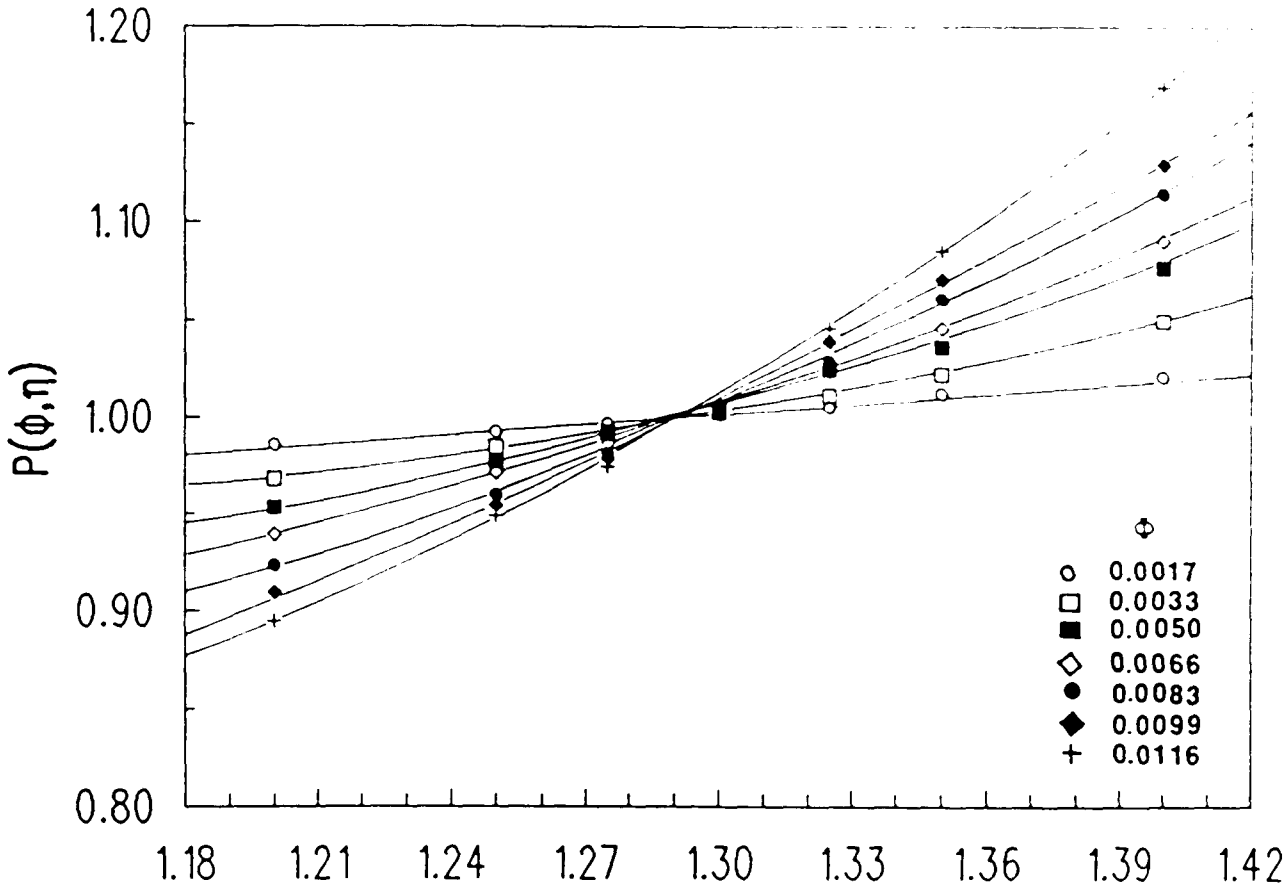
1.20
1.10
1.00
0.90
0.80
P(ϕ,η)
1.18
1.21
1.24
1.27
1.30
1.33
1.36
1.39
1.42
η = exp(1/k_BT)
0.0017
0.0033
0.0050
0.0066
0.0083
0.0099
0.0116

Figure 5.12c

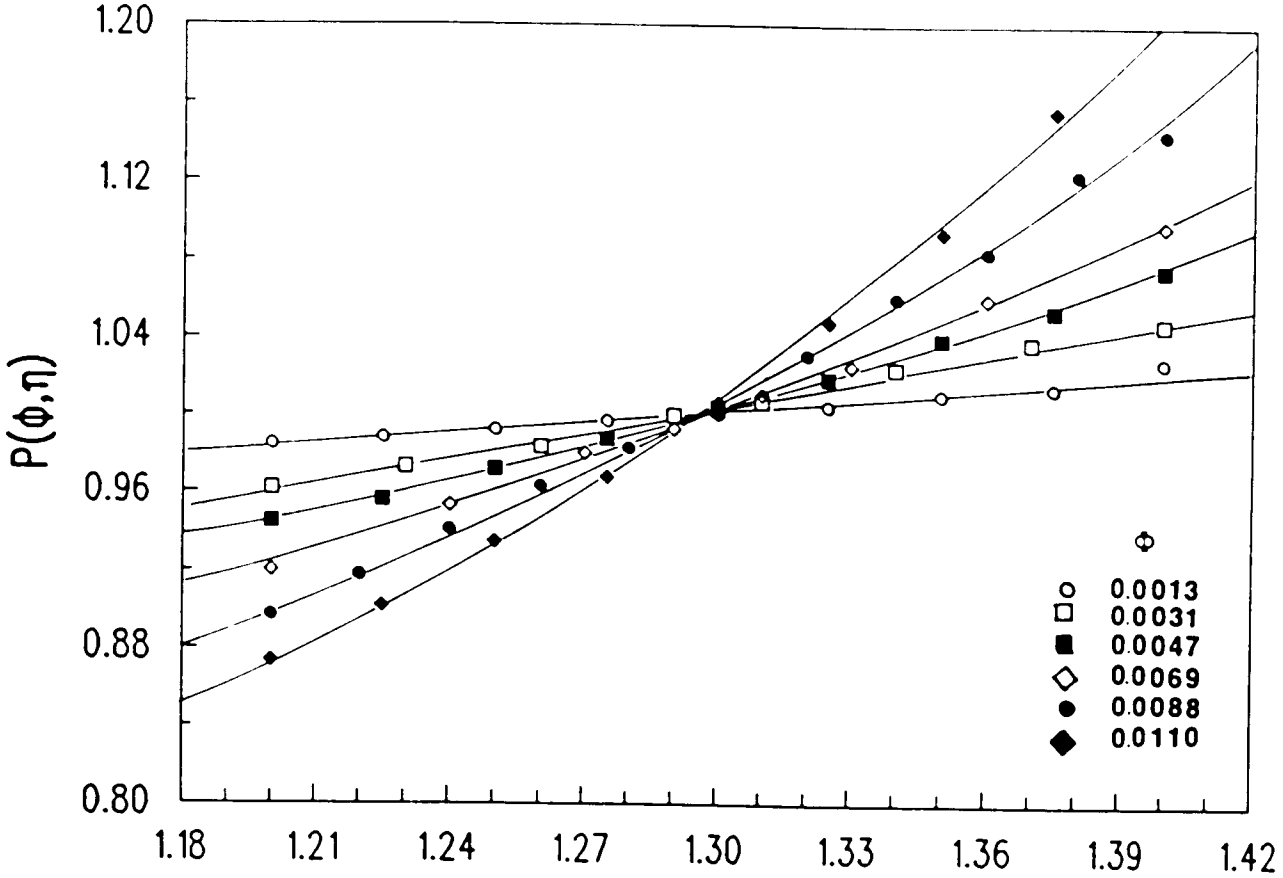
1.20
1.12
1.04
0.96
0.88
0.80
P(Φ,η)
1.18
1.21
1.24
1.27
1.30
1.33
1.36
1.39
1.42
η = exp(1/k_BT)
Φ
0.0013
0.0031
0.0047
0.0069
0.0088
0.0110

Figure 5.12d

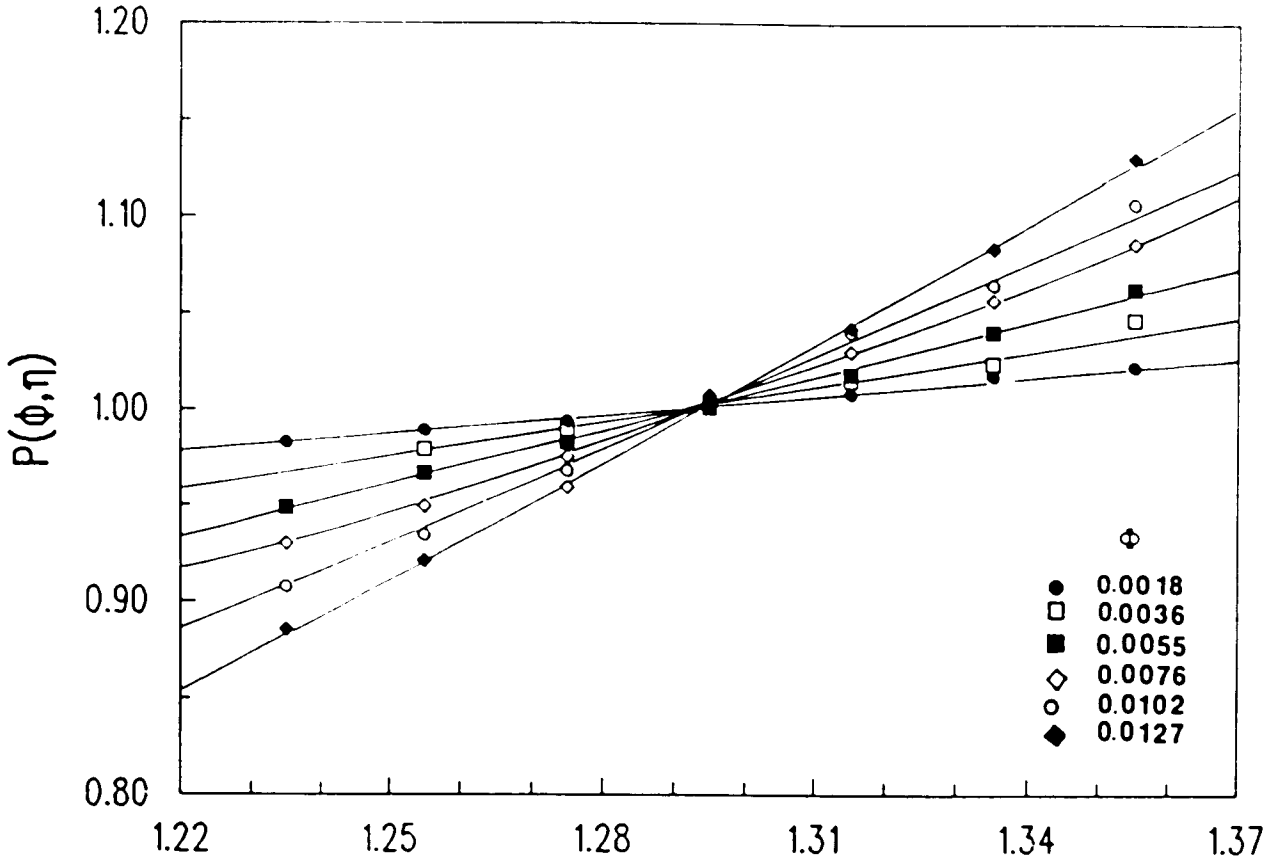
1.20
1.10
1.00
0.90
0.80
P(ϕ,η)
1.22
1.25
1.28
1.31
1.34
1.37
η = exp(1/k_BT)
ϕ
0.0018
0.0036
0.0055
0.0076
0.0102
0.0127

Figure 5.12e

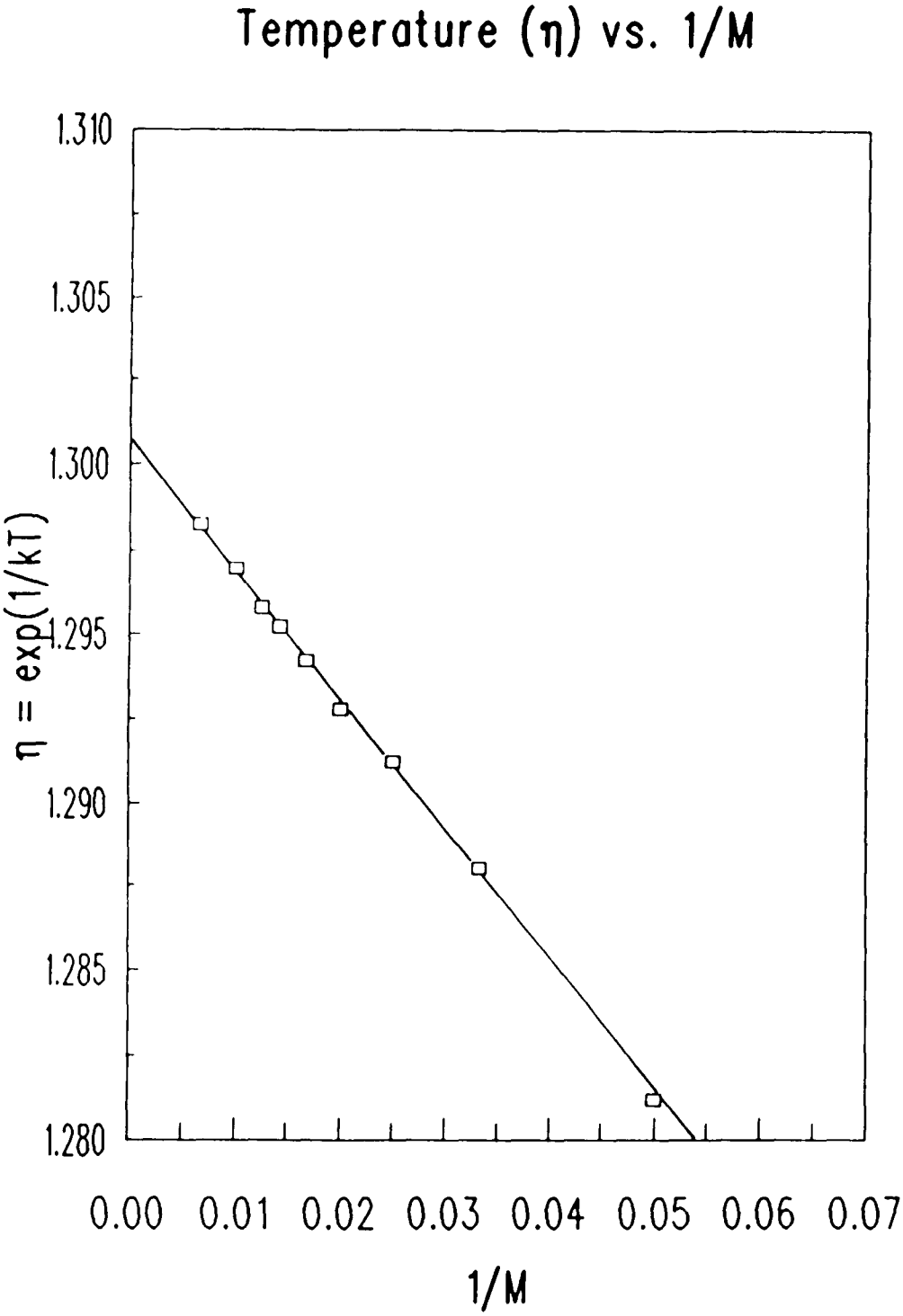
Temperature (η) vs. 1/M
1.310
1.305
1.300
1.295
1.290
1.285
1.280
η = exp(1/kT)
0.00
0.01
0.02
0.03
0.04
0.05
0.06
0.07
1/M

Figure 5.13

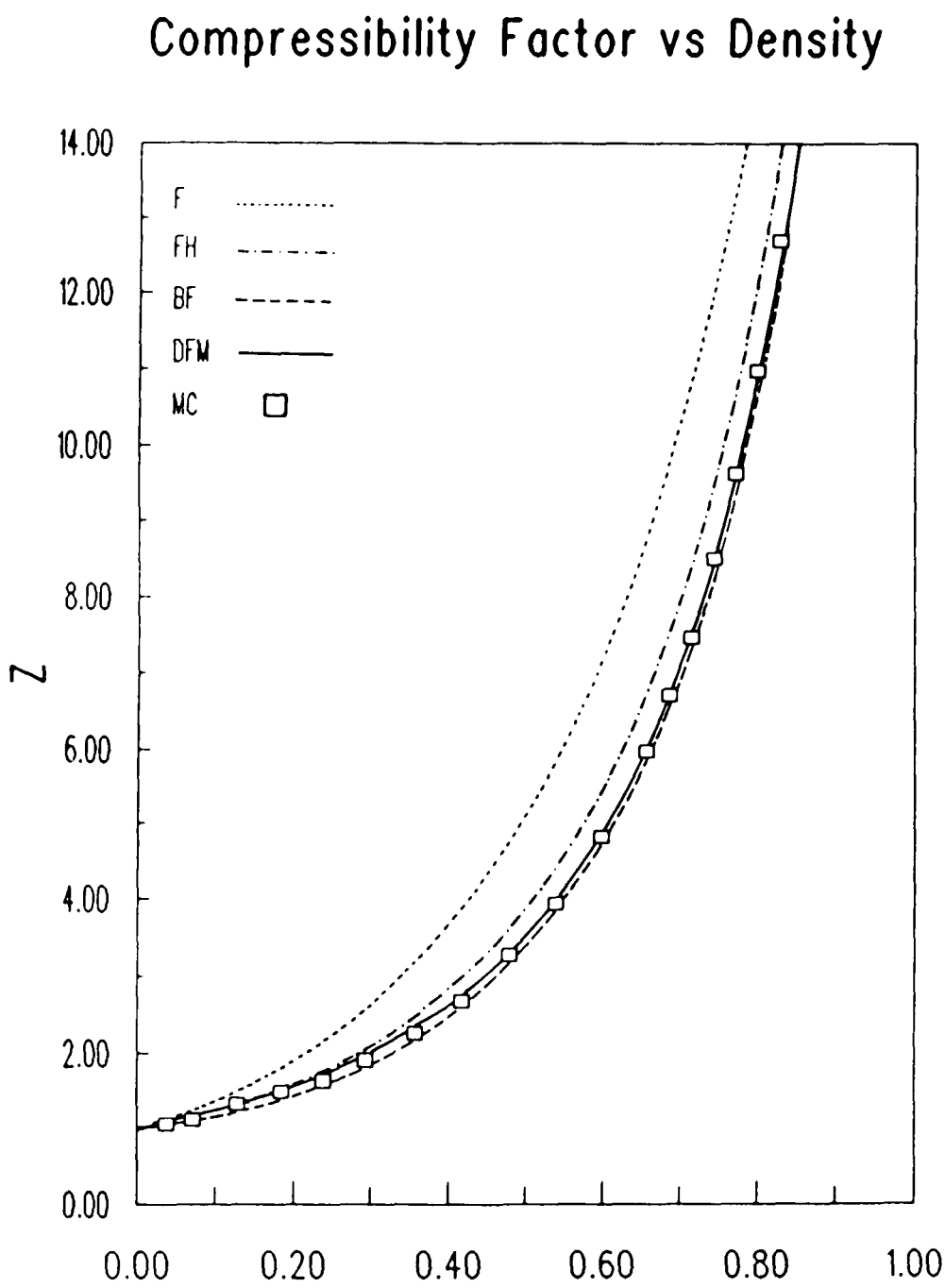
Compressibility Factor vs Density
14.00
12.00
10.00
8.00
6.00
4.00
2.00
0.00
Z
F
FH
BF
DFM
MC
0.00
0.20
0.40
0.60
0.80
1.00
Density (ϕ)

Figure 5.14a

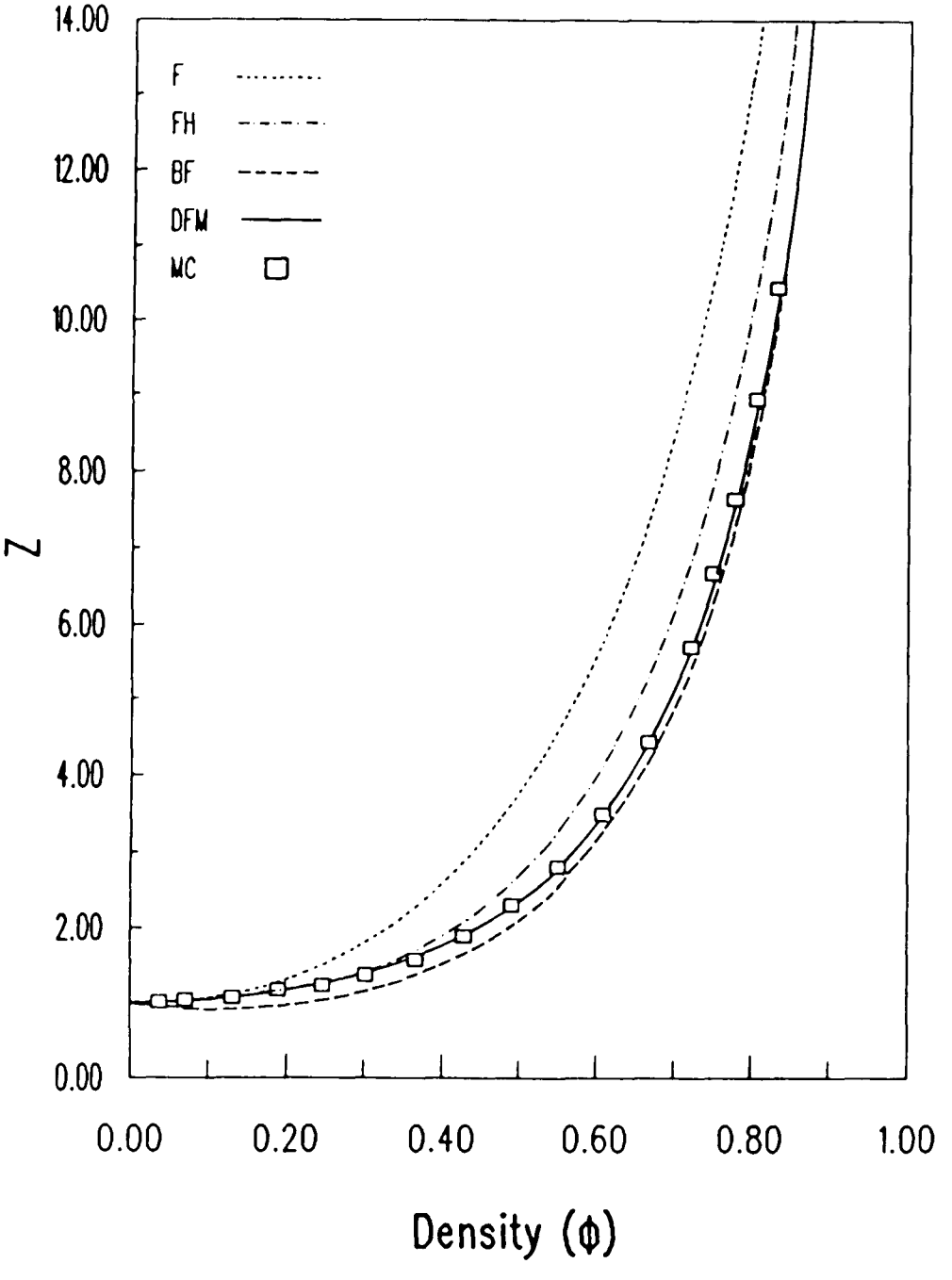
Compressibility Factor vs. Density
F
FH
BF
DFM
MC
Z
14.00
12.00
10.00
8.00
6.00
4.00
2.00
0.00
0.00
0.20
0.40
0.60
0.80
1.00
Density (ϕ)

Figure 5.14b

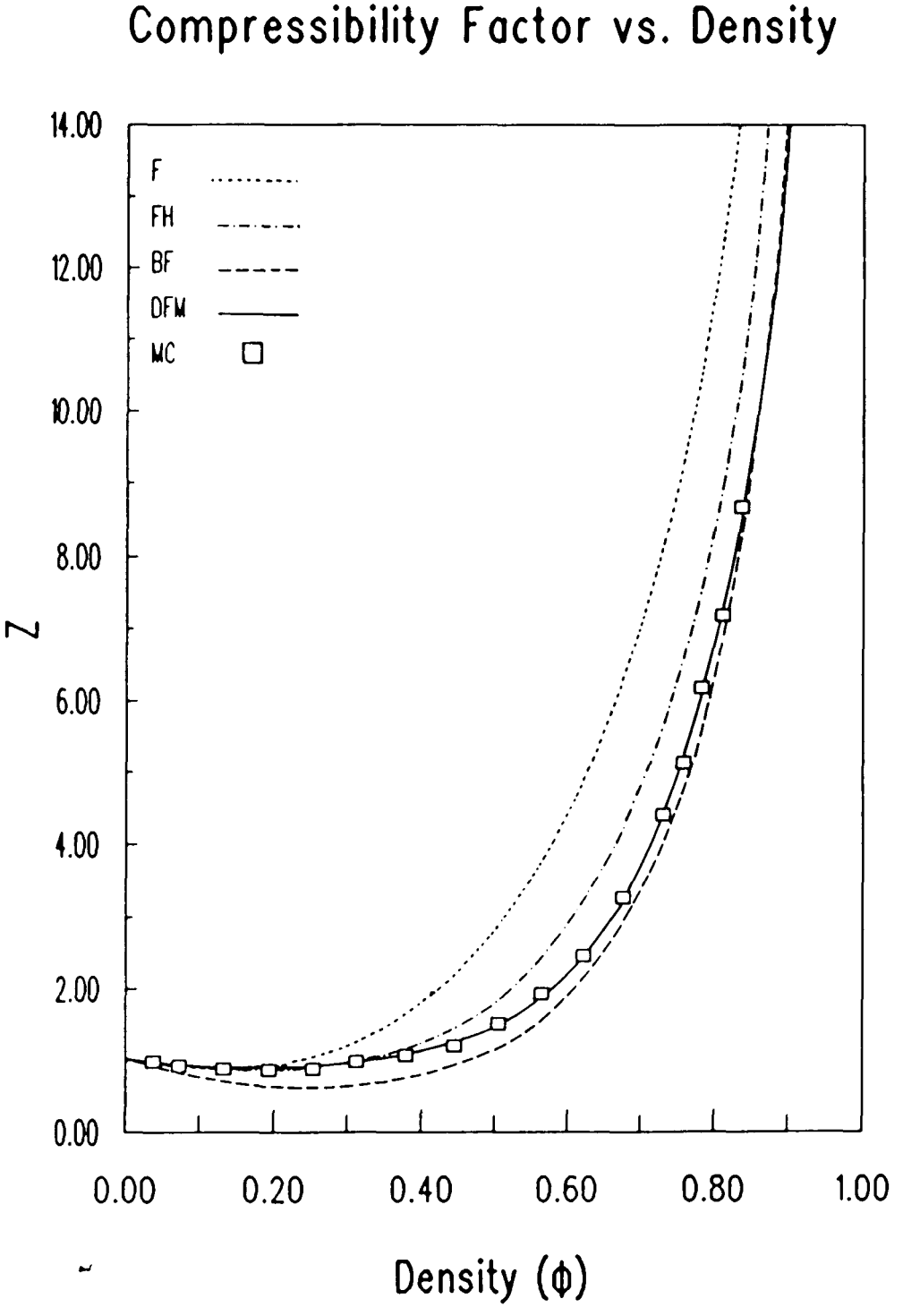
Compressibility Factor vs. Density
14.00
12.00
10.00
8.00
6.00
4.00
2.00
0.00
Z
F
FH
BF
DFM
MC
0.00
0.20
0.40
0.60
0.80
1.00
Density (ϕ)

Figure 5.14c

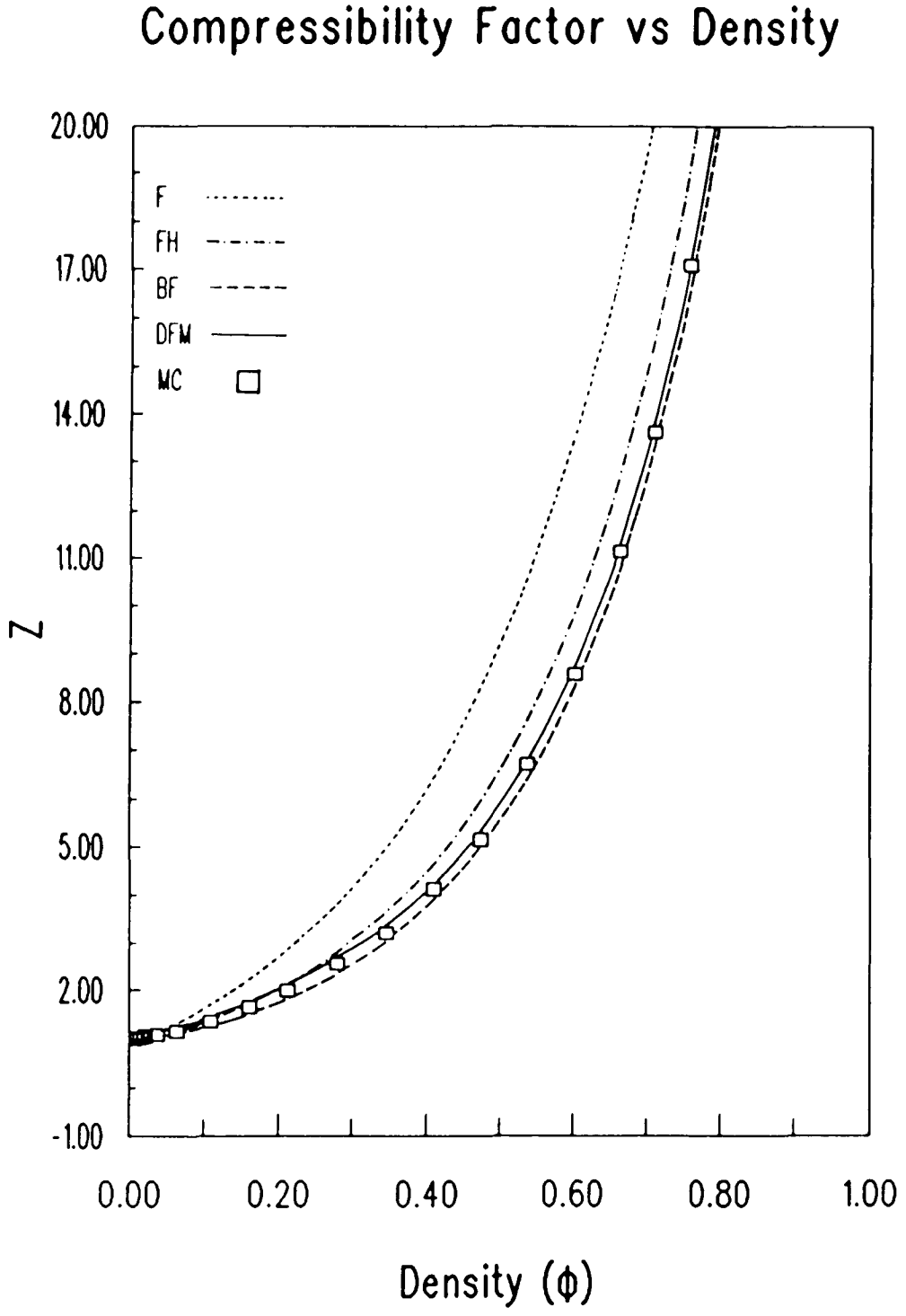
Compressibility Factor vs Density
20.00
17.00
14.00
11.00
8.00
5.00
2.00
-1.00
Z
F
FH
BF
DFM
MC
0.00
0.20
0.40
0.60
0.80
1.00
Density (ϕ)

Figure 5.14d

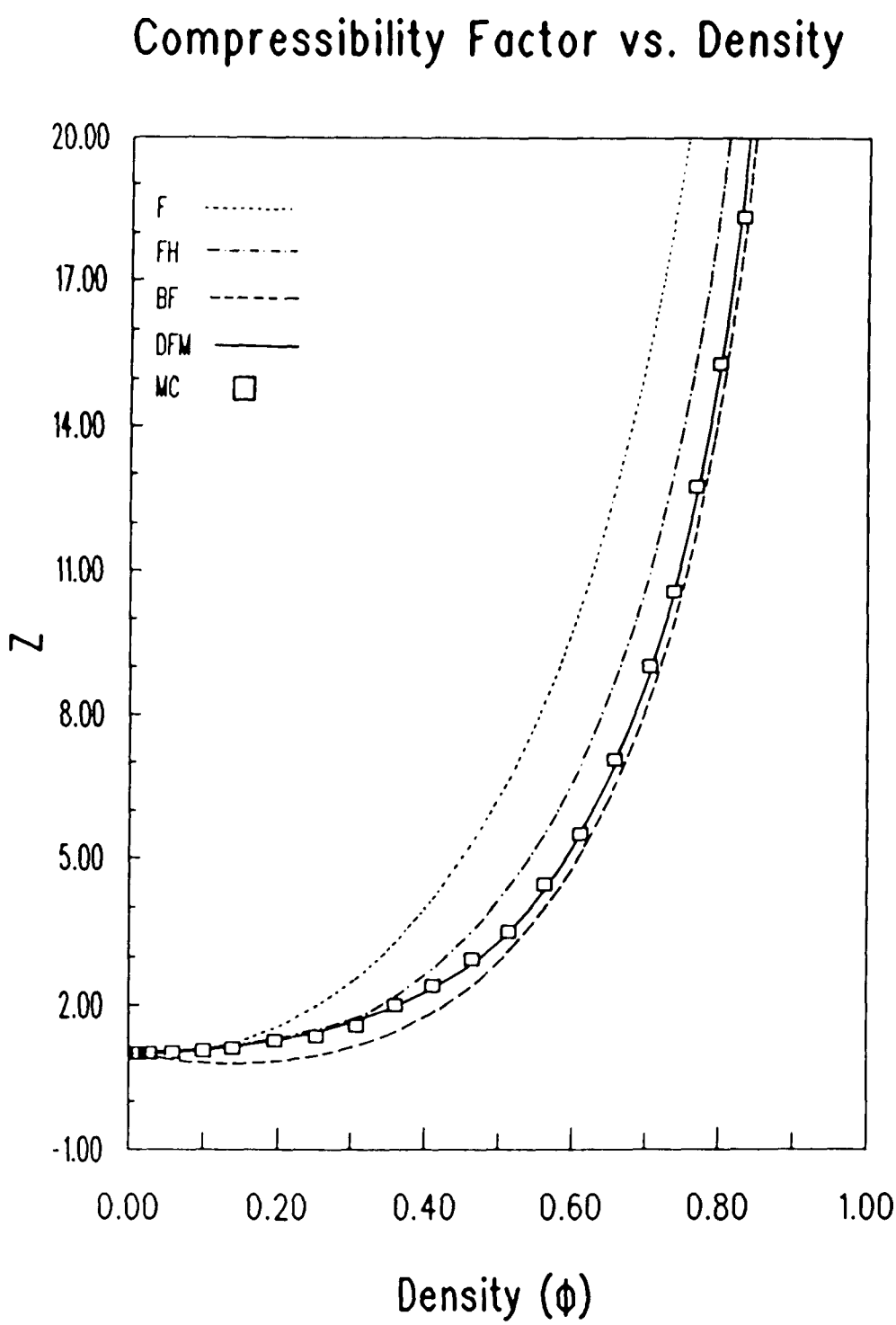
Compressibility Factor vs. Density
20.00
17.00
14.00
11.00
8.00
5.00
2.00
-1.00
Z
F
FH
BF
DFM
MC
0.00
0.20
0.40
0.60
0.80
1.00
Density (ϕ)

Figure 5.14e

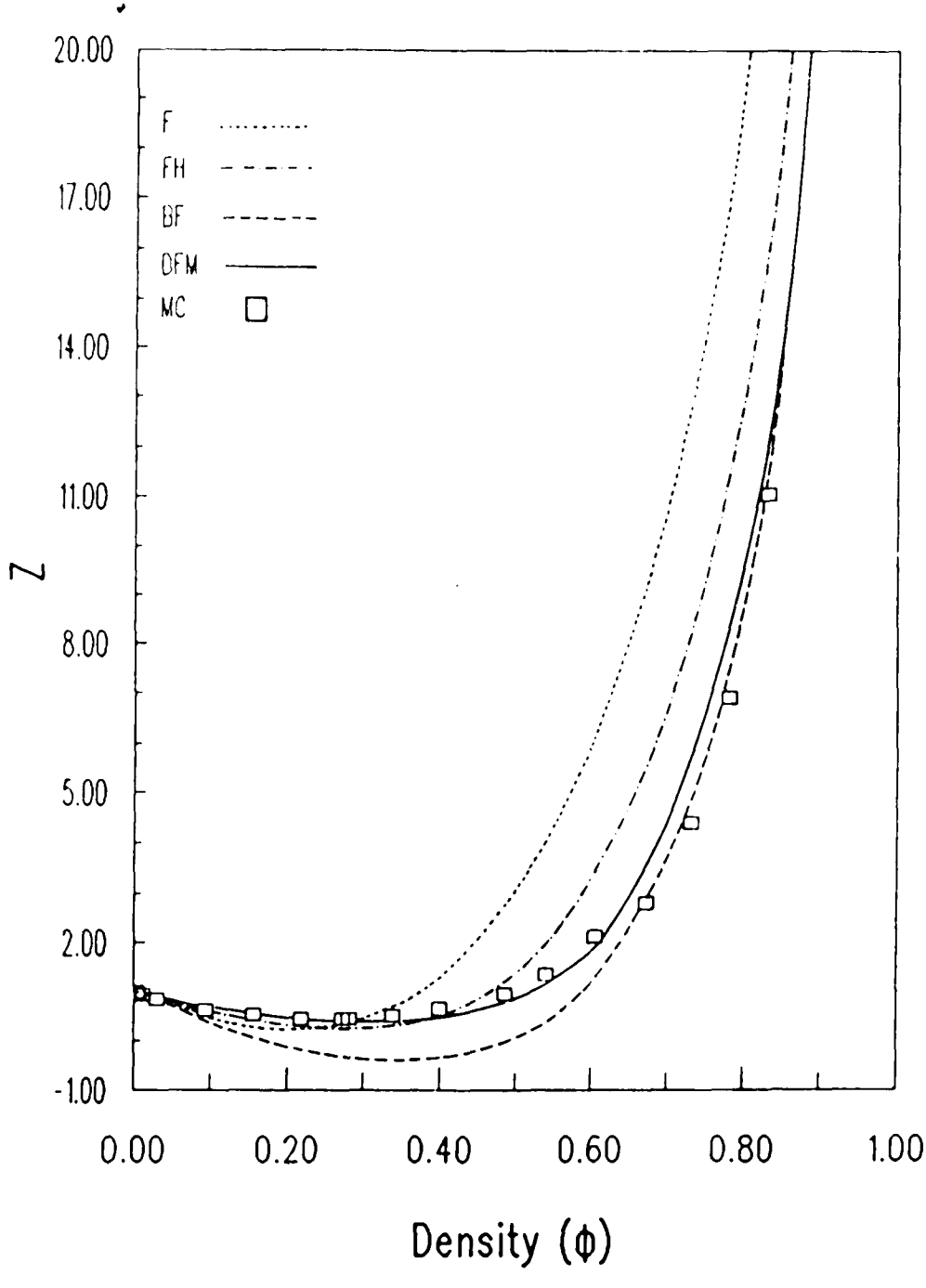
Compressibility Factor vs. Density
20.00
17.00
14.00
11.00
8.00
5.00
2.00
-1.00
Z
F
FH
BF
BFM
MC
0.00
0.20
0.40
0.60
0.80
1.00
Density (ϕ)

Figure 5.14f

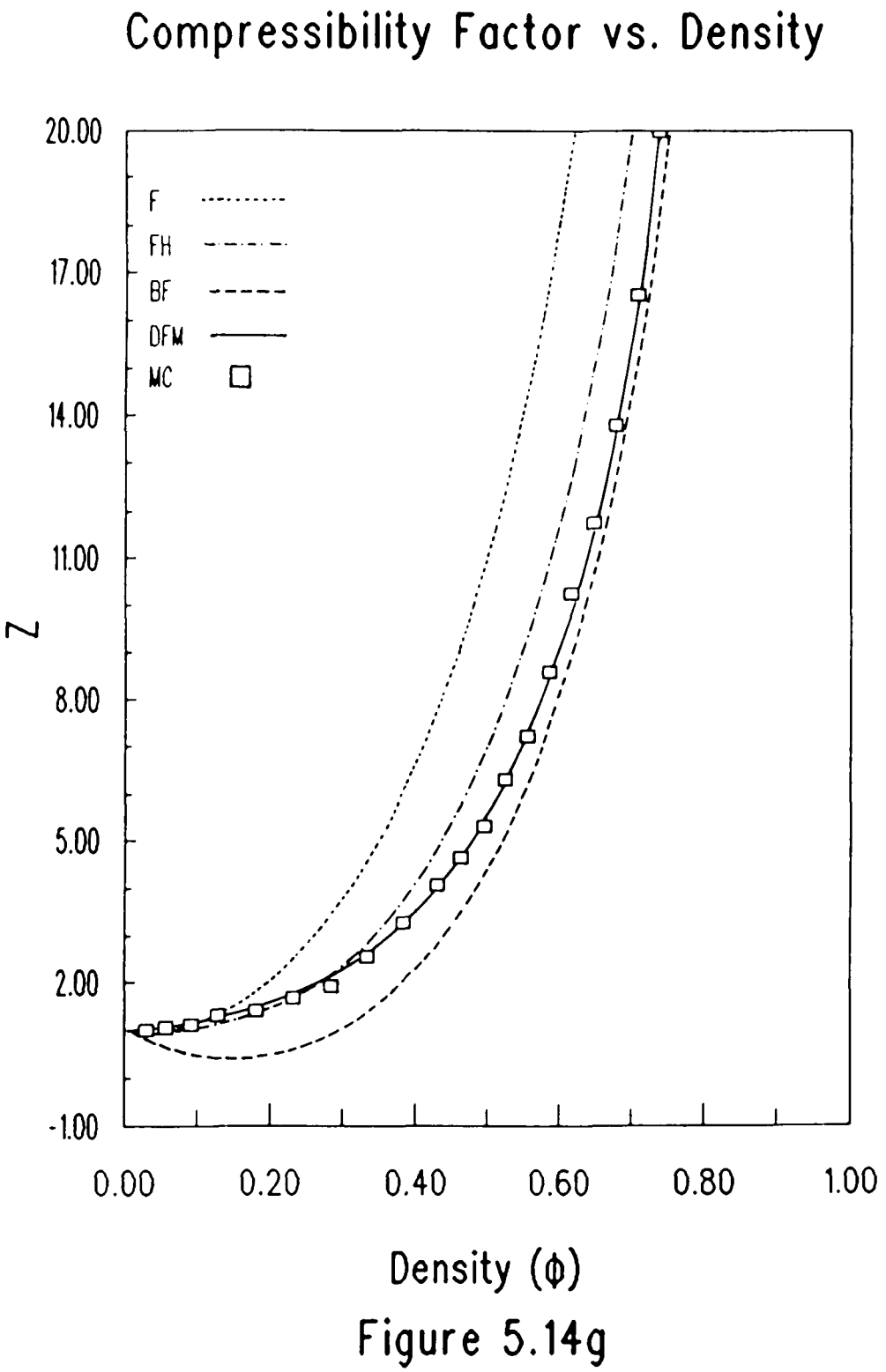
Compressibility Factor vs. Density
20.00
17.00
14.00
11.00
8.00
5.00
2.00
-1.00
Z
F
FH
BF
DFM
MC
0.00
0.20
0.40
0.60
0.80
1.00
Density (ϕ)

Figure 5.14g

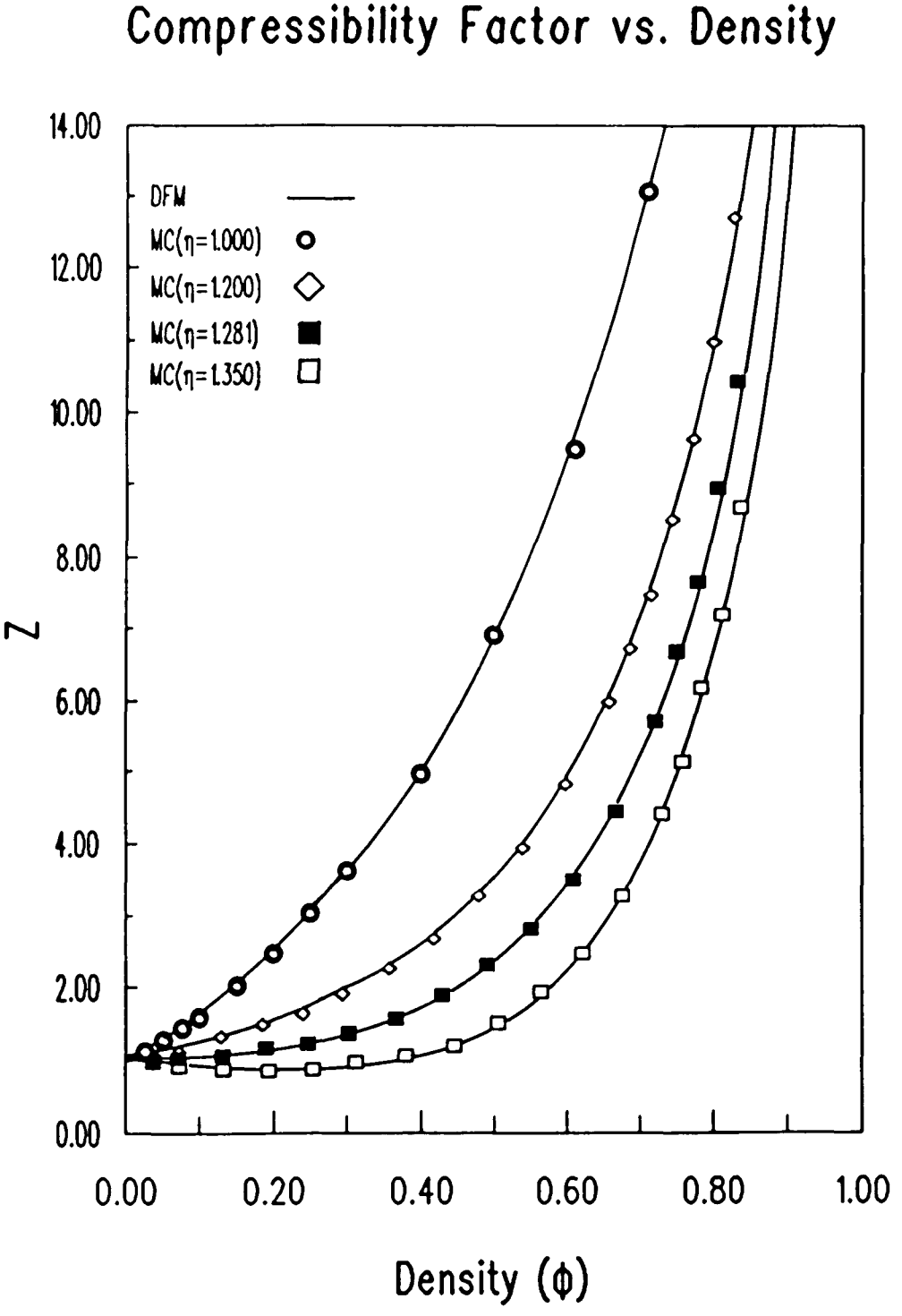
Compressibility Factor vs. Density
DFM
MC(η=1.000)
MC(η=1.200)
MC(η=1.281)
MC(η=1.350)
Z
14.00
12.00
10.00
8.00
6.00
4.00
2.00
0.00
0.00
0.20
0.40
0.60
0.80
1.00
Density (ϕ)

Figure 5.15a

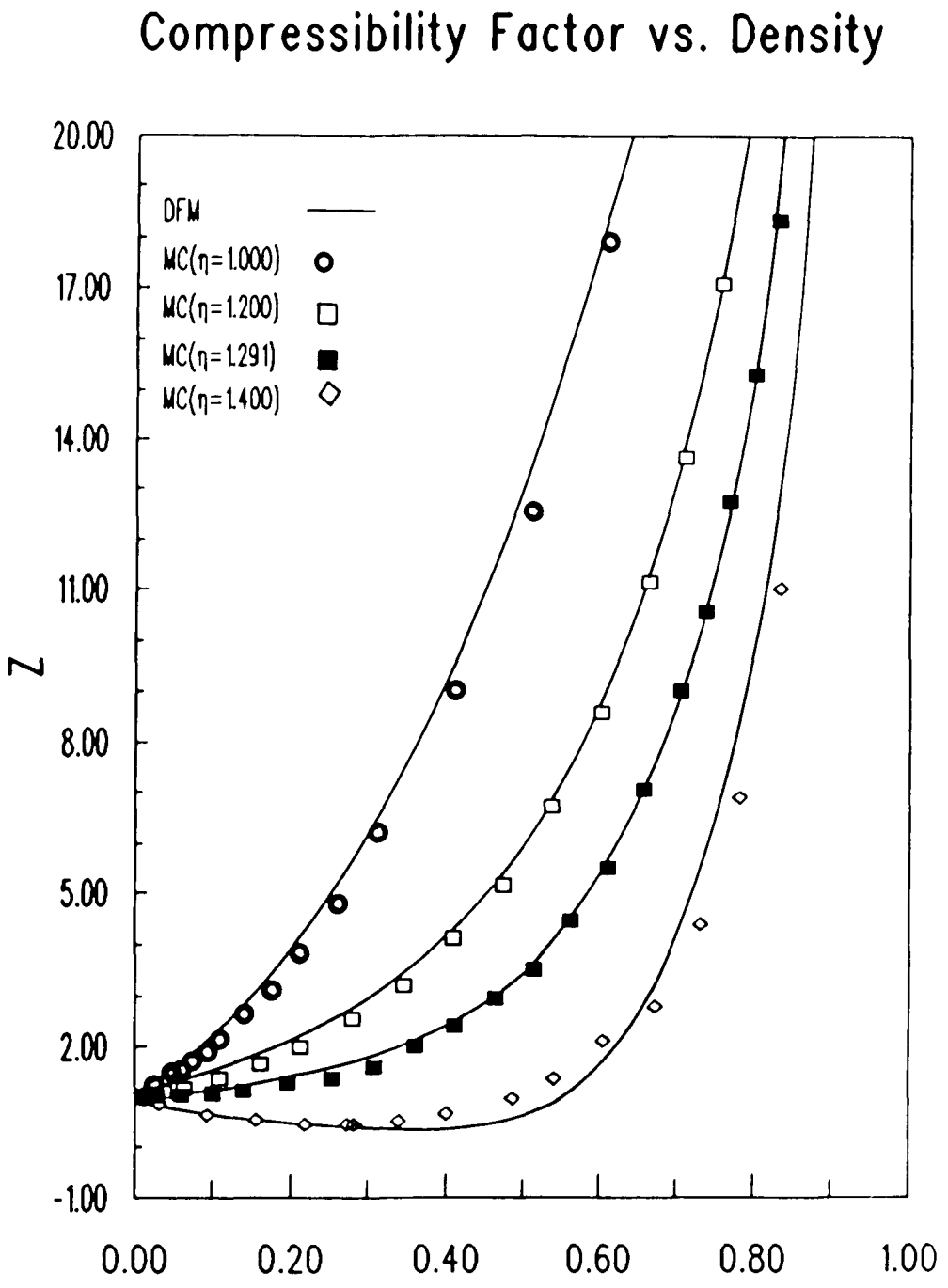
Compressibility Factor vs. Density
DFM
MC(η=1.000)
MC(η=1.200)
MC(η=1.291)
MC(η=1.400)
Z
20.00
17.00
14.00
11.00
8.00
5.00
2.00
-1.00
0.00
0.20
0.40
0.60
0.80
1.00
Density (ϕ)

Figure 5.15b

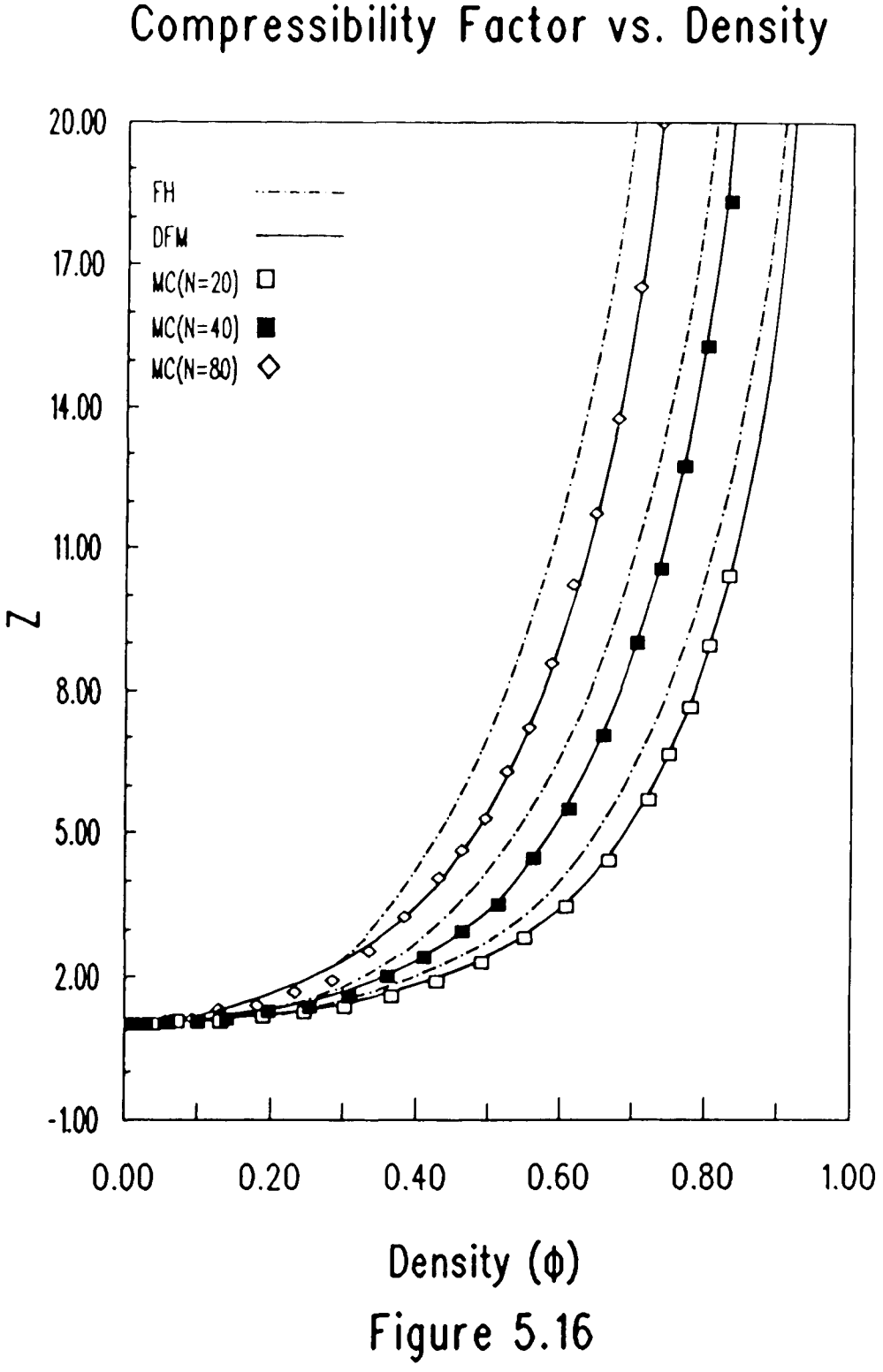
Compressibility Factor vs. Density
20.00
17.00
14.00
11.00
8.00
5.00
2.00
-1.00
Z
FH
DFM
MC(N=20)
MC(N=40)
MC(N=80)
0.00
0.20
0.40
0.60
0.80
1.00
Density (ϕ)

Figure 5.16

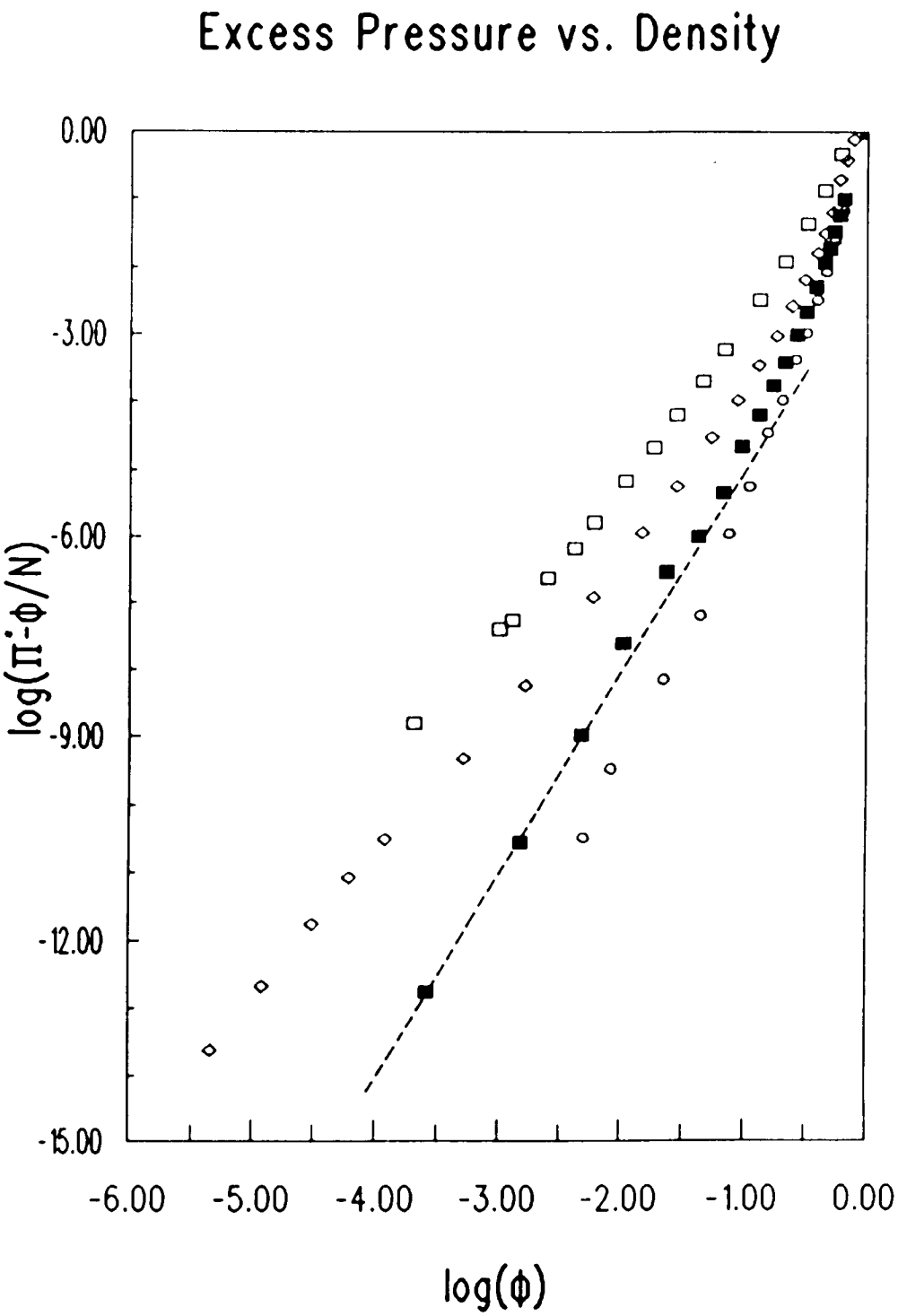
Excess Pressure vs. Density
0.00
-3.00
-6.00
-9.00
-12.00
-15.00
log(Π*-ϕ/N)
-6.00
-5.00
-4.00
-3.00
-2.00
-1.00
0.00
log(ϕ)

Figure 5.17a

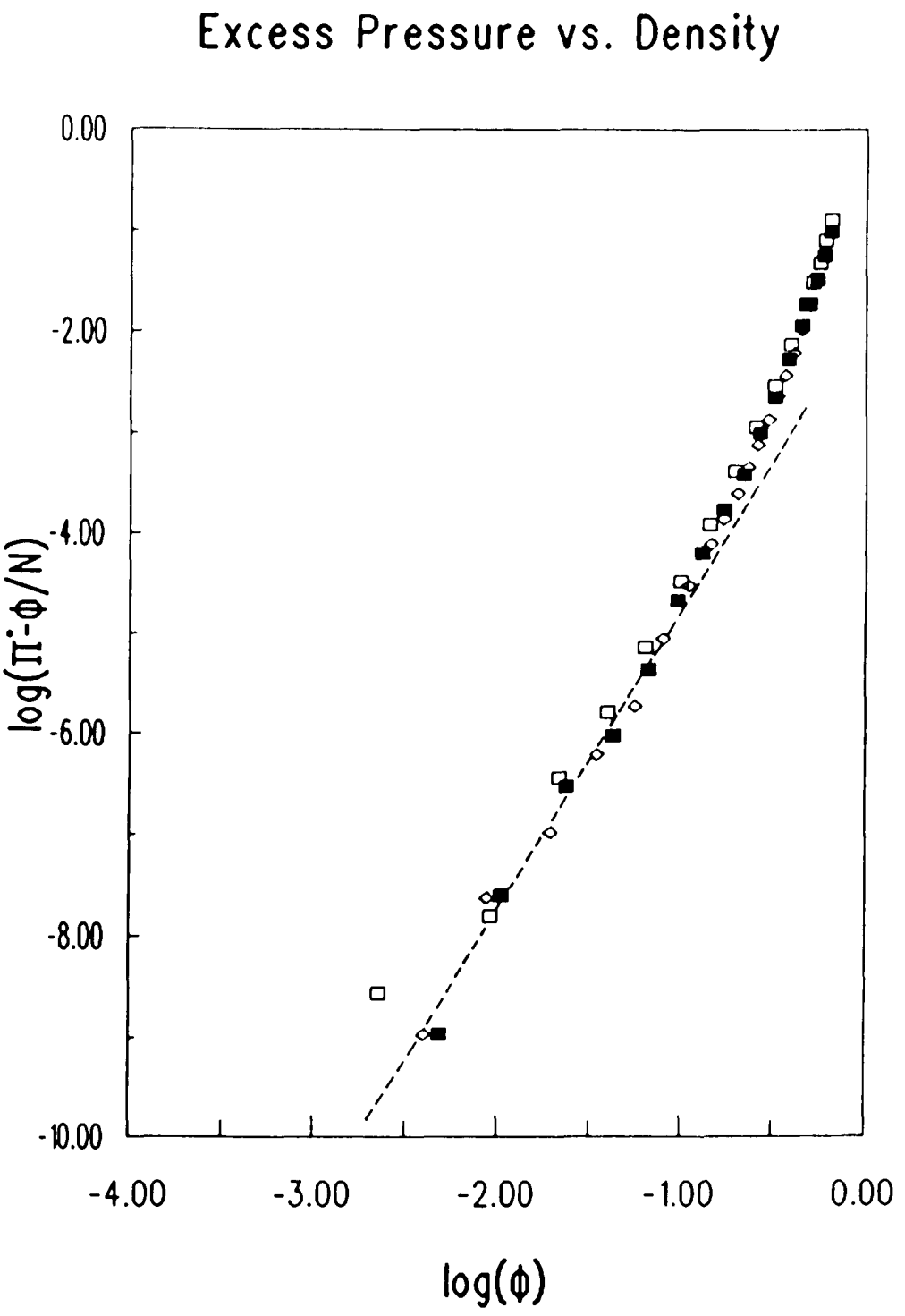
Excess Pressure vs. Density
0.00
-2.00
-4.00
-6.00
-8.00
-10.00
log(Π*-Φ/N)
-4.00
-3.00
-2.00
-1.00
0.00
log(Φ)

Figure 5.17b

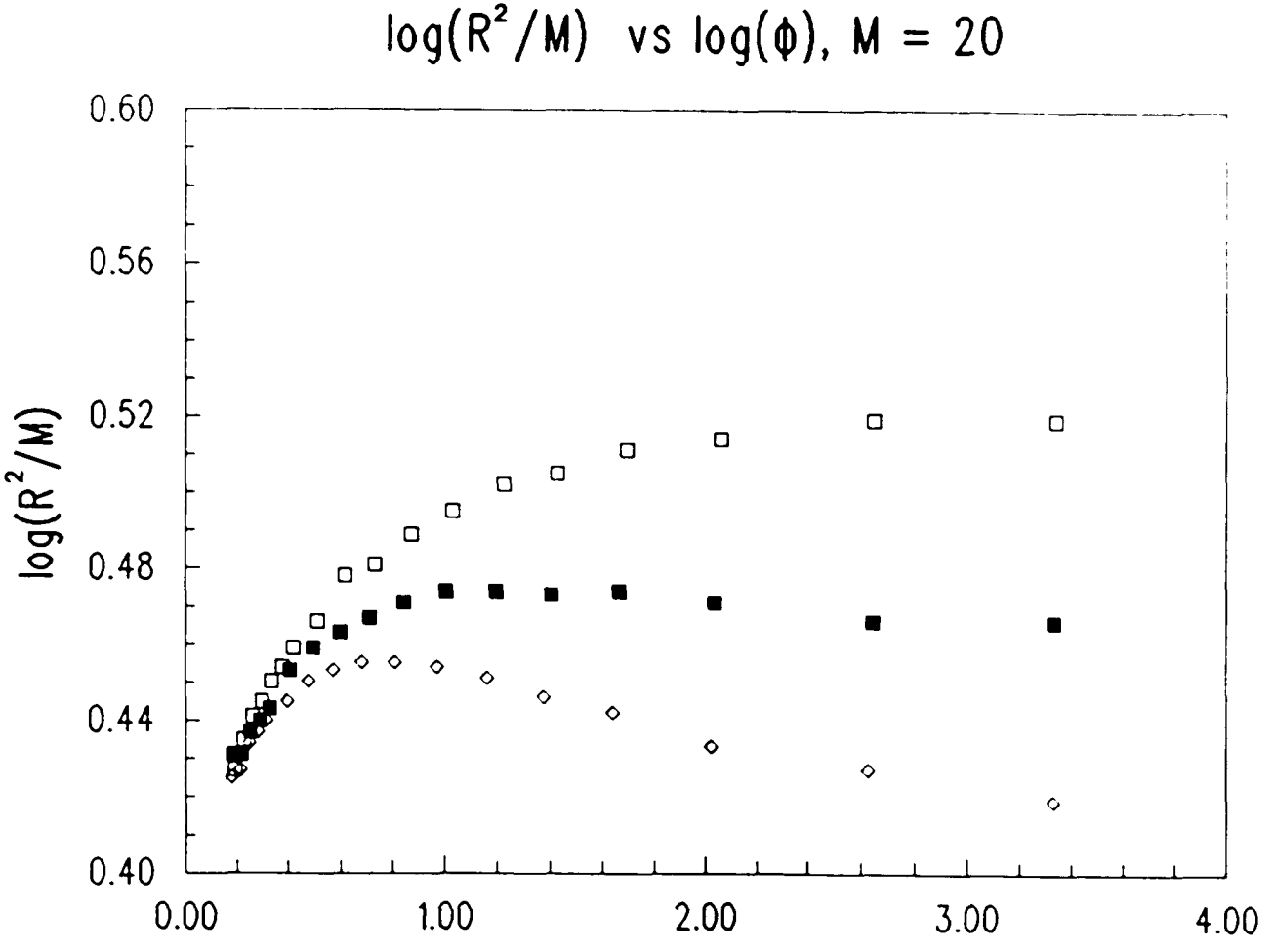
log(R²/M) vs log(ϕ), M = 20
0.60
0.56
0.52
0.48
0.44
0.40
log(R²/M)
0.00
1.00
2.00
3.00
4.00
-log(ϕ)
Figure 5.18a

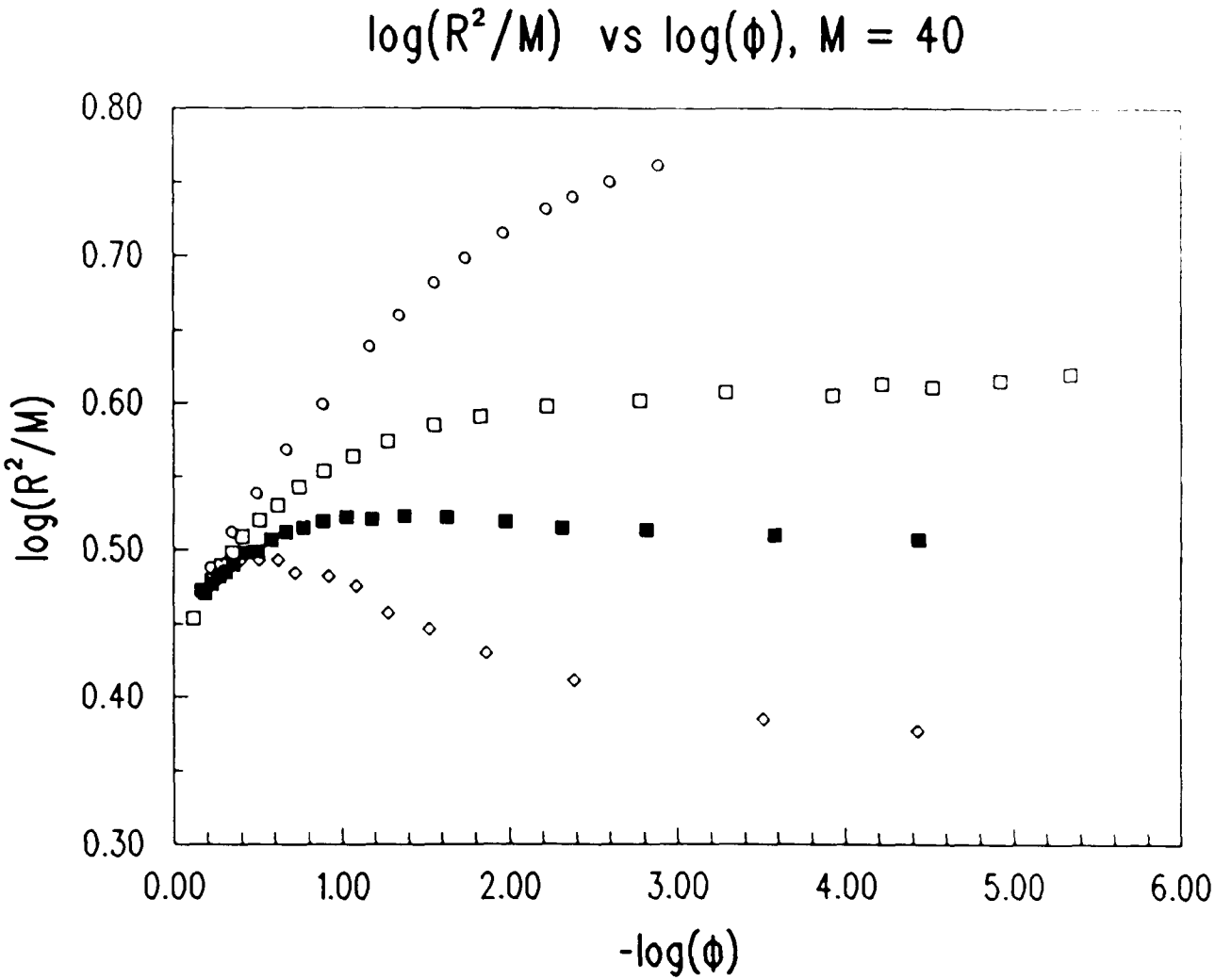
log(R²/M) vs log(ϕ), M = 40
0.80
0.70
0.60
0.50
0.40
0.30
log(R²/M)
0.00
1.00
2.00
3.00
4.00
5.00
6.00
-log(ϕ)

Figure 5.18b

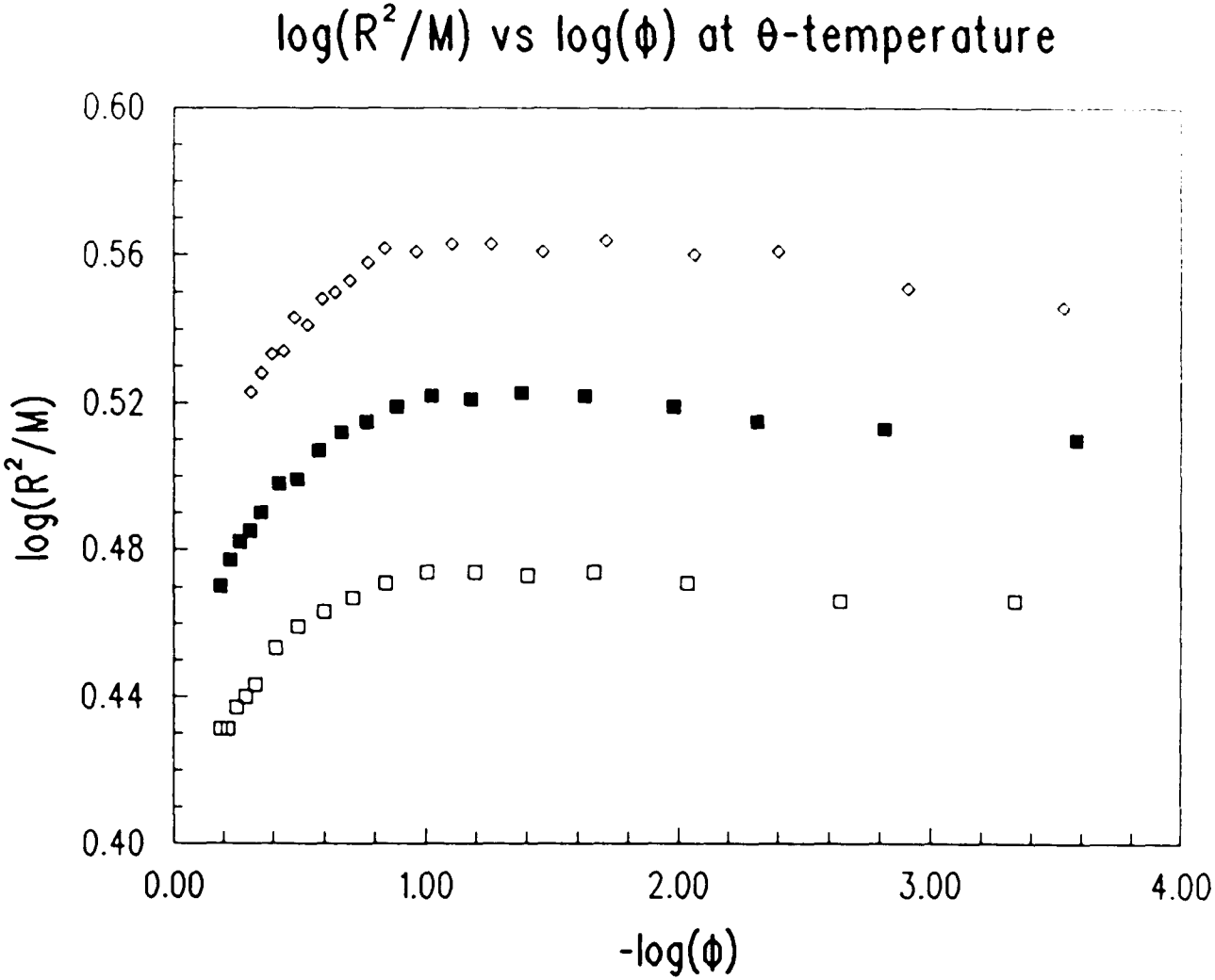
log(R²/M) vs log(ϕ) at θ-temperature
0.60
0.56
0.52
0.48
0.44
0.40
log(R²/M)
0.00
1.00
2.00
3.00
4.00
-log(ϕ)

Figure 5.18c

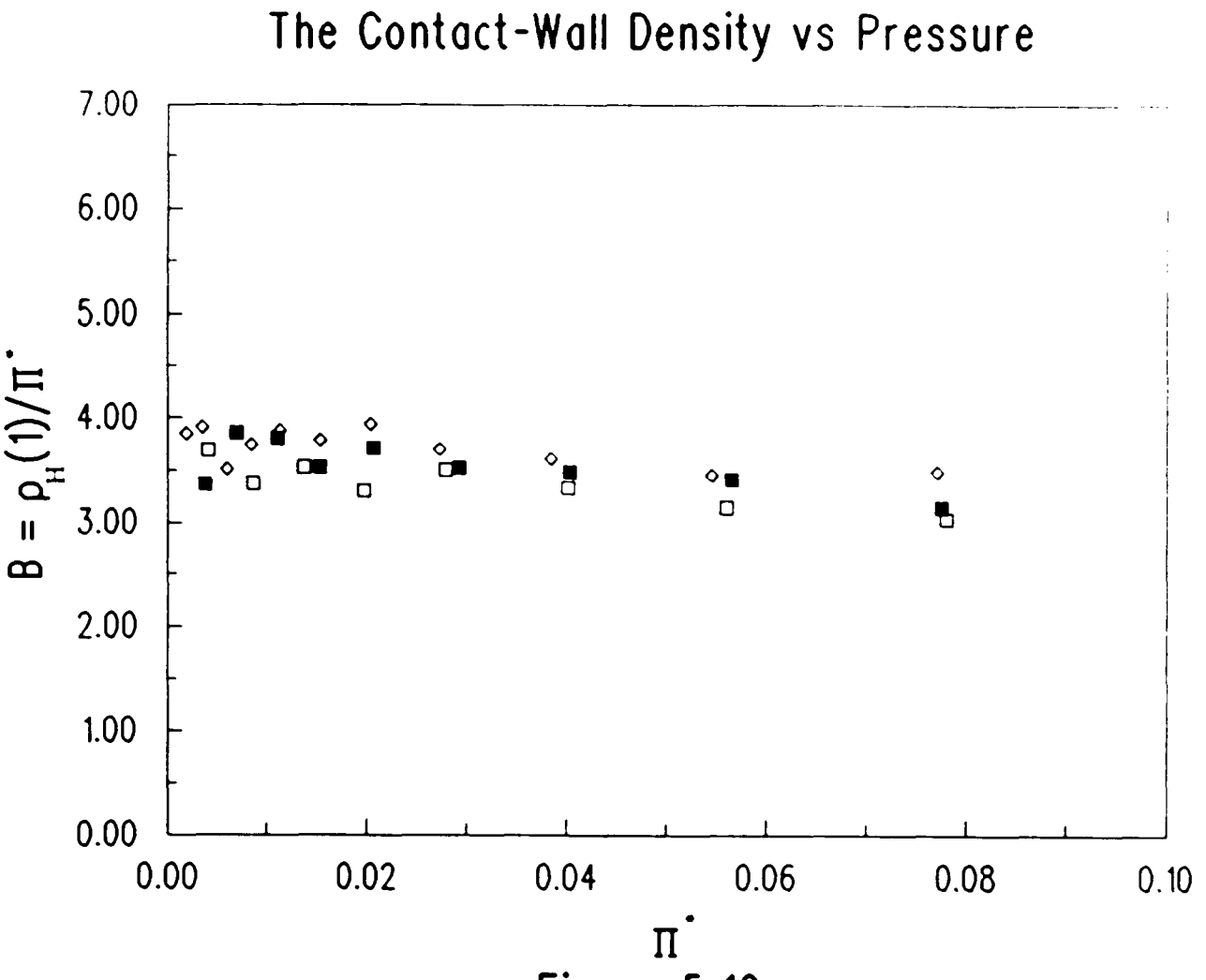
The Contact-Wall Density vs Pressure
7.00
6.00
5.00
4.00
3.00
2.00
1.00
0.00
B = ρH(1)/Π*
0.00
0.02
0.04
0.06
0.08
0.10
Π*

Figure 5.19a

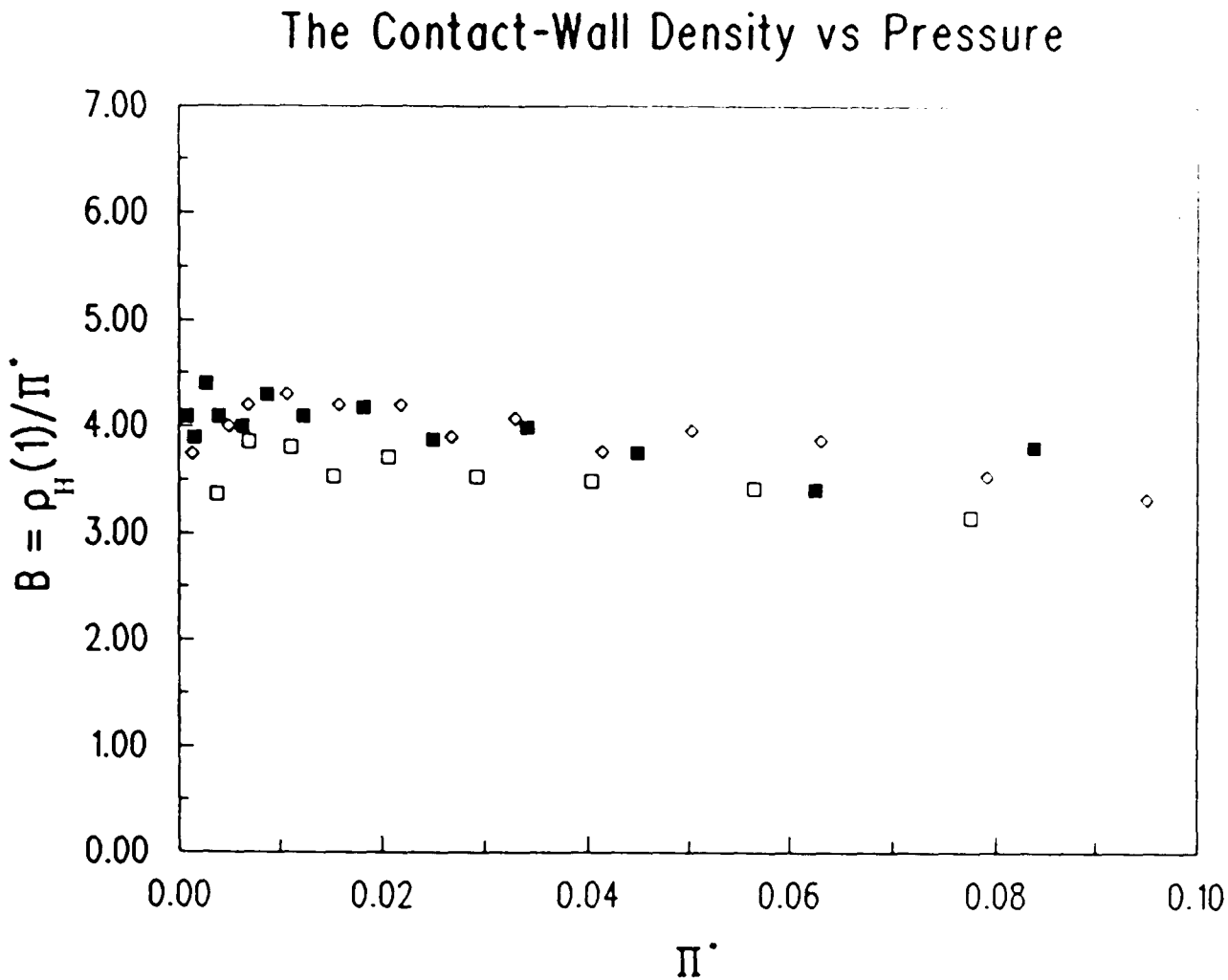
The Contact-Wall Density vs Pressure
7.00
6.00
5.00
4.00
3.00
2.00
1.00
0.00
B = ρH(1)/Π*
0.00
0.02
0.04
0.06
0.08
0.10
Π*

Figure 5.19b

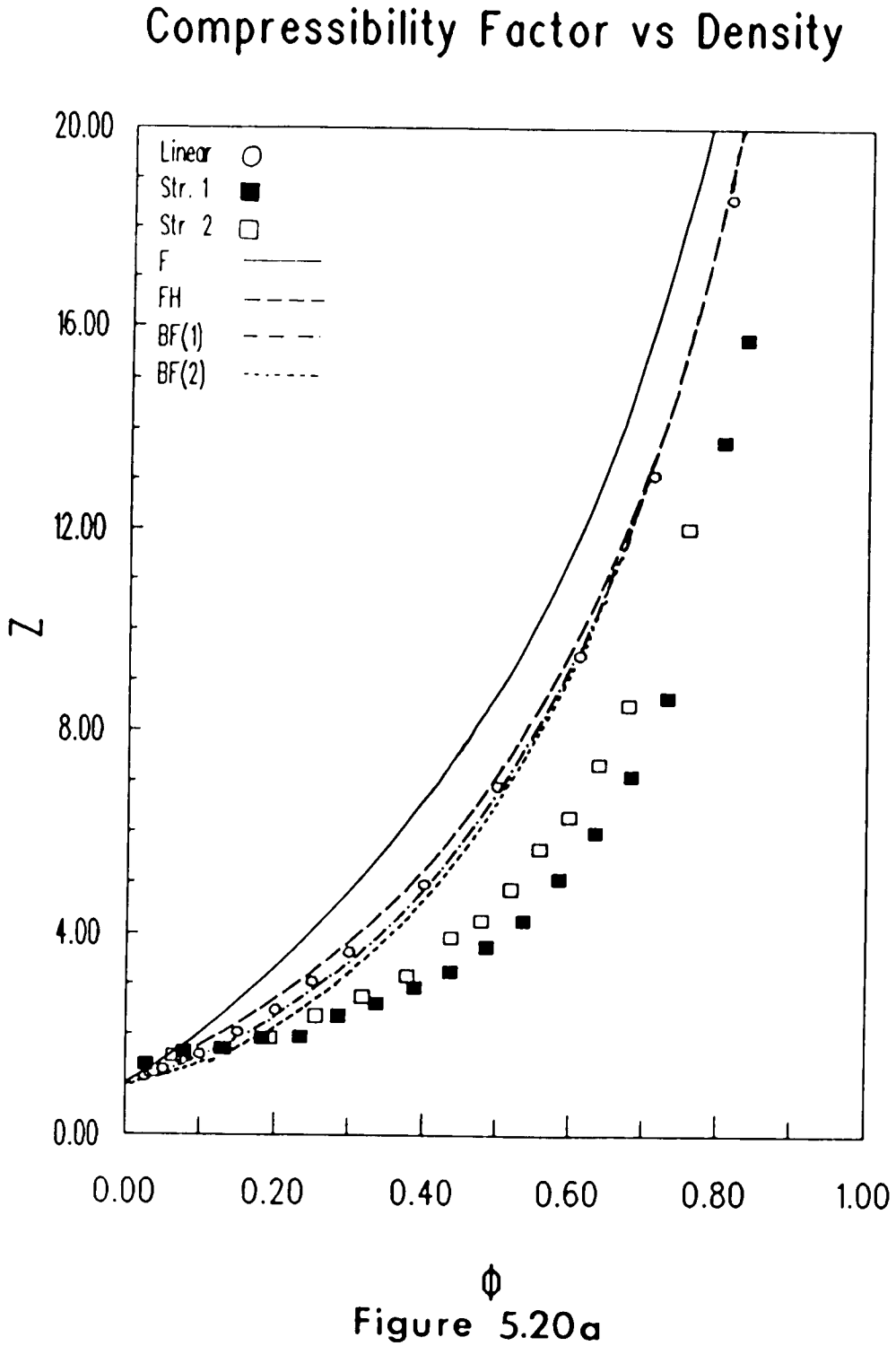
Compressibility Factor vs Density
Linear
Str. 1
Str 2
F
FH
BF(1)
BF(2)
Z
20.00
16.00
12.00
8.00
4.00
0.00
0.00
0.20
0.40
0.60
0.80
1.00
Φ

Figure 5.20a

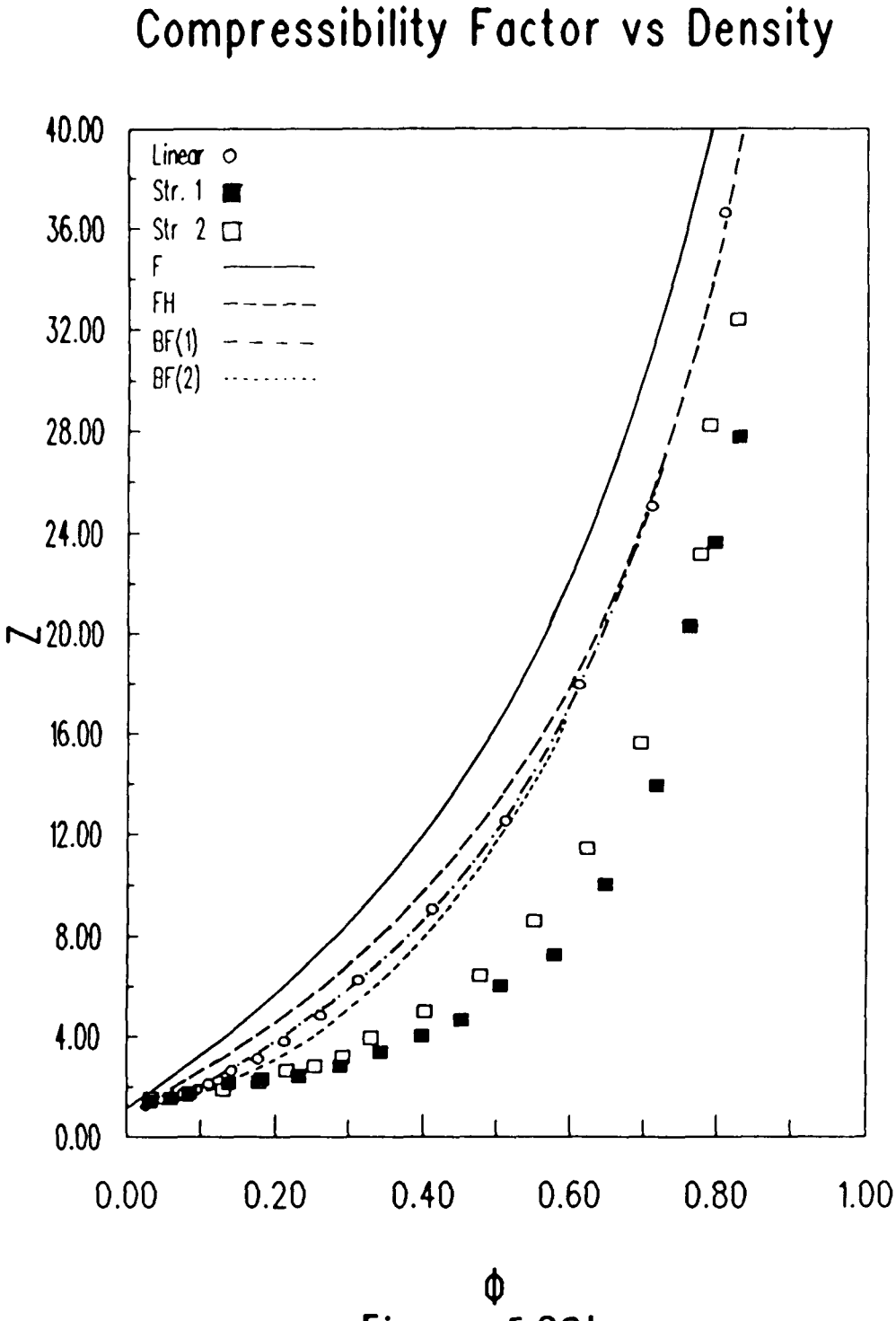
Compressibility Factor vs Density
Linear
Str. 1
Str 2
F
FH
BF(1)
BF(2)
Z
40.00
36.00
32.00
28.00
24.00
20.00
16.00
12.00
8.00
4.00
0.00
0.00
0.20
0.40
0.60
0.80
1.00
Φ

Figure 5.20b

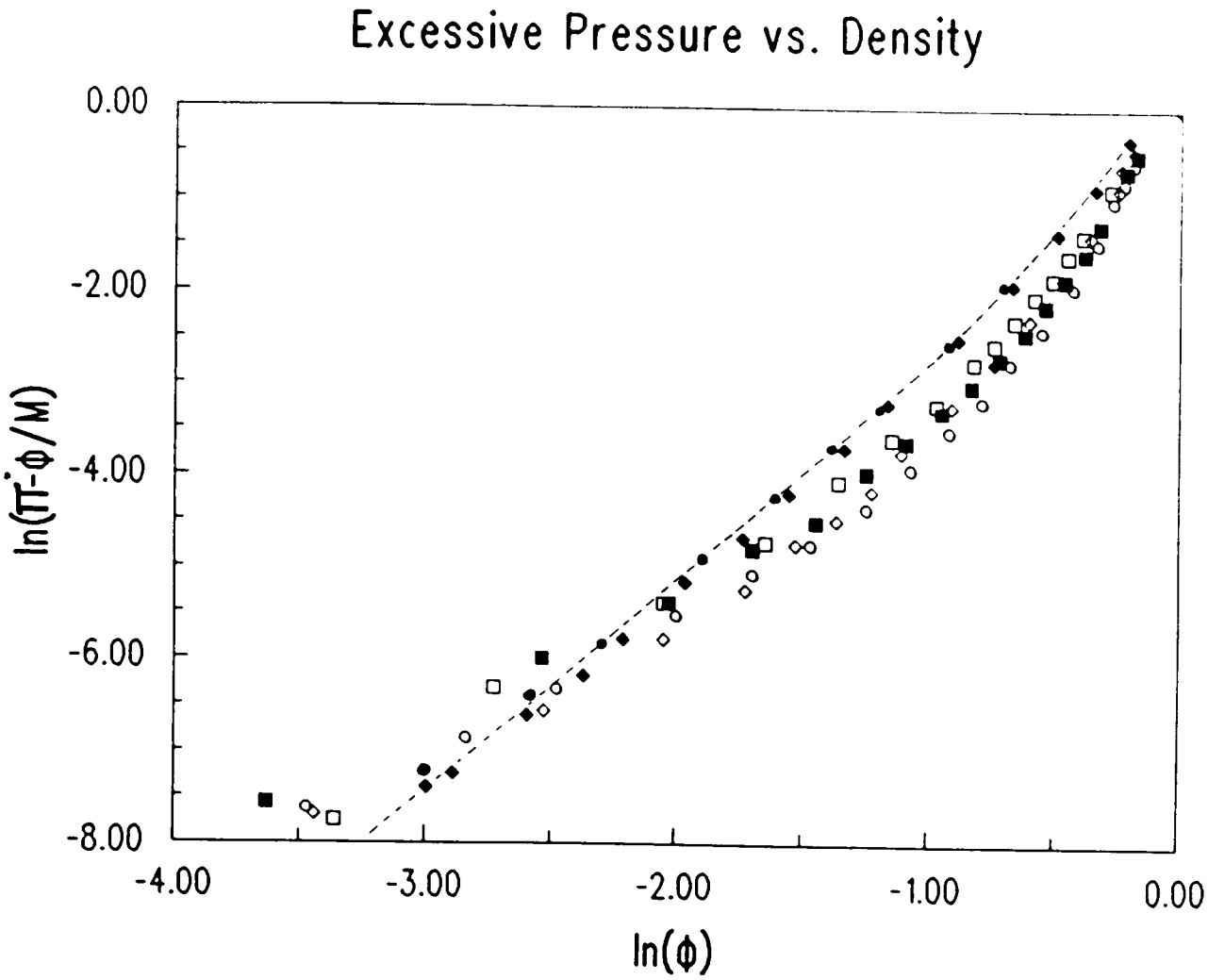
Excessive Pressure vs. Density
0.00
-2.00
-4.00
-6.00
-8.00
ln(Π*-φ/M)
-4.00
-3.00
-2.00
-1.00
0.00
ln(φ)

Figure 5.21

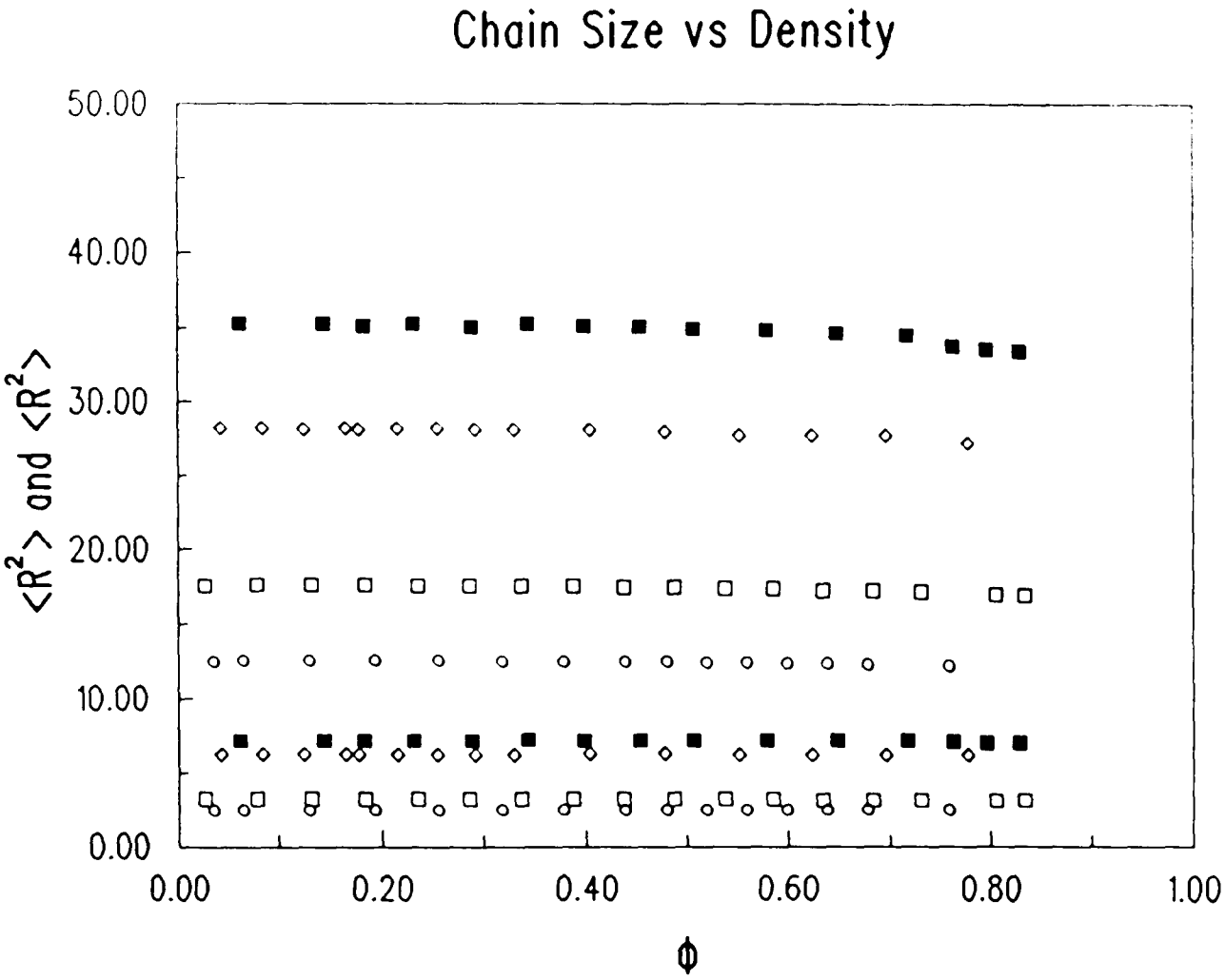
Chain Size vs Density
50.00
40.00
30.00
20.00
10.00
0.00
<R²> and <R²>
0.00
0.20
0.40
0.60
0.80
1.00
Φ

Figure 5.22

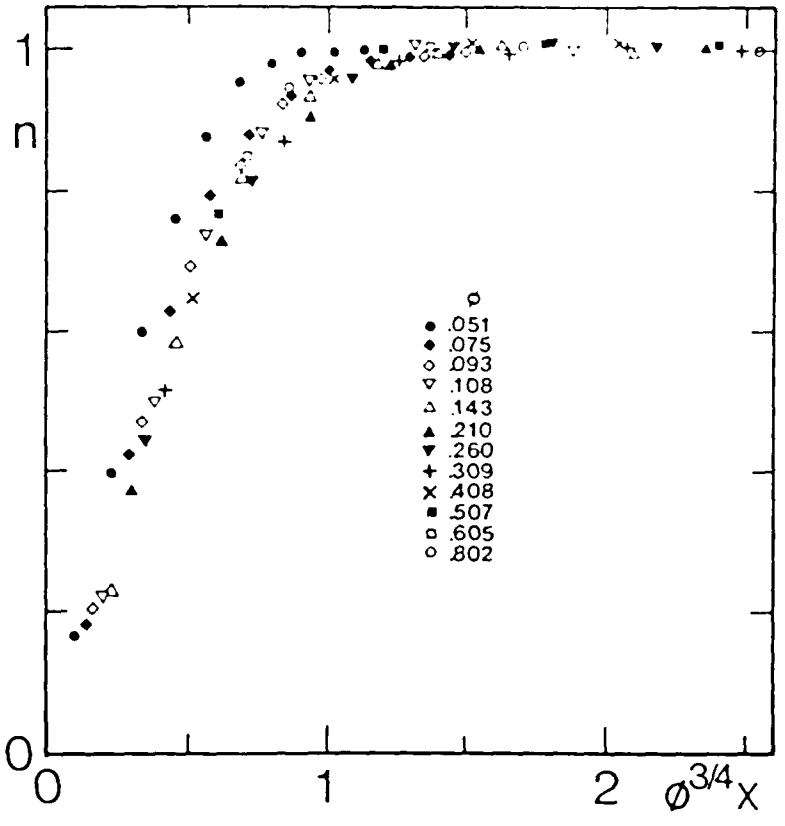

Figure 5.23

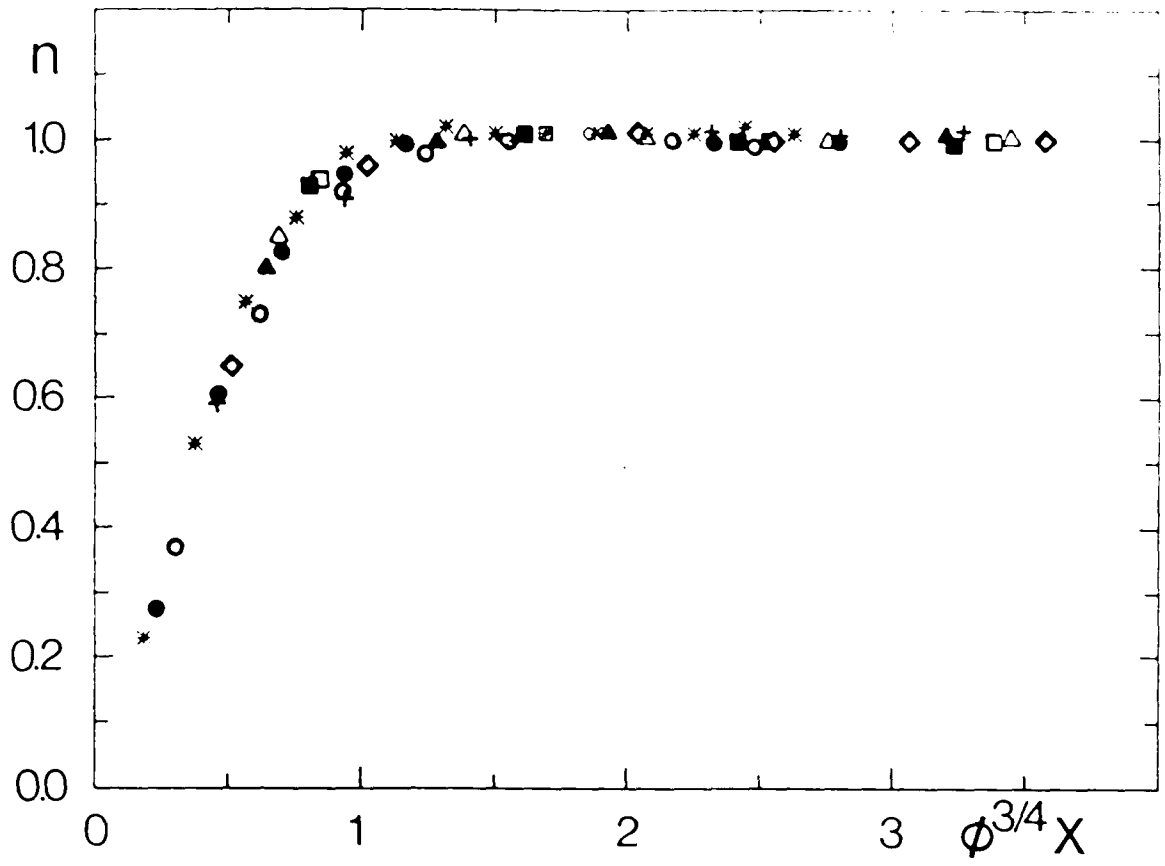

Figure 5.24

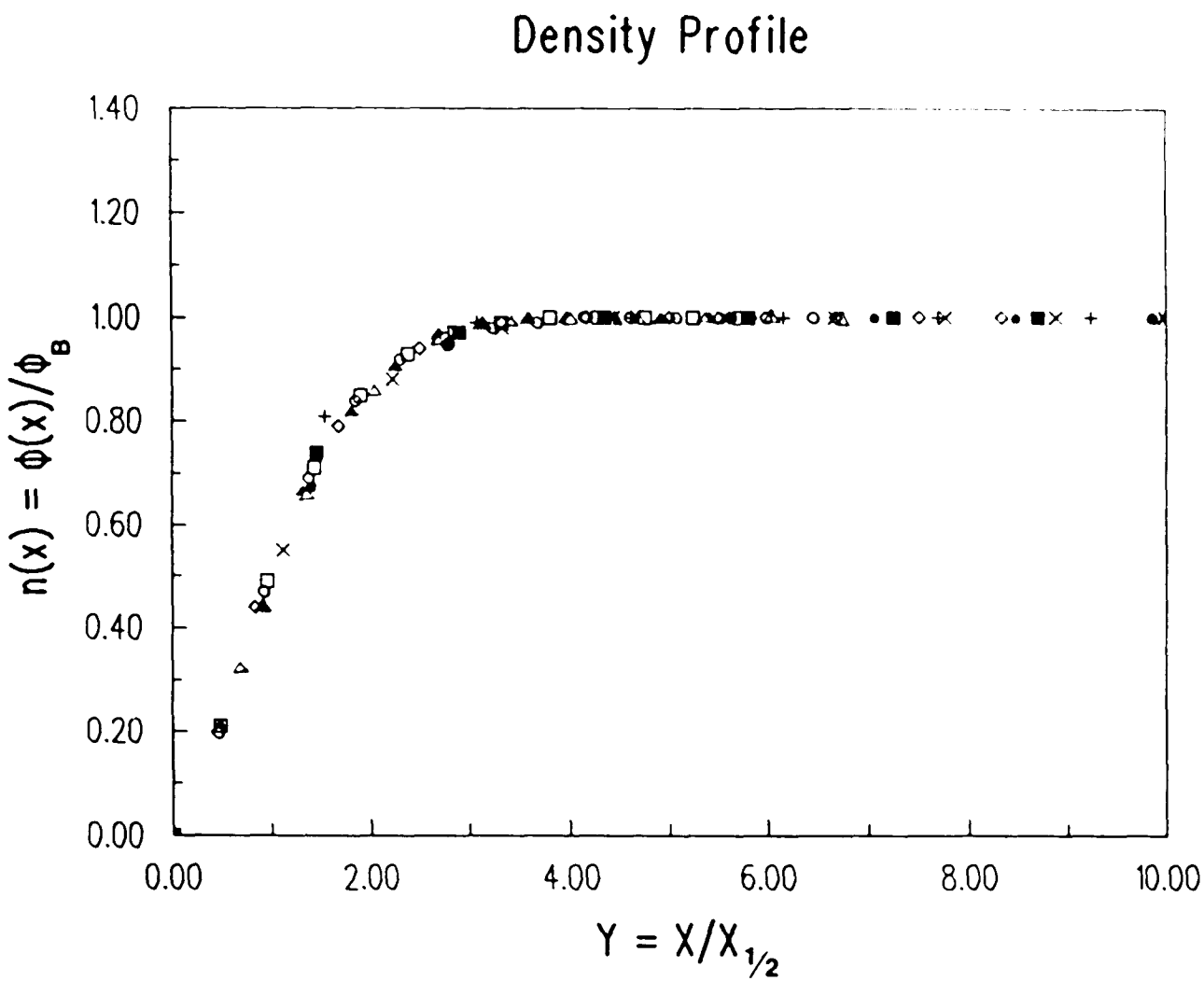
Density Profile
1.40
1.20
1.00
0.80
0.60
0.40
0.20
0.00
n(x) = φ(x)/φB
0.00
2.00
4.00
6.00
8.00
10.00
Y = X/X1/2

Figure 5.25a

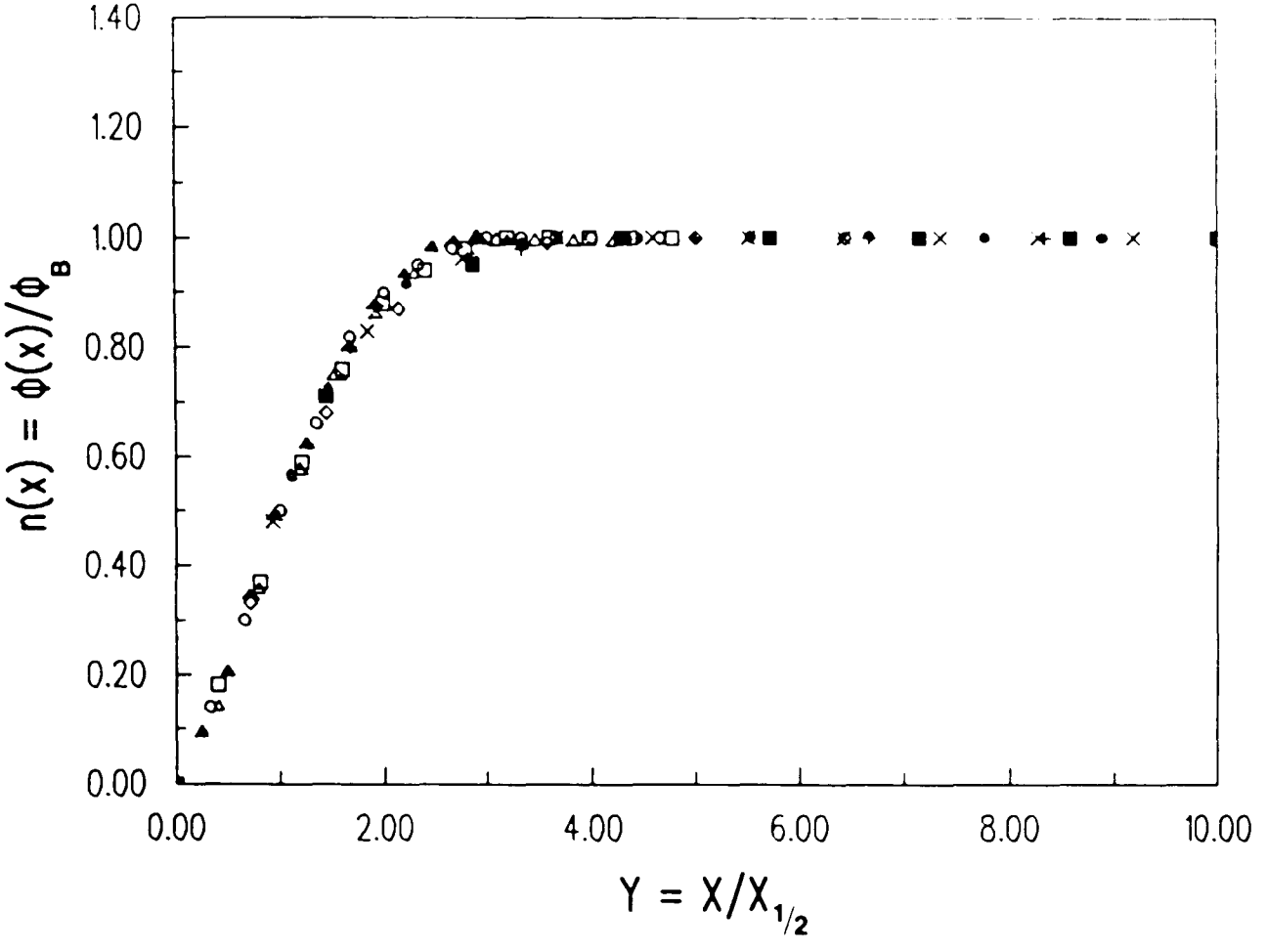
Density Profile
1.40
1.20
1.00
0.80
0.60
0.40
0.20
0.00
n(x) = φ(x)/φB
0.00
2.00
4.00
6.00
8.00
10.00
Y = X/X1/2

Figure 5.25b

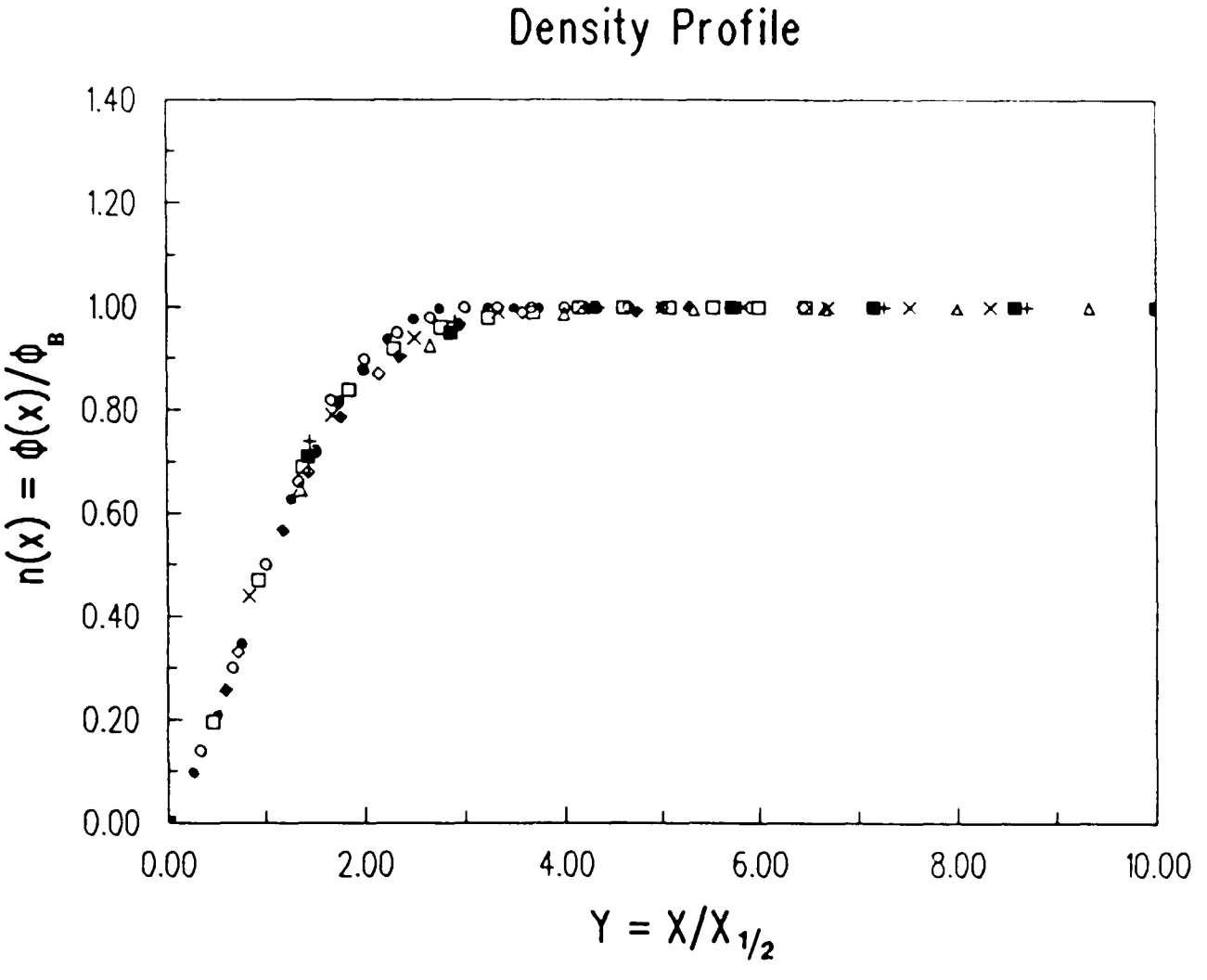
Density Profile
1.40
1.20
1.00
0.80
0.60
0.40
0.20
0.00
n(x) = φ(x)/φB
0.00
2.00
4.00
6.00
8.00
10.00
Y = X/X1/2

Figure 5.25c

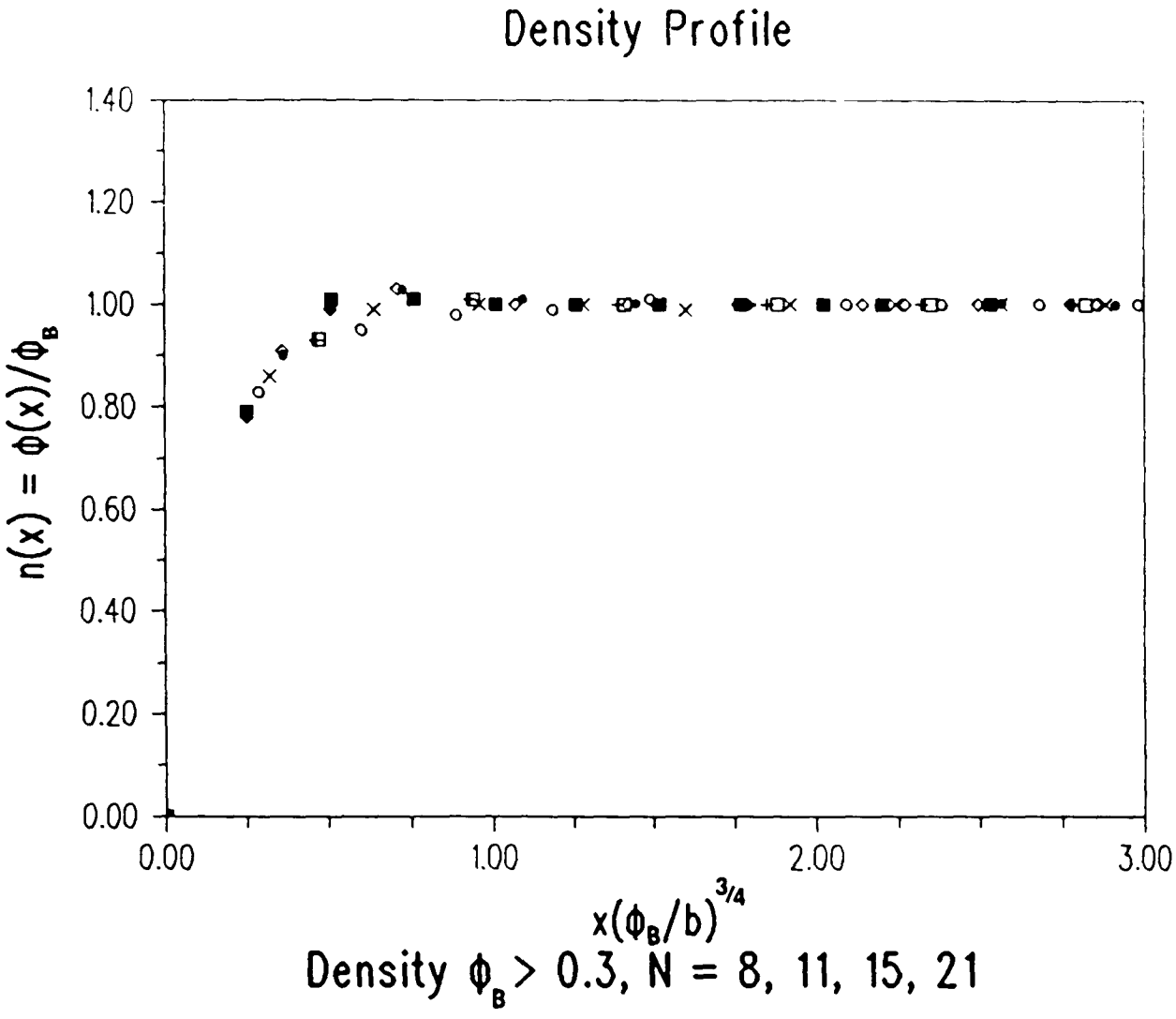
Density Profile
1.40
1.20
1.00
0.80
0.60
0.40
0.20
0.00
n(x) = φ(x)/φB
0.00
1.00
2.00
3.00
x(φB/b)3/4
Density φB > 0.3, N = 8, 11, 15, 21

Figure 5.26

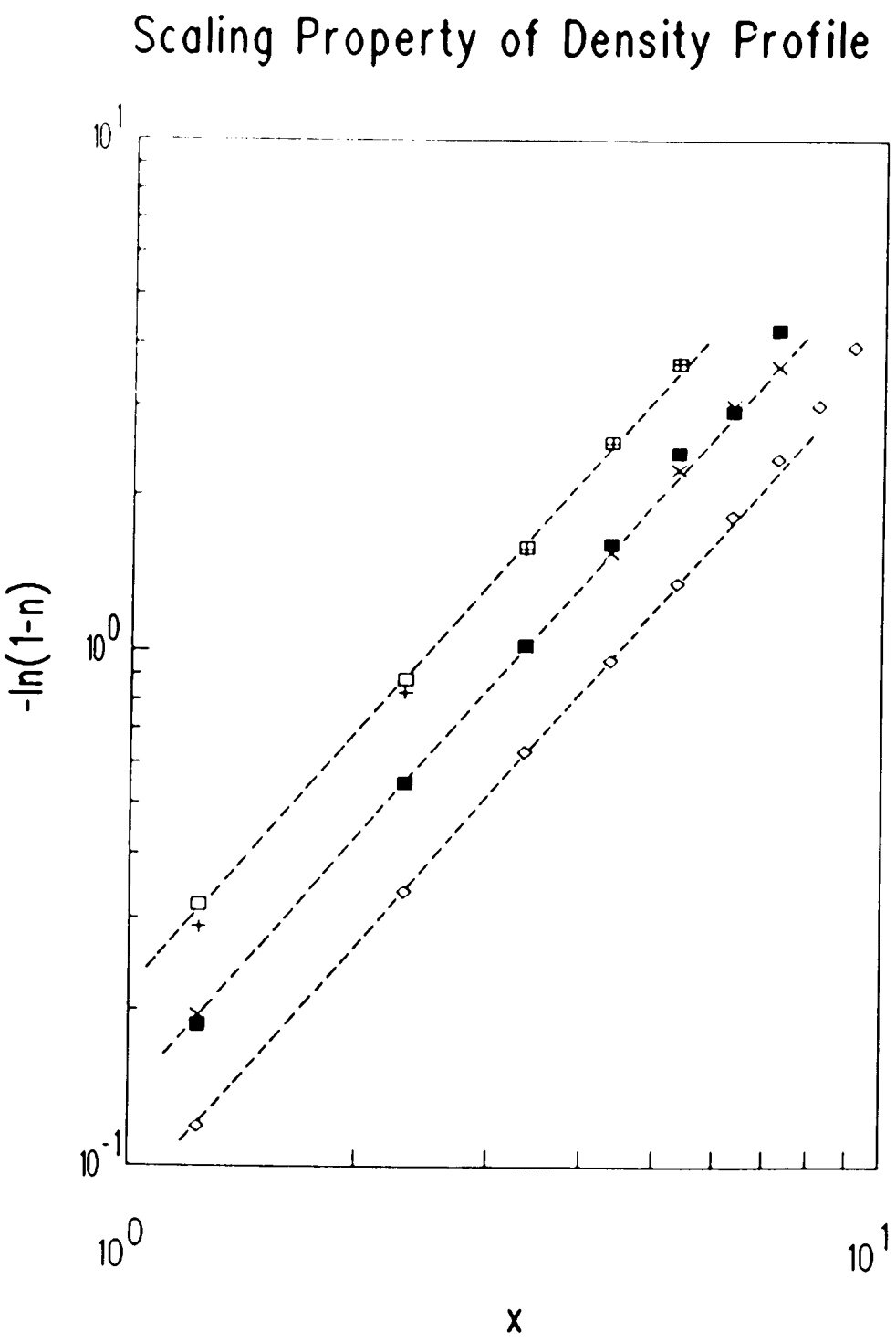
Scaling Property of Density Profile
10^1
10^0
10^{-1}
-ln(1-n)
10^0
10^1
x

Figure 5.27a

Scaling Property of Density Profile

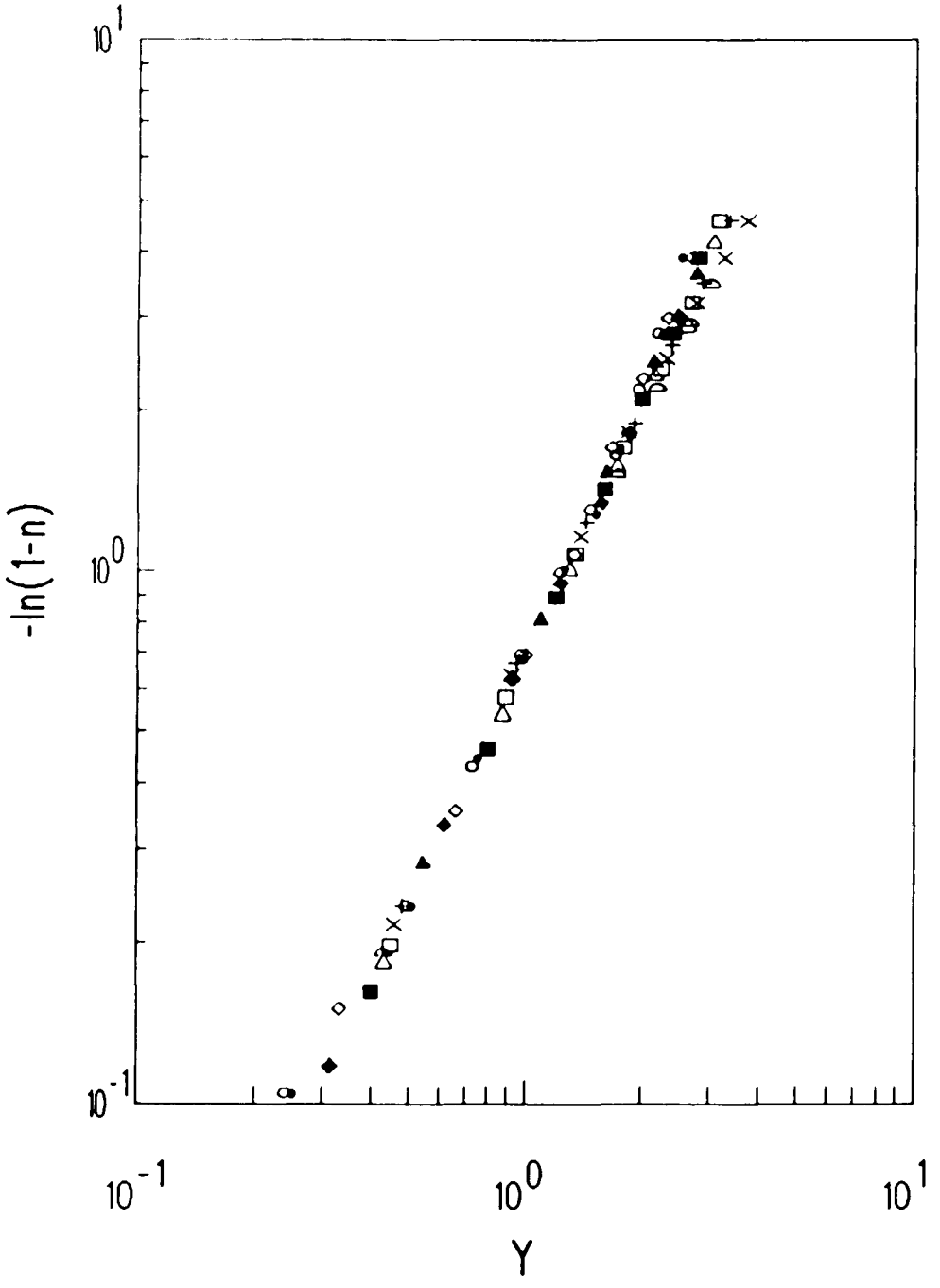

Figure 5.27b

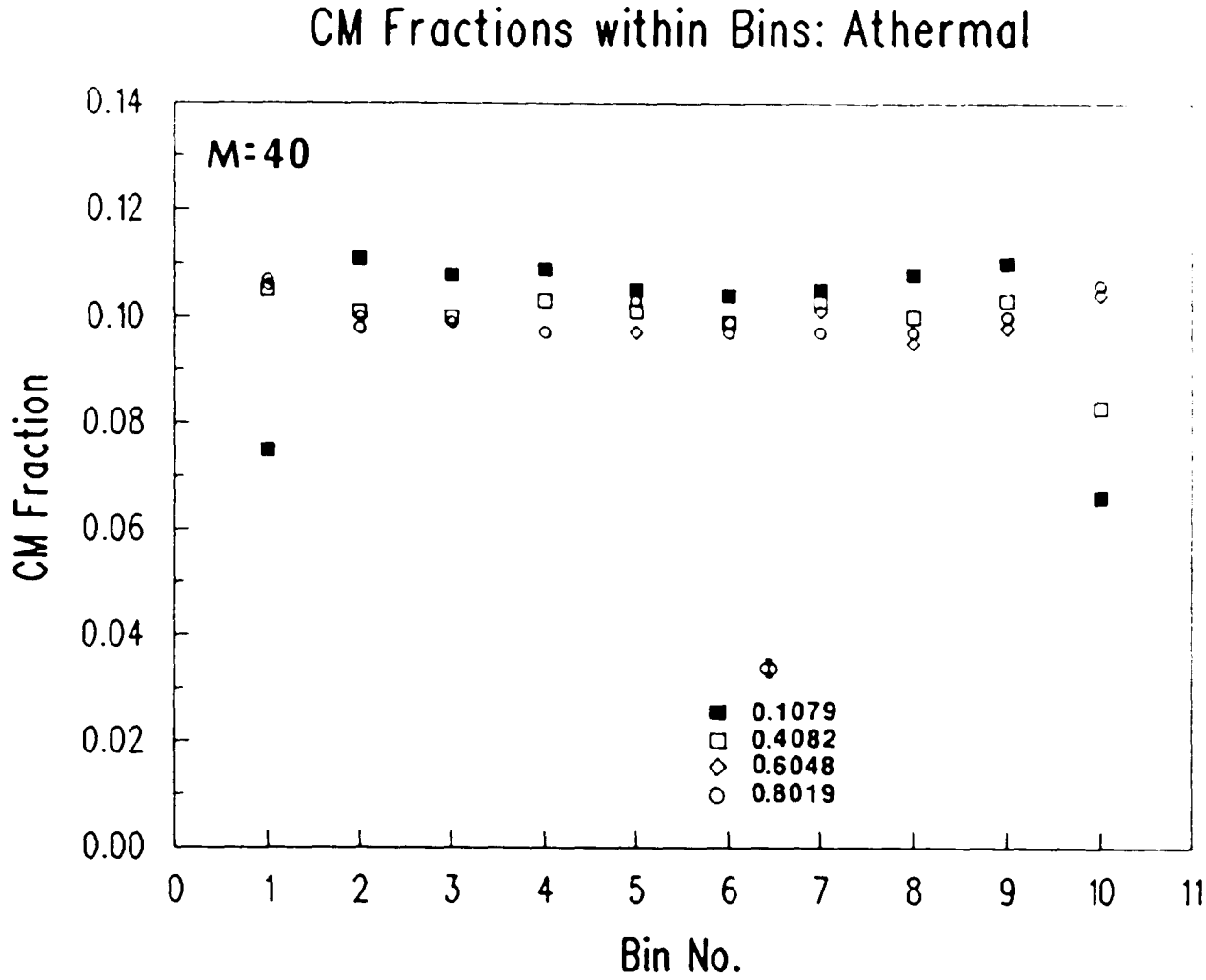
CM Fractions within Bins: Athermal
M=40
CM Fraction
Bin No.
0.14
0.12
0.10
0.08
0.06
0.04
0.02
0.00
0
1
2
3
4
5
6
7
8
9
10
11
Φ
0.1079
0.4082
0.6048
0.8019

Figure 5.28

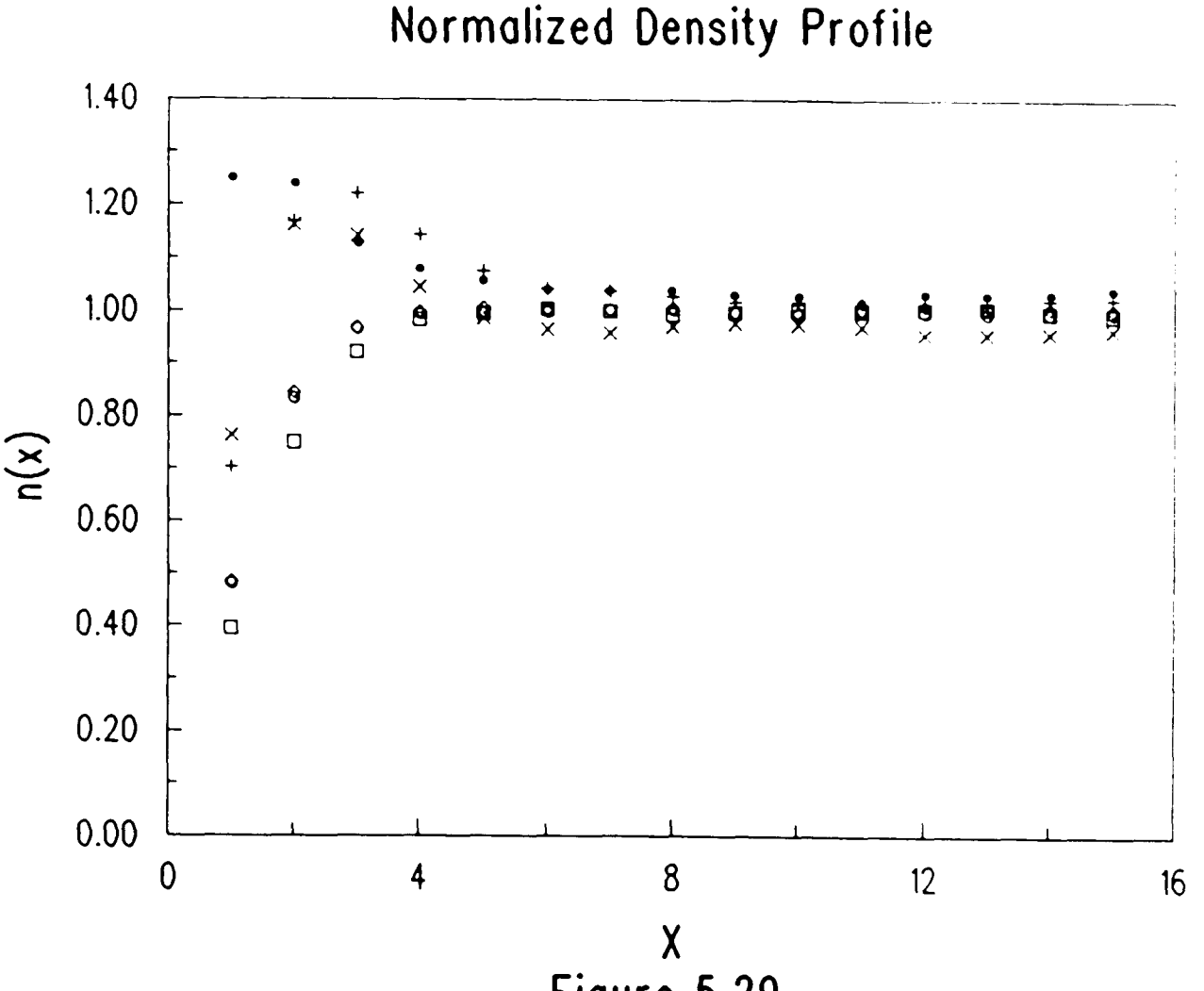
Normalized Density Profile
1.40
1.20
1.00
0.80
0.60
0.40
0.20
0.00
n(x)
0
4
8
12
16
X

Figure 5.29

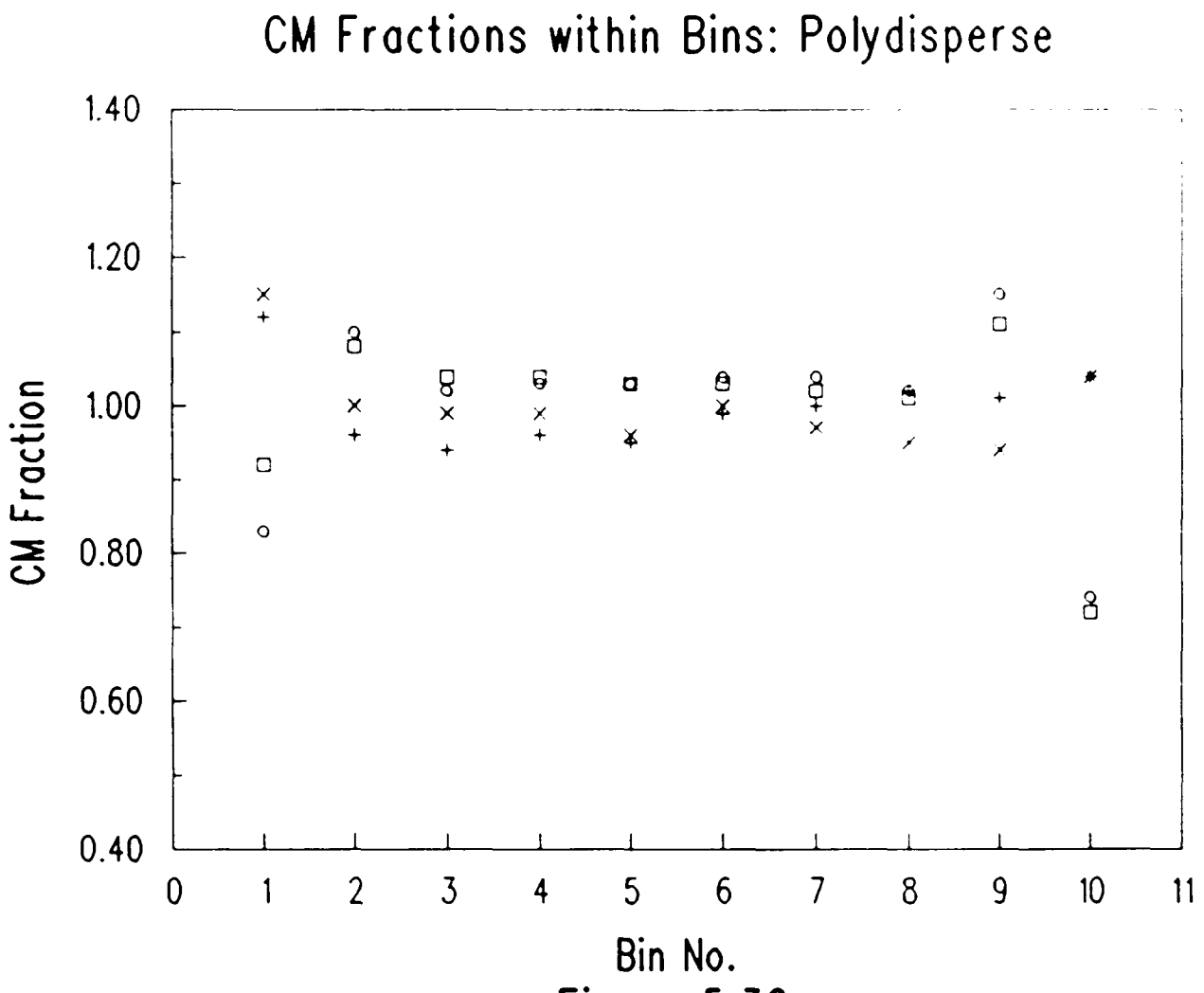
CM Fractions within Bins: Polydisperse
CM Fraction
1.40
1.20
1.00
0.80
0.60
0.40
0
1
2
3
4
5
6
7
8
9
10
11
Bin No.

Figure 5.30

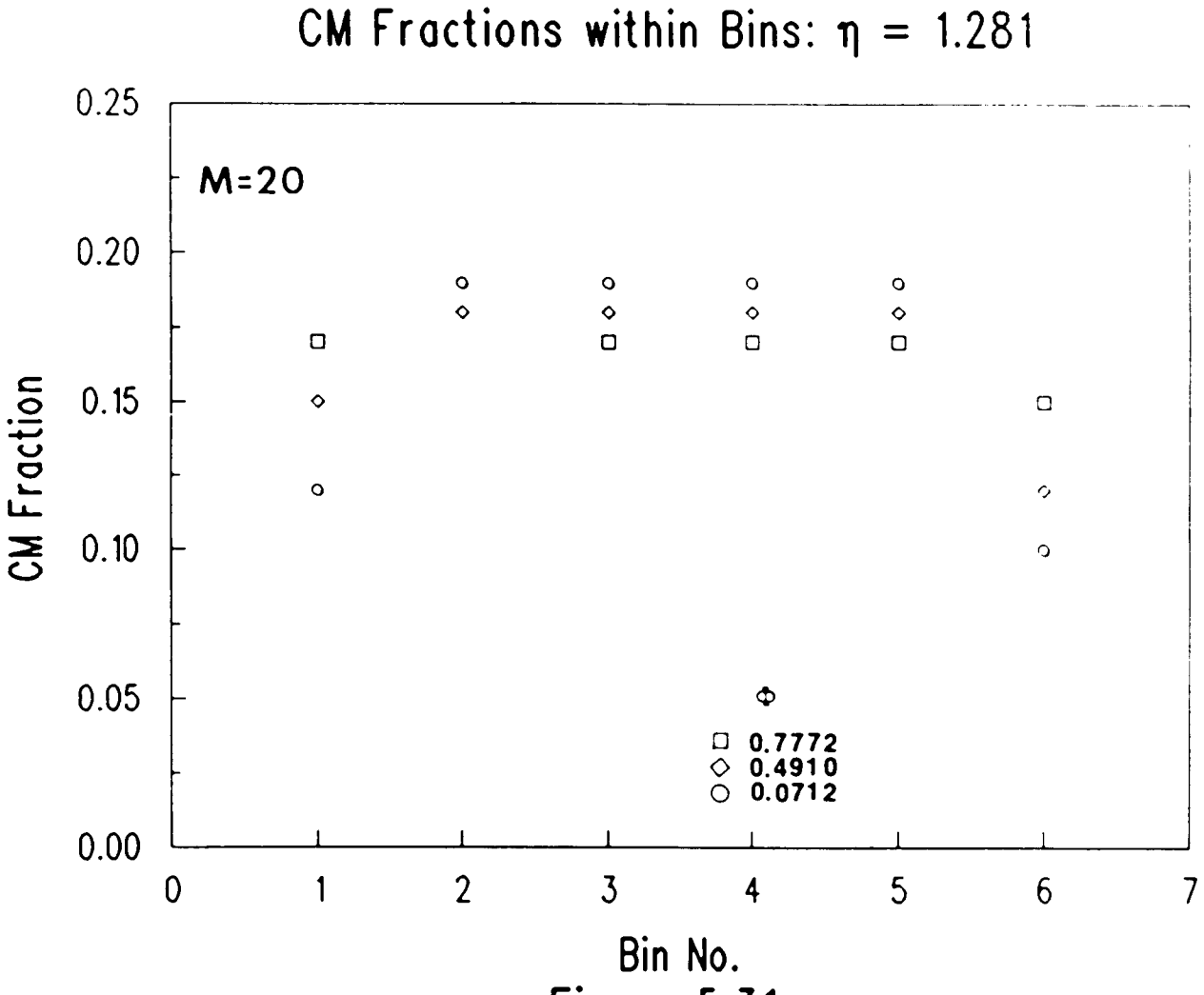
CM Fractions within Bins: η = 1.281
M=20
0.25
0.20
0.15
0.10
0.05
0.00
CM Fraction
0
1
2
3
4
5
6
7
Bin No.
0.7772
0.4910
0.0712

Figure 5.31a

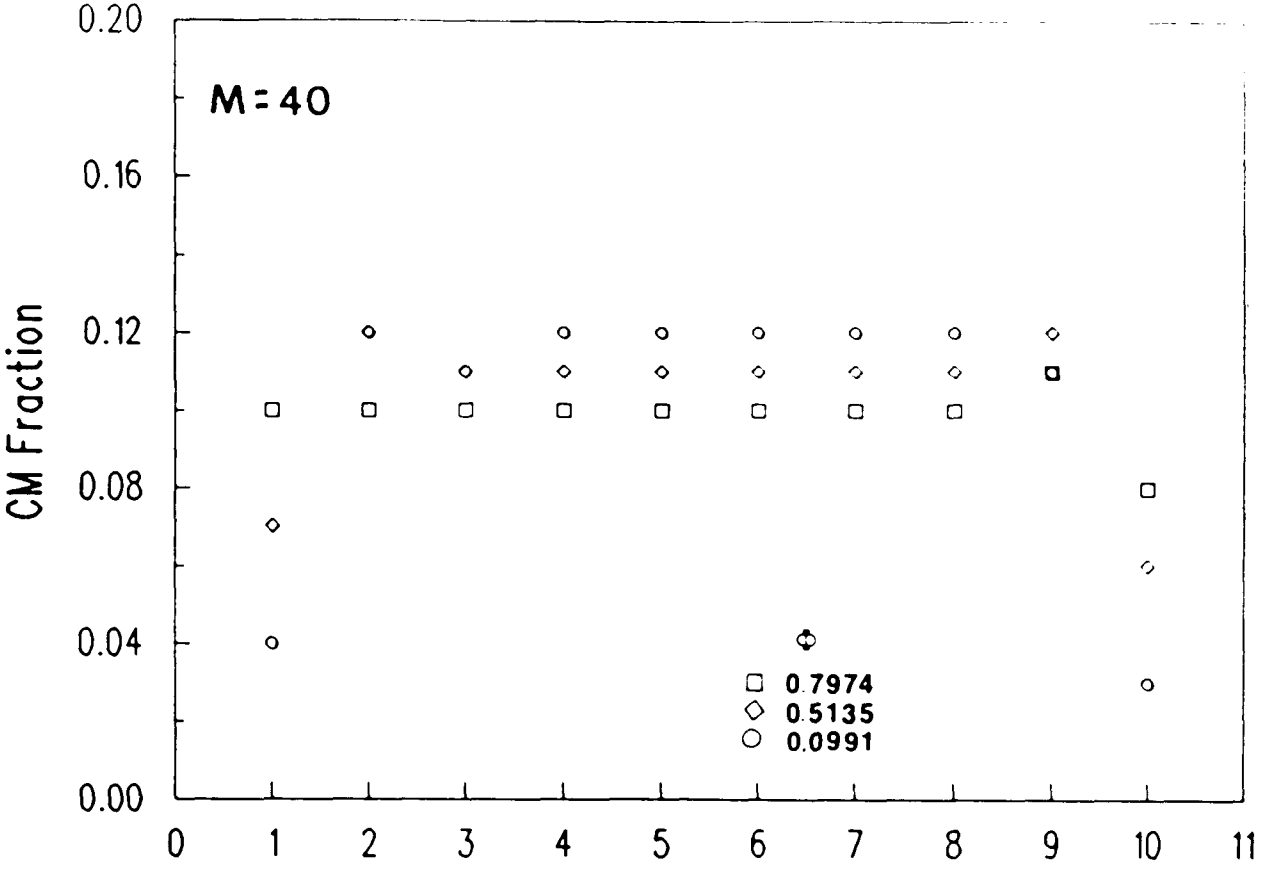
CM Fractions within Bins: η = 1.291
M=40
CM Fraction
0.20
0.16
0.12
0.08
0.04
0.00
0
1
2
3
4
5
6
7
8
9
10
11
Bin No.
0.7974
0.5135
0.0991

Figure 5.31b

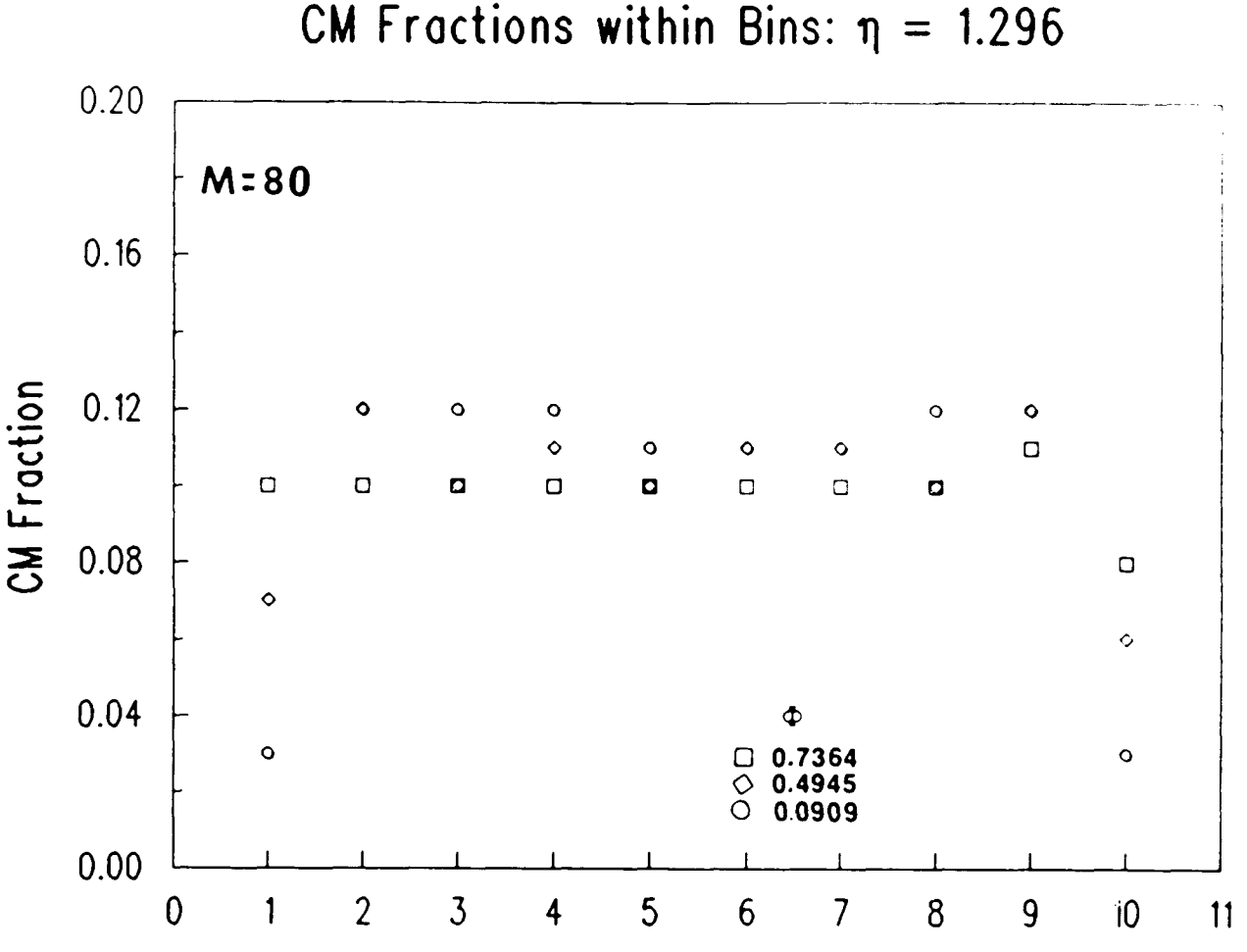
CM Fractions within Bins: η = 1.296
M=80
CM Fraction
0.20
0.16
0.12
0.08
0.04
0.00
0
1
2
3
4
5
6
7
8
9
10
11
Bin No.
0.7364
0.4945
0.0909

Figure 5.31c

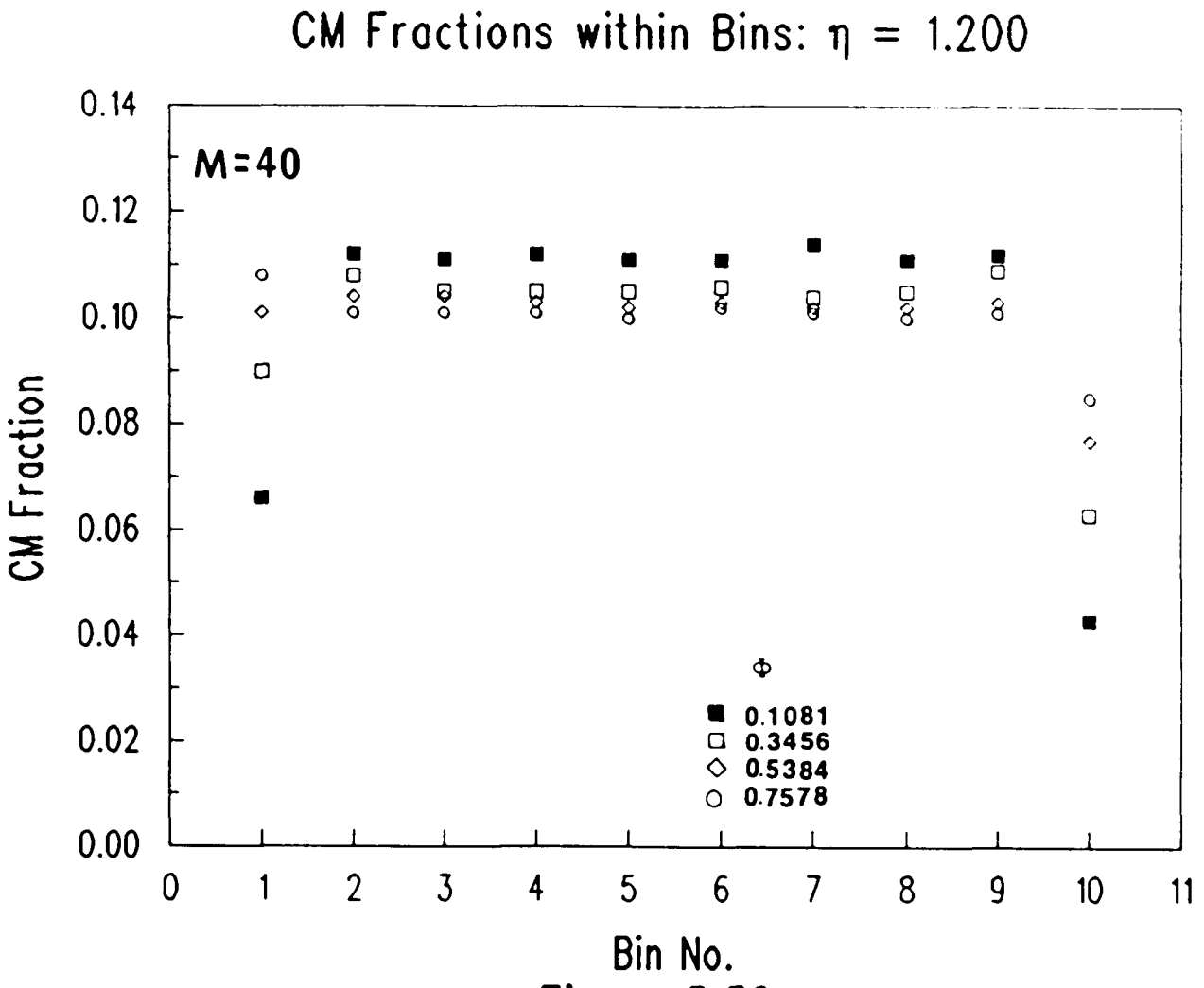
CM Fractions within Bins: η = 1.200
M=40
CM Fraction
Bin No.
0.14
0.12
0.10
0.08
0.06
0.04
0.02
0.00
0
1
2
3
4
5
6
7
8
9
10
11
Φ
0.1081
0.3456
0.5384
0.7578

Figure 5.32a

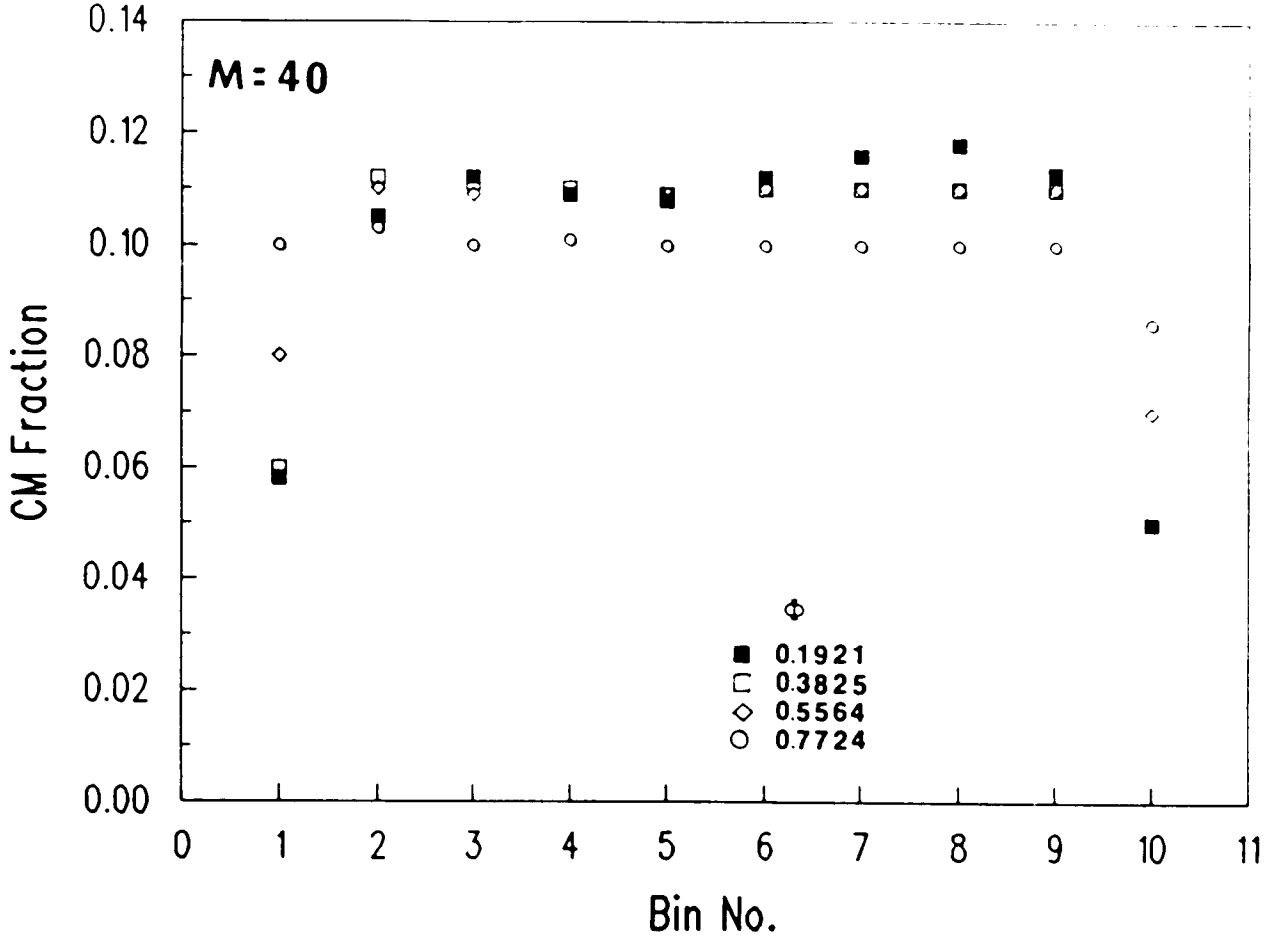
CM Fractions within Bins: η = 1.300
M=40
CM Fraction
Bin No.
Φ
0.1921
0.3825
0.5564
0.7724
0.00
0.02
0.04
0.06
0.08
0.10
0.12
0.14
0
1
2
3
4
5
6
7
8
9
10
11

Figure 5.32b

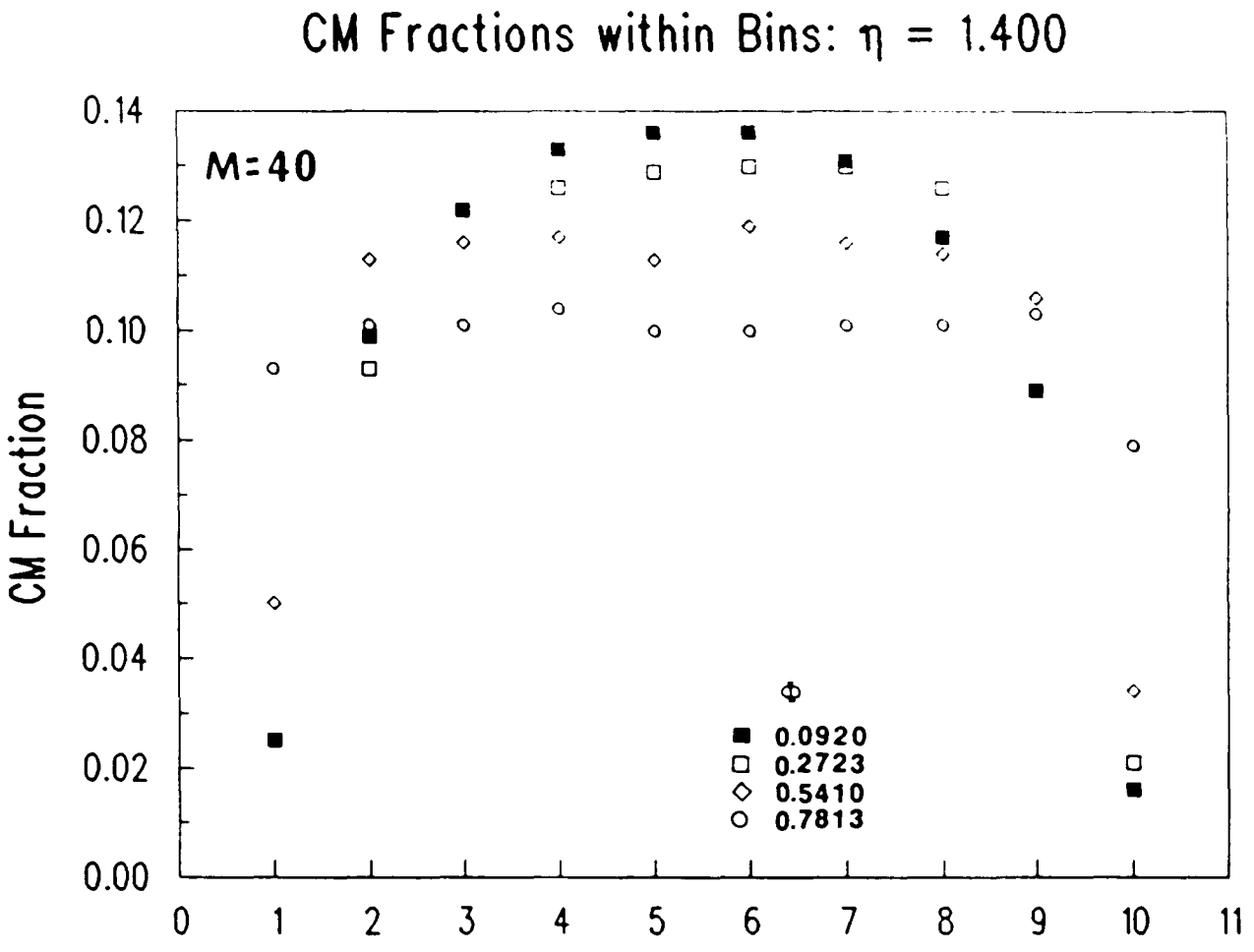
CM Fractions within Bins: η = 1.400
M=40
CM Fraction
Bin Bo.
Φ
0.0920
0.2723
0.5410
0.7813
0.00
0.02
0.04
0.06
0.08
0.10
0.12
0.14
0
1
2
3
4
5
6
7
8
9
10
11

Figure 5.32c

VI. CONCLUSIONS.

In this chapter I summarize the results of my studies, and mention possible directions for future work.

In Chapter II, I reviewed Edwards' model and functional integration techniques to derive the scaling behavior of polymer solutions. Scaling properties of a single chain and chains at finite concentration are given. To investigate the effect of confinement, I also studied the scaling laws of chains in a confined space (chains located between two walls).

The problems of chains near an interface have attracted new attention because of their application in engineering and in biology. One of these problems is the segment distribution adjacent to an interface. My work, in Chapter III, tries to address the density profile near a repulsive wall. First, I studied this profile via scaling theories in a more systematic way than that of de Gennes. In the second part, I used the Gaussian model to represent ideal chains. The segment density profile near an interface was established. My result is in agreement with previous studies using the n-vector model[164]. I also derived the density distribution of ideal chains confined between two repulsive walls. Finally, I used Edwards' model and the renormalization group equation to derive the scaling law for the segment density as a function of the

distance from a wall. The perturbation method was employed to the lowest order to obtain the scaling exponent.

Edwards' model is defined in continuous space, so it is not appropriate for comparison with Monte Carlo studies employing a lattice model. In addition, the δ-potential does not restrict segment occupancy. To emulate polymer at finite concentrations, we use a lattice model. We derive the Flory and Flory-Huggins mean field approximations for athermal and non-athermal chains. Since polymers on a lattice are defined as sequences of occupied sites, bond or segment correlations play a significant role in the chain configuration. To study the effect of bond correlations on the equation of state, I used Freed's n-vector model. In chapter IV, I summarize earlier works of Freed and coworkers[15,94-105]. I also provide some algebraic corrections, and derive the equation of state for a system of chains with a uniform-length distribution and of chains in non-athermal solutions.

To test theoretical predictions, I run extensive Monte Carlo simulations. The models used were of polymer chains defined on a three-dimensional (cubic) lattice. Athermal and non-athermal systems of monodisperse chains were studied. I also studied the effect of polydispersity and chain structure on the equation of state. In my simulations I employed the test-chain insertion and repulsive wall methods to obtain the compressibility factor. Other conformational properties, such as the mean-square end-to-end distance and density profile

were obtained. I found preliminary indications that des Cloizeaux' scaling law is observed in the non-athermal system. It was also shown that polydispersity does not affect the equation of state. The non-athermal systems, I employed the test-chain insertion technique to determine the values of the θ-temperature at different chain lengths, and extrapolated these results to obtain the θ-temperature in the limit $N\to\infty$. I also showed that Freed's n-vector model provides the best estimate for the equation of state of linear chains. There are some discrepancies observed between theory and simulation. First, the scaling law cannot explain the conformational properties of nonathermal chains (e.g., the increase of the average chain size around ϕ_m, and the dependence of density profile on temperature and bulk density). Secondly, the lattice n-vector model overestimates the osmotic pressure of polymer systems with branched structure.

These discrepancies raise questions: How to include the temperature in scaling theories? How to improve calculations of the density profile for multichain systems? What is the functional form of the segment density in a system with more general polymer-wall interactions. How do higher order interactions (e.g., three-body interaction for polymers at the θ-temperature) affect the density profile. Since our results indicate that the equation of state of branched-polymers is far off from the improved predictions of Freed's n-vector model, it is also necessary to test the accuracy of this

theoretical model by including higher order bond-diagrams.

Several theoretical models have been devised, however the transition from one model to another is not obvious. For example: What kind of model is obtained when the correlating-bond corrections of the lattice model are included in the continuum limit? A new polymer model, the fluctuating bond model[173,174], has been devised to study dynamics and to avoid ergodicity problems in simulations. This model is more representative than that of the regular lattice model with fixed bond length. The monomer size is also taken into account in the fluctuating bond model. However, the basic structure remains defined on a lattice. This computer model lacks its theoretical counterpart. It is necessary to extend the Freed's n-vector model to incorporate the fluctuating chain length.

Addressing the aforementioned issues is important for the advancement of polymer science. I plan to explore these problems in my future work.

Appendix A. Definition of Kuhn Step Length[2,149]

Consider a real chain with the average end-to-end distance $\langle R^2 \rangle$, and the maximum elongation R_{max}. $\langle R^2 \rangle$ can be determined from neutron scattering, and R_{max} can be calculated if its chemical bond length, bond angle, and steric hindrance are known. Kuhn[149] suggested that this chain could be replaced by an equivalent Gaussian chain consisting of N_k bonds. Each bond has an effective length l_k, which is known as the Kuhn step length. N_k and l_k are determined as follows:

$$l_k = \frac{\langle R^2 \rangle}{R_{max}}$$
$$N_k l_k = R_{max} \qquad \text{(A.1)}$$

For example[148], a cis-polyisoprene chain [$\left(\text{CH}_2\text{-}\underset{\text{H}}{\overset{}{\text{C}}}\text{=}\overset{\text{CH}_3}{\overset{|}{\text{C}}}\text{-CH}_2 \right)_N$] in rubber, where N is the polymerization index (the number of segments), has a bond length = 4.6×10^{-10} m. So the fully extended length $R_{max} = 4.6\ N \times 10^{-10}$ m. The root-mean-square end-to-end distance of polyisoprene molecule is determined to be $16.2\ N \times 10^{-10}$ m. Therefore, Eqn. (A.1) will give $l_k = 3.52 \times 10^{-10}$ m. and $N_k = 1.31\ N$. In this case the effective Kuhn length is less than the physical bond length.

To see the application of Kuhn's concepts to a rigid chain, consider a freely rotating chain with N bonds (Figure A.1). If the bond angle θ is fixed, the mean square of the

end-to-end distance is

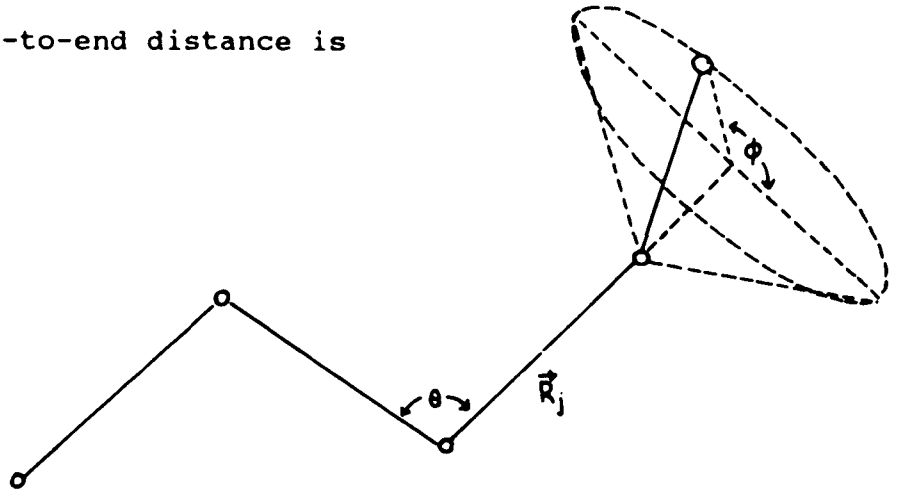

Figure A.1. A schematic representation of a freely rotating chain.

$$\langle \vec{R}^2 \rangle = \langle (\sum_{j=1}^{N} \vec{R}_j)^2 \rangle$$

$$= \sum_{j=1}^{N} \langle \vec{R}_j^2 \rangle + 2 \sum_{j=1}^{N} \sum_{s=1}^{N-j} \langle \vec{R}_j \cdot \vec{R}_{j+s} \rangle \qquad \text{(A.2)}$$

where <...> is the configuration average and R_j is the j^{th} bond vector. The projection of the $(j+1)^{th}$ bond vector on the j^{th} bond vector is $-l^2\cos\theta$. Hence, equation (A.2) becomes

$$\langle \vec{R}^2 \rangle = Nl^2 + 2l^2 \sum_{j=1}^{N} \sum_{s=1}^{N-j} (-\cos\theta)^s$$

$$= Nl^2 \left[\frac{1-\cos\theta}{1+\cos\theta} + \frac{2\cos\theta}{N} \frac{1-(-\cos\theta)^N}{(1+\cos\theta)^2} \right] \qquad \text{(A.3)}$$

The quantity $1/(1+\cos\theta) = 1/(2\lambda)$ is defined as the persistence length[69]. This definition represents a physical situation in which the polymer strand becomes rigid when $\theta\to\pi$ (large persistence length). The 'worm-like' chain[69] is defined such that $l\to 0$, $N\to\infty$, $Nl=L$ (maximum length), $\theta\to\pi$, $1/(1+\cos\theta)\to 1/(2\lambda)$. Under this limit, Eqn. (A.3) becomes

$$\lim_{worm} \langle \vec{R}^2 \rangle = \frac{L}{\lambda} - \frac{1}{2\lambda^2}\left[1 - e^{-2\lambda L}\right] \qquad (A.4)$$

Following Kuhn, a 'worm-like' chain may be replaced by an equivalent Gaussian chain with l_k and N_k given by

$$l_k = \frac{1}{\lambda} - \frac{1}{2L\lambda^2}\left[1 - e^{-2\lambda L}\right]$$

$$N_k = \frac{2L^2\lambda^2}{2L\lambda - 1 + e^{-2\lambda L}} \qquad (A.5)$$

For a rigid rod ($\lambda\to 0$) $l_k=L$ and $N_k=1$. The whole chain is replaced by a single bond of length L. In the flexible chain limit ($0 \le \theta \le \pi$), the cross-term in Eqn. (A.2) vanishes. We obtain $l_k=l$ and $N_k= N$. From the definition of Kuhn length, it is obvious that the rigidity, steric-constraint, and segment-segment interaction (including short-range excluded volume effects) are already taken into account.

Appendix B. Proof of Equation (4.35).

Consider the right side of equation (4.35), and let the exponent in the numerator be

$$I = \sum_i (\vec{S}^*_{i,\alpha+1} \cdot \vec{\Phi}_{i,\alpha} + \vec{S}_{i,\alpha} \cdot \vec{\Phi}^*_{i,\alpha}) - \sum_{i,j} \tilde{V}_{ij} \vec{\Phi}^*_{i,\alpha} \cdot \vec{\Phi}_{j,\alpha} \qquad \text{(B.1)}$$

Introduce the following transformations

$$\vec{\Phi}'_{j,\alpha} = \vec{\Phi}_{j,\alpha} - \sum_m A_{jm} \vec{S}_{m,\alpha} \qquad \text{(B.2a)}$$

$$\vec{\Phi}'^*_{i,\alpha} = \vec{\Phi}^*_{i,\alpha} - \sum_m B_{im} \vec{S}^*_{m,\alpha} \qquad \text{(B.2b)}$$

The exponent in the denominator of equation (4.35) can be written as

$$-\sum_{i,j} \tilde{V}_{ij} \vec{\Phi}'^*_{i,\alpha} \cdot \vec{\Phi}'_{j,\alpha} = -\sum_{i,j} \tilde{V}_{ij} \vec{\Phi}^*_{i,\alpha} \cdot \vec{\Phi}_{j,\alpha} + \sum_{i,j} \sum_m \tilde{V}_{ij} B_{im} \vec{S}^*_{m,\alpha+1} \cdot \vec{\Phi}_{j,\alpha}$$
$$+ \sum_{i,j} \sum_m \tilde{V}_{ij} A_{jm} \vec{S}_{m,\alpha} \cdot \vec{\Phi}^*_{i,\alpha} - \sum_{i,j} \sum_{m,n} B_{im} \tilde{V}_{ij} A_{jn} \vec{S}^*_{m,\alpha+1} \cdot \vec{S}_{n,\alpha}$$

(B.3)

Eqn. (B.3) will produce Eqn. (B.1) and the exponent on the left side of Eqn. (4.35), if we set

$$\sum_{i,j} B_{im}\tilde{V}_{ij}A_{jn} = \begin{cases} +K & \text{if } |n-m|=1 \\ 0 & \text{otherwise} \end{cases} \qquad \text{(B.4)}$$

and

$$\sum_{i} B_{im}\tilde{V}_{ij} = \delta_{m,j}$$

$$\sum_{j} \tilde{V}_{ij}A_{jm} = \delta_{i,m} \qquad \text{(B.5)}$$

Substituting Eqn. (B.5) into Eqn. (B.4), we obtain

$$A_{mn} = \begin{cases} +K & \text{if } |n-m|=1 \\ 0 & \text{otherwise} \end{cases} \qquad \text{(B.6)}$$

A similar result is obtained for B_{mn}. Let us transform A_{mn} and $\tilde{V}_{ij}$ into their Fourier-components,

$$A_{mn} = \frac{1}{N_1}\sum_{\vec{k}} e^{-i\vec{k}\cdot(\vec{r}_m-\vec{r}_n)}A_{\vec{k}} \qquad \text{(B.7a)}$$

$$\tilde{V}_{ij} = \frac{1}{N_1}\sum_{\vec{k}} e^{-i\vec{k}\cdot(\vec{r}_i-\vec{r}_j)}\tilde{V}_{\vec{k}} \qquad \text{(B.7b)}$$

where the summation is over the first Brilloin-zone. The product in Eqn. (B.5) is

$$\sum_j \tilde{V}_{ij} A_{jm} = N_1^{-2} \sum_j \sum_{\vec{k},\vec{k}'} A_{\vec{k}} \tilde{V}_{\vec{k}'} e^{i\vec{k}\cdot(\vec{r}_j - \vec{r}_m) + i\vec{k}'\cdot(\vec{r}_i - \vec{r}_j)}$$

$$- N_1^{-1} \sum_{\vec{k}} A_{\vec{k}} \tilde{V}_{\vec{k}} e^{+i\vec{k}\cdot(\vec{r}_i - \vec{r}_m)} \qquad \text{(B.8)}$$

which is equal to $\delta_{i,m}$ if $\tilde{V}_{\vec{k}} = (A_{\vec{k}})^{-1}$. Using equation (B.6) in (B.7a), we obtain

$$A_{\vec{k}} = K \sum_{\{\vec{a}_i\}} e^{-i\vec{k}\cdot\vec{a}_i} = K f(\vec{k}) \qquad \text{(B.9)}$$

where $\{ \vec{a}_i \}$ is the set of unit vectors on the lattice. Therefore, $\tilde{V}_{ij}$ is given by

$$\tilde{V}_{ij} = \sum_{\vec{k}} e^{i\vec{k}\cdot(\vec{r}_i - \vec{r}_j)} [N_1 K f(\vec{k})]^{-1} \qquad \text{(B.10)}$$

which is the identity in equation (4.36).

Appendix C. Diagramatic Rules and The Calculation of The Third and Forth Order Corrections.

A diagram is made up of segments and bonds. Suppose that a diagram possesses s segments and b bonds, then the following rules apply:

o — An open dot (a vertex) symbolizes the chain segment, and for every dot we assign a coordinate $\vec{r}_i$.

------ — A dashed line represents a bond connecting two vertices. Every line is assigned a 'momentum' $\vec{q}_i$ such that if this line links two segments with coordinates $\vec{r}_l$ and $\vec{r}_m$, it contributes a factor

$$e^{-i\vec{r}_l\cdot(\vec{r}_l-\vec{r}_m)}\,\frac{f(\vec{q}_i)}{z} \qquad \text{(C.1)}$$

The value of the diagram is given by the product of all factors representing the b bonds, and is summed over b non-zero momenta and s distinct lattice sites. The result should take into account all possible ways of placing the b (non-) consecutive bonds and be divided by the number of choices to put s segments on N_l lattice sites in without overlap and in an ordered-fashion. The latter means that permutations of s

segments are not allowed. The correction to the partition function is obtained by multiplying the result by the partition function in the mean-field approximation. For clarity, let us apply this rule to the third order correction depicted in the next figure.

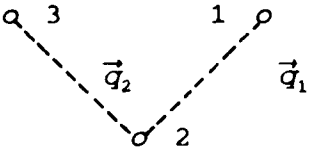

Figure C.1. A consecutively-placed-two-bond diagram

The numbers {1,2,3} correspond to the position of the three sequential chain segments $\{\vec{r}_1, \vec{r}_2, \vec{r}_3\}$. $\vec{q}_1$ and $\vec{q}_2$ are momenta assigned to the bonds connecting the sites $\{\vec{r}_1, \vec{r}_2\}$ and $\{\vec{r}_2, \vec{r}_3\}$ respectively. Using equation (C.1), this diagram will give

$$\sum_{1\neq 2\neq 3} \sum_{\vec{q}_1,\vec{q}_2}{}' e^{-i\vec{q}_1\cdot(\vec{r}_1-\vec{r}_2)-i\vec{q}_2\cdot(\vec{r}_2-\vec{r}_3)} \frac{f(\vec{q}_1)\, f(\vec{q}_2)}{z^2} \qquad (C.2)$$

There are $(N-1)n_p$ ways to place two consecutive bonds on n_p chains and $N_l(N_l-1)(N_l-2)$ ways to put three segments on N_l sites in an ordered fashion (without permutation of {1,2,3}). Therefore, the correction to the partition function is

$$Z^{(3)} = Z_{n_p} \frac{n_p(N-1)}{N_1(N_1-1)(N_1-2)} \sum_{1\neq 2\neq 3} \sum_{\vec{q}_1,\vec{q}_2}{}' e^{-i\vec{q}_1\cdot(\vec{r}_1-\vec{r}_3)-i\vec{q}_2\cdot(\vec{r}_2-\vec{r}_3)} \frac{f(\vec{q}_1)\,f(\vec{q}_2)}{z^2}$$

(C.3)

The restricted summation can be rewriten using equation (4.70) in terms of an ordinary summation involving Kronecker-δ's. Hence,

$$Z^{(3)} = Z_{n_p} \frac{n_p(N_1-1)}{N_1(N_1-1)(N_1-2)} [P_{3,1} + P_{3,2} + P_{3,3} + P_{3,4} + P_{3,5}]$$

(C.4)

The first term, $P_{3,1}$, is given by

$$P_{3,1} = \sum_{1,2,3} \sum_{\vec{q}_1,\vec{q}_2}{}' e^{-i\vec{q}_1\cdot(\vec{r}_1-\vec{r}_3)-i\vec{q}_2\cdot(\vec{r}_2-\vec{r}_3)} \frac{f(\vec{q}_1)\,f(\vec{q}_2)}{z^2} \quad \text{(C.5)}$$

$P_{3,1}$ is zero since summation with respect to coordinates will give a Kronecker-δ which is non-zero only for $\vec{q} = 0$, while the summation over momenta is constrained to non-zero values. The summations involving $\delta_{1,2}$, $\delta_{1,3}$, $\delta_{2,3}$, and $\delta_{1,2,3}$ can be described using contracted diagrams (figure C.2).

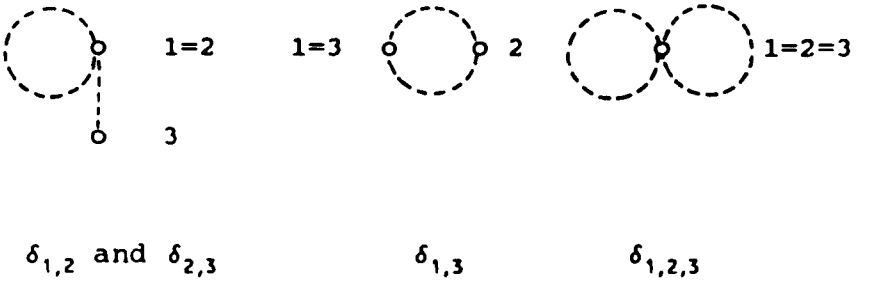

Figure C.2. Contractions of a two-bond diagram.

$P_{3,2}$ and $P_{3,3}$ after contraction yiled the same topological diagram, which is represented by the first picture in figure C.2. Its value is given by

$$P_{3,2} = P_{3,3} = -\sum_{1,2,3} \delta_{1,2} \sum_{\vec{q}_1,\vec{q}_2}{}' e^{-i\vec{q}_1\cdot(\vec{r}_1-\vec{r}_2)-i\vec{q}_2\cdot(\vec{r}_2-\vec{r}_3)} \frac{f(\vec{q}_1)\,f(\vec{q}_2)}{z^2} \tag{C.6}$$

$P_{3,2}$ and $P_{3,3}$ vanish for the reason described previously. In fact all diagrams containing dangling (uncontracted) sites give zeros. The second diagram produces

$$\begin{aligned} P_{3,4} &= \sum_{1-2-3} \delta_{1,3} \sum_{\vec{q}_1,\vec{q}_2}{}' e^{-i\vec{q}_1\cdot(\vec{r}_1-\vec{r}_2)-i\vec{q}_2\cdot(\vec{r}_2-\vec{r}_3)} \frac{f(\vec{q}_1)\,f(\vec{q}_2)}{z^2} \\ &= N_1^2 \sum_{\vec{q}}{}' \frac{f(\vec{q})\,f(\vec{q})}{z^2} \\ &= \frac{N_1^3}{z} = N_1^2 \end{aligned} \tag{C.7}$$

and the last diagram contributes

$$P_{3,5} = \sum_{1-2-3} \delta_{1,2,3} \sum'_{\vec{q}_1,\vec{q}_2} e^{-i\vec{q}_1\cdot(\vec{r}_1-\vec{r}_3)-i\vec{q}_2\cdot(\vec{r}_2-\vec{r}_3)} \frac{f(\vec{q}_1)\,f(\vec{q}_2)}{z^2}$$

$$- N_1 \left[\sum'_{\vec{q}} \frac{f(\vec{q})}{z}\right]^2 - N_1 \qquad (C.8)$$

Hence, P_3 and the partition function follow as in equations (4.72) and (4.73) respectively.

For the forth order corrections, there are three diagrams involving three consecutive bonds, two non-consecutive bonds located on the same chain and two non-consecutive bonds on different chains. Consider the first diagram depicted in the following figure

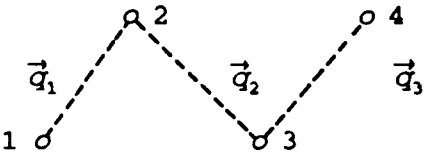

Figure C.3. A consecutively-placed-three-bond diagram.

This diagram will give

$$Z_{n_p}^{(4a)} = \frac{(N-2)\,n_p}{N_1 \ldots (N_1-3)}\, P_{4a}\, Z_{n_p,MF} \qquad (C.9)$$

where

$$P_{4a} = \sum_{1\neq 2\neq 3\neq 4} \sum_{\vec{q}_1,\vec{q}_2,\vec{q}_3}{}' e^{-i\vec{q}_1\cdot(\vec{r}_1-\vec{r}_2)-i\vec{q}_2\cdot(\vec{r}_2-\vec{r}_3)-i\vec{q}_3\cdot(\vec{r}_3-\vec{r}_4)} \frac{f(\vec{q}_1)\,f(\vec{q}_2)\,f(\vec{q}_3)}{z^3} \qquad (C.10)$$

The restricted sum can be expressed as an unrestricted summation involving Kronecker-δ

$$\sum_{1\neq 2\neq 3\neq 4} = \sum_{1,2,3,4} (1-\delta_{1,2})(1-\delta_{1,3})\ldots(1-\delta_{3,4}) \qquad (C.11)$$

Let us define the following convention: $\delta_{i,j}\delta_{j,k} = \delta_{i,j,k}$ which, unlike the standard rule of δ-Kronecker summation, means that the indices $\vec{r}_i=\vec{r}_j=\vec{r}_k$; $\delta_{i,j}\delta_{j,k}\delta_{k,l} = \delta_{i,j}\delta_{j,k}\delta_{j,l} = \ldots = \delta_{i,j,k,l}$ etc. Finally we can write equation (C.11) as

$$\begin{aligned}\sum_{1\neq 2\neq 3\neq 4} = \sum_{1,2,3,4} (1 &- \delta_{1,2} - \delta_{1,3} - \ldots - \delta_{1,4} \\ &+ 2\delta_{1,2,3} + 2\delta_{1,2,4} + 2\delta_{1,3,4} + 2\delta_{2,3,4} \\ &+ \delta_{1,2}\delta_{3,4} + \delta_{1,3}\delta_{2,4} + \delta_{1,4}\delta_{2,3} - 6\delta_{1,2,3,4})\end{aligned} \qquad (C.12)$$

If we define $\delta[m]$ as the Kronecker-δ with m indices chosen from all segments (dots) in a diagram, equation (C.12) can be rewritten in a compact form

$$\sum_{1\neq 2\neq 3\neq 4} - \sum_{1,2,3,4} (1 - \delta[2] + 2\delta[3] + \delta[2]\delta[2] - 6\delta[4])$$

(C.13)

The contribution of uncontracted diagrams to P_{4a} is zero, and the non-vanishing results come from the following diagrams

$\delta[2]$ (from $\delta_{1,4}$) $\rightarrow P_{4a,1} \rightarrow$

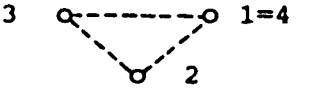

$\delta[3]$ (from $\delta_{1,2,4}$ and $\delta_{1,3,4}$) $\rightarrow$ $P_{4a,2} \rightarrow$

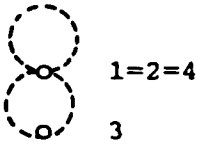

$\delta[2]\delta[2]$ (from $\delta_{1,3}\delta_{2,4}$ and $\delta_{2,3}\delta_{1,4}$) $\rightarrow P_{4a,3} \rightarrow$

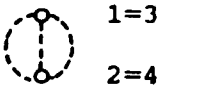

$\delta[4]$ (from $\delta_{1,2,3,4}$) $\rightarrow P_{4a,4} \rightarrow$

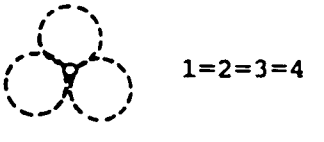

Using the mathematical tools collected in Appendix D, one may obtain

$$P_{4a,1} = N_l^3 \sum_{\vec{q}}{}' \frac{f(\vec{q})\, f(\vec{q})\, f(\vec{q})}{z^3} = -N_l^3 \tag{C.14a}$$

$$P_{4a,2} = N_l^2 \sum_{\vec{q}}{}' \frac{f(\vec{q})\, f(\vec{q})}{z^2} = -\frac{N_l^3}{z} + N_l^2 \tag{C.14b}$$

$$P_{4a,3} = N_l^2 \sum_{\vec{q}_1,\vec{q}_2}{}' \frac{f(\vec{q}_1)\, f(\vec{q}_2)\, f(\vec{q}_1+\vec{q}_2)}{z^3} = \frac{N_l^4}{z^2} - 3\frac{N_l^3}{z} + 2N_l^2 \tag{C.14c}$$

$$P_{4a,4} = N_l \left(\sum_{\vec{q}}{}' \frac{f(\vec{q})}{z} \right) = -N_l \tag{C.14d}$$

Hence,

$$P_{4a} = \frac{N_l^4}{z^2} - 8\frac{N_l^3}{z} + N_l^3 + 7N_l^2 + 6N_l \tag{C.15}$$

The number of ways to place three consecutive bonds among n_p chains is $(N-2)n_p$, while the number of an ordered arrangement of four segments among N_l sites is $N_l(N_l-1)(N_l-2)(N_l-3)$. The correction to the partition function is

$$Z_{n_p}^{(4a)} = \frac{(N-2)\, n_p}{N_l \ldots (N_l-3)} Z_{n_p,MF} P_{4a} \tag{C.16}$$

The arrangement of two non-consecutive bonds is given by the diagrams in figure (C.4)

Figure C.4. A non-consecutively-placed-two-bond diagram.

The left side corresponds to the bond configuration on different chains. On the right side, a wiggly line is used to indicate that the two bonds separated by this line are placed non-consecutively on the same chain. Both diagrams give the same value P_{4b} where

$$P_{4b} = \sum_{1\neq 2\neq 3\neq 4} e^{-i\vec{q}_1\cdot(\vec{r}_1-\vec{r}_2)-i\vec{q}_2\cdot(\vec{r}_3-\vec{r}_4)} \frac{f(\vec{q}_1)\,f(\vec{q}_2)}{z^2} \qquad (C.17)$$

However, the number of ways in regard to bond-placement is different; the left side gives $n_p N(n_p-1)N/2$, while the right picture is $n_p(N-1)(N-2)/2$. The factor 1/2 is to take into account bond symmetry.

Consider the diagram on the left side. The contraction of the monomer sites requires $\delta[4]$ and $\delta[2]\delta[2]$ only.

$\delta[2]\delta[2]$

(from $\delta_{1,2}\delta_{3,4}$) → $P_{4b,1}$ → 1=2 3=4

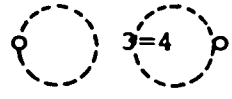

(from $\delta_{1,3}\delta_{2,4}$ and $\delta_{1,4}\delta_{2,3}$) → $P_{4b,2}$ →

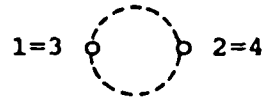

$\delta[4]$

(from $\delta_{1,2,3,4}$) → $P_{4b,3}$ →

Note that $P_{4b,2}$ and $P_{4b,3}$ are similar to $P_{3,4}$ and $P_{3,5}$ while $P_{4b,1}$ is

$$P_{4b,1} = [N_1 \sum_{\vec{q}}{}' \frac{f(\vec{q})}{z}]^2 - N_1^2 \qquad \text{(C.18)}$$

The analysis of the diagram on the right side follows similarly, and

$$P_{4b} = \frac{2N_1^3}{z} - N_1^2 - 6N_1 \qquad \text{(C.19)}$$

Dividing by the number of permutations of segment placement, one obtains

$$Z^{(4b)} = Z_{n_p,MF}\{\frac{Nn_pN(n_p-1)}{2N_1\ldots(N_1-3)} + \frac{n_p(N-1)(N-2)}{2N_1\ldots(N_1-3)}\} \times [\frac{2N_1^3}{z} - N_1^2 - 6N_1] \tag{C.20}$$

From the previous discussion, it is obvious that all diagrams with dangling sites or diagrams which can be disconnected into two subdiagrams by cutting a single bond vanish. In field theory language, 1 Particle Irreducible diagrams without dangling vertices give non-vanishing contributions.

Appendix D. A List of Mathematical Results and The Rules of Contracted Diagrams.

The following results are used in the calculations,

$$f(\vec{q})|_{\vec{q}=0} = z \qquad and \qquad \sum_{\vec{q}}{}' f(\vec{q}) = -z \tag{D.1}$$

$$\sum_{i_1 \neq i_2 \neq \cdots \neq i_s} = \sum_{i_1, i_2, \ldots, i_s} \{1 - \delta[2] + 2\delta[3] - 6\delta[4] + \ldots \tag{D.2}$$

$$+ \cdots + \prod_{\substack{j=1 \\ \sum_j m_j \leq s}}^{p} (-1)^{m_j - 1} (m_j - 1)!\, \delta[m_j] + \cdots + (-1)^{s-1} (s-1)!\, \delta[s] \}$$

$$\sum_{\vec{q}}{}' f(\pm\vec{q}) f(\pm\vec{q}) = N_1 z - z^2 \tag{D.3}$$

$$\sum_{\vec{q}}{}' f(\pm\vec{q}) f(\pm\vec{q}) f(\pm\vec{q}) = -z^3 \tag{D.4}$$

$$\sum_{\vec{q}}{}' [f(\pm\vec{q})]^4 = N_1 (3z^2 - 3z) - z^4 \tag{D.5}$$

$$\sum_{\vec{q}}{}' f(\pm\vec{q}) f(\pm\vec{q} \pm \vec{k}) = (N_1 - z) f(\vec{k}) \tag{D.6}$$

$$\sum_{\vec{q}}{}' [f(\pm\vec{q})]^2 f(\pm\vec{q} \pm \vec{k}) = -z^2 f(\vec{k}) \tag{D.7}$$

$$\sum_{\bar{\alpha}, \bar{\beta}, \bar{\gamma}, \bar{\delta}} \delta_{\bar{\alpha} + \bar{\beta} + \bar{\gamma} + \bar{\delta}, 0} = 3z^2 - 3z \tag{D.8}$$

$$\sum_{\vec{q}_1, \vec{q}_2}{}' f(\pm\vec{q}_1) f(\pm\vec{q}_2) f(\pm\vec{q}_1 \pm \vec{q}_2) = N_1^2 z - 2N_1 z^2 + z^3 \tag{D.9}$$

Note that the previous results are obtained for a hypercubic lattice with the coordination number z. Different lattice structure yields different result[94]. For example, in a triangular lattice equation (D.4) is replaced by $2N_l z - z^3$.

We find out that the following diagrams are the most primitive (with their values on the right side). Other diagrams can be constructed by attaching additional bonds or by merging them on a common lattice site.

$- N_l$

$N_l^3/z - N_l^2$

$- N_l^3$

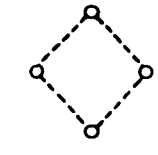

$(3N_l^5)/z^2 - (3N_l^5)/z^3 - N_l^4$

Figure D.1. The primitive diagrams.

For example diagram in $P_{4a,3}$ can be constructed from the second diagram by attaching an additional bond

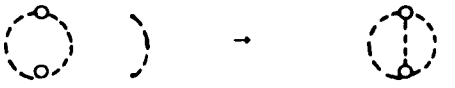

$$(N_l^3/z - N_l^2)(N_l/z - 2)$$

Figure D.2. An example of construction of a three-bond diagram out of a two-bond diagram and a bond.

It can be easily shown that by attaching a single line between two adjacent sites in 1-PI diagram, the original value is multiplied by $(N_l/z - 2)$. This is another example

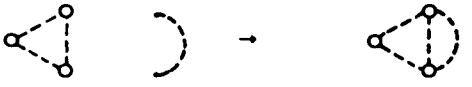

$$(-N_l^3)(N_l/z - 2)$$

Figure D.3. Construction of a four-bond diagram out of a three-bond diagram and a correlating bond.

Also diagram $P_{4a,2}$ is the product of the first and second diagram in figure D.1

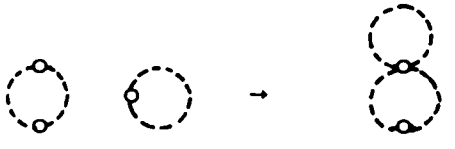

$$(N_l^3/z - N_l^2)(-N_l)/N_l$$

Figure D.4. An example of construction of a three-bond diagram out of two primitive diagrams.

Division by N_l is neccessary since by collapsing two segments on a single site we have to take care of the overcount.

Appendix E. The contracted diagrams and Their Values.

When we rewrite the restricted summation in term of the ordinary sums, contraction occurs on some diagrams because of the δ-Kronecker. In thermodynamic limit ($N_l \to \infty$) only few contracted diagrams contribute to the cummulant. The following figures are the surviving contracted diagrams and their values.

$$R_{1,1} = - N_l$$

$$R_{2,1} = (N_l^3)/z - N_l^2$$

$$R_{3,1} = (N_l^4)/z^2 - (3N_l^3)/z + 2N_l^2$$

$$R_{3,2} = R_{2,1}R_{1,1}$$

$$R_{4,1} = (R_{2,1})^2$$

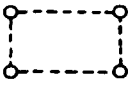

$$R_{4,2} = (3N_l^5)/z^2 - (3N_l^5)/z^3 - N_l^4$$

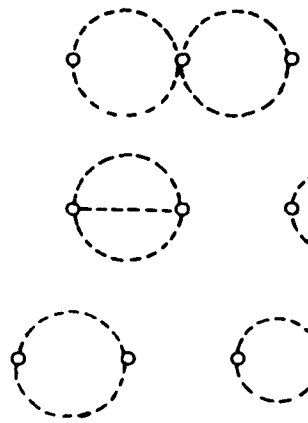

$$R_{4,3} = (R_{2,1})^2/N_1$$

$$R_{4,4} = R_{3,1}R_{1,1}$$

$$R_{4,5} = R_{2,1}(R_{1,1})^2$$

Note that our results, $R_{3,1}$ and $R_{4,2}$, are different from Nemirovsky et. al.[97].

Appendix F. A List of The Values of N_i and $N_{i,j}$.

We follow the convention of Nemirovski et. al.[97]: N_i is the number of ways to place i consecutive bonds on a chain; $N_{i,j}$ is the number of possible placement of two bond-sequences on a chain, one with i consecutive bonds and the other with j consecutive bonds; $N_\perp$, $N_\perp'$, and N_* are respectively the number of ways to put the structure F, O, and Q on a chain. F, O, and Q are depicted in the diagram set I of Appendix H. For our purpose we only need the results for a linear chain, a chain with branch structure 1 and 2. M is the number of segments per unit chain. Our result $N_\perp$ for structure 1 is different from Ref.[97].

	Linear Chain	Structure 1	Structure 2
M	N+1	2N	3N-1
N_1	N	2N-1	3N-2
N_2	N-1	3(N-1)	6(N-1)
N_3	N-2	4(N-2)	9(N-2)
N_4	N-3	4(N-3)	9(N-3)
$N_\perp$	0	(N-1)	4(N-1)
$N_\perp'$	0	4(N-2)	18(N-2)
N_*	0	0	N-1
$N_{1,1}$	(N-1)(N-2)	4(N-1)(N-2)	9(N-1)(N-2)
$N_{1,2}$	(N-2)(N-3)	2(N-2)(3N-7)	$18(N-2)^2$
$N_{2,2}$	(N-3)(N-4)	$9N^2-51N+74$	$36N^2-180N+234$

Appendix G. The Value of Diagrams of Monodisperse Chains.

The following results are the values of cummulant diagrams obtained from the diagram sets in Appendix H. M is the molecular weight which is equal to the number of segments per unit chain. The calculation was performed in thermodynamic limit ($N_l \to \infty$), and only the dominant terms proportional to N_l were retained. Our results are in agreement with Ref.[105].

Diagram set I.

A → $-(N_2\phi N_l)/(Mz)$

B → $(N_1^2\phi^2 N_l)/(M^2 z)$

C → $(N_3\phi N_l)/(Mz^2)$

D → $-(4N_1N_2\phi^2N_l)/(Mz)^2$

E → $(16N_1^3\phi^3N_l)/(6M^3z^2)$

F → $(2N_\perp\phi N_l)/(Mz^2)$

G → $O(N_l^0)$

H → $(-2N_1N_3\phi^2N_l)/(Mz)^2$

I → $(2N_2^2\phi^2N_l)/(2Mz)^2$

J → $(N_{2,2}\phi N_l)/(2Mz^2)$

K → $(2N_1^2N_2\phi^2N_l)/(Mz)^2$

L → $(-2N_1N_{1,2}\phi^2N_l)/(Mz)^2$

M → $(2N_1^4\phi^4N_l)/(M^4z^2) + (-2N_1^4\phi^3N_l)/(M_3z_2)$

N → $(2N_1^2N_{1,1}\phi^3N_l)/(M^3z^2)$

O → $(N_\perp'\phi N_l)/(Mz^2)$

$P \rightarrow (-6N_1N_\perp\phi^2N_1)/(Mz)^2$

$Q \rightarrow (3N_*\phi N_1)/(Mz^2)$

Diagram set II

$A_2 \rightarrow (N_1\phi^4z)/4\ [\ \epsilon^2 + \epsilon^3 + 7\epsilon^4/12\ ]$

$B_2 \rightarrow -(N_1\phi^3z)/2\ [\ \epsilon^2 + \epsilon^3 + 7\epsilon^4/12\ ]$

$A_3 \rightarrow (N_1\phi^6z)/3\ [\ \epsilon^3 + 3\epsilon^4/2\ ]$

$B_3 \rightarrow -(N_1\phi^5z)\ [\ \epsilon^3 + 3\epsilon^4/2\ ]$

$C_3 \rightarrow (N_1\phi^4z)/2\ [\ \epsilon^3 + 3\epsilon^4/2\ ]$

$D_3 \rightarrow (N_1\phi^4z)/3\ [\ \epsilon^3 + 3\epsilon^4/2\ ]$

$A_4 \rightarrow (3N_1\phi^8z)/8\ [\ \epsilon^4\ ]$

$B_4 \rightarrow -(3N_1\phi^7z)/2\ [\ \epsilon^4\ ]$

$C_4 \rightarrow (N_1\phi^6z)/2\ [\ \epsilon^4\ ]$

$D_4 \rightarrow (N_1\phi^6z)/2\ [\ \epsilon^4\ ]$

$E_4 \rightarrow (N_1\phi^6z)\ [\ \epsilon^4\ ]$

$F_4 \rightarrow (N_1\phi^5z)/2\ [\ \epsilon^4\ ]$

$G_4 \rightarrow -(N_1\phi^5z)\ [\ \epsilon^4\ ]$

$H_4 \rightarrow -(N_1\phi^5z)/4\ [\ \epsilon^4\ ]$

$I_4 \rightarrow -(N_1\phi^4z)/4\ [\ \epsilon^4\ ]$

Diagram Set III.

$B_1 \rightarrow N_1N(1)\phi^3\ [\ \epsilon + \epsilon^2/2\ ]$

$B_2 \rightarrow -2N_1N(1)\phi^2\ [\ \epsilon + \epsilon^2/2\ ]$

$B_3 \rightarrow N_1N(1)\phi\ [\ \epsilon + \epsilon^2/2\ ]$

$C_1 \rightarrow -2N_l N(2)\phi\ \epsilon/z$

$C_2 \rightarrow 2N_l N(2)\phi^2\ \epsilon/z$

$C_3 \rightarrow 2N_l N(2)\phi^2\ \epsilon/z$

$C_4 \rightarrow -2N_l N(2)\phi^3\ \epsilon/z$

$D_1 \rightarrow 2N_l N(1)N(1)\phi^2\ \epsilon/z$

$D_2 \rightarrow -8N_l N(1)N(1)\phi^3\ \epsilon/z$

$D_3 \rightarrow 4N_l N(1)N(1)\phi^4\ \epsilon/z$

$D_4 \rightarrow 2N_l N(1)N(1)\phi^2\ \epsilon/z$

$E_1 \rightarrow -2N_l N(3)\phi\ \epsilon/z$

$E_2 \rightarrow 2N_l N(3)\phi^2\ \epsilon/z$

$E_3 \rightarrow -N_l N(3)\phi^3\ \epsilon/z$

$E_4 \rightarrow N_l N(3)\phi\ \epsilon/z$

$F_1 \rightarrow 2N_l N(1)N(2)\phi^2\ \epsilon/z$

$F_2 \rightarrow 4N_l N(1)N(2)\phi^2\ \epsilon/z$

$F_3 \rightarrow N_l N(1)N(2)\phi M\ \epsilon/z$

$F_4 \rightarrow N_l N(1)N(2)\{4\phi^3 - 6\phi^2 - 2\phi^2 M\}\ \epsilon/z$

$F_5 \rightarrow -4N_l N(1)N(2)\phi^3\ \epsilon/z$

$F_6 \rightarrow -6N_l N(1)N(2)\phi^3\ \epsilon/z$

$F_7 \rightarrow N_l\ [N(1)N(2)M\phi^3 + 6N(1)N(2)\phi^3]\ 4\epsilon/z$

$G_1 \rightarrow -2N_l[N(1)]^3 M\phi^2\ \epsilon/z$

$G_2 \rightarrow -4N_l[N(1)]^3\phi^3\ \epsilon/z$

$G_3 \rightarrow N_l\{4[N(1)]^3 M\phi^3 + 8[N(1)]^3\phi^3\}\ \epsilon/z$

$G_4 \rightarrow N_l[N(1)]^3\ \{-2M\phi^4 - 8\phi^4 + 4\phi^5\}\ \epsilon/z$

$H_1 \rightarrow N_l\ [-N(1,2)\phi^3]\ \epsilon/z$

$H_2 \rightarrow N_l\ [2N(1,2)\phi^2]\ \epsilon/z$

$H_3 \rightarrow N_l\ [-N(1,2)\phi]\ \epsilon/z$

$I_1 \rightarrow N_l\ [\ -3N(\perp)\phi^3]\ \epsilon/z$

$I_2 \rightarrow N_l\ [\ 3N(\perp)\phi^2]\ \epsilon/z$

$I_3 \rightarrow N_l\ [\ 3N(\perp)\phi^2]\ \epsilon/z$

$I_4 \rightarrow N_l\ [\ -3N(\perp)\phi]\ \epsilon/z$

$J_1 \rightarrow N_l\ [\ 4N(1)N(1,1)\phi^4\ ]\ \epsilon/z$

$J_2 \rightarrow N_l\ [-8N(1)N(1,1)\phi^3\ ]\ \epsilon/z$

$J_3 \rightarrow N_l\ [\ 4N(1)N(1,1)\phi^2\ ]\ \epsilon/z$

Diagram Set IV.

$A_1 \rightarrow N_l\ [\ -\phi^3 z\ ]\ \epsilon^2/2$

$A_2 \rightarrow N_l\ [\ \phi^4 z\ ]\ \epsilon^2/4$

$B_1 \rightarrow N_l\ [\ -2N(1)\phi^2]\ \epsilon^2$

$B_2 \rightarrow N_l\ [\ 2N(1)\phi^3]\ \epsilon^2$

$B_3 \rightarrow N_l\ [\ 2N(1)\phi^3]\ \epsilon^2$

$B_4 \rightarrow N_l\ [\ -2N(1)\phi^4]\ \epsilon^2$

$B_5 \rightarrow N_l\ [\ N(1)\phi^3]\ \epsilon^2$

$B_6 \rightarrow N_l\ [\ -4N(1)\phi^4]\ \epsilon^2$

$B_7 \rightarrow N_l\ [\ N(1)\phi^3]\ \epsilon^2$

$B_8 \rightarrow N_l\ [\ 2N(1)\phi^5]\ \epsilon^2$

$C_1 \rightarrow N_l\ [3N(2)\phi^3]\ \epsilon^2/2$

$C_2 \rightarrow N_l\ [-2N(2)\phi^2]\ \epsilon^2$

$C_3 \rightarrow N_l\ [N(2)\phi]\ \epsilon^2$

$C_4 \rightarrow N_l\ [N(2)\phi^2]\ \epsilon^2$

$C_5 \rightarrow N_l\ [N(2)\phi^3]\ \epsilon^2$

$C_6 \rightarrow N_l\ [N(2)\phi^3]\ \epsilon^2$

$C_7 \rightarrow N_l\,[N(2)\phi^4 - 9N(2)\phi^3/2]\,\epsilon^2$

$C_8 \rightarrow N_l\,[2N(2)\phi^3]\,\epsilon^2$

$C_9 \rightarrow N_l\,[2N(2)\phi^3]\,\epsilon^2$

$C_{10} \rightarrow N_l\,[-2N(2)\phi^2]\,\epsilon^2$

$C_{11} \rightarrow N_l\,[-3N(2)\phi^4]\,\epsilon^2$

$C_{12} \rightarrow N_l\,[-2N(2)\phi^4]\,\epsilon^2$

$C_{13} \rightarrow N_l\,[3N(2)\phi^4]\,\epsilon^2$

$D_1 \rightarrow N_l\,[-4N(1)N(1)\phi^2]\,\epsilon^2$

$D_2 \rightarrow N_l\,[4N(1)N(1)\phi^3]\,\epsilon^2$

$D_3 \rightarrow N_l\,[4N(1)N(1)\phi^3]\,\epsilon^2$

$D_4 \rightarrow N_l\,[-6N(1)N(1)\phi^4]\,\epsilon^2$

$D_5 \rightarrow N_l\,[-4N(1)N(1)\phi^4]\,\epsilon^2$

$D_6 \rightarrow N_l\,[6N(1)N(1)\phi^4]\,\epsilon^2$

$D_7 \rightarrow N_l\,[-2N(1)N(1)\phi^4]\,\epsilon^2$

$D_8 \rightarrow N_l\,[N(1)N(1)\phi^2]\,\epsilon^2$

$D_9 \rightarrow N_l\,[4N(1)N(1)\phi^2 + 2N(1)N(1)\phi^2M]\,\epsilon^2$

$D_{10} \rightarrow N_l\,N(1)N(1)\,\{4\phi^4 - 10\phi^3 - 2\phi^3M\}\,\epsilon^2$

$D_{11} \rightarrow N_l\,[-N(1)N(1)M\phi]\,\epsilon^2/2$

$D_{12} \rightarrow N_l\,[-2N(1)N(1)\phi^4]\,\epsilon^2$

$D_{13} \rightarrow N_l\,[-N(1)N(1)M\phi^3 - 4N(1)N(1)\phi^3]\,\epsilon^2$

$D_{14} \rightarrow N_l\,[2N(1)N(1)M\phi^4 + 16N(1)N(1)\phi^4]\,\epsilon^2$

$D_{15} \rightarrow N_l\,[N(1)]^2\,\{-M\phi^5/2 - 10\phi^5 + 3\phi 6\}\,\epsilon^2$

$E_1 \rightarrow N_l\,[N(1,1)\phi^5]\,\epsilon^2$

$E_2 \rightarrow N_l\,[-4N(1,1)\phi^4]\,\epsilon^2$

$E_3 \rightarrow N_l\,[2N(1,1)\phi^3]\,\epsilon^2$

$E_4 \rightarrow N_l\,[N(1,1)\phi]\,\epsilon^2$

$E_5 \rightarrow N_l\ [4N(1,1)\phi^3]\ \epsilon^2$

$E_6 \rightarrow N_l\ [-4N(1,1)\phi^2]\ \epsilon^2$

Appendix H. Diagrams Depicting Correlating Bonds And Nearest-Neighbor Intreactions.

Diagram set I provide corrections to the entropic part of the free energy in the lattice model up to $O(z^{-2})$. The corresponding values obtained in Appendix G are calculated using the cummulant expansion described in Chapter IV. Diagram F, O, P, and Q are required for polymers with branched-structure 1 and 2.

Diagram Set I[95,97]

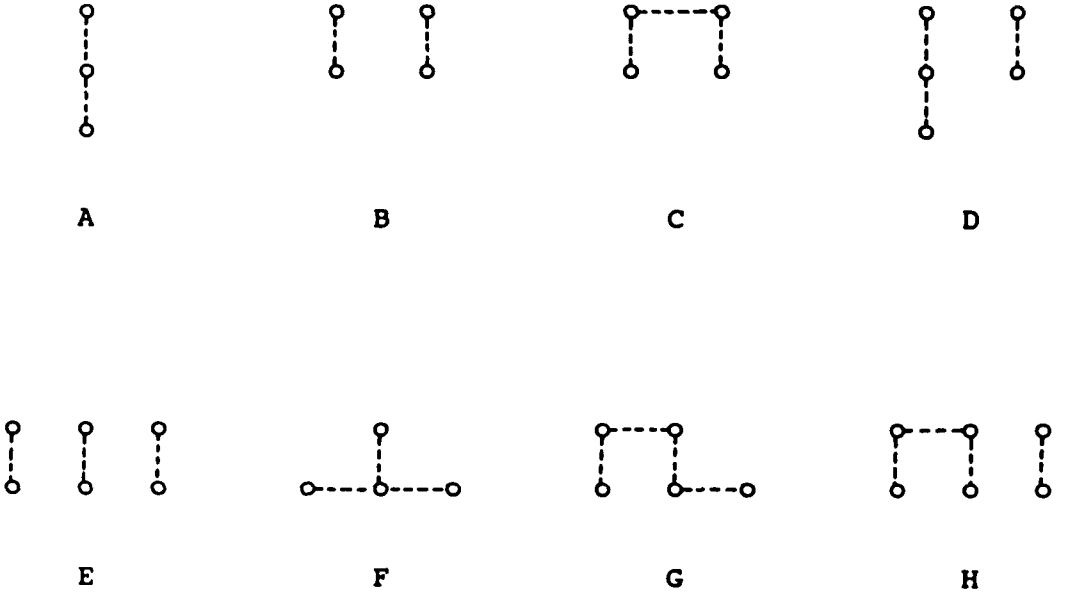

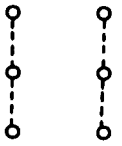

I

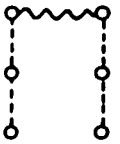

J

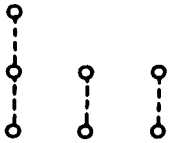

K

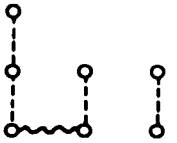

L

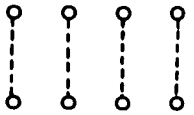

M

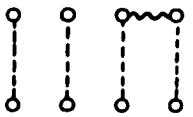

N

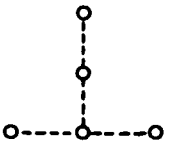

O

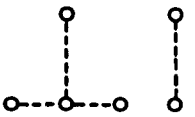

P

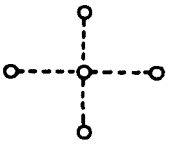

Q

Corrections to the energetic-part of the free energy require diagram set II, III, and IV[103,105]. Diagram set II give corrections up to $O(\varepsilon^4)$, diagram set III and IV correspond to corrections up to $O(\varepsilon, z^{-1})$ and $O(\varepsilon^2)$ respectively. Note that the solid line represents the interaction between two nearest-neighbor segments. We use a diagrammatic notation to conform the results in Ref. [103] and [105].

Diagram Set II

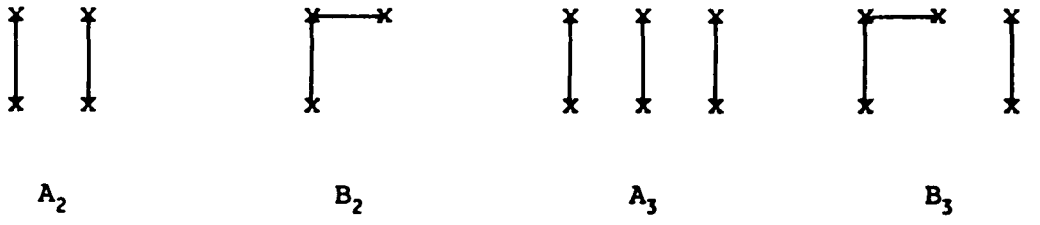

A_2 B_2 A_3 B_3

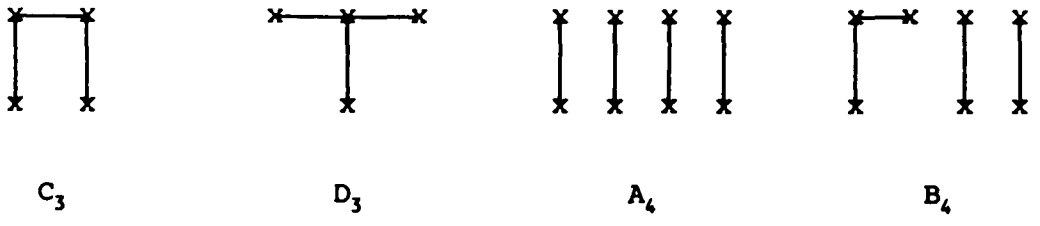

C_3 D_3 A_4 B_4

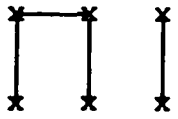

C_4

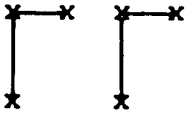

D_4

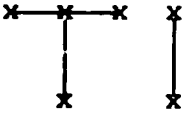

E_4

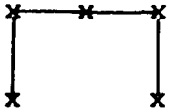

F_4

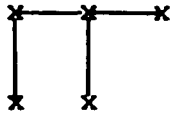

G_4

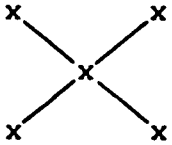

H_4

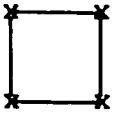

I_4

Diagram Set III.

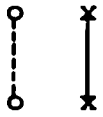

B_1

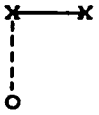

B_2

B_3

C_1

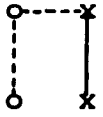

C_2

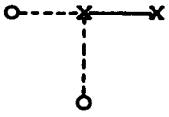

C_3

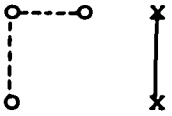

C_4

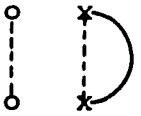

D_1

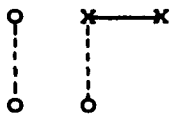

D_2

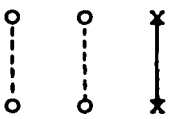

D_3

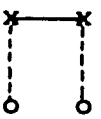

D_4

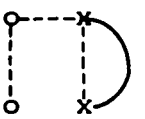

E_1

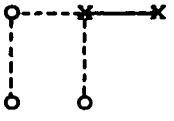

E_2

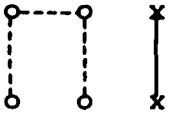

E_3

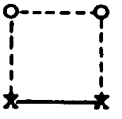

E_4

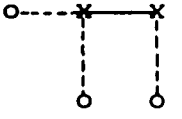

F_1

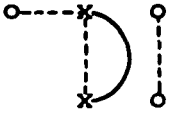

F_2

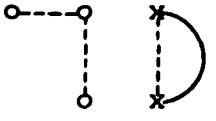

F_3

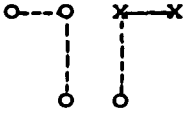

F_4

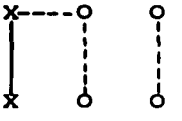

F_5

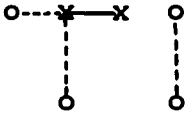

F_6

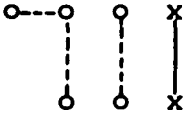

F_7

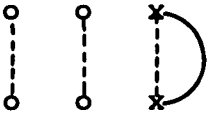

G_1

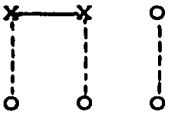

G_2

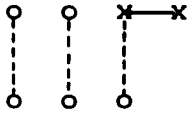

G_3

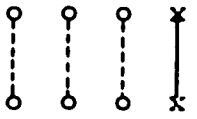

G_4

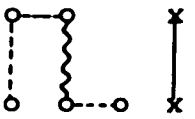

H_1

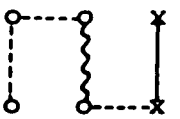

H_2

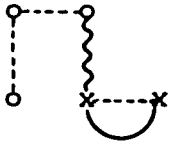

H_3

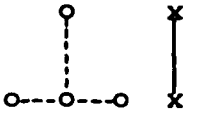

I_1

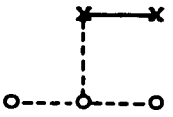

I_2

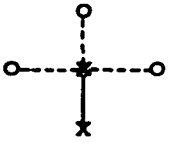

I_3

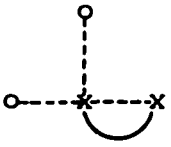

I_4

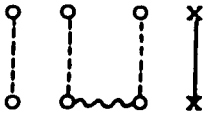

J_1

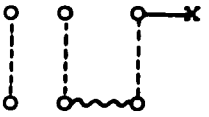

J_2

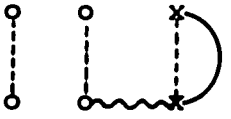

J_3

Diagram Set IV.

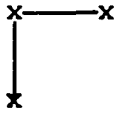

A_1

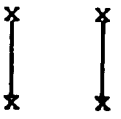

A_2

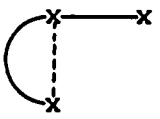

B_1

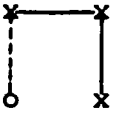

B_2

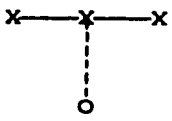

B_3

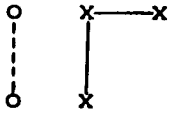

B_4

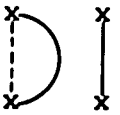

B_5

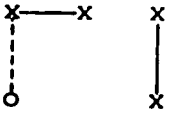

B_6

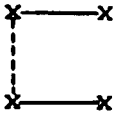

B_7

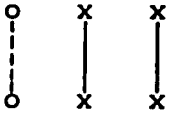

B_8

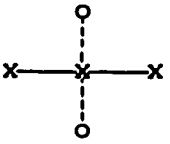

C_1

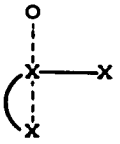

C_2

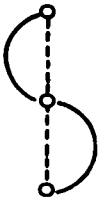

C_3

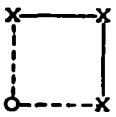

C_4

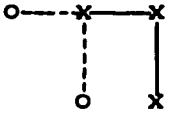

C_5

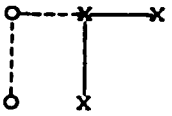

C_6

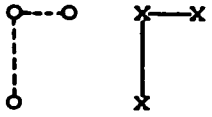

C_7

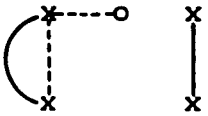

C_8

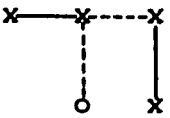

C_9

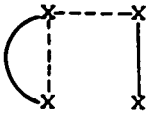

C_{10}

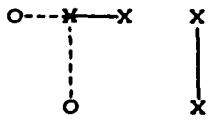

C_{11}

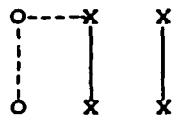

C_{12}

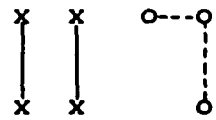

C_{13}

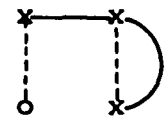

D_1

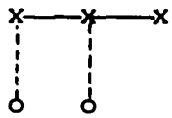

D_2

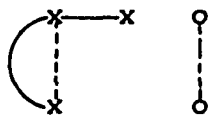

D_3

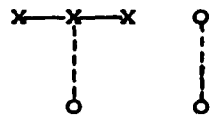

D_4

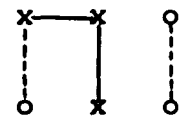

D_5

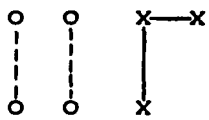

D_6

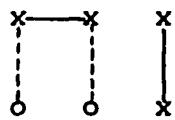

D_7

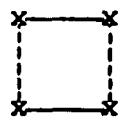

D_8

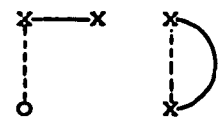

D_9

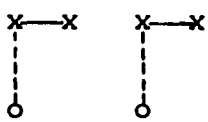

D_{10}

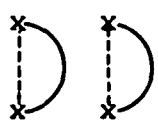

D_{11}

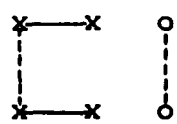

D_{12}

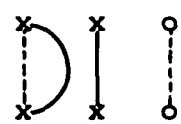

D_{13}

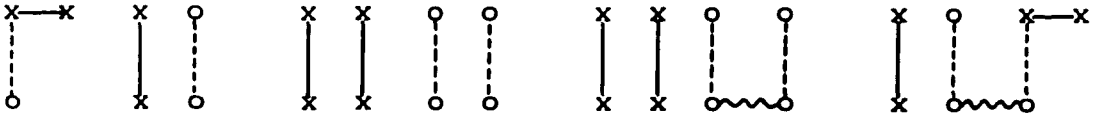

D_{14} D_{15} E_1 E_2

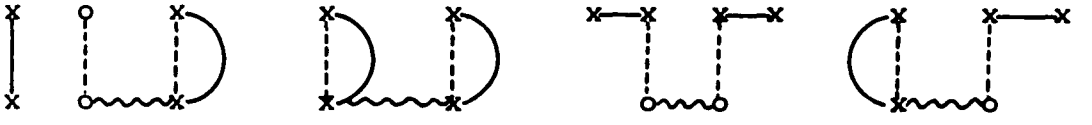

E_3 E_4 E_5 E_6

REFERENCES.

1. J. des Cloizeaux and G. Jannink, "Polymers in Solution: Their Modelling and Structure", Oxford Univ. Press, New York (1989).
2. P.J. Flory, "Principles of Polymer Chemistry", Cornell Univ. Press, Ithaca, New York (1953).
3. K.H. Meyer, Z. Phys. Chem. Abt. **B44**, 383 (1939).
4. R.H. Fowler and G.S. Rushbrooke, Trans. Faraday Soc. **33**, 1272 (1937).
5. T.S. Chang, Proc. Cambridge Philos. Soc. **35**, 265 (1939).
6. A.R. Miller, Proc. Cambridge Philos. Soc. **38**, 109 (1942).
7. E.A. Gugenheim, Proc. R. Soc. London **A183**, 203 (1944). E.A. Gugenheim, "Mixtures", Oxford Univ. Press, Oxford (1952).
8. P.J. Flory, J. Chem. Phys. **9**, 660 (1941).
9. P.J. Flory, J. Chem. Phys. **10**, 51 (1942).
10. P.J. Flory, Proc. R. Soc. London, **A234**, 60 (1956).
11. P.J. Flory, Proc. Natl. Acad. Sci. **79**, 4510 (1982).
12. M.L. Huggins, J. Chem. Phys. **9**, 440 (1941).
13. M.L. Huggins, J. Phys. Chem. **46**, 151 (1942).
14. M.L. Huggins, Ann. N.Y. Acad. Sci. **44**, 431 (1943).
15. K.F. Freed, J. Phys. **A18**, 871 (1985).
16. R. Zallen, "The Physics of Amorphous Solids", John-Wiley, New York (1983).

17. H. Yamakawa, "Modern Theory of Polymer Solutions", Harper and Row, New York (1971).

18. P.J. Flory, J. Chem. Phys. **17**, 303 (1949).

19. M.E. Fisher, J. Phys. Soc. Japan **26**, S44 (1969).

20. J.P. Cotton, J. Phys. Lett. (Paris) **41**, L231 (1980).

21. N. Madras and A. Sokal, J. Stat. Phys. **50**, 109 (1988).

22. R. Dickman, J. Chem. Phys. **87**, 2246 (1987).
A. Hertanto and R. Dickman, J. Chem. Phys. **89**, 7577 (1988).

23. E. De Vos and A. Bellemans, Macromolecules **7**, 812 (1974).

24. E. De Vos and A. Bellemans, Macromolecules **8**, 651 (1975).

25. H. Okamoto, J. Chem. Phys. **79**, 3976 (1983).

26. A. Sariban and K. Binder, Macromolecules **21**, 711 (1988).

27. F.T. Wall and J.P. Erpenbeck, J. Chem. Phys. **30**, 634 (1959).

28. M.G. Watts, J. Phys. **A7**, 489 (1974).

29. B. Nienhuis, Phys. Rev. Lett. **49**, 1063 (1982).

30. R. Vilanove and F. Rondelez, Phys. Rev. Lett. **45**, 1502 (1980).

31. M. Daoud, J.P. Cotton, B. Farnoux, G. Jannink, G. Sarma, H. Benoit, R. Duplessix, C. Picot, and P.G. de Gennes, Macromolecules **8**, 804 (1975).

32. K. Okano, E. Wada, Y. Taru, H. Hiramatsu, Rep. Prog. Polym. Sci. Japan **17**, 141 (1974).

33. R.P. Feynman, Rev. Mod. Phys. **20**, 367 (1948).

34. R.P. Feynman and A.R. Hibbs, "Quantum Mechanics and Path Integrals", McGraw-Hill, New York (1965).

35. L.S. Schulman, "Techniques and Applications of Path Integration", Wiley, New York (1981).

36. S.F. Edwards, Proc. Phys. Soc. London **85**, 613 (1965).

37. S.F. Edwards, Proc. Phys. Soc. London **88**, 265 (1966).

38. N. Saito, K. Takahashi, and Y. Yunoki, J. Phys. Soc. Japan **22**, 219 (1967).

39. K.F. Freed, Adv. Chem. Phys. **22**, 1 (1972).

40. L.P. Kadanoff, Physics **2**, 263 (1966).

41. L.P. Kadanoff, W. Gotze, D. Hamblen, R. Hecht, E.A.S. Lewis, V.V. Pakiauskas, M.Rayl, J. Swift, D. Aspnes, and J. Kane, Rev. Mod. Phys. **39**, 395 (1967).

42. B. Widom, J. Chem. Phys. **43**, 3892, 3898 (1965).

43. C. Domb and D.L. Hunter, Proc. Phys. Soc. London **86**, 1147 (1965).

44. H.E. Stanley, "Introduction to Phase Transtitions and Critical Phenomena", Oxford Univ. Press, London (1972).

45. S.K. Ma, "Modern Theory of Critical Phenomena", Benjamin/ Addison-Wesley, New York (1976).

46. P.G. de Gennes, Phys. Lett. **38A**, 339 (1972); J. Phys. (Paris) **36**, L55 (1975); **39**, L299 (1978).

47. P.G. de Gennes, "Scaling Concepts in Polymer Physics", Cornell Univ. Press, Ithaca, New York (1971).

48. J. des Cloizeaux, J. Phys. (Paris) **36**, 281 (1975); **41**, L151 (1980).

49. D.J. Burch and M.A. Moore, J. Phys. **A9**, 435, 451 (1976).

50. M. Gell-Mann and F.E. Low, Phys. Rev. **95**, 1300 (1954).

51. K.G. Wilson, Phys. Rev. **B4**, 3174, 3184 (1971).

52. K.G. Wilson and M.E. Fisher, Phys. Rev. Lett. **28**, 240 (1972).

53. K.G. Wilson, Phys. Rev. Lett. **28**, 548 (1972).

54. E. Brezin, J.C. le Guillou, J. Zinn-Justin and B.G. Nickel, Phys. Lett. **44A**, 227 (1973).

55. E. Brezin, D.J. Wallace and K.G. Wilson, Phys. Rev. Lett. **29**, 591 (1972); Phys. Rev. **B7**, 232 (1973).

56. K.G. Wilson and J. Kogut, Phys. Rep. **12C**, 75 (1974).

57. K.G. Wilson, Rev. Mod. Phys. **47**, 773 (1975).

58. E. Brezin, J.C. le Guillou and J. Zinn-Justin, in "Phase Transitions and Critical Phenomena", vol. 6, C. Domb and M.S. Green, eds., Academic Press, London (1976).

59. E. Brezin, in "Methods in Field Theory", Les Houches 1975, R. Balian and J. Zinn-Justin, eds., North-Holland, Amsterdam (1976).

60. J. Illiopoulos, C. Itzykson, and A. Martin, Rev. Mod. Phys. **47**, 165 (1975).

61. C. Itzykson and J.B. Zuber, "Quantum Field Theory", McGraw-Hill, New York (1980).

62. P. Ramond, "Field Theory, A Modern Primer", Benjamin/ Cummings, Reading, Massachusetts (1981).

63. D.J. Amit, "Field Theory, The Renormalization Group and Critical Phenomena", World Scientific, Singapore (1984).

64. J. Zinn-Justin, "Quantum Field Theory and Critical Phenomena", Oxford Univ. Press, New York (1989).

65. T.A. Witten and L. Schafer, J. Phys. **A11**, 1843 (1978); J. Chem. Phys. **74**, 2582 (1981).

66. L. Schafer and T.A. Witten, J. Chem. Phys. **66**, 2121 (1977).

67. M. Gabay and T. Garel, J. Phys. (Paris) **39**, L123 (1978).

68. M.K. Kosmas, J. Phys. **A14**, 931, 2779 (1981); **A15**, 1667 (1982).

69. K.F. Freed, "Renormalization Group Theory of Macromolecules", Wiley, New York (1987).

70. Y. Oono, T. Ohta and K.F. Freed, J. Chem. Phys. **74**, 645 (1981); Macromolecules **14**, 880 (1981).

71. Y. Oono and K.F. Freed, J. Chem. Phys. **75**, 993 (1981); J. Phys. **A15**, 1931 (1982).

72. T. Ohta and Y. Oono, Phys. Lett. **89A**, 460 (1982).

73. Y. Oono, Adv. Chem. Phys. **61**, 301 (1985).

74. T. Ohta, Y. Oono, and K.F. Freed, Phys. Rev. **A25**, 2801 (1982); Macromolecules **14**, 1588 (1981).

75. J.F. Douglas and K.F. Freed, Macromolecules **16**, 1800 (1983); **17**, 1854, 2344, 2354 (1984); **18**, 2445 (1985).

76. A.L. Kholodenko and K.F. Freed, J. Chem. Phys. **78**, 7390 (1983); **80**, 900 (1984).

77. A. Miyake and K.F. Freed, Macromolecules **16**, 1228 (1983); **17**, 678 (1984).

78. B.J. Cherayil, J.F. Douglas, and K.F. Freed, J. Chem. Phys. **83**,5293 (1985).

79. K.F. Freed, J. Chem. Phys. **79**, 3121, 6357 (1983).

80. A. Nakamichi and T. Ohta, J. Phys. **A16**, 4155 (1983).

81. B.J. Cherayil, M.G. Bawendi, A. Miyake, and K.F. Freed, Macromolecules **19**, 2770 (1986).

82. B.J. Cherayil, A.L. Kholodenko, and K.F. Freed, J. Chem. Phys. **86**, 7204 (1987).

83. Z.G. Wang, A. Nemirovsky, and K.F. Freed, J. Chem. Phys. **86**, 4266 (1987).

84. A.M. Nemirovsky and K.F. Freed, J. Chem. Phy. **83**, 4166 (1985); Nucl. Phys. **B270**, 423 (1986).

85. Z.G. Wang, A.M. Nemirovsky, and K.F. Freed, J. Chem. Phys. **85**, 3068 (1986).

86. B.J. Cherayil and K.F. Freed, J. Chem. Phys. **88**, 7851 (1988).

87. G. Stratouras, A.M. Kosmas, and M.K. Kosmas, J. Phys. **A23**, L1317 (1990).

88. J.F. Douglas, A.M. Nemirovsky, K.F. Freed, Macromolecules **19**, 2041 (1986).

89. J.F. Douglas, S.Q. Wang, K.F. Freed, Macromolecules **19**, 2207 (1986); **20**, 543 (1987).

90. J.F. Douglas and K.F. Freed, J. Chem. Phys. **86**, 4280 (1987).

91. G. 't Hooft and M. Veltman, Nucl. Phys. **B44**, 189 (1972).

92. G. 't Hooft and M. Veltman, "Diagrammar", CERN Report 73-9 (1973).

93. G. 't Hooft, Nucl. Phys. **B61**, 465 (1973).

94. M.G. Bawendi, K.F. Freed, U. Mohanty, J. Chem. Phys. **84**, 7036 (1986).

95. K.F. Freed, M.G. Bawendi, J. Chem. Phys. **88**, 2741 (1988).

96. M.G. Bawendi, K.F. Freed, U. Mohanty, J. Chem. Phys. **87**, 5534 (1987).

97. A.M. Nemirovsky, M.G. Bawendi, K.F. Freed, J. Chem. Phys. **87**, 7272 (1987).

98. K.F. Freed, A.I. Pesci, J. Chem. Phys. **87**, 7342 (1987).

99. A.I. Pesci, K.F. Freed, J. Chem Phys. **90**, 2003, 2017 (1989).

100. M.G. Bawendi, K.F. Freed, J. Chem. Phys. **85**, 3007 (1986).

101. M.G. Bawendi, K.F. Freed, J. Chem. Phys. **86**, 3720 (1987).

102. K.F. Freed and M.G. Bawendi, J. Phys. Chem. **93**, 2194 (1989).

103. J. Dudowicz, K.F. Freed, W.G. Madden, Macromolecules **23**, 4803 (1990).

104. W.G. Madden, A.I. Pesci, K.F. Freed, Macromolecules **23**, 1181 (1990).

105. J. Dudowicz and K.F. Freed, Univ. Chicago preprints (1991).

106. B.E. Eichinger and P.J. Flory, Trans. Faraday Soc. **64**, 2035, 2053, 2061, 2066 (1968).

107. P.J. Flory, Discuss. Faraday Soc. **49**, 7 (1970).

108. C.T. Murray, J.W. Gilmer, and R.S. Stein, Macromolecules **18**, 996 (1985).

109. F.T. Wall, L.A. Hiller, D.J. Wheeler, J. Chem. Phys. **22**, 1036 (1954).

110. F.T. Wall, L.A. Hiller, W.F. Atchison, J. Chem. Phys. **23**, 2314 (1955); **26**, 1742 (1957).

111. F.T. Wall, R.J. Rubin, L.M. Isaacson, J. Chem. Phys. **27**, 186 (1957).

112. M.E. Fisher and M.F. Sykes, Phys. Rev. **114**, 45 (1959).

113. M.N. Rosenbluth and A.W. Rosenbluth, J. Chem. Phys. **23**, 356 (1955).

114. H. Meirovitch, J. Phys. **A15**, L735 (1982).

115. P.G. Khalatur, S.G. Pletneva, Y.G. Papulov, J. Chem. Phys. **83**, 97 (1984).

116. H.C. Ottinger, Macromolecules **18**, 93, 1348 (1985).

117. F.T. Wall and F. Mandel, J. Chem. Phys. **63**, 4592 (1975).

118. F. Mandel, J. Chem. Phys. **70**, 3934 (1979).

119. P.H. Verdier and W.H. Stockmayer, J. Chem. Phys. **36**, 227 (1962).

120. P.H. Verdier, J. Chem. Phys. **45**, 2122 (1966).

121. P.H. Verdier, J. Chem. Phys. **52**, 5512 (1970).

122. P.H. Verdier, J. Chem. Phys. **59**, 6119 (1973).

123. D.E. Kranbuehl and P.H. Verdier, J. Chem. Phys. **71**, 2662 (1979).

124. H.J. Hilhorst and J.M. Deutch, J. Chem. Phys. **63**, 5153 (1975).

125. H. Boots and J. M. Deutch, J. Chem. Phys. **67**, 4608 (1977)

126. A. Baumgartner and K. Binder, J. Chem. Phys. **71**, 2541 (1979).

127. A. Baumgartner and K. Binder, J. Chem. Phys. **75**, 2994 (1981).

128. M. Lal, Molec. Phys. **17**, 57 (1969).

129. O.F. Olaj and K.H. Pelinka, Makromol. Chem. **177**, 3413 (1976).

130. B. Mac Donald, N. Jan, D.L. Hunter and M.O. Steinitz, J. Phys. **A18**, 2627 (1985).

131. D.L. Hunter, N.Jan, and B. Mac Donald, J. Phys. **A19**, L543 (1986).

132. A. Baumgartner and K. Binder, Eds. "Applications of the Monte Carlo Method in Stastistical Physics", Springer-Verlag, New York 1984.

133. K. Binder and D.W. Heermann, "The Monte Carlo Method in Statistical Physics", Springer-Verlag, New York 1988.

134. D.W. Heermann, "Computer Simulation Methods in Theoretical Physics", Springer-Verlag, Berlin 1990.

135. K. Kremer and K. Binder, Comp. Phys. Repts. **7**, 259 (1988).

136. H. Okamoto, J. Chem. Phys. **64**, 2686 (1975).

137. H. Okamoto and A. Bellemans, J. Phys. Soc. Jpn. **47**, 955 (1979).

138. H. Okamoto, J. Chem. Phys. **70**, 1690 (1979).

139. H. Okamoto, K. Itoh, and T. Araki, J. Chem. Phys. **78**, 975 (1983).

140. H. Okamoto, J. Chem. Phys. **83**, 2587 (1985).

141. H. Okamoto, J. Chem. Phys. **88**, 5095 (1988).

142. A. Bellemans and E. De Vos, J. Polym. Sci. : Symp. No. **42**, 1195 (1973).

143. R. Dickman and C.K. Hall, J. Chem. Phys. **85**, 3023 (1986).

144. R. Dickman, J. Chem. Phys. **91**, 454 (1989).

145. A. Hertanto and R. Dickman, J. Chem. Phys. **93**, 774 (1990).

146. M.K. Kosmas and K.F. Freed, J. Chem. Phys. **69**, 3647 (1978).

147. U. Eisele, "Introduction to Polymer Physics", Springer-Verlag, Berlin (1990).

148. A. Rudin, "The Elements of Polymer Science and Engineering", Acad. Press, London (1982).

149. W. Kuhn, Kolloid Z. **68**, 2 (1934).

150. D.S. McKenzie, Phys. Rep. **27**, 35 (1976).

151. C.D. Domb, Adv. Chem. Phys. **30**, 634 (1985).

152. I. Webman, J.L. Lebowitz, M.H. Kalos, Phys. Rev. **21**, 5540 (1980).

153. H. Benoit, D. Decker, J.S. Higgins, C. Picot, J.P. Cotton, B. Farnoux, G. Jannink, and R. Ober, Nat. Phys. Sci. **245**, 13 (1973).

154. J.P. Cotton, D. Decker, H. Benoit, B. Farnoux, J.S. Higgins, G. Jannink, C. Picot, and J. des Cloizeaux, Macromolecules **7**, 863 (1974).

155. R.G. Kirste, W.A. Kruse, and K. Ibel, Polymer **16**, 120 (1975).

156. D.G. Ballard, J. Schelten, G.D. Wignall, Euro. Polym. J. **9**, 965 (1973).

157. M. Nierlich, J.P. Cotton, and B. Farnoux, J. Chem. Phys. **69**, 1379 (1978).

158. G. Swislow, S. T. Sun, I. Nishio, and T. Tanaka, Phys. Rev. Lett. **44**, 796 (1980).

159. P.G. de Gennes, Macromolecules **14**, 1637 (1981).

160. W. Weibull, J. Appl. Mech. **18**, 293 (1951).

161. W.Y. Shih, W.H. Shih and I.A. Aksay, Macromolecules **23**, 3291 (1990).

162. J. des Cloizeaux, J. Phys. (Paris) **49**, 699 (1988).

163. A.L. Kholodenko and K.F. Freed, J. Phys. **A17**, 2703 (1984).

164. E. Eisenrigler, K. Kremer and K. Binder, J. Chem. Phys. 77, 6296 (1982).

165. K. Binder, in "Phase Transitions and Critical Phenomena", Vol. 8 (C.Domb and M.S. Green, Eds.), Academic Press, New York, 1983.

166. I.S. Gradshteyn and I.M. Ryzhik, "Table of Integrals, Series, and Products", Academic Press, New York, 1980.

167. W. Magnus, F. Oberhettinger, F.G. Tricomi, "Tables of Integral Transforms", McGraw-Hill, New York, 1954.

168. R. Dickman and C.K. Hall, J. Chem. Phys. **85**, 4108 (1986).

169. H. Muler-Krumbhaar and K. Binder, J. Stat. Phys. **8**, 1 (1973).

170. N. Metropolis, A.W. Rosenbluth, M.N. Rosenbluth, A.H. Teller, and E. Teller, J. Chem. Phys. **21**, 1087 (1953).

171. M.L. Mansfield, J. Chem. Phys. **77**, 1554 (1982).

172. W. G. Madden, J. Chem. Phys. **88**, 3934 (1988); **87**, 1405 (1987).

173. I. Carmesin and K. Kremer, Macromolecules **21**, 2819 (1988).

174. H. Deutsch and R. Dickman, J. Chem. Phys. **93**, 8983 (1990).

175. A. Bellemans and M. Janssens, Macromolecules, **7**, 809 (1974).

176. M. Bishop, M. Kalos, A.D. Sokal, and H.L. Frisch, J. Chem. Phys. **79**, 3496 (1983).

177. A. Baumgartner, J. Chem. Phys. **72**, 871 (1980); J. Physique **43**, 1407 (1982).

178. R. Finsy, M. Janssens, and A. Bellemans, J. Phys. **A8**, L106 (1975); M. Janssens and A. Bellemans, Macromolecules, **9**, 303 (1976).

179. R. Dickman, J. Chem. Phys. **96**, 1516 (1992).